INVESTIGATION OF TROGLITAZONE TOXICITY USING TRANSCRIPTOMIC ANALYSIS IN *IN VIVO* MOUSE AND *IN VITRO* STEM CELL BASED MODELS

Thesis submitted for the degree of

Doctor of Philosophy

at the University of Leicester

by

Harsharon Kaur Bahia BSc MSc (Birmingham)

Medical Research Council Toxicology Unit

University of Leicester

2016

Harsharon Kaur Bahia

Investigation Of Troglitazone Toxicity Using Transcriptomic Analysis In

In Vivo Mouse And In Vitro Stem Cell Based Models

Troglitazone (TRO), an anti-diabetic drug, was withdrawn from the market due to incidences of idiosyncratic hepatotoxicity and to a lesser extent cardiotoxicity in a small sub-set of the patient population. Post-marketing drug withdrawal emphasises the requirement for better predictive toxicity assays for use during drug development. Stem cells can potentially be differentiated into any cell type and thus could be utilised in novel in vitro assays to predict toxicity during preclinical drug development. The hypothesis for this thesis was that transcriptomic changes in mouse embryonic stem (mES) cell derived cardiomyocytes and hepatocytes are signatures for cardiotoxic and hepatotoxic effects of troglitazone in the mouse.

Standardised and reproducible protocols were developed for chemical induced differentiation of mES cells into cardiomyocytes and hepatocytes. The differentiated cells expressed key cardiac and hepatic marker genes, however, cell cultures were heterogeneous and contained a mixture of immature and terminally differentiated cells. Transcriptomic signatures of TRO toxicity in vivo were obtained using normal and high fat diet induced diabetes mouse models. These signatures were compared with those obtained from TRO treatment of mES cell derived cardiomyocytes and hepatocytes.

In vitro transcriptomic signatures implicated an endoplasmic reticulum (ER) stress based mechanism for TRO induced toxicity in both hepatocytes and cardiomyocytes. In vivo transcriptomic data also indicated that TRO induced hepatic ER stress. In particular, the up-regulation of Trib3 was observed in vivo, in the livers of normal and diabetic mice and in vitro, in mES cell derived hepatocytes and cardiomyocytes. Increased expression of genes involved in cardiac remodelling due to TRO induced plasma volume increase were observed in vivo, however, in vitro, these genes were down-regulated. These data indicate that there is some correlation between in vitro and in vivo hepatic transcriptomic signatures of TRO toxicity but no correlation between the cardiac signatures.

Acknowledgements

Contents

List of Figures

List of Tables

Abbreviations

2D	Two dimensional
3D	Three dimensional
ADR(s)	Adverse drug reaction(s)
ALT	Alanine aminotransferase
ANOVA	Analysis of variance
ANP	Atrial natriuretic peptide
AP	Alkaline phosphatase
APS	Ammonium persulphate
AST	Aspartate aminotransferase
ATP	Adenosine triphosphate
AUC	Area under the curve
BG	Blood glucose
BMP	Bone morphogenic proteins
BSA	Bovine serum albumin
^{o}C	Degrees Celsius
Ca^{2+}	Calcium
cDNA	Complementary DNA
CIG	Ciglitazone
CM	Cardiomyocyte
cm	Centimetre
CO_2	Carbon dioxide
cRNA	Complementary RNA
Ct	Cycle threshold
Cy3	Cyanine-3
Cy5	Cyanine-5
Cyp	Cytochrome P450
DAR	Darglitazone
Dex	Dexamethasone
DMSO	Dimethyl sulphoxide
DNA	Deoxyribonucleic acid

E.coli	Escherichia coli
EB(s)	Embryoid body(-ies)
EBiSC	European Bank for Induced Pluripotent Stem Cells
EDTA	Ethylenediaminetetraacetic acid
ENG	Englitazone
ER	Endoplasmic reticulum
ES	Embryonic stem
EST	Embryonic stem cell test
ETC	Electron transport chain
FA(s)	Fatty acid(s)
FACS	Fluorescence-activated cell sorting
$FADH_2$	Flavin adenine dinucleotide
FCS	Foetal calf serum
FDA	U.S. Food and Drug Administration
FFAs	Free fatty acids
g	Gram
GAL	GenePix array list
GLP	Good laboratory practice
GMEM	Glasgow's minimal essential medium
gp130	Glycoprotein 130
GPR	GenePix text file
GSH	Glutathione
GSK	GlaxoSmithKline
H_2O	Water
HBSS	Hank's buffered salt solution
Hep	Hepatocyte
hES	Human embryonic stem
HFD	High fat diet
HLA	Histocompatibility complex
HTS	High throughput screening
IC_{50}	Concentration causing 50% inhibition of cell viability
ICM	Inner cell mass
IDAT	Illumina intensity data file

IgG	Immunoglobulin G
IL6	Interleukin 6
IMDM	Iscove's modified Dulbecco's Medium
Iono	Ionomycin
IPA	Ingenuity pathway analysis
iPS	Induced pluripotent stem
ITS	Insulin-transferrin-selenium supplement
kDa	Kilodalton
kg	Kilogram
KO-DMEM	Knockout Dulbecco's modified eagle medium
L	Litre
LB	Liquid broth medium
LC-MS	Liquid chromatography-mass spectrometry
LD_{50}	Dose required to kill 50% of the population
LIF	Leukaemia inhibitory factor
LIFR	LIF specific receptor
Lowess	Locally weighted polynomial regression
MEEBO	Mouse Exonic Evidence Based Oligonucleotide
MEFs	Mouse embryonic fibroblasts
mES	Mouse embryonic stem
mg	Milligram
ml	Millilitre
mLIF	Murine LIF
mM	Millimolar
mRNA	Messenger RNA
MTT	(3-(4,5-dimethylthiazol-2-yl)-2,5-diphenyltetrazolium bromide)
NADH	Nicotinamide adenine dinucleotide
NAPQI	N-acetyl-p-benzoquinone
NCBI	National Center for Biotechnology Information
ng	Nanogram
nm	Nanometre
nM	Nanomolar

OGTT	Oral glucose tolerance test
PBS	Phosphate buffered saline
PFA	Paraformaldehyde
PIO	Pioglitazone
pmol	Picomole
QSAR	Quantitative structure-activity relationship
RIN	RNA integrity number
RNA	Ribonucleic acid
ROSI	Rosiglitazone
ROS	Reactive oxygen species
rpm	Revolutions per minute
RT	Room temperature
RT-PCR	Quantitative real time polymerase reactions
SC4SM	Stem Cells for Safer Medicine
SCN	Suprachiasmatic nuclei
SD	Standard deviation
SDS	Sodium dodecyl sulphate
SDS-PAGE	Sodium dodecyl sulphate – polyacrylamide gel electrophoresis
SR	Sarcoplasmic reticulum
SSC	Saline sodium citrate
T2D	Type 2 diabetes
TCA	Tricarboxylic acid
TdP	Torsades de Pointes
TEMED	Tetramethylethylenediamine
TMRM	Tetramethylrhodamine methyl ester
TRO	Troglitazone
TZD	Thiazolidinedione
UPR	Unfolded protein response
UK	United Kingdom
USA	United States of America
USD	U. S. Dollar
V	Volts

v/v	Volume-volume percentage
w/v	Weight-volume percentage
w/w	Weight-weight percentage
Wnt	wingless
ΔCt	Delta Ct
ΔΔCt	Delta-delta Ct
µg	Microgram
µl	Microlitre

Chapter 1: Introduction

The purpose of this work was to examine the concept that embryonic stem cells differentiated to hepatocytes and cardiomyocytes could be used to test for idiosyncratic drug reactions during pre-clinical testing. Troglitazone was the chosen test drug because it was withdrawn from the market due to primarily liver but also cardiac toxicity in a subset of patients to whom it was administered. The *in vitro* model was compared with data from *in vivo* administration in a normal and diabetic model reflecting the therapeutic application of Troglitazone. Chapter one provides a general overview of the challenge, troglitazone, the cells and the methods used in this work.

1.1 Toxicity Testing in Drug Discovery and Development

Drug discovery and development is an expensive and time-consuming multi-stage process that is estimated to cost in excess of $1 billion USD per marketed drug (Morgan et al., 2011). The process of discovering and developing new drugs can be broadly divided into 5 stages of identifying the biological target, selecting a lead candidate drug, performing preclinical safety, toxicity, pharmacology and pharmacokinetic studies, undertaking clinical studies in patients and gaining regulatory approval for marketing (Figure 1.1) (Hughes et al., 2011). The designs of the studies in each stage are adapted according to the properties of the drug being developed and the nature of the disease being treated. For example, during clinical development the 'first time in man' studies usually involve healthy male volunteers. However, in the development of inherently toxic anti-cancer drugs patients with advanced stage cancer are used in place of healthy volunteers (Gupta et al., 2012). The assortment of *in silico, in vitro, ex vivo, in vivo animal* and human clinical trial studies that are undertaken during drug development are completed to ascertain the efficacy and safety of the new drug entity. There can

be an overlap between the studies used in each stage of drug development and some studies, such as long term animal reproductive studies and phase I clinical trials, may be performed in parallel.

2 - 5 Years	**Target Identification**	Biology, biochemistry, genetic studies for target ID High throughput screening assays
	Lead Selection	Medicinal chemistry Structure-activity relationship studies X-ray crystallography
6 - 10 Years	**Preclinical Development**	*In vitro* & *in vivo* safety & toxicity studies Pharmacology studies Absorption, distribution, metabolism and excretion
	Clinical Development	Phase I – First time in humans (10 – 80 volunteers) Phase II – Proof of principle testing (100 – 300 patients) Phase III – Safety study (1000 – 3000 patients)
1 - 2 Years	**Approval & Marketing**	Submission for drug approval to regulatory authority Phase IV – post launch trials Post-marketing surveillance, Adverse event reporting

Figure 1.1 – Drug discovery and development process. The drug discovery and development process can be divided into 5 overlapping stages. In the first stage a suitable biological target, which plays a significant role in a particular disease or medical syndrome, is identified. A potential lead candidate drug is then selected that has affinity for the biological target and can improve the disease state. The lead drug is further developed during preclinical development and its properties are determined by a series of *in vitro* and *in vivo* safety, toxicity, pharmacology and pharmacokinetic studies. Successful completion of these studies leads to the first test of the drug in humans followed by larger clinical trials. Preclinical and clinical data is then submitted to the regulatory authorities for approval to market the drug. The drug manufacturer continues surveillance of the effects of the drug via collection of post-marketing data.

Parallel studies are undertaken when the results of the two studies are unlikely to affect each other. New drugs entities can be tested for the first time in man whilst reproductive toxicity tests in animals are being concluded because the phase I trials do not utilise pregnant women. If a drug is found to cause reproductive toxicity it is likely to be given a warning label when marketed, advising for the drug not to be prescribed to pregnant women, rather than be discarded at such a late stage of development (Hartung, 2013).

1.1.1 Target Identification

The initial stage of the discovery process begins with identifying a suitable druggable biological macromolecule for the treatment of a disease or medical syndrome. Traditionally, cellular proteins such as G-protein coupled receptors, ion channels, nuclear receptors and kinases have been the target biological entities of drug discovery pathways. However, advancements in genomic and proteomic technologies such as microarrays and genome sequencing, have allowed genes, RNA and novel proteins to become drug discovery targets (Tyers and Mann, 2003, Wang et al., 2004).

1.1.2 Lead Drug Candidate Selection

Once a target has been chosen potential drug candidate molecules need to be selected. This is achieved by screening compound libraries using high throughput screening (HTS) or by using computational methods such as quantitative structure-activity relationship (QSAR) modelling to identify small molecules or siRNAs with suitable affinity for the biological target (Bleicher et al., 2003, Cumming et al., 2013). The challenge then is to filter through the potential candidates and identify a lead drug candidate that is likely to have good efficacy and safety and in humans. Toxicity testing in drug discovery and development

starts during the process of selecting a lead candidate drug. The results of the HTS and QSAR studies often provide a number of potential drug candidates from which the pharmaceutical company chooses one to develop further. In order to minimise drug attrition at a later stage, a number of toxicology studies are commenced during the lead selection stage to deduce which of the potential drug candidates is likely to be the safest and thus is most suitable for further investment and development. During this early phase of drug development several *in vitro* and a few *in vivo* studies are undertaken to inform on the properties of the potential drug candidates (Pritchard et al., 2003).

If the therapeutic route of application for the potential drugs is to be via oral administration then the absorption of the compounds is assessed. In humans, absorption of drugs occurs in the small intestine via trans-epithelial transport routes. Absorption of drug candidates across the intestinal mucosa is assessed using a combination of *in silico* mathematical modelling, *in vitro* cell based assays such as the Caco-2 cell model and *ex vivo* models utilising animal intestinal sections. These models help to determine whether the drug candidate will cross the intestinal mucosa via gradient dependent passive routes or active transporter dependent pathways (Deferme et al., 2008). Drugs absorbed across the intestinal mucosa are transported via the portal vein to the liver where they are metabolised (Pang, 2003).

The metabolism of potential lead drug candidates is assessed using human hepatocellular carcinoma derived cell lines, primary human hepatocytes, human liver microsomes and transgenic animal cell lines. These *in vitro* cell based assays are used in conjunction with liquid chromatography, mass spectrometry and/or nuclear magnetic resonance technologies to assess the biotransformation

5

of the drug and consequent metabolite formation during Phase I and Phase II metabolism (Brandon et al., 2003).

Drugs and their metabolites enter the systemic circulatory system through which they can have an effect on target and non-target organs. Early safety pharmacology studies are used to screen candidate molecules for the potential to cause Torsades de Pointes (TdP), a type of ventricular tachycardia. The ability to cause TdP is not limited to just drugs used for the treatment of cardiac ailments and in the UK 3% of all prescription drugs carry warnings regarding their potential to cause TdP (Yap and Camm, 2003). The onset of TdP is associated with inhibition of the human ether-a-go-go (hERG) potassium channel, which is encoded for by the KCNH2 gene and is involved in the repolarisation stage during action potential generation. The effect of candidate molecules on the hERG potassium channel is assessed *in vitro* using cell lines such as the hERG expressing Chinese Hamster Ovary cell line and patch-clamp electrophysiology techniques (Hancox et al., 2008).

In addition to early stage assessment of potential cardiotoxicity, genotoxicity testing is undertaken during early drug development to detect potential mutagenic and carcinogenic properties of candidate drugs. Mutagenic potential of drug candidates is initially assessed *in vitro* using the Ames test, the mouse lymphoma assay and the micronucleus test, which collectively provide information on the potential of the candidate drug to cause chromosomal damage, alterations in the number of chromosomes and induce gene mutations. Subsequent *in vivo* testing in rodents is undertaken to determine potential somatic and germ cell genotoxicity and mutagenicity of drugs that may be used for extended periods of time. Aneuploidic and clastogenic potential is determined using the bone marrow

micronucleus assay, the ability to cause reversible and irreversible DNA damage is assessed using the Comet assay and contact site, somatic and germ tissue genotoxicity is ascertained using the transgenic rodent mutation assay (Müller et al., 1999, Dearfield et al., 2002).

The data from early stage toxicity studies are used by pharmaceutical companies to deduce which of the candidate drugs has the greatest chances of making it through development and onto the market. The chosen lead drug then enters preclinical development where that safety and efficacy of the drug is further evaluated.

1.1.3 Preclinical Development

The preclinical and clinical drug development stages can be the most time and cost consuming phases of the process. During these stages the lead drug undergoes extensive testing to ascertain the efficacy and safety of the drug in humans. Before the drug can be tested in humans its toxicity is assessed using *in vivo* animal studies. Early *in* vitro metabolic studies, conducted using human hepatic cell lines and primary cells, will have informed on the primary metabolites that are produced when the drug is metabolised. During preclinical toxicity testing, at least one animal species used will also form the primary metabolites that were identified in the early *in vitro* studies (Liu and Jia, 2007).

Acute toxicity testing is undertaken to ascertain the LD_{50} concentration of the drug, this is the dose that causes death in 50% of the test population. These studies use as few animals as possible, are often performed on male and female mice and rats, the drug is administered once at a high dose via the route of intended exposure and the animals are observed for 14 days. During the study the food and water consumption, behaviour and mortality of the animals is

recorded (Parasuraman, 2011). Sub-chronic toxicity studies are then undertaken to establish the 'no observed adverse effect level' and the 'lowest observed adverse effect level'. These studies typically last for 90 days, utilise one rodent and one non-rodent species with up to 20 animals of each gender, the drug is administered repeatedly at a high dose that induces toxicity but not mortality and during the study the food and water consumption, animal behaviour and any mortalities are noted. At termination of the study blood and organs are collected, histopathology, haematology and biochemical analysis is undertaken to assess the effects of the drug on target and non-target organs (Adler et al., 2011). The data from sub-chronic studies are used to select the doses for chronic toxicity studies. Chronic toxicity studies utilising rats last for 2 years and studies utilising non-rodent species last for one year. These studies involve repeat administration of the drug at the estimated maximum tolerated dose. At the termination of the study, histopathology, haematology and biochemical analysis is undertaken and the animals are assessed for tumours to inform on the potential carcinogenicity of the drug (Jacobs and Hatfield, 2012). In addition to ascertaining the toxicity of the drug on the parent ingesting the compound the toxicity, studies are also undertaken to evaluate potential developmental and reproductive toxicity. The importance of such tests was highlighted by the catastrophic effects of thalidomide. Reproductive toxicity studies commonly utilise rats. Male rats are administered the drug for 60 days leading up to mating and females are exposed for 14 days before mating; the females are then administered the drug through gestation and lactation. During these studies the number of females that get pregnant are noted and the mortality and morbidity of the off-spring is also noted. Studies to assess developmental toxicity typically utilise rats and rabbits and the

drug is administered during the first trimester to assess potential teratogenicity (Barrow, 2009). Toxicity data collected from the preclinical animal studies forms part of the drug development portfolio that is submitted to regulatory authorities for approval to begin testing the drug in humans.

1.1.4 Clinical Development

The starting dose for human clinical trials is often a tenth of the lowest maximum tolerated dose observed in the *in vivo* chronic toxicity animal studies (Newell et al., 1999). Phase I clinical trials are undertaken in a small number of healthy, often male, human volunteers. These studies are used to determine the drug dosing regimen that is to be utilised in future trials, to identify any safety or toxicity concerns and to establish the pharmacokinetic profile of the drug in humans. Phase I trials are used to confirm the safety of the drug in humans and successful completion leads to commencement of Phase II clinical trials. The format of Phase II trials varies depending on how the drug is to be administered and the type of disease or medical syndrome that is being treated. The primary aim of Phase II trials is to determine efficacy of the new drug in the patient population. These trials are undertaken using 100 to 300 patients and will include division of the patients into two groups wherein one group is administered the drug and the other groups is given a placebo. Phase III trials are initiated to expose a larger patient population to the drug to confirm its safety and efficacy and to determine the therapeutic dose range (ABPI, 2012, ABPI, 2014). The data collected from the drug discovery and development process are used by the pharmaceutical company to apply for regulatory approval and a licence to market the drug.

1.1.5 Regulatory Approval and Marketing

There are numerous international regulatory authorities that have the power to approve new drugs, including the Medicines and Healthcare products Regulatory Agency in the UK, the European Medicines Agency, which covers members of the European Union, the Food and Drug Administration (FDA) in the USA and the Pharmaceuticals and Medical Devices Agency in Japan (WHO, 2012).

The numerous *in vitro*, *in vivo* animal and human toxicity studies undertaken during drug development are designed to inform on the potential toxicity of the new drug. In order to gain approval for marketing, pharmaceutical companies have to illustrate the safety of the new drug in patients. Thus, the clinical trials are deemed to be a crucial part of drug development as they illustrate the safety of the drug in patients. However, there have been occasions where the ability of a drug to cause serious adverse reactions in some patients only became apparent after millions of patients had been administered the drug. One high profile example of such an incidence is the drug Troglitazone (TRO), which was found to cause severe and in some instances fatal hepatotoxicity in a small number of patients after it had been prescribed to millions of Type 2 diabetics (Gale, 2001).

1.2 Troglitazone

TRO was the investigative compound for this project and the first member of the thiazolidinedione (TZD) compound family to be marketed. TZDs are peroxisome proliferator activated receptor gamma (PPARγ) agonists, which are prescribed for oral administration in the treatment of insulin resistance in patients with type 2 diabetes (T2D). Each member of the TZD family contains a common thiazolidinedione functional group, which is a heterocyclic 5 membered saturated ring with a thioether group at position 1, an amine group at position 3 and two

ketone groups at positions 2 and 4. The TZD drugs vary by the composition of their side chains at position 5 of the heterocyclic 5 membered saturated ring (Figure 1.2) (Day, 1999). In addition to structural differences, the TZD drugs also differ in their affinity for PPARγ. Rosiglitazone (ROSI) has the highest binding affinity for PPARγ followed by pioglitazone (PIO), TRO, darglitazone (DAR), ciglitazone (CIG) and englitazone (ENG) (Aleo et al., 2003, Mabilleau et al., 2011).
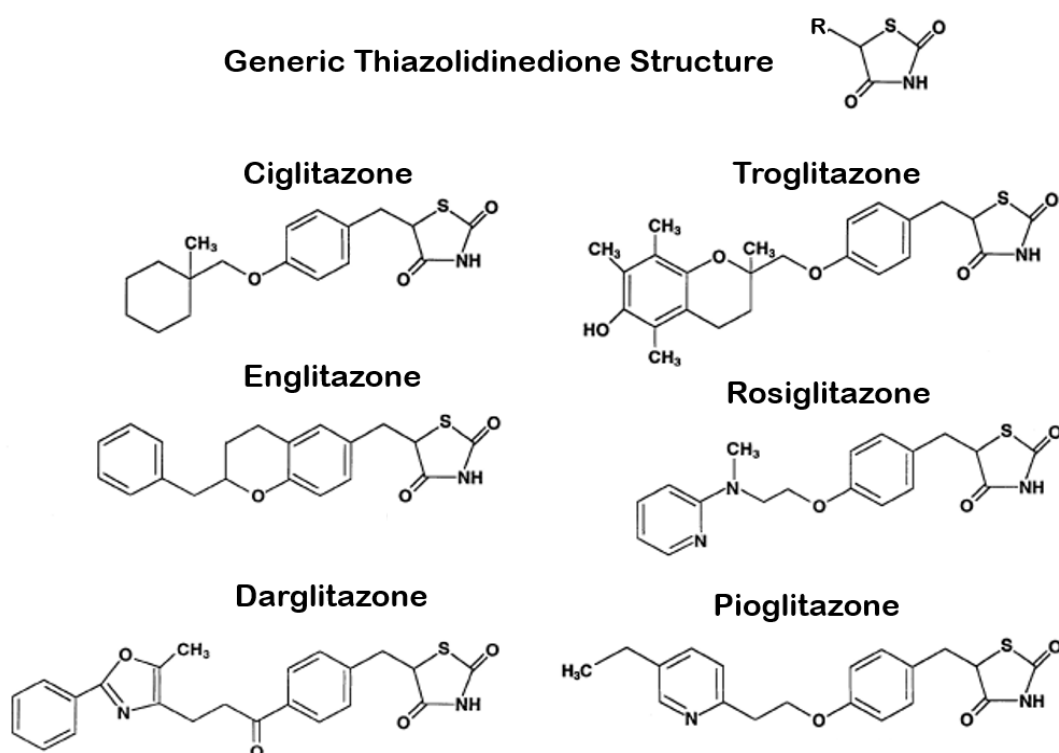
Figure 1.2 – Structures of the thiazolidinedione anti-diabetic drug family. All members of the TZD drug family contain a common thiazolidinedione group, which is a heterocyclic 5 membered saturated ring with a thioether group at position 1, an amine group at position 3 and two ketone groups at positions 2 and 4. The drugs vary by the composition of their side chains at position 5 of the heterocyclic 5 membered saturated ring.

CIG, ENG and DAR were shown to cause liver toxicity during development and consequently were not marketed (Hulin et al., 1996). TRO first entered the market in Japan in January 1997 followed by release in the USA in April and in the UK

in October of the same year. However, it was withdrawn from worldwide sale in February 2000 due to incidences of idiosyncratic toxicity (Gale, 2001). ROSI was withdrawn from sale in the UK in September 2010 due to increased risk of heart attacks associated with its use but is still market in the USA (MHRA, 2010). PIO is the only TZD drug currently marketed for the treatment for T2D in the UK. However, prolonged use has been linked to increased risk of bladder cancer and because of this in 2011 it was withdrawn from the market in France and Germany (Schernthaner et al., 2013).

1.2.1 Insulin and Type 2 Diabetes

Insulin is a hormone that is produced and secreted by the β-cells of the Islets of Langerhans in the pancreas and plays a vital role in glucose homeostasis (Cheatham and Kahn, 1995). Secretion of insulin is predominantly triggered by blood glucose levels although fatty acids and amino acids can also influence this process (Straub and Sharp, 2002). The insulin signalling cascade has the greatest influence on the liver, skeletal muscle and adipose tissue and helps to maintain plasma glucose levels between 4-7 mM in normal individuals (Saltiel and Kahn, 2001). Plasma insulin binds to its tyrosine kinase receptor, which is found on the outer cell surface of insulin responsive tissues. This stimulates uptake of glucose, fatty acids and amino acids from the blood into tissues and subsequently modulates their conversion into glycogen, triglycerides and proteins, respectively. When glucose levels are high, such as after eating, insulin also acts to inhibit glycogenolysis, lipolysis and breakdown of proteins in tissues (Figure 1.3) (Lizcano and Alessi, 2002).

Dysregulation of post feeding nutrient uptake and storage processes results in insulin resistance and the onset of T2D. Patients with T2D have increased plasma

levels of free fatty acids (FFAs), which accumulate in the liver and muscle tissue instead of being taken up by adipose tissue. Obesity and T2D are often associated and there is an established relationship between increased body fat content and decreased sensitivity to insulin. Elevated plasma FFA levels decrease the efficiency of insulin signalling resulting in decreased uptake of glucose into tissues, this consequently leads to high circulating levels of insulin and glucose, a measurable characteristic of T2D (Frayn, 2001).

Third party content removed

Figure 1.3 – Effect of insulin signalling on glucose metabolism. Binding of insulin to its receptor promotes glycogenesis and lipogenesis whilst inhibiting glycogenolysis and lipolysis (adapted from (Saltiel and Kahn, 2001)).

1.2.2 Peroxisome Proliferator Activated Receptor Gamma

The Peroxisome Proliferator Activated Receptor (PPAR) family of ligand activated transcription factors is composed of three members PPARα (alpha), PPARγ (gamma) and PPARδ (delta) that play important roles in the regulation of metabolic homeostasis (Tontonoz and Spiegelman, 2008). PPARα is highly

expressed in the liver, heart, kidney and in skeletal muscle, PPARγ is highly expressed in adipose tissue with much lower expression found in the liver and skeletal muscle and PPARδ is uniformly expressed in all tissues (Willson et al., 2001). Activated PPARs form heterodimers with retinoid X receptors, which then bind to peroxisome proliferator response elements of target genes subsequently increasing their transcription (Berger and Moller, 2002). PPARγ can be activated by endogenous ligands such as free fatty acids and eicosanoid derivatives, as well as by synthetic ligands such as members of the TZD class of anti-diabetic drugs (Berger and Moller, 2002).

1.2.3 Mechanism of Action

TRO binds to PPARγ, which in turn regulates the transcription of insulin responsive genes that are involved in glucose and lipid metabolism. Binding of TRO to PPARγ leads to the transcription of genes such as fatty-acid transport-protein, lipoprotein lipase, acyl-CoA synthase and glycerol transporter aquaporin 7, which are involved in the uptake of circulating fatty acids into adipocytes (Rosen et al., 2000). Activation of PPARγ in adipose tissue results in adipogenesis, a process by which fibroblast like pre-adipocytes differentiate into mature fat storing adipocytes (Lehrke and Lazar, 2005). The high levels of PPARγ expression in adipose tissue make it the primary target of TRO but subsequent increased sensitivity to insulin is also observed in the liver and skeletal muscle (Picard and Auwerx, 2002). TRO increases the uptake of FFAs into adipose tissue, decreasing their deposition into the liver and skeletal muscle (Frayn et al., 2006). The accepted mechanism of the anti-diabetic effect of TZDs is via insulin dependent sensitisation of adipose tissue, hepatocytes and skeletal muscle to the action of insulin (Table 1.1) (Day, 1999).

Third party content removed

Table 1.1 – Ex vivo and in vitro effects of TZDs (Day, 1999)

1.2.4 Metabolism

TRO is metabolised in the liver via a number of pathways (Figure 1.4) Metabolism by cytochrome P450 (CYP) 3A4 and 2C8 produces a quinone metabolite (M3) that can be conjugated with glutathione (GSH) via glutathione-*S*-transferase (GST) enzymes or metabolised further generating epoxide and hydroquinone metabolites. Hydroquinone metabolites can undergo sulphation or glucuronidation (Smith, 2003, Lauer et al., 2009). Phase II metabolism predominantly occurs via phenolsulphotransferase isoenzyme 1A3 (SULT1A3) and produces a sulphate metabolite (M1) (Smith, 2003). To a lesser extent the products of the phase I oxidative metabolism are also metabolised by uridine diphosphate glucuronyl transferase enzymes producing a glucuronide metabolite (M2). The major plasma metabolites found in healthy male volunteers who were administered a single 400 mg dose were M1 and M3, whilst M2 was detected in the urine but not in the plasma. Levels of M1 were 6-7 times higher than those of TRO and M3 in both normal and T2D patients. At clinically relevant concentrations TRO does not inhibit any of the major CYP enzymes although it does induce expression of CYP3A4 (FDA, 1999b).

Third party content removed

Figure 1.4 – Pathways of troglitazone metabolism
The enzymes involved in TRO metabolism are: phenolsulphotransferase 1A3 (SULT1A3), cytochrome P450 3A4 and 2C8 (CYP3A4/CYP2C8) and glutathione-S-transferase (GST) (adapted from (Smith 2003))

1.2.5 Possible Causes of Toxicity

During clinical trials it was noted that TRO caused reversible elevation (>3 times the upper limit of normal values) of serum alanine transaminase (ALT) levels in 1.9% of the study's 2510 patients and was discontinued in 0.8% of these patients (Bailey, 2000). Serum ALT is a commonly used biomarker in the detection of liver injury. Despite this indication of hepatotoxicity, TRO was marketed in January 1997 however, by November of the same year there had been 135 reports of severe hepatotoxicity and six fatalities (Gale, 2001). TRO was withdrawn from the market in March 2000 by which point there had been 60 deaths due to TRO induced liver failure and 10 patients had undergone liver transplantation. The incidence of acute liver failure among patients treated with TRO is estimated to be between 1 in 8000 and 1 in 20,000 and thus TRO induced toxicity was classified as idiosyncratic (Gale, 2001, Smith, 2003). In 1999, 50 spontaneous adverse reaction cases of TRO induced heart failure, including six fatalities, were reported by the Endocrinologic and Metabolic Drugs Advisory Committee to the FDA. The committee also noted that in a particular patient trial 4% of the test group developed peripheral oedema and one patient developed pulmonary oedema, whereas no adverse cardiovascular effects were reported in the placebo group (FDA, 1999a). Incidences of TRO induced cardiac toxicities included fluid retention leading to oedema, deterioration of pre-existing heart failure and pseudo-anaemia resulted in physicians being prohibited from prescribing TRO to T2D patients with known cardiac abnormalities (Sarafidis, 2008).

TRO was prescribed to patients on a daily oral administration regime. Clinical reports of the onset of TRO induced hepatotoxicity vary greatly in the length of

TRO therapy undertaken by the patient before liver injury was detected. In some patients TRO induced hepatotoxicity occurred after the patient had taken the drug for 2 weeks whereas in others symptoms did not become apparent till after 9 months of treatment (Graham et al., 2003). Possible mechanisms proposed for TRO induced hepatotoxicity include protein conjugation via toxic intermediates, bile salt export protein inhibition resulting in cholestasis, mitochondrial dysfunction leading to apoptosis and genetic susceptibility such as single nucleotide polymorphisms in genes involved in the metabolism and transport of TRO (Chojkier, 2005, Masubuchi, 2006). Oxidation of TRO during phase I metabolism by the enzymes CYP3A4 and CYP2C8 generates a highly electrophilic open ring intermediate. This reactive intermediate is conjugated with GSH in a reaction mediated by the enzyme GST resulting in a non-toxic metabolite that is excreted. However, it is hypothesised that accumulation of the electrophilic open ring intermediate could deplete cellular GSH levels allowing the reactive metabolite to covalently bind with cellular macromolecules resulting in toxicity (Narayanan et al., 2003). *In vitro* studies have shown that both the parent compound and its primary metabolite, a sulphate conjugate produced via metabolism of TRO by the enzyme SULT1A3, are toxic to hepatocytes (Kostrubsky et al., 2000). Polymorphisms of SULT1A3 are observed in the general population, which affect the level of enzyme activity in hepatocytes (Hildebrandt et al., 2004). These variances in SULT1A3 would cause differences in the rate of TRO to TRO-sulphate conversion between individuals and lead to accumulation of either the parent compound or its primary metabolite. In *in vitro* and *in vivo* rat models, TRO and TRO-sulphate have been shown to inhibit the bile salt export pump (BSEP) causing a significant reduction in bile acid excretion

from hepatocytes into the bile canaliculus. The TRO-sulphate metabolite has been shown to be 10 times more potent than TRO at inhibiting Bsep in rats. (Funk et al., 2001). The function of BSEP is to export bile acids and xenobiotic conjugates from hepatocytes into the bile canaliculus. Inhibition of BSEP leads to accumulation of bile acids and drug conjugates within hepatocytes causing injury via cholestasis, which can further progress into liver failure. Thus the idiosyncratic nature of TRO induced hepatotoxicity could stem from variances in SULT1A3 activity within the patient population, which could lead to accumulation of the TRO-sulphate metabolite in some individuals making them more susceptible to developing cholestatic liver injury. As with SULT1A3, there are known polymorphisms of BSEP in humans that affect the expression and subsequent activity of the transporter in hepatocytes (Meier et al., 2006). Variances in the metabolism of TRO to TRO-sulphate and in the clearance of TRO and its metabolites from the liver could make certain individuals more susceptible to TRO induced hepatotoxicity than others. There is a reported case of a patient admitted to hospital because of TRO induced hepatotoxicity who presented with hepatic cholestasis (Menon et al., 2001). The exact cause of TRO induced toxicity is still undetermined however, it is likely that toxicity occurs via a number pathways and is dependent on the patient's genetic makeup hence the idiosyncratic nature of the observed adverse reactions (Smith, 2003). TRO is one of numerous drugs that have been withdrawn from the market due to incidences of severe toxicity in the patient population.

1.3 Adverse Drug Reactions

An adverse drug reaction (ADR) is defined as a toxic and unintended response to a therapeutic compound (Edwards and Aronson, 2000). ADRs are a leading cause of patient morbidity and mortality across the world and it is estimated that 6.7% of adult hospital admissions are for patients experiencing an ADR (Pirmohamed et al., 2004). Improvements and advancements of technologies utilized to evaluate drug safety are constantly being sought to prevent ADRs such as those observed with TRO. In 2006 the FDA issued a report that emphasized the need of scientific advancement in predictive toxicology studies to enable better prediction and understanding of ADRs (FDA, 2006). Between 1994 and 2006, 38 approved drugs were withdrawn from the market by the FDA and many more were issued 'black box warnings'; these are notices that are placed on patient information leaflets warning about serious ADRs associated with use of the drug (Dykens and Will, 2007). The primary toxicological reasons for post marketing drug withdrawal are liver and cardiac toxicity based ADRs. Drugs that are withdrawn post marketing will have passed all toxicological assessment during development and their potential to cause serious ADRs only becomes apparent when large populations have been exposed. Rare drug induced toxicities that only occur in a small subset of the patient population are termed idiosyncratic. The frequency of idiosyncratic ADRs can be as little as 1 in 100,000 drug treated patients. Considering that phase III clinical trials typically consist of 1000-3000 patients, it is not surprising that the potential of a drug to cause idiosyncratic toxicity is not detected before the drug is marketed and administered to millions of patients (FDA, 2009, Daly, 2013). ADRs can present a significant danger to the health of a patient, thus the ability to detect if a drug can cause

ADRs is of utmost importance. Understanding the mechanisms of ADRs should enable better predictions to be made regarding the potential of a new drug to cause such reactions during development.

ADRs can be divided into two categories; 'Type A' reactions, which account for the majority of ADRs, are often related to the pharmacology of the drug and can usually be predicted whereas 'Type B' reactions are idiosyncratic and difficult to detect because their mechanisms are often unrelated to the pharmacology of the drug (Park et al., 1992). Individual ADRs to a drug can be governed by genetic differences between patients. The study of how genetic variances between patients affect the absorption, distribution, metabolism, excretion, efficacy and toxicity of a drug is termed pharmacogenomics (ICH, 2008). Pharmacogenomics is increasingly being utilised during drug development to evaluate if genetic variances can make some patients more susceptible to ADRs than others. To date, the FDA has issued pharmacogenomic warnings to 138 drugs, some examples are listed in Table 1.2 (FDA, 2014). Some pharmacogenomic notices are regarding drug efficacy, for example some anti-cancer drugs such as everolimus are only efficacious in patients with hormone receptor positive cancer (Baselga et al., 2012). Other warnings are for potential drug induced toxicity in patients who possess polymorphisms in Phase I metabolising enzymes. For example, patients who possess the CYP2D6*10 variant are poor metabolisers and are at increased risk of bradycardia when prescribed the beta-blocker drug metoprolol at the same dose as a normal CYP2D6 metabolisers. The increased toxicity is due to slower metabolism of metoprolol in CYP2D6 poor metabolisers resulting in several fold higher drug plasma levels and increased drug half-life (Wuttke et al., 2002). Thus polymorphisms in the CYP2D6 genes makes some

patients more susceptible than others to experiencing a 'Type A' ADR when taking metoprolol.

Third party content removed

Table 1.2 – Drugs with FDA issued pharmacogenomic warnings (FDA, 2014)

Pharmacogenomic warnings have also been issued regarding drug hypersensitivity in patients with polymorphisms in genes encoding for the immune system component major histocompatibility complex (HLA). One such example is the anti-retroviral drug Abacavir that is used in the treatment of human immunodeficiency virus infection. Patients with the HLA allele HLA-B*5701 are susceptible to hypersensitivity reactions when treated with Abacavir and can experience symptoms ranging from fever and rash to renal impairment and respiratory failure, which in some cases have resulted in death (Hewitt, 2002, Mallal et al., 2002). Genetic polymorphisms can make some patients more susceptible to ADRs, however drug induced toxicity can also occur via mechanisms involving drug-receptor interactions in on and off-target tissues.

Drug induced toxicity can occur via receptor specific mechanisms, which result from interactions between drugs and their target receptors in off-target tissues. For example, statins lower cholesterol levels by inhibiting hydroxymethylglutaryl co-enzyme A (HMG CoA) in the liver however, inhibition of HMG CoA in muscle tissue can cause muscle weakness and damage (Gotto Jr, 2006). Some drugs are non-specific and thus able to bind to multiple receptors. This can result in off-target toxicity where a drug activates a receptor that was not its intended target. The post marketing withdrawal of terfenadine was a result of such off-target toxicity. Terfenadine was originally marketed for the treatment of allergic reactions as its interaction with the H_1 receptor resulted in an antihistamine response. However, it also interacted with the cardiac potassium channel hERG, causing cardiac arrhythmias. (Sanguinetti and Tristani-Firouzi, 2006).

Some drugs are bio-activated into reactive metabolites, which if allowed to accumulate within cells can bind to cellular macromolecules and consequently lead to toxicity (Figure 1.5) (Park et al., 2010).

Third party content removed

Figure 1.5 – Bioactivation of drugs into reactive metabolites. Many drugs are bioactivated into reactive metabolites that can react with cellular macromolecules resulting in toxicity (adapted from Park et al 2010).

This mechanism has been shown to occur in paracetamol induced hepatotoxicity. Paracetamol is metabolized in the liver by the phase I metabolizing enzyme CYP2E1 into a reactive quinone metabolite, which at therapeutic doses is detoxified via conjugation with GSH. However, in cases of overdose, cellular GSH levels are depleted allowing the reactive quinone metabolite to accumulate in hepatocytes. In the absence of GSH the electrophilic metabolite covalently binds to nucleophilic cellular macromolecules such as DNA and proteins, resulting in apoptosis (Gonzalez, 2005). The binding of reactive metabolites to cellular

proteins can also induce an immunological response. Such reactions were observed at a frequency of 1 patient in 35,000, with the use of the general anaesthetic halothane (Sanderson et al., 2006). In susceptible patients, the reactive metabolite trifluoroacetyl chloride covalently bound to lysine residues of cellular proteins in the liver and caused halothane-hepatitis (Park et al., 2011). Drugs, such as TRO, which are withdrawn post-marketing due to drug induced toxicity, often cause 'Type B' idiosyncratic toxicity and the mechanisms of these ADRs are often unknown. It has been proposed that some idiosyncratic ADRs are the result of immune system mediated toxicity caused by chemically active drug metabolites. The 'Hapten' hypothesis proposes that electrophilic low molecular weight metabolites react and covalently bind with nucleophilic cellular macromolecules producing conjugates that initiate an immune response and cause hypersensitive reactions (Park et al., 1998). The 'Danger' hypothesis extends the 'Hapten' model by proposing that if the conjugate is assessed as being dangerous an immune system reaction is initiated and if the conjugate is judged as non-dangerous then an immune system reaction is not initiated and the conjugate is allowed to accumulate in the cell (Anderson and Matzinger, 2000). As the understanding of the mechanisms of ADRs advances the demand for assays to predict such toxicities during drug development increases.

1.4   Current *In Vitro* Models Used in Predictive Toxicology Studies

A variety of cell types are used as the basis of *in vitro* models in the preclinical stage of drug development to assess the potential toxicity of new drug candidates. Many of these are immortalised cancer derived cell lines or primary rodent or human tissue cells (Zucco et al., 2004). There are several issues related to the use of these cells as the basis of models used to predict potential drug

induced toxicity. Immortalised cancer derived cell lines neither represent the normal physiological nor the diseased state of an organism. There are issues relating to the availability of human primary cells as liver tissue from which cells are extracted is often acquired from biopsy samples taken during surgery or from cadavers. Heterogeneity of samples results in batch to batch variance in the cells making it difficult to compare data acquired from different experiments. Furthermore, primary cells are known to de-differentiate in culture becoming less comparable to cells *in vivo* (Wilkening and Bader, 2003).

It is anticipated that the current advances in mammalian stem cell technologies will result in the development of stem cell based models for use in compound screening, pharmacological assessment, metabolic profiling and toxicological studies in drug development (Pouton and Haynes, 2007). Embryonic stem (ES) cells possess the ability to differentiate into the three germ layers, ectoderm, mesoderm and endoderm as well as primordial germ cells. This gives rise to the potential to differentiate ES cells into most cell types (Thomson et al., 1998). Phenotypically and genotypically, differentiated ES cells are anticipated to be similar enough to adult cells *in vivo,* for them to be utilised in pharmacological and toxicological studies. The advantages of using ES cells over immortalised cell lines and primary cells, which are currently used in *in vitro* studies, are listed in Table 1.3 (McNeish, 2004).

Third party content removed

Table 1.3: Properties of cell types used in drug development (McNeish, 2004)

1.5 Embryonic Stem Cells

The definition of a stem cell is a cell that can self-renew generating exact copies of itself but can also differentiate into any cell type (Reya et al., 2001). The first ES cell lines were derived in 1981 from the inner cell mass (ICM) of mouse blastocysts (Evans and Kaufman, 1981, Martin, 1981). In 1998 the first human ES cell lines were derived from human blastocysts (Thomson et al., 1998). In mammalian fertilization zygotes undergo many rounds of division to produce blastocysts, which are composed of two distinct lineages, the trophectoderm and the ICM (Figure 1.6). ES cells isolated from the ICM are pluripotent and can differentiate into the three embryonic germ layers, mesoderm, endoderm and ectoderm (Nichols and Smith, 2011).

With mouse embryonic stem (mES) cells the efficiency of derivation initially proved to be strain dependent and the most successful isolation was from 5-7 day old blastocysts from the 129 inbred mouse strain; generating the parental E14 cell line. *In vitro*, mES cells divide every 12-15 hours and maintain a normal

and stable karyotype even when continually passaged (Wobus and Boheler, 2005).

Third party content removed

Figure 1.6 – Embryonic stem cells are derived from the inner cell mass of blastocysts. ES cells isolated from the ICM are pluripotent and can be cultured *in vitro* where they can undergo serial passage in their undifferentiated state or be prompted to differentiate into cells of the three germ layers (adapted from Wobus and Boheler, 2005).

1.5.1   Control of mES Cell Pluripotency

Mouse ES cells can be cultured *in vitro* however maintenance of their undifferentiated phenotype is not cell-autonomous. To maintain mES cells in an undifferentiated state they were initially cultured in the presence of foetal calf serum (FCS) on feeder layers consisting of mitotically inactivated mouse embryonic fibroblasts (MEFs). MEFs conditioned the media with factors that supported stem cell pluripotency, allowing the cells to self-renew without differentiating. Leukaemia inhibitory factor (LIF) was identified as the key factor secreted by MEFs, which allowed mES cells to proliferate whilst maintaining their pluripotent nature (Smith et al., 1988, Williams et al., 1988). However, without FCS, LIF alone was not sufficient enough to support undifferentiated self-renewal of mES cells, indicating that FCS also contributed key factors that were required to maintain pluripotency. Further analysis indicated that bone morphogenic

proteins (BMPs) were the critical FCS components involved in maintaining mES cell pluripotency (Ying et al., 2003). A combination of MEFs/LIF and FCS/BMPs is required to maintain mES cell self-renewal and pluripotency *in vitro* and purified recombinant LIF can replace MEFs allowing mES cells to be cultured in feeder free conditions (Hoffman and Merrill, 2007).

LIF is a glycoprotein member of the interleukin 6 (IL6) cytokine family that binds to a heterodimeric membrane protein consisting of glycoprotein 130 (gp130) and a LIF specific receptor (LIFR) (Metcalf, 2003). Binding of LIF to this heterodimer produces a trimeric complex consisting of LIF:LIFR:gp130. This then activates Jak/Stat3 and p42/p44/Mapk pathways, which control the expression of a number of downstream targets that control mES cell self-renewal (Smith, 2001). The targets of Jak/Stat3 and p42/p44/Mapk have not been fully characterized but are proposed to include c-myc, which has been shown to be involved in the maintenance if self-renewal (He et al., 2009).

Bmp4 activates members of the Smad family of transcription factors, which in turn results in activation of the inhibitor of differentiation gene family and supports ES cell self-renewal. LIF is a major factor in maintaining ES pluripotency however in the absence of LIF the wingless/integrated (Wnt) pathway can control self-renewal. Binding of the Wnt protein to the Fizzled receptor activates the Wnt pathway, which results in inhibition of glycogen-synthase kinase-3 beta allowing expression of β-catenin target genes, which promote self-renewal (Boiani and Schöler, 2005). Thus stem cell pluripotency is controlled by overlapping signal transduction pathways (Figure1.7).

Third party content removed

Figure 1.7 – Multiple signal transduction pathways are involved in maintaining mES cell pluripotency. There is crosstalk between the different signalling pathways. The LIF/Stat3 pathway promotes self-renewal through transcription of c-myc target genes and is supported by Bmp4/Smad mediated inhibition of differentiation. (Okita and Yamanaka, 2006)

In addition to extrinsic control, pluripotency of mES cells is also regulated at the transcriptional level by the transcription factors Nanog homeobox (Nanog), POU class 5 transcription factor 1 (Pou5f1 also known as Oct4) and SRY-box containing gene 2 (Sox2). (Chambers, 2004). Oct4 is a well characterized regulator of pluripotency that is expressed in all pluripotent cells both *in vivo* in mouse embryos and *in vitro* in mES cells. Lack of Oct4 *in vivo* prevents mouse embryos from developing past the blastocyst stage as without Oct4 the ICM is unable to form. *In vitro,* down regulation of Oct4 results in differentiation of mES cells and loss of pluripotency (Pan et al., 2002). Sox2 functions as a heterodimer with Oct4 and half of the pluripotency genes regulated by Oct4 are also under the transcriptional control of Sox2 (Loh et al., 2006). In the absence of LIF, forced expression of Oct4 is not enough to maintain pluripotency whereas increased expression of Nanog is. However, the ability of Nanog to support self-renewal is

dependent on functional Oct4 activity, thus regulation of mES cell self-renewal and pluripotency relies on the activity of both Oct4 and Nanog (Hoffman and Merrill, 2007). Both extrinsic and intrinsic control of pluripotency is required to inhibit differentiation and to support self-renewal of mES cells. There is no conclusive evidence on the direct link between LIF and Nanog expression though it has been shown that there is a Stat3 binding site in the Nanog 5' promoter region (Suzuki et al., 2006).

1.5.2 Differentiation of mES Cells

Pluripotency is a unique characteristic of stem cells, which under the right culture conditions allows them to differentiate into cells of the three germ layers and subsequently be directed to form a particular cell type. Cells of the ectoderm germ layer can be differentiated to give rise to cells of the brain and skin, endoderm cells can be directed into cells of the gastrointestinal tract, liver and lung and cells from the mesoderm layer can produce cells of the cardiovascular system and bone cells (Wobus and Boheler, 2005). A popular method of mES cell differentiation is through the formation of cell aggregates termed embryoid bodies (EBs) in the absence of LIF. These aggregates replicate, in part, the ICM environment found *in vivo* and help mES cells differentiate into the three germ layers (Wobus, 2001).

Differentiation can be directed towards a specific germ layer and cell type by forming and culturing EBs in medium supplemented with chemicals or protein growth factors. Retinoic acid has been shown to promote differentiation of mES cells into inhibitory, excitatory and telencephalic neurons and glia cells. Use of the growth factors sonic hedgehog, basic fibroblast growth factor and fibroblast growth factor 8 has produced dopaminergic and serotonergic neurons.

Differentiation into cardiomyocytes has been induced using a cocktail of Activin A, bone morphogenetic protein 4 and Wnt proteins (Keller, 2005). The formation of pancreatic cells requires a number of different medium compositions including EB formation using medium supplemented with Activin A and retinoic acids followed by culture in medium containing fibroblast growth factor 10 and maintenance of differentiated cells in medium supplemented with nicotinamide and fibroblast growth factor 2 (Murry and Keller, 2008).

1.5.3 Use of ES cells in Drug Development

The requirement for novel, more predictive cell based assays for the detection of drug induced toxicity lead to the formation of the UK Stem Cell Initiative in 2005. The primary focus of this government, industry and academic collaboration was to develop stem cell technologies for use in predictive toxicology studies during drug development. The ability of stem cells to differentiated into any cell type was anticipated to allow the development of better predictive cell models for use in pre-clinical drug testing (SC4SM, 2008).

The use of ES cell based assays in drug development has been exemplified by the approval granted by the European Centre for the Validation of Alternative Methods for use of the 'embryonic stem cell test' (EST). The EST was approved for use in *in vitro* embryotoxicity studies to evaluate teratogenic potential of new drug candidates (Genschow et al., 2004). The EST uses the D3 mES cell line and assess the ability of new drug candidates to inhibit spontaneous differentiation into contracting cardiomyocytes. New drug candidates are added to the differentiation medium during EB formation, EBs are seeded on day 3 of differentiation and cultures are observed for 10 days. Experimental endpoints include determination of cytotoxicity of compounds using the MTT assay,

calculating inhibition of cell growth and inhibition of differentiation. Depending on the results compounds are subsequently labelled as weakly embryotoxic, strongly embryotoxic or not embryotoxic (Scholz et al., 1999, Genschow et al., 2002). The EST illustrates the advancements being made in the utilisation of stem cell based assays in drug development. The EST is aiding a reduction and refinement in the use of animals in preclinical studies however, it has not replaced *in vivo* animal models of embryotoxicity (McNeish, 2004).

The EST is currently the only stem cell based assay used during drug development that has been approved by a regulatory authority. Other stem cell based assays are being used during toxicity testing in drug development but they are being used in addition and not in place of existing methods. The difficulty in fully integrating stem cell based models into the drug development pipeline is due to limitations of differentiation protocols, the length of time taken to generate differentiated cells and the high costs involved in generating differentiated stem cells. Many stem cell differentiation protocols last at least 20-30 days and some can take several months and protocols are labour intensive, often requiring daily cell culture maintenance. Long culture time makes it difficult for the cells to be utilised in the drug development process where the pressure is on to acquire *in vitro* results quickly in order to initiate *in vivo* studies. Furthermore, the costs of stem cell culture can be 10 times as much as the costs of culturing primary cells and immortalised cell lines (McGivern and Ebert, 2014). There is also the issue of being able to produce enough differentiated stem cells for use in drug development assays. Many protocols for stem cell differentiation are able to generate small numbers of differentiated cells whereas millions of cells are required for use in drug development assays. Furthermore, variances between

different batches of differentiated stem cells make it difficult to compare data from assays using different lots of differentiated cells. As these limitations are overcome, it is anticipated that stem cell based models will become an integral part of the *in vitro* assays utilised in drug development.

1.6 Transcriptomics

Transcriptomics is the study of RNA transcripts produced by the genome under specific conditions such as during development, disease and drug treatment (Waters and Fostel, 2004). Global mRNA profiling techniques are being increasingly utilised in risk assessment and predictive toxicology studies during the development of new drugs. By utilising *in vitro* and *in vivo* models and genome profiling techniques, such as microarray analysis, it is possible to assess global changes in gene expression in response to xenobiotic exposure; The work of consortiums such as the American Tox21 (Toxicology in the 21st Century) program is centred on this concept. Projects within Tox21 are using high-throughput screening assays, including whole genome analysis, to assess the toxicity pathways activated by 10,000 compounds. This list includes chemicals, pesticides, approved drugs, drinking water contaminants among others. Profiling toxicity induced by these agents will allow a database consisting of toxicity profiles to be built, which could be used to predict the potential toxicity of new drugs (Schmidt, 2009).

1.6.1 Microarray Technology

The advantage of using microarrays is that they allow the expression of many genes to be assessed simultaneously in one experiment. A microarray is typically a glass slide containing thousands of arrayed gene probes. Older arrays utilised

cDNA gene clones as probes, however due to problems with clone identity and perceived specificity of these arrays they have now been replaced in most experiments by a variety of microarrays that use short oligonucleotide probes (~20 to 80 bases each) (Mah et al., 2004). Two microarray platforms have been utilised within this project, one is an in-house printed version of the Mouse Exonic Evidence Based Oligonucleotide (MEEBO) oligo probe set (DeRisi et al., 1996) and the other the commercially available Illumina Mouse WG-6 v2.0 Expression Beadchip platform. Both arrays used the publically available MEEBO set, which provides 88.05% coverage of the mouse genome (Verdugo and Medrano, 2006). The in-house microarrays were two colour arrays and the Illumina microarrays were one colour arrays. With two colour microarrays, each sample, control and treated, is labelled with either a Cy3 or Cy5 fluorophore. Labelling is achieved by integrating either the Cy3 or Cy5 fluorophore into cDNA during reverse transcription of the sample mRNA. The newly synthesized cDNA-fluorophore conjugates are mixed and hybridized to the same microarray slide. Spot intensity is measured by scanning the slide at 532 nm to activate Cy3 (green) and 635 nm to activate Cy5 (red) fluorescence. The fluorescence is then detected by a photomultiplier tube. The ratio of the Cy5/Cy3 intensities of each spot relate to the level of expression of that gene in each sample. For example if the control sample is labelled with Cy3 and the treated with Cy5, a spot with ratio of Cy5/Cy3 >1 will be red in colour and is indicative of up regulation of that gene in the treated sample and a spot with a ratio <1 will be coloured green and illustrates down regulation of that gene in the treated sample (Figure 1.8).
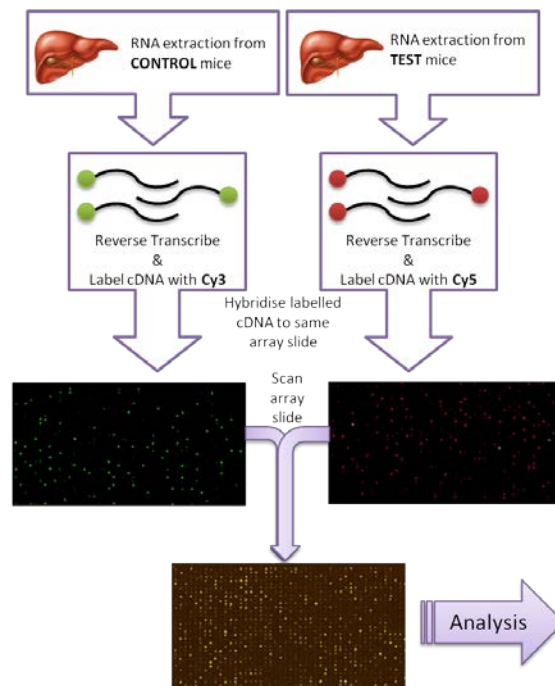
Figure 1.8 – Transcriptomic profiling using a two colour microarray.
Control RNA is labelled with Cy3 and treated RNA is labelled with Cy5, both
samples are hybridizes to the same array. Scanning of the slide gives ratio
values of the two dyes with ratios >1 indicative of up regulation and <1
indicative of down regulation for each gene.

The Illumina platform is a one colour microarray with each sample, control and

treated being labelled with a Cy3 fluorophore. As opposed to two colour arrays

where both control and test sample are hybridized to the same array, with the

Illumina platform, one sample is hybridized to each single array. The expression

of the Cy3 fluorophore is assumed to be proportional to gene expression and thus

the ratio of the Cy3 intensities of the control and treated samples indicates the

change in gene expression between the two samples. The advantage of one

colour microarrays is that each sample is hybridized to a single array whereas

with a two colour array each test sample must be co-hybridized with a control

sample and thus less control mRNA is utilised when using one colour array

systems. However the major disadvantage of one colour microarrays is that

variability between the microarrays is uncontrolled and in the event of their being a fault with the control microarray there is a loss of the remaining data in the experiment. This does not happen with a two colour system. Zhang and Gant (2008) have analysed different experimental designs and arguably the best design is two colour but with one reference sample being utilized on each slide. Thus control and test samples are hybridized against the same reference sample but the analysis is as for a one colour system. Variations in across the microarrays in the experiment are though controlled by the used of the same standard reference on each slide (Zhang and Gant, 2008).

For both the one and two sample experimental designs microarray data was processed and analysed using ArrayTrack software from the National centre for Toxicological Research at the FDA (Tong et al., 2003). To adjust for variation in the hybridisations between slides the data have to be normalised before cross array comparisons are made. This process controls for various biases from occurrences such as alterations in RNA extraction, inefficient reverse transcription or fluorophore labelling, differences in hybridization of labelled cDNA to the gene probe and variances in scanning of arrays (Smyth and Speed, 2003). Normalisation of 2 colour microarrays was done using the Lowess normalisation algorithm and for Illumina data normalisation was performed using the quantile algorithm. The principle assumption of the Lowess normalisation method is that most genes will not be differentially expressed and thus have a Log_2 ratio of 0 (Yang et al., 2002). With quantile normalisation the distribution of intensities of each probe in a set of arrays is made the same (Bolstad et al., 2003). Comparison of microarray data from normal and drug treated tissue from animals or cells

provides a list of genes that were up or down regulated by drug treatment; this list is referred to as a gene signature.

1.6.2 Toxicogenomics

It has been widely hypothesized that these gene expression signatures or profiles are highly indicative of toxicity. Furthermore is it considered that these data may allow prediction or elucidation of the pharmacological and toxicological mechanisms of new drugs in pre-clinical drug development (Lord, 2004). This area of research is classified as toxicogenomics and uses mRNA expression profiling to examine cellular, tissue and whole organism responses to xenobiotic exposure (DeCristofaro and Daniels, 2008). The principle of toxicogenomics is that compounds that have similar mechanisms of action will affect related molecular pathways and thus will induce similar gene expression changes (Blomme and Warder, 2008). By utilising microarray technologies in conjunction with toxicogenomic databases it may be possible to develop transcriptomic signatures of ADRs that may provide insight into the mechanisms of such toxicities. This implies it may be possible to develop genomic biomarkers to both recognize and predict types of toxicity associated with new drugs during preclinical studies, before further costs are endured and before the patient population is exposed. Furthermore, circulating biomarkers that can be extracted from the blood would be particularly useful as they could be obtained from animals during preclinical studies using minimally invasive procedures. During injury or toxic insult mRNAs are released from damaged cells via extracellular vesicles such as exosomes into the blood and these nucleic acids can be used as biomarkers of drug induced toxicity (Mathivanan et al., 2010). It is anticipated that mRNA biomarkers will be better indicators of specific organ toxicity than

currently used serum biomarkers such as aspartate aminotransferase (AST). AST is an FDA approved serum biomarker of toxicity however, increased levels of AST do not provide information on which specific organ is being affected by the administered drug. Increased AST levels are often indicative of liver damage but levels can also be raised when cardiac or skeletal muscle are damaged (Nathwani et al., 2005, Ozer et al., 2008).

The benefit of profiling transcriptomic data in understanding and detecting drug-induced toxicity was illustrated in a study by Bushel et al (2007). Microarray technology was used to profile changes in blood gene expression in rats exposed to subtoxic and toxic doses of acetaminophen. Comparison of array data identified 152 genes that were differentially expressed between the two dose groups. This list was further filtered to produce a gene signature of the top 35 differentially expressed genes that allowed for highly accurate (89-95%) prediction of acetaminophen induced hepatotoxicity. Furthermore, the study showed that transcriptomic data was more accurate at predicating drug induced toxicity than traditional biochemical and histopathological analysis (Bushel et al., 2007).

Advances have also been made in the search for mRNA biomarkers of reproductive toxicity. During preclinical drug development assessment of drug induced testicular toxicity from animal studies is made using analysis of testosterone, luteinizing hormone, follicle-stimulating hormone or inhibin B levels in serum or by assessment of semen count, motility and morphology. However, semen analysis can be highly variable and thus ineffective at accurately assessing testicular toxicity and changes in serum hormone levels are not always supported by changes in testicular histopathology (Buck et al., 2008). Thus, more

sensitive biomarkers of testicular toxicity are constantly being sought and work published by Pacheco et al (2012) and Champion et al (2013) indicates that mRNA biomarkers of early reproductive toxicity are detectable in sperm samples from rats exposed to known reproductive toxicants. Rats exposed to the Sertoli cell toxicants 2,5-hexanedione, the active metabolite of the gasoline constituent *n*-hexane and carbendazim, the active metabolite of Benlate fungicide, had differential expression of several sperm mRNA transcripts. The expression of four mRNA transcripts for the genes Clu, Ptgds, Sil1 and Ift81 was significantly altered in both chemical exposure groups and indicates that these transcripts could be utilised as mRNA biomarkers of testicular toxicity (Pacheco et al., 2012). Exposure of rats to a number of Sertoli cell and germ cell toxicants at various doses and time points followed by transcriptomic analysis has identified a core group of four mRNA transcripts, Abi2, Clu, Ptgds and Sod3, from which the expression of at least one transcript was significantly altered in each of the 17 test groups (Campion et al., 2013). The use of toxicogenomics to identify biomarkers of toxicity could help to predict and identify toxicity of new drug candidates during preclinical drug development.

1.7   Summary

Toxicology studies are a vital component of the drug discovery and development process. The safety of all new drugs depends on the outcomes of *in vitro* and *in vivo* studies and clinical trials. Prevalence of drug induced toxicity is a leading cause of late stage drug attrition and post-marketing drug withdrawal. These losses are financially detrimental to pharmaceutical companies and drugs that are withdrawn post-market will have caused serious and at times fatal ADRs in the patient population. To overcome these issues the development of more

predictive assays for the detection of drug induced toxicity during drug development is constantly being sought. Advancements in cell culture techniques, especially the differentiation of stem cells into any cell type in conjunction with advancing molecular technologies in the field of transcriptomics are anticipated to aid in the development of more predictive *in vitro* assays for use in toxicology studies during drug development.

1.8   Thesis Hypothesis

The hypothesis for this thesis was that transcriptomic changes in mES cell derived cardiomyocytes and hepatocytes are signatures for cardiotoxic and hepatotoxic effects of troglitazone in the mouse.

TRO was chosen as the drug to test this hypothesis because it was withdrawn from the market due to incidences of idiosyncratic toxicity, which in particular affected the liver and the heart. To test this hypothesis a number of aims were devised which correlate with each results chapter.

The aim of Chapter 3 was to develop reproducible methods for the differentiation of pluripotent E14Tg2a.4 mES cells into cardiomyocytes and hepatocytes; generating cells that could be used to evaluate TRO toxicity.

The aim of Chapter 4 was to acquire an *in vivo* transcriptomic signature of TRO induced gene changes in heart and liver tissue using a normal mouse model.

The aim of Chapter 5 was to use a T2D mouse model, one that mimicked the disease state of the patient population, to acquire an *in vivo* transcriptomic signature of TRO induced gene changes in heart and liver tissue.

The aims of Chapter 6 were to assess the transcriptional responses of mES cell derived cardiomyocytes and hepatocytes (developed in Chapter 3) to TRO, to compare these changes in gene expression with those observed in heart and

liver tissues from *in vivo* normal and diabetic mouse studies (data from Chapters 4 and 5) and to evaluate if *in vitro* gene expression changes could provide information on the mechanisms of TRO induced toxicity.

Chapter 2: Materials and Methods

2.1 Materials

Troglitazone was sourced from the GSK compound bank (The Frythe, Welwyn, Hertfordshire). Male strain 129P2/OlaHsd mice and male and female strain C57 BL/6J mice, were sourced from Charles River (Wilmington, Massachusetts, USA). Mouse standard chow and high fat diet were purchased from Test Diet Ltd (London, UK). Cell culture media and supplements were purchased from Invitrogen (Paisley, UK). Cell culture plates and dishes were purchased from Grenier Bio-One (Stonehouse, UK). All other chemicals were sourced from Sigma (Poole, UK) or Fisher Scientific (Loughborough, UK) unless otherwise stated.

2.2 General Methods

2.2.1 RNA Isolation from Frozen Tissue

RNA was extracted from tissue samples that had been flash frozen in liquid nitrogen and stored at -80°C until use. To minimise thawing of tissues a cutting block was placed over dry ice and sections (max 100 mg) were cut from the frozen tissue using a scalpel. Excised tissue samples were added to 2 ml Eppendorf tubes containing TRI reagent (1 ml) and homogenized using an Ultra Turrax T8 homogenizer for 40 seconds. Samples were incubated at room temperature (RT) for 5 minutes following which 1-bromo-3-chloro-propane (200 µl) was added. Samples were vortexed for 15 seconds, incubated at RT for 3 minutes and then centrifuged at 4°C, 12000 revolutions per minute (rpm) for 14 minutes. The upper aqueous layer (600 µl) was pipetted into a new 2 ml Eppendorf tube, isopropanol (600 µl) was added following which samples were mixed thoroughly by pipetting. Samples were incubated at RT for 10 minutes and then centrifuged at 4°C, 12000

rpm for 10 minutes. The supernatant was discarded and remaining pellet was washed with ice cold ethanol (75% v/v, 1 ml) and centrifuged at $4^{\circ}C$, 12000 rpm for 5 minutes. Again the supernatant was removed and pellet was washed with ice cold ethanol (75% v/v, 500 µl) and centrifuged at $4^{\circ}C$, 12000 rpm for 5 minutes. All traces of ethanol were removed and RNA pellets were dried using a Savant Speed Vac on a medium heat setting. Dried pellets were resuspended in RNase free water (50 µl) water and stored at $-80^{\circ}C$ until use.

2.2.2 RNA Isolation from Cultured Cells

RNA was extracted from cultured cells using Qiagen miRNeasy Mini Kits as according to manufacturer's guidelines.

2.2.2.1 Preparation of Cultures of Attached cells

Culture medium was aspirated, cells were washed with phosphate buffered saline (PBS) (138 mM NaCl, 8.06 mM Na_2HPO_4, 2.67 mM KCl, 1.47 mM KH_2PO_4 final concentration, pH 7.4) and QIAzol Lysis Reagent (700 µl) was added directly onto the cells. Cells were detached from the culture plate using a cell scraper and the cell/lysis reagent mixture was pipetted into 2 ml Eppendorf tubes.

2.2.2.2 Preparation of Cultures of Embryoid Bodies in Suspension

Medium containing suspended embryoid bodies (EBs) was gently pipetted into a 15 ml conical Falcon tube. Samples were left at RT for 1 minute to allow EBs to sink to the bottom of the tube under gravity. Medium was pipetted off taking care not to disturb the EBs. PBS (5 ml) was added and EBs were left for 1 minute to allow them to settle. PBS was gently removed and EBs were washed again with PBS (5 ml). PBS was removed and QIAzol Lysis Reagent (700 µl) was added to the tube. The EBs/lysis reagent mixture was pipetted into 2 ml Eppendorf tubes.

2.2.2.3 RNA Isolation from Cells and Embryoid Bodies in Lysis Reagent

RNA extraction from cells and EBs in lysis reagent was performed in the same manner. To the 2 ml Eppendorf tubes containing the cell/lysis reagent mixtures, 1-bromo-3-chloro-propane (140 µl) was added and samples were centrifuged 4°C, 12000 rpm for 15 minutes. The upper aqueous layer was transferred into a new 2 ml Eppendorf tube, ethanol was added (100%, 1.5 volumes of aqueous layer) and samples were mixed by pipetting and transferred into RNeasy Mini spin columns. Samples were centrifuged for 15 seconds and the flow-through was discarded. Columns were washed once with buffer RWT (700 µl) and twice with buffer RPE (500 µl). To elute the RNA, RNeasy Mini spin columns were placed into new 2 ml Eppendorf tubes, RNase free water (50 µl) was pipetted directly onto the column membrane, samples were incubated at RT from 1 minute and then centrifuged at 10000 rpm for 1 minute. Eluted RNA was stored at -80°C until use.

2.2.3 Nanodrop Assessment of RNA Concentration and Quality

RNA concentration and quality was measured using a Nanodrop 2000 spectrophotometer. Nanodrop software was opened, the nucleic acid measurement program was selected and when prompted RNase free water (1 µl) was loaded onto the instrument pedestal and the arm was lowered. After initialization of the instrument the RNA-40 sample type setting was selected and the instrument was blanked using the previously loaded water sample. The instrument arm was lifted and the water sample was removed from the pedestal and arm using lint free tissue. A sample (1 µl) of the RNA to be assessed was loaded onto the instrument and its concentration and quality were measured and noted. Each RNA sample was assessed in the same manner with the instrument

pedestal and arm being cleaned between each reading. The RNA concentration was noted in µg/µl and the quality was assessed by the ratio of absorbance at wavelengths 260 and 280 nm. Samples with 260/280 ratios of ~2 were considered to be of good quality.

2.2.4 Bioanalyzer Assessment of RNA Integrity for Microarrays

RNA integrity was assessed using the Agilent 2100 Bioanalyzer micro-fluidics based platform and the RNA Nano 6000 LabChip kit, as according to manufacturer's instructions. Briefly, a LabChip kit was removed from the fridge and left to equilibrate at RT for 30 minutes. Filtered gel matrix (65 µl) and fluorescent RNA intercalating dye (1 µl) were added to a 0.5 ml microfuge tube, mixed by vortex and centrifuged at RT, 14000 rpm for 10 minutes. The Gel/dye mix (9 µl) was pipetted into to three specific wells on the LabChip and the RNA 6000 Nano marker (5 µl) was added to each of the 12 sample wells and the ladder well. RNA samples (1 µl) of concentrations between 5 to 500 ng/µl (RNA concentrations were measured using the Nanodrop 2000 spectrophotometer) were added to each of the 12 sample wells. The LabChip was placed on a vortex for 60 seconds at 2400 rpm and loaded onto the Bioanalyzer within 5 minutes. The eukaryote total RNA assay program was loaded and the run was started. The Agilent 2100 Bioanalyzer used electrophoretic separation to separate RNA samples based on their molecular weight. The fluorescent dye intercalated with the separated RNA allowing these complexes to be detected by laser induced fluorescence. RNA integrity was determined by RIN (RNA Integrity Number) analysis, which was calculated from the ratio of the areas of the ribosomal 18S and 28S regions compared with the total area under the curve. Each sample was scored on RIN scale of 1 – 10, with a score of 1 signifying a highly degraded RNA

sample and a score of 10 identifying a highly intact sample. RNA samples with a RIN score ≥8 were used in microarray experiments.

2.2.5 In-house Printed Mouse Whole Genome Microarrays

2.2.5.1 Printing Microarray Slides

Two colour microarrays were printed in-house by Dr Gant. The Mouse Exonic Evidence Based Oligonucleotide (MEEBO) set (Invitrogen, Paisley, UK) was printed onto 1 x 3 inch aldehyde and poly-l-lysine coated glass slides (Genetix, Wokingham, UK) using the ArrayJet Ultra-Marathon Arrayer (Edinburgh, Scotland). The MEEBO set contained a total of 38,467 oligos covering exonic, alternatively spliced, non-coding RNA, mitochondrial and murine viral gene probes as well as negative and positive controls. The probes had a 5' amino modification and were designed to minimise cross-hybridisation and secondary structure. The whole MEEBO probe set was printed across two glass slides thus one array consisted of an A and B array slide.

2.2.5.2 Preparation of Microarray Slides and Coverslips for Use

Prior to use, in-house printed microarray slides were prepared using a three step wash process. Slides were washed with shaking in sodium dodecyl sulphate (SDS) (0.2% w/v) for 2 minutes followed by two washes in water, each for 2 minutes. Slides were quickly transferred to a centrifuge and dried by spinning the slides at RT, 1000 rpm for 4 minutes. Dried slides were stored in protective cases and kept in the dark until use. Coverslips were washed with shaking in SDS (1% w/v) for 30 minutes followed by five washes in water, each for 5 minutes. Coverslips were dried in an oven at 42°C overnight and stored in sealed containers until use.

2.2.5.3 Sample Preparation and Array Hybridisation

Sample preparation was performed using the Agilent Low Input Quick AMP Two Colour Labelling Kit with amendments to the manufacturer's protocol.

2.2.5.3.1 cDNA Synthesis

RNA samples were diluted in RNase free water to give a concentration of 200 ng in 3.5 µl water. The T7 promoter primer master mix was prepared using T7 Promoter Primer (0.8 µl per reaction) and nuclease free water (1 µl per reaction) and 1.8 µl of the primer mix was added to each 0.25 ml microfuge tube containing the diluted RNA. Samples were mixed by pipetting and incubated at 65°C for 10 minutes and then placed on ice for 5 minutes. The cDNA master mix was prepared using 5X first strand buffer (2 µl per reaction), 0.1 M DTT (1 µl per reaction), 10 mM dNTP (0.5 µl per reaction) and AffinityScript RNase Block Mix (1.2 µl per reaction). To each sample tube 4.7 µl of the cDNA master mix was added, samples were mixed by pipetting and incubated at 40°C for 2 hours then at 70°C for 15 minutes and then placed on ice for 5 minutes.

2.2.5.3.2 cRNA Synthesis and Amplification

Two lots of the transcription master mix were prepared using nuclease free water (0.75 µl per reaction), 5X transcription buffer (3.2 µl per reaction), 0.1 M DTT (0.6 µl per reaction), NTP mix (1 µl per reaction) and T7 RNA polymerase blend (0.21 µl per reaction). Cyanine 3-CTP (0.24 µl per reaction) was added to one lot of the transcription master mix and Cyanine 5-CTP (0.24 µl per reaction) was added to the other. To each control cDNA sample 6 µl of the Cyanine 3-CTP transcription mix was added and to each test cDNA sample 6 µl of the Cyanine 5-CTP transcription mix was added. Samples were mixed by pipetting and incubated at 40°C for 2 hours and then placed on ice for 5 minutes.

2.2.5.3.3 cRNA Purification

Amplified cRNA samples were purified using Qiagen RNeasy mini spin columns. To each cRNA sample (of volume 16 µl), nuclease free water (84 µl), buffer RLT (350 µl) and ethanol (100%, 250 µl) were added in order and samples were mixed by pipetting. Samples were pipetted into RNeasy mini columns placed in 2 ml collection tubes and centrifuged at 4°C, 13000 rpm for 30 seconds. The flow-through was discarded, buffer RPE (500 µl) was added to each column and samples were centrifuged at 4°C, 13000 rpm for 30 seconds. Again the flow-through was discarded, buffer RPE (500 µl) was added to each column and samples were centrifuged at 4°C, 13000 rpm for 30 seconds. To elute the purified cRNA sample, columns were placed into new 1.5 ml collection tubes, RNase free waster (14 µl) was pipetted directly onto the column membranes, samples were incubated at RT for 1 minute and then centrifuged at 4°C, 13000 rpm for 30 seconds. The eluted purified cRNA was kept on ice.

2.2.5.3.4 Quantification of Purified cRNA

Purified cRNA samples were quantified using the Nanodrop 2000 spectrophotometer and the microarray measurement program. The instrument was initialised and blanked using nuclease free water and the RNA-40 sample type setting was selected. An aliquot (1 µl) of each cRNA sample was used to measure the cyanine-3 (Cy3) or cyanine-5 (Cy5) dye concentration (pmol/µl), the RNA absorbance ratio (260 nm/280nm) and the cRNA concentration (ng/µl). The cRNA yield and dye activity were calculated for each control and test sample and compared to the recommended values listed in the Agilent Low Input Quick AMP Two Colour Labelling kit protocol. Only samples meeting the cRNA yield and dye activity requirements were used, for failed samples cRNA was prepared again.

2.2.5.3.5 Fragmentation of cRNA

Corresponding control and test cRNA samples were combined and dried using a Savant Speed Vac on a medium heat setting till the volume of each combined sample was 9 µl. The Ambion RNA fragmentation reagent kit was used to fragment cRNA samples. To each combined control and test sample fragment reagent (1 µl) was added and samples were incubated at 70°C for 15 minutes following which stop solution (1 µl) was added and sampled were placed on ice.

2.2.5.3.6 Array Hybridisation

Nuclease free water (29 µl), yeast tRNA (1 µl) and hybridisation buffer (40 µl) were added to each combined control and test reaction and samples were incubated at 100°C for 5 minutes and then held at 42°C until they could be loaded onto array slides. Microarray slides and cover slips were prepared as stated in section 2.2.5.2. Each reaction was hybridised across two array slides, onto which the whole MEEBO set had been printed. Coverslips were placed over the printed A and B slides and half of each sample reaction (40 µl) was pipetted along the coverslip edge allowing it to be drawn across the array by capillary action. Slides were placed into a Genetix hybridisation chamber and incubated at 42°C for 18 hours.

2.2.5.4 Post-hybridisation Washing of Microarrays

Array slides were washed in three different buffers that were prepared using ultra-pure water (1 L). The first buffer contained SDS (0.03%) and saline sodium citrate (SSC) (1x), the second contained SSC (0.2x) and the third contained SSC (0.05x). Slides were washed in each buffer on an orbital shaker for 5 minutes. After the third wash, slides were quickly transferred to a centrifuge and dried by

spinning at RT, 1000 rpm for 4 minutes. Slides were transferred into carry cases, which shielded them from light and were scanned within a few hours.

2.2.5.5 Scanning of In-house Printed Microarrays

Microarrays were scanned using the laser based Axon 4200A scanner with GenePix software version 6.0. Arrays were scanned with laser beams at 532 nm to excite the Cy3 dye and 647 nm to excite the Cy5 dye, with laser intensity set at 80%. The light emitted from the excited cyanine dyes was collected and amplified by the photomultiplier tube and converted into a digital image. Array scans were saved as TIFF image files. A GenePix Array List (GAL) file was overlaid onto each array image, this contained the position and identity of each probe on the array. The GAL file was auto-aligned to the spots on the array and each array was reviewed by eye to exclude any artefacts that had falsely been identified as array probes. The sum of all the pixel intensities of each identified probe and the array background was calculated and saved as a GenePix text file (GPR file).

2.2.5.6 Data Analysis of In-house Printed Microarrays

The raw array results saved within the GPR files contained the signal intensities for the green (532 nm) and red channels (647 nm) for each spot on the array. The ratio of the green to red channel for a particular probe identified the expression of that gene in the control sample compared with the test sample. GPR files were processed and analysed using ArrayTrack software from the National centre for Toxicological Research at the FDA (Tong et al., 2003). The raw data files were normalised using the locally weighted polynomial regression (Lowess) algorithm in ArrayTrack to account for labelling variances between the Cy3 and Cy5 dyes. The principle assumption of the Lowess normalisation method

is that most genes will not be differentially expressed and thus have a Log_2 ratio of 0 (Yang et al., 2002). Normalised data were statistically analysed using the Welch t-test, which assumes unequal variance between control and test groups.

2.2.6 Illumina MouseWG-6 v2.0 Expression BeadChip Microarrays

The one-colour Illumina MouseWG-6 v2.0 expression BeadChip microarray platform contained 45,200 probes that had been derived from the National Center for Biotechnology Information (NCBI) Reference Sequence database build 36 release 22 and the MEEBO set.

2.2.6.1 Sample Preparation and Array Hybridisation

Sample preparation was performed using the Ambion Illumina TotalPrep RNA Amplification kit as according to the manufacturer's protocol.

2.2.6.1.1 Reverse Transcription to Synthesise First Strand cDNA

RNA samples were diluted in RNase free water to give a concentration of 500 ng in 11 µl water. The reverse transcription master mix was prepared using T7 Oligo (dT) Primer (1 µl), 10X first strand buffer (2 µl), dNTP mix (4 µl), RNase script inhibitor (1 µl) and ArrayScript (1 µl) and added to each diluted RNA sample. Samples were mixed by pipetting and incubated at 42°C for 2 hours and then placed on ice.

2.2.6.1.2 Second Strand cDNA Synthesis

The second strand master mix was prepared using nuclease free water (63 µl), 10X second strand buffer (10 µl), dNTP mix (4 µl), DNA polymerase (2 µl) and RNase H (1 µl) and was added to each reaction. Samples were mixed by pipetting and incubated at 16°C for 2 hours and then placed on ice.

2.2.6.1.3 Purification of cDNA

To each reaction, binding buffer (250 µl) was added, samples were mixed by pipetting and transferred into a cDNA filter column. Samples were centrifuged at 10000 rpm for 1 minute and the flow-through was discarded. Wash buffer (500 µl) was added to each column and again samples were centrifuged at 10000 rpm for 1 minute and the flow-through was discarded. The cDNA filter column was transferred into a 2 ml collection tube, nuclease free water (55°C, 20 µl) was pipetted directly onto the column membrane. Samples were incubated at RT for 2 minutes and then centrifuged at 10000 rpm for 1 minute. The elute was transferred from the collection tube into a 0.25 ml microfuge tube.

2.2.6.1.4 *In Vitro* Transcription to Synthesize cRNA

The *in vitro* transcription master mix was prepared using T7 10X reaction buffer (2.5 µl), T7 enzyme mix (2.5 µl) and Biotin-NTP mix (2.5 µl) and added to each purified cDNA sample. Samples were mixed by vortex and incubated at 48°C for 14 hours, reactions were stopped by adding nuclease free water (75 µl).

2.2.6.1.5 Purification of cRNA

To each reaction, cRNA binding buffer (350 µl) and ethanol (100%, 250 µl) were added and samples were mixed by pipetting up and down three times. Samples were transferred into cRNA filter columns and centrifuged at 10000 rpm for 1 minute. The flow-through was discarded, wash buffer (650 µl) was added to each column and samples were centrifuged at 10000 rpm for 1 minute. Columns were placed into 2 ml collection tubes, nuclease free water (55°C, 200 µl) was pipetted directly onto the column filter and samples were incubated at 55°C for 10 minutes. To elute the purified cRNA, samples were centrifuged at 10000 rpm for 1.5 minutes.

2.2.6.1.6 Quantification of Purified cRNA

Purified cRNA samples were quantified using the Nanodrop 2000 spectrophotometer and the nucleic acid measurement program. The instrument was initialised and blanked using nuclease free water and the RNA-40 sample type setting was selected. An aliquot (1 µl) of each sample was used to measure the cRNA concentration (ng/µl). Analysis of the size distribution of the purified cRNA was performed using the Agilent 2100 Bioanalyzer and the RNA Nano 6000 LabChips using the same protocol as outlined in section 2.2.4.

2.2.6.1.7 BeadChip Array Hybridisation

The Illumina BeadArray equipment within the Genomics Department at the University of Leicester was used to hybridise and process Illumina one-colour microarrays. The Illumina MouseWG-6 v2.0 Expression BeadChip microarrays contained six independent arrays on each slide. For each array, 1.5 µg of total cRNA in 10 µl of nuclease free water was pipetted into 0.5 ml microfuge tubes and incubated at 65°C for 5 minutes. To each sample, hybridisation buffer (20 µl) was added, samples were mixed by pipetting and loaded onto the arrays. Array slides were loaded into Illumina hybridisation chambers and incubated in an Illumina hybridisation oven at 58°C, with a rocker speed of 5 for 18 hours.

2.2.6.2 Washing of BeadChip Microarrays

Array slides were submerged into wash buffer E1BC and the loading gaskets covering the arrays were peeled off using tweezers. The arrays were racked and transferred into a Hybex water bath containing high temperature wash buffer that had been heated to 55°C. Arrays were submerged in the heated buffer for 10 minutes. Arrays then underwent three RT washes on an orbital shaker in wash buffer E1BC for 5 minutes then in ethanol (100%) for 10 minutes and then in wash

buffer E1BC again for 2 minutes. Arrays were removed from the washing racks and placed horizontally into wash trays. Block E1 buffer (4 ml) was pipetted over each arrays slide, completely covering all 6 arrays on each slide and placed on a rocking platform for 10 minutes. To prepare for signal detection a 1:1000 solution of Cy3-Streptavidin in block E1 buffer was prepared. Array slides were transferred into new wash trays, covered with the Cy3-Streptavidin/block E1 buffer solution and placed on a rocking platform for 10 minutes. Arrays were then racked and washed at RT in buffer E1BC on an orbital shaker for 5 minutes. Arrays slides were dried by centrifugation at 1400 rpm for 4 minutes and then transferred into protective cases.

2.2.6.3 Scanning and Analysis of BeadChip Microarrays

One-colour Illumina MouseWG-6 v2.0 expression BeadChip microarrays were scanned using the Illumina BeadArray Reader. Arrays were scanned with a laser beam at 532 nm to excite the Cy3 dye with laser intensity set at 80%. Array scans were saved as TIFF image files and raw spot intensities were saved as Illumina intensity data files (IDAT). IDAT files were imported into GenomeStudio analysis software to check array quality and the gene intensity values were exported as text files. These raw data files were imported into ArrayTrack and normalised using the quantile algorithm, which the distribution of intensities of each probe in a set of arrays is made the same (Bolstad et al., 2003). Normalised data were statistically analysed using the Welch t-test, which assumes unequal variance between control and test groups.

2.2.7 Quantitative Real Time Polymerase Chain Reactions

Quantitative real time polymerase reactions (RT-PCR) were used to assess changes in gene expression between control and test samples.

2.2.7.1 Primers

Forward and reverse primer sequences were obtained from the Harvard Primer Bank (Appendix A1) with the exception of the primer pair for Cyp3a11, which was designed using Primer Express software and the sequence was checked using the NCBI Primer Blast tool (Appendix B1) (Wang and Seed, 2003, Koressaar and Remm, 2007, Spandidos et al., 2008, Spandidos et al., 2010). Primers were ordered as desalted from Sigma, resuspended in nuclease free water. Gapdh was validated as an endogenous housekeeping gene with minimal variability between all control and test samples (Appendix Two).

2.2.7.2 RT-Protocol

Single strand cDNA synthesis was performed using the High Capacity RNA to cDNA kit (Applied Biosystems, UK) as according to manufacturer's protocol. Briefly, 2 µg RNA (in a maximum volume of 9µl), reaction buffer (10 µl), reverse transcription enzyme mix (1 µl), nuclease free water (to give a final reaction volume of 20 µl) were mixed together in a 0.25 ml microfuge tube. Reaction mixtures were incubated in a thermal cycler at 37°C for 60 minutes, 95°C for 5 minutes and then kept at 4°C until use (cDNA was prepared fresh for each RT-PCR reaction and was not kept for longer than 1 hour at 4°C). Concentration of cDNA was measured using the Nanodrop 2000 spectrophotometer. Reaction mixtures for RT-PCR were composed of SYBR® Green Fast Master Mix (final concentration 1x), single strand cDNA (100 ng), forward and reverse primers (1 µl each) and nuclease free water (to make a final reaction volume of 10 µl). Reaction mixtures were pipetted into MicroAmp Optical 96-well plates (Life Technologies, Paisley, UK) and sealed with transparent PCR plate film. Plates were centrifuged at RT, 1000 rpm for 2 minutes and reactions were run using ABI

7500 Fast Real-Time PCR Machine using default thermal cycling conditions for comparative delta-delta Ct (ΔΔCt) and melt curve analysis. Each cDNA sample and test gene was assayed in triplicate and the mean of the three Ct values was used in calculating gene expression changes. Expression (Ct values) of target genes for each sample was normalized against expression of Gapdh (endogenous housekeeping gene) and ΔΔCt of treated samples against control were used to calculate $\log_2$ fold changes in gene expression. Statistical analysis was performed using GraphPad Prism software (GraphPad, San Diego, USA).

2.3 Mouse Embryonic Stem Cell Culture Protocols

The E14Tg2a.4 mouse embryonic stem (mES) cell line was sourced from the Mutant Mouse Regional Resource Center (University of California, Davis, USA). The cell line was originally derived from the 129P2/OlaHsd mouse strain and had been adapted for growth in feeder-free conditions.

2.3.1 Production of Leukaemia Inhibitory Factor

Mouse Leukaemia Inhibitory Factor (LIF) was purified from an *Escherichia coli* (*E. coli*) culture transfected with the construct pGEX-2T-MLIF. Glycerol stock of JM109 cells, a strain of chemically competent *E.coli* cells, carrying the LIF vector was kindly provided by Dr Shaun Cowley of the Department of Biochemistry at the University of Leicester.

2.3.1.1 Synthesis of LIF

2.3.1.1.1 Growing Cultures of Transformed JM109 Bacteria

Liquid broth medium (LB) and agar plates were prepared with ampicillin (50 µg/ml) and stored at 4ºC until use. An aliquot of the glycerol stock of JM109 cells

transformed with the LIF vector was thawed and streaked across an agar plate. Plates were incubated at 37°C overnight to generate colonies. Four bacterial colonies were selected from the plates, inoculated in LB (1 ml) and incubated with shaking (250 rpm) at 37°C for 8 hours. Cultures were diluted with LB (50 ml) and incubated with shaking (250 rpm) at 37°C overnight.

2.3.1.1.2 Cell Lysis

Cultures were inoculated with LB (500 ml) and incubated with shaking (200 rpm) at 37°C for 2 hours. Isopropyl β-D-1thiogalactopyranoside (0.1 M, 500 µl) was added to the culture and it was incubated with shaking (200 rpm) at 37°C for 3 hours. Cultures were centrifuged at 4°C, 3600 rpm for 15 minutes; the supernatant was discarded and the cell pellet was resuspended in 5 ml of MTPBS buffer (150 mM NaCl, 16 mM Na_2HPO_4, 4 mM NaH_2PO_4 final concentration, pH 7.3). The cell suspension was placed on ice and sonicated for 4 minutes in total consisting of 8 cycles of 15 seconds pulse then 15 seconds rest. Triton X-100 (10%) was prepared in MTPBS buffer, 600 µl was added to the sonicated cell suspension. The mixture was incubated on ice for 5 minutes, then centrifuged at 4°C, 3800 rpm for 10 minutes after which the cell suspension was decanted and kept on ice.

2.3.1.1.3 Binding of Glutathione-LIF to Glutathione-Sepharose Beads

An aliquot (4 ml) of Glutathione-Sepharose bead suspension (GE Healthcare, Buckinghamshire, UK) was centrifuged at 4°C, 2500 rpm for 2 minutes. The supernatant was discarded and the beads were resuspended in MTPBS (20 ml) and centrifuged at 4°C, 2500 rpm for 2 minutes; this was repeated twice more. After the beads were centrifuged for the third time they were resuspended in MTPBS (4 ml, 4°C). The beads were added to the cell suspension and the

mixture was placed on a rotating disk (speed 50) in a cold room (4°C) and mixed for 2 hours. The cell suspension and beads were layered on top of a 20% sucrose solution (20 ml) and centrifuged at RT, 2500 rpm for 5 minutes. The supernatant was discarded and the beads were washed in 10 ml of wash buffer 1 (1 % Triton X-100 in MTPBS) and then centrifuged at RT, 2500 rpm for 5 minutes. The supernatant was discarded and the beads were washed in 10 ml wash buffer 2 (50 mM Tris pH8.5 and 150 mM NaCl in H_2O) and centrifuged at RT, 2500 rpm for 5 minutes. Again the supernatant was discarded and the beads were washed in 10 ml elution buffer (50 mM Tris pH 8.5, 150 mM NaCl and 2.5 mM $CaCl_2$ in H_2O) and centrifuged at RT, 2500 rpm for 5 minutes. The supernatant was discarded and the beads were resuspended in elution buffer (3 ml).

2.3.1.1.4 Thrombin Digestion

An aliquot (300 µl) of thrombin (500 U resuspended in 450 µl elution buffer) was added to the bead suspension and incubated with shaking at RT for 6 hours. After which the suspension was placed on a rotating disc and incubated at 4°C overnight. The bead suspension was centrifuged at 4°C, 3800 rpm for 5 minutes after which the supernatant was decanted and centrifuged again at 4°C, 3800 rpm for 5 minutes to remove any residual beads. LIF (the supernatant) was decanted, and filter sterilised through a 0.2 µm filter in a cell culture hood and stored as 500 µl aliquots in 1.5 ml cryo tubes at -80°C until use.

2.3.1.2 Identification of Purified Protein from an SDS-PAGE Gel by Mass Spectrometry

The purified protein, commercially available LIF (Millipore, Watford, UK) and LIF synthesised by another research laboratory at the University of Leicester using the same protocol (sourced LIF), were compared using one dimensional sodium

dodecyl sulphate – polyacrylamide gel electrophoresis (SDS-PAGE). Samples were separated using a 10% SDS-PAGE gel and a Tris/Glycine buffer system. Gel casting equipment was set up, filled with water to check for any leaks and when the equipment seals proved to be air tight the water was removed and the equipment was dried. Resolving gel solution (5 ml) was prepared using H_2O (2 ml), 30% w/v acrylamide mix (1.65 ml), 1.5 M Tris pH 8.8 (1.25 ml), 10% w/v SDS (50 µl), 10% w/v ammonium persulphate (APS) (50 µl) and tetramethylethylenediamine (TEMED) (3.5 µl) and poured into the gel casting equipment. It was covered with isopropanol and left to set. Once the gel had set the isopropanol was poured off and the gel was rinsed with water then left to air dry. Stacking gel solution (1 ml) was prepared using H_2O (700 µl), 30% w/v acrylamide mix (165 µl), 1 M Tris pH 6.8 (125 µl), 10% w/v SDS (10 µl), 10% w/v APS (10 µl) and TEMED (2 µl), it was poured on top of the set resolving gel and a comb was inserted to produce 6 sample loading lanes. Stock solution of running buffer (10X) consisting of 25 mM Tris base, 250 mM glycine and 0.1% w/v SDS was prepared and diluted 1:10 in water to produce a working solution. The 1X running buffer was poured over the gel and a voltage of 100 volts (V) was passed through the gel for 30 minutes. Sample buffer (2X) was prepared to give final concentrations of 100 mM Tris-hydrochloride pH 6.8, 25% w/v glycerol, 2% w/v SDS and 0.01% w/v bromophenol blue. Sample buffer (10 µl) was mixed with 10 µl of each of the three LIF samples (purified, commercial and sourced) and the protein marker. Each prepared sample buffer/LIF sample (20 µl) was added to the sample loading lanes and a voltage of 150 V was passed through the gel until the blue bands neared the bottom of the gel. The gel was placed into a staining dish, covered with Coomassie blue stain and placed on an orbital shaker for 30

minutes. Coomassie blue stain was poured off and the gel was covered with destaining solution (40% methanol and 10% acetic acid in H_2O) and placed on an orbital shaker. The destaining solution was replaced every 10 minutes for 1 hour. The gel was imaged and then transferred into a storage container containing water and placed in the fridge for storage. The protein band corresponding to the purified LIF was given to Rebekah Jukes-Jones of the MRC Toxicology Unit's Proteomics Group for mass spectrometry based identification of the protein. This was to confirm that the purified protein was murine LIF.

2.3.1.3 Protein Assay to Determine Concentration of LIF

The concentration of in-house purified solubilized LIF was determined using the Bio-Rad protein assay (Bio-Rad Laboratories Ltd, Hertfordshire, UK), which is based on the protein quantitation assay as described by (Bradford, 1976). Bovine serum albumin (BSA) standards of concentration 0.1, 0.25, 0.50, 0.75 and 1 mg/ml were prepared using elution buffer. Samples (20 µl) of each BSA standard and LIF were prepared in triplicate by diluting each sample in Bio-Rad dye reagent (980 µl) and mixing by pipetting. Samples were incubated at RT for 5 minutes and their absorbance at 595 nm was read using the Eppendorf BioPhotometer Plus spectrophotometer. The average absorbance of the triplicate samples was taken as the final sample reading. The measurements from the BSA standards were used to produce a standard curve and this was used to calculate the relative absorbance of LIF.

2.3.2 LIF Potency Assay

E14Tg2a.4 mES cells were cultured in varying concentrations of in-house synthesised LIF to assess its potency for promoting mES cell proliferation. Six aliquots of cell culture medium was prepared as stated in section 2.3.3.2 but

without the addition of LIF. To each of the aliquots LIF was added at concentrations of 0, 250, 500, 1000, 1500, 2000 units/ml. Cells were seeded at a density of 25000 cells/ml into 6-well plates in each of the six different LIF media. Cells were imaged 2 hours and 26 hours after seeding using a Leica light microscope and a 10x magnification lens. Images were compared to observe the effect of varying LIF concentrations on cell proliferation.

2.3.3 Media and Reagents Used For Culturing E14Tg2a.4 mES Cells

2.3.3.1 Preparing Gelatin Coated Tissue Culture Vessles

Cell culture grade bovine gelatin (2% in H_2O) was diluted in sterile PBS to produce a 0.1% gelatin solution. Tissue culture dishes and plates were coated with gelatin solution (0.1%) and incubated at RT for at least 1 hour prior to use. Gelatin was removed immediately before use and medium was pipetted into the plates before the gelatin coating dried out.

2.3.3.2 Medium for Seeding and Culturing Undifferentiated E14Tg2a.4 mES Cells

Maintenance medium used to routinely culture pluripotent mES cells consisted of Glasgow's minimal essential medium (GMEM) supplemented with foetal calf serum (FCS) (1X), l-glutamine (1X), sodium pyruvate (1X), non-essential amino acids (1X), β-mercaptoethanol (0.1 mM) and in-house synthesised LIF (131 µl/500 ml medium). Maintenance medium was stored at 4°C and prior to use it was aliquoted and warmed to 37°C. Cell maintenance medium was changed daily during routine culture of E14Tg2.4 mES cells.

2.3.3.3 Reagents for Passaging E14Tg2a.4 mES Cells

E14Tg2a.4 mES cells were detached from cell culture vessels during passage using 0.25 % trypsin-EDTA (1X) with phenol red warmed to 37°C. The volume of trypsin used was a third of the culture medium volume for that cell culture vessel.

2.3.3.4 Medium for Freezing of E14Tg2a.4 mES Cells

Medium used to preserve E14Tg2a.4 mES cells during freezing was produced by supplementing maintenance medium (as described in section 2.3.3.2) with 20% FCS and 20% dimethyl sulphoxide (DMSO).

2.3.4 Routine Culture of Undifferentiated E14Tg2a.4 mES Cells

2.3.4.1 Thawing of E14Tg2a.4 mES Cells

Prior to thawing of E14Tg2a.4 mES cells, a 6-well plate was coated with gelatin (as described in section 2.3.3.1). One cryo vial of E14Tg2a.4 cells was thawed by submerging the lower half of the vial in a water bath set to 37°C. The thawed cell suspension was diluted into maintenance medium and centrifuged at 1000 rpm for 5 minutes. The supernatant was discarded and the cell pellet was resuspended in maintenance medium (3 ml) and seeded into one well of a 6-well plate. Cells were incubated at 37°C with 5% CO_2.

2.3.4.2 Passage of E14Tg2a.4 mES Cells

Cells were passaged once they had reached approximately 80% confluency. One hour prior to passaging, cell culture maintenance medium was replaced with fresh medium. To dissociate cells, medium was removed, cells were washed with PBS (at RT) and incubated in trypsin (as described in section 2.3.3.3) for 5 minutes at 37°C with 5% CO_2. The trypsin/cell suspension was diluted in maintenance medium and centrifuged at 1000 rpm for 3 minutes. The supernatant was

discarded and the cell pellet was resuspended in maintenance medium (10 ml) and seeded into a gelatinised 10 cm cell culture dish. Cells were incubated at 37°C with 5% CO_2.

2.3.4.3 Freezing of E14Tg2.4 mES Cells

E14Tg2a.4 mES cells were dissociated from cell culture dishes as described in section 2.3.4.2. Cell pellets were resuspended in equal volumes of maintenance medium and freezing medium and 1 ml of cell suspension was pipetted into labelled cryo vials. Two cryo vials of cells were produced from each 10 cm cell culture dish. Cryo vials were stored at -80°C for 24 hours and then transferred into liquid nitrogen for long term storage.

2.3.5 Formation of Embryoid Bodies

Differentiation of E14Tg2a.4 mES cells was induced via formation of EBs. Pluripotent cells cultured in 10 cm culture dishes were dissociated as described in section 2.3.4.2. After centrifugation, cell pellets were resuspended in maintenance medium without LIF (-LIF medium) and counted using a Schärfe Casy-1 cell counter. EBs were produced by either the highly cited suspension (Doetschman et al., 1985) or 'hanging drop' (Wobus et al., 1997) methods or by the in-house devised ultra-low attachment U/V-bottomed 96-well plate method. After 6 days, formed EBs were transferred into gelatinised 10 cm culture dishes.

2.3.5.1 Suspension Culture Method

Cells were diluted in -LIF medium to give 25,000 cells/ml and 10 ml cell suspension was pipetted into 10 cm bacteriological grade Petri dishes. Plates were incubated at 37°C with 5% CO_2.

2.3.5.2 'Hanging Drop' Method

Cell suspension was diluted in -LIF medium to give 500 cells/20 µl and seeded in 20 µl drops onto the inside of a 15 cm Petri dish lid. PBS (5 ml) was placed into the base of each Petri dish and lids were carefully inverted onto the base. Plates were incubated at 37°C with 5% CO_2.

2.3.5.3 Ultra-low Attachment U/V-bottomed 96-well Plate Method

Cell suspension was diluted in -LIF medium to give 500 cells/100 µl and 100 µl of cell suspension was pipetted into each well of an ultra-low attachment U or V-bottomed 96-well plate. Plates were incubated at 37°C with 5% CO_2.

2.3.6 Differentiation of E14Tg2a.4 Cells into Cardiomyocytes

2.3.6.1 Effect of Small Molecules on Cardiomyocyte Differentiation

The effect of ascorbic acid (10 µM), DMSO (1% v/v) and ascorbic acid (10 µM) plus DMSO (1%) on cardiomyocyte differentiation was observed. The basal medium used for cardiomyocyte differentiation protocols was Knockout-Dulbecco's modified eagle medium (KO-DMEM) supplemented with foetal calf serum (FCS) (1X), l-glutamine (1X), sodium pyruvate (1X), non-essential amino acids (1X) and β-mercaptoethanol (0.1 mM) and is referred to as CM-basal medium. EBs were produced and differentiated for 12 days in CM-basal medium only or medium supplemented with either ascorbic acid, DMSO or a combination of both. On day 12 RNA was extracted (as described in section 2.2.1.3) and RT-PCR (as described in section 2.2.7) was performed. This was repeated twice with a new batch of undifferentiated E14Tg2a.4 mES cells and medium being used for each batch of experiments.

2.3.6.2 Effect of Ascorbic Acid on Cardiomyocyte Differentiation

The effect of varying ascorbic acid concentrations on cardiomyocyte differentiation was assessed. EBs were produced and differentiated for 12 days in CM-basal medium supplemented with 0, 10, 20, 50 and 100 µM ascorbic acid. On day 12 RNA was extracted (as described in section 2.2.1.3) and RT-PCR (as described in section 2.2.7) was performed. This was repeated twice with a new batch of undifferentiated E14Tg2a.4 mES cells and medium being used for each batch of experiments. All further experiments involving differentiation of E14Tg2a.4 mES cells into cardiomyocytes utilised CM-basal medium supplemented with 10 µM ascorbic acid, referred to as CM medium.

2.3.6.3 Detecting Presence of Pluripotent E14Tg2a.4 mES Cells in Differentiated Cultures

Alkaline phosphatase (AP) is expressed on the cell membranes of pluripotent mES cells. As differentiation proceeds AP activity decreases indicating a loss of pluripotency. AP activity was measured using the Millipore Alkaline Phosphatase ES Characterization Kit. Cells used in this assay were pluripotent E14Tg2a.4 mES cells and E14Tg2a.4 mES cells differentiated into cardiomyocytes for 3, 6 and 9 days using CM medium. Attached cells (pluripotent and day 9 differentiated cells) were dissociated using trypsin and EBs in suspension (day 3 and 6 differentiated cells) were collected into 15 ml centrifuge tubes and centrifuged at RT, rpm for 5 minutes. Cell pellets were resuspended in wash buffer (2 ml), counted and 20,000 cells were aliquoted into three 2 ml Eppendorf tube, to produce technical replicates for each sample. Cells were centrifuged at RT, 2000 rpm for 5 minutes. Supernatant was discarded, cell pellets were resuspended in p-NPP buffer (50 µl) and each sample was transferred into one well of a 96-well

assay plate. The enzymatic reaction was initiated by addition of 2X p-NPP substrate solution (50 µl) and plates were incubated in the dark at RT for 20 minutes. Reactions were stopped by adding stop solution (50 µl) and absorbance was read at 405 nm using a Tecan plate reader. The average of the three technical samples for each cell type was taken as the sample value. This assay was repeated twice with a new batch of undifferentiated and differentiated E14Tg2a.4 mES cells. The average of the experimental readings for each cell type was taken as the final measurement.

2.3.6.4 Observation of Spontaneous Contractions in EBs Differentiated into Cardiomyocytes

E14Tg2a.4 mES cells were differentiated into cardiomyocytes via EB formation (as described in section 2.3.5.3) using CM-basal medium supplemented with 0 or 10 µM ascorbic acid (as described in section 2.3.6.2.1). Differentiation was initiated on three different occasions with 96 EBs being produced per medium type. After day 1 of differentiation EBs were visible under a light microscope at 10x magnification. The number of spontaneously contracting EBs was noted each day for 12 days. The average of the three batches of differentiation was taken for each time point.

2.3.6.5 Morphology of E14Tg2a.4 mES Cells Differentiated into Cardiomyocytes

E14Tg2a.4 mES cells were differentiated into cardiomyocytes via EB formation (as described in section 2.3.5.3) using CM medium (as described in section 2.3.6.2.1). On day 6 of differentiation, 72 EBs were seeded into each gelatinised 10 cm culture plates. Differentiated cultures were maintained for 25 days with medium being replaced every other day. Images of were taken on day 1, 2, 4, 6,

7 and 25 of differentiation. All images were acquired using a Zeiss LSM 510 confocal microscope at 10x magnification with AxioVision software.

2.3.6.6 Visualization of Cardiac Structural Proteins in E14T2a.4 mES Cells Differentiated into Cardiomyocytes

E14Tg2a.4 mES cells were differentiated into cardiomyocytes via EB formation (as described in section 2.3.5.3) using CM medium (as described in section 2.3.6.2.1).

2.3.6.6.1 Isolating Differentiated Cells from Embryoid Bodies and Re-Plating

On day 23 of differentiation, medium was removed and cell culture plates were washed with calcium and magnesium free Hank's Buffered Salt Solution (HBSS) (10 ml). Worthington type 2 collagenase (5ml, 1mg/ml) was added and culture plates were incubated at 37°C for 30 min. Cell suspension was collected into a 15 ml Falcon tube and centrifuged at RT, 1000 rpm for 5 minutes. Supernatant was discarder, cell pellet was resuspended in CM medium and the number of cells was counted. Gelatin coated 13 mm glass coverslips were placed into the wells of 24-well plates and cells were seeded at a density of 50,000 cell/well. Cultures were incubated at 37°C with 5% CO_2 with medium being replaced every other day.

2.3.6.6.2 Immunostaining Differentiated mES Cells Isolated from EBs

E14Tg2a.4 derived cardiomyocytes where characterized using the Millipore Cardiomyocyte Characterization Kit, which contained antibodies to troponin I, desmin, actinin, atrial natriuretic peptide (ANP) and tropomyosin. Differentiated cells were isolated from EBs and seeded onto glass coverslips as described in section 2.3.6.6.1. Medium was removed, cells were washed with PBS and fixed

with paraformaldehyde (PFA) (4%) for 15 minutes at RT. PFA was removed and cells were washed with PBS for 10 minutes, the was step was repeated twice. Blocking solution (5% donkey serum and 0.3% Triton X-100 in PBS) was applied cell were incubated at 4°C overnight. Primary antibodies were diluted in blocking solution at the following concentrations; sheep anti-tropomyosin (1/500), mouse anti-troponin I (1/100), mouse anti-actinin (1/200), rabbit anti-ANP (1/200) and mouse anti-desmin (1/100). Control mouse, rabbit and sheep immunoglobulin G (IgG) were used as negative staining isotype controls (Appendix Five). Blocking solution was removed and primary antibodies and negative staining controls were added into four wells each. Cells were incubated with primary antibodies at 4°C overnight. The following day, cells were washed twice in PBS for 10 minutes, then washed twice with blocking solution and then left in blocking solution for 30 minutes. Fluorophore conjugated secondary antibodies were prepared just before use, cells were incubated with the appropriate antibody for 2 hours a RT, in a cupboard. Cells were washed three times with PBS (10 minutes each), the last wash contained the nuclear stain Hoechst 33342 (50 µg/ml). Coverslips were mounted on to glass microscope slides using a mounting solution and imaged using a Zeiss LSM 510 confocal microscope at 40x magnification.

2.3.6.7 Isolation of Pure Cardiomyocytes from Differentiated mES Cell Cultures

The fluorescence-activated cell sorting (FACS) method published by Hattori et al., (2010) was used to isolate a population of pure cardiomyocytes from E14Tg2a.4 mES cells that had been differentiated into cardiomyocytes for 23 days. Differentiated cultures consisted of six 10 cm plates each containing 72 EBs. To detach and disperse the EBs Worthington type 2 collagenase (1mg/ml)

was prepared in Ads buffer (116 mM NaCl, 20 mM HEPES, 12.5 mM NaH_2PO_4, 5.6 mM glucose, 5.4 mM KCl and 0.8 mM $MgSO_4$ final concentration; pH 7.4) to produce the digestion medium. Culture medium was removed, EBs were washed with HBBS and then incubated in digestion medium (5 ml) at 37°C for 30 minutes. Digestion medium was transferred into a 15 ml centrifuge tube and centrifuged at RT, 1000 rpm for 5 minutes. The supernatant was discarded and the cell pellet was resuspended in Ads buffer containing the fluorescent mitochondrial dye tetramethylrhodamine methyl ester (TMRM) (10 nM) (Life Technologies, Paisley, UK) and incubated at 37°C for 30 minutes. The cell suspension was subsequently sorted using the FACS Aria (Becton Dickinson) with the assistance of Mr Roger Snowden. Cells with the highest TMRM fluorescence were collected into CM medium and seeded onto gelatinised 13 mm glass coverslips placed in wells of 24-well plates.

2.3.6.8 Visualizing Mitochondrial Content of Spontaneously Contracting mES Cell Differentiated Cardiomyocytes

E14Tg2a.4 mES cells were differentiated into cardiomyocytes as described in section 2.3.6.6. On day 24 of differentiation, CM-medium was removed and cells were incubated in imaging medium supplemented with TMRM (10 nM) at 37°C for 30 minutes. Cells were washed twice in PBS and fresh imaging medium was add to the culture plates. Phase contrast and fluorescent images were acquired of the same imaging area using a Zeiss LSM 510 confocal microscope at 20x magnification.

2.3.6.9 Intracellular Calcium Measurements of mES Cell Differentiated Cardiomyocytes

A population of differentiated cardiomyocytes was isolated using FACS as described in section 2.3.6.8 and seeded onto 13 mm glass coverslips. CM medium was removed and replaced with imaging medium (121 mM NaCl, 5.4 mM KCl, 800 µM MgCl$_2$, 1.8 mM CaCl2, 6 mM NaHCO$_3$, 5.5 mM glucose and 25 mM HEPES; pH 7.3) containing the calcium specific dye Fura-2 AM (2 µM) (Life Technologies, Paisley, UK). Cells were incubated in imaging medium for 30 minutes at 37°C in the dark. For imaging, glass coverslips were loaded onto the heated stage of a Zeiss Axiovert microscope and maintained at 37°C in imaging medium. Calcium imaging was performed using fluorescent microscopy with the help of Dr Kenneth Young of the MRC Toxicology Unit. Images were acquired using a 40x oil immersion lens, the Fura-2 AM dye was alternatively excited at wavelengths of 340 and 380 nm and emitted fluorescence was collected.

2.3.7 Differentiation of E14Tg2a.4 Cells into Hepatocytes

Several medium compositions were trialled for the differentiation of E14Tg2a.4 mES cells into hepatocytes. Basal differentiation medium consisted of IMDM supplemented with FCS (1X), l-glutamine (1X), sodium pyruvate (1X), non-essential amino acids (1X) and β-mercaptoethanol (0.1 mM) and is referred to as HEP-basal medium. For differentiation HEP-basal medium was supplemented with varying concentration of FCS, insulin-transferrin-selenium supplement (ITS), dexamethasone (Dex) and sodium butyrate at different time points. Differentiation cultures were maintained for a maximum of 25 days after which RNA was extracted (as described in section 2.2.1.3) and RT-PCR (as described in section 2.2.7) was performed to assess for the presence of hepatic marker

genes. Differentiation was repeated twice for each medium composition with a new batch of undifferentiated E14Tg2a.4 mES cells and medium being used for each lot of experiments.

2.3.7.1 Hepatocyte Differentiation Using High FCS Concentration

Differentiation was induced via EB formation as described in section 2.3.5.3 using HEP-basal medium supplemented with 15% FCS (termed HEP-medium 1). Cells differentiated using HEP-medium 1 were maintained in culture for 25 days.

2.3.7.2 Hepatocyte Differentiation Using Low FCS Concentration

Differentiation was induced via EB formation as described in section 2.3.5.3 using HEP-basal medium supplemented with 5% FCS (termed HEP-medium 2). EBs produced using HEP-medium 2 did not attach to gelatinised culture plates day 6 of differentiation and thus this medium composition was deduced to be unsuitable for use.

2.3.7.3 Hepatocyte Differentiation Using Varying FCS Concentrations

Differentiation was induced via EB formation as described in section 2.3.5.3 using HEP-basal medium supplemented with 15% FCS with EBs being seeded onto gelatinised cell culture plates on day 6 of differentiation. On day 7 of differentiation medium was changed to HEP-basal medium supplemented with 4% FCS, 1% ITS and 10^{-7} M Dex (termed HEP-medium 3). Cells differentiated using HEP-medium 3 were maintained in culture for 25 days.

2.3.7.4 Hepatocyte Differentiation Using Sodium Butyrate to Form EBs

Differentiation was induced via EB formation as described in section 2.3.5.3 using HEP-basal medium supplemented with 15% FCS and 1 mM sodium butyrate

(termed HEP-medium 4). EBs failed to form in HEP-medium 3 and thus this medium composition was deduced to be unsuitable for use.

2.3.7.5 Hepatocyte Differentiation Using Sodium Butyrate to Mature EBs

Differentiation was induced via EB formation as described in section 2.3.5.3 using HEP-basal medium supplemented with 15% FCS. On day 3 of differentiation medium was supplemented with 1 mM sodium butyrate. On day 6 of differentiation EBs were seeded into gelatinised cell culture plates however after 48 hours EBs had not attached and thus this medium composition was deduced to be unsuitable for use.

2.3.7.6 Hepatocyte Differentiation Using FCS, Sodium Butyrate and Dex

Differentiation was induced via EB formation as described in section 2.3.5.3 using HEP-basal medium supplemented with 15% FCS. On day 3 of differentiation medium was supplemented with 1 mM sodium butyrate. On day 6 of differentiation medium was changed to HEP-basal medium supplemented with 10% FCS and 10^{-7} M Dex (termed HEP-medium 6) and EBs were seeded into gelatinised cell culture plates. After 24 hours EBs had attached and cell cultures were maintained using HEP-medium 6 for up to 25 days.

2.3.7.7 Detecting Presence of Pluripotent E14Tg2a.4 mES Cells in Differentiated Cultures

AP activity was measured as described in section 2.3.6.4. Cells used in this assay were pluripotent E14Tg2a.4 mES cells and E14Tg2a.4 mES cells differentiated into hepatocytes for 3, 6 and 9 days using HEP-medium 6.

2.3.8 Treatment of Differentiated Cells with Troglitazone

2.3.8.1 Effect of FCS Free Medium on Differentiated mES Cells

Cardiomyocytes and hepatocytes were differentiated using CM medium and HEP-medium 6, respectively. On day 23 of differentiation, medium was replaced with test medium, consisting of KO-DMEM (for cardiomyocyte cultures) and IMDM (for hepatocyte cultures) supplemented with ITS supplement (5%), l-glutamine (1X), sodium pyruvate (1X), non-essential amino acids (1X) and β-mercaptoethanol (0.1 mM). Cultures were maintained in test medium for 48 hours after which RNA was extracted (as described in section 2.2.1.3) and RT-PCR (as described in section 2.2.7) was performed.

2.3.8.2 Treating Differentiated mES Cells with Troglitazone

TRO was dissolved in DMSO to produce a 1000x stock solution of the required final concentration. For cell treatment, 0.1% DMSO was used as a control and the final DMSO concentration in TRO treated wells was also 0.1%. TRO concentrations ranged from 0 to 100 µM were added to test medium and cells were treated with the selected does for 24 hours.

2.3.8.3 Assessment of Cell Viability After Troglitazone Treatment

Cell viability in response to TRO treatment was assessed using the Promega CellTiter 96® AQueous One Solution Cell Viability Assay. EBs differentiated into cardiomyocytes and hepatocytes were dispersed to produce a single cell suspension. Cells were plated into 96-well plates at a density of 2×10^5 cells/well. Cells were allowed to attach for 24 hours prior to treatment. Cells were treated with TRO for 24 hours following which 20 µl of CellTiter 96® AQueous One

Solution was added to each well and plates were incubated for 3 hours at 37°C and 5% CO_2. Absorbance was read at 490 nm.

2.3.8.4 Assessment of Intracellular Calcium Fluctuations Using Cellomics ArrayScan VTI

Differentiated cardiomyocytes were isolated from day 22 EBs and re-plated as single cells at a density of 250,000 cells/well in 24-well plates. Cells were allowed to attach overnight. Prior to imaging cells were incubated with medium containing Fluo-4 AM (50 nM) and Hoechst 33342 (50 µg/ml) for 30 minutes at 37°C and 5% CO_2. After loading, cells were washed twice with PBS and fresh test medium (500 µl/well) was added. Using the Cellomics software Hoechst stained nuclei were detected and a cell mask was added to outline the cytoplasm of the cell. Either control medium, TRO (5 or 10 µM) or Ionomycin (1 µM) were added and changes in florescence were recorded for up to 75 seconds. The average cell intensity algorithm was used to measure increase fluorescence of Fluo-4 AM in the cytoplasm of the cell.

2.4 *In Vivo* Study Protocols

Both studies were performed in accordance with the Animal Scientific Procedures Act (1986), under project license 80/2126. Dosing suspensions were prepared in accordance with Good Laboratory Practice (GLP) guidelines. For both studies TRO was prepared in arachis oil (1% w/w) and was mixed with diet for 60 min (three cycles of 20 minutes) in an orbital mixer and stored at 4°C until use. For control mice only vehicle was mixed into the diet. Dosing suspension and drug-diet mixtures were prepared 24 hours before commencement of each study. Troglitazone was administered for 7 and 14 days via the diet and the diet was

changed daily. Body weight, diet and water consumption were measured each day. Changing of diet and taking of weight and diet and water consumption was undertaken by technicians of the Biomedical Sciences Division of The University of Leicester. Dr Gant's assisted with the culling of the mice, which was performed by anaesthetic overdose using isoflurane. Liver and heart tissues were excised and a small section of each organ from three mice per dose group was preserved in formalin for histopathological analysis. The remainder of the tissue was flash frozen in liquid nitrogen and stored at -80°C until use. Blood was collected by either cardiac puncture or by vena cava bleeds and stored on ice for up to 2 hours. For plasma extraction, blood samples were centrifuged at 4°C, 13000 rpm for 20 minutes. The plasma was pipetted into Eppendorf tubes and stored at -80°C until use, freeze-thawing of plasma was minimised as much as possible.

2.4.1 Investigation of Troglitazone Toxicity in a Normal Mouse Model

Adult male, strain 129P2/OlaHsd mice were used for this study. Six mice were assigned to each of the five dosing groups; 0 (control), 200, 400, 800 and 1200 mg/kg/day and each group was administered TRO for 7 and 14 days.

2.4.1.1 Histopathology

At the point of necropsy in both 7 and 14 day studies, small sections of liver tissue from 3 mice per dose group were taken and preserved in formalin (10%). Samples were sent to GSK for histopathological assessment.

2.4.2 Investigation of Troglitazone Toxicity in a High Fat Diet Induced Diabetic Mouse Model

2.4.2.1 Administering a High Fat Diet

Adult male and female, strain C57 BL/6J mice were used for this study. Mice were administered a high fat diet (HFD) for 16 weeks in order to allow them to develop an insulin resistant phenotype.

2.4.2.2 Measuring Blood Glucose

Blood glucose was measured from tail vein blood samples using either a Glucose-6-phosphate Assay Kit (Sigma) or an Accu-Check blood glucose meter and strips.

2.4.2.3 Performing Oral Glucose Tolerance Tests

Mice were fasted for 6 hours prior to commencement of the oral glucose tolerance test (OGTT). At T0, a drop of blood was taken from the tail vein and an Accu-Check blood glucose meter and strips were used to measure initial blood glucose levels. Immediately after blood sampling, a bolus of glucose (2 g/kg body weight) was administered to each mouse by oral gavage. Blood glucose levels were measured at 15, 30, 60, 90 and 120 minutes after glucose administration.

2.4.2.4 LC-MS Analysis of Plasma for Detection of Troglitazone

Sample preparation and analysis was undertaken at the Medical Toxicology Centre at the University of Newcastle under the supervision of Dr Michael Dunn. Plasma clean-up was undertaken using Varian Bond Elut Plexa PCX 96-well plates as according to manufacturer's instructions (Agilent Technologies). Briefly, 150 µl of plasma, 20 µl of internal standard (benzoylecgonine 1mg/ml) and 450 µl of phosphoric acid (2%) were added to an Eppendorf tube. The suspension

was mixed by vortexing and incubated at room temperature for 1 hour. The Bond Elut Plexa plate was conditioned with a 2 step wash, firstly with MeOH and then with H_2O (500 µl/well), drawing the solution through the well filters by vacuum suction. Plasma sample mixtures were added to the plate and eluted through the filters that were then washed with 500 µl of formic acid (2%). Metabolites were eluted in two aliquots, the first using 500 µl of MeOH:ACN (1:1) and the second using 500 µl of MeOH:ACN (1:1) + 5% ammonia. Elutes 1 and 2 were collected in separate test tubes and evaporated to dryness at $40^{O}C$ under nitrogen. Dried samples were reconstituted in H_2O:MeOH (9:1) + formic acid (0.01%). Samples were stored at $4^{o}C$ and analysed for TRO by Dr Michael Dunn.

Chapter 3: Differentiation of Mouse Embryonic Stem Cells into Derived Cardiomyocytes and Hepatocytes

3.1 Introduction

The pharmaceutical industry is in need of improved *in vitro* model systems to utilize in drug development to predict potential toxicity of new drug entities. ES cells can be differentiated along the three germ lineages and into any cell type. The ability to produce cells *in vitro* that are phenotypically similar to cells *in vivo* could revolutionize drug development by providing novel *in vitro* systems for use in testing the safety and toxicity of new drugs (Pouton and Haynes, 2007). Reproducible and standardized protocols for the culture and differentiation of stem cells are required in order for them to be utilised in drug development assays (Thomson, 2007).

Cardiotoxicity and hepatotoxicity are the two most commonly reported drug induced adverse reactions. It is anticipated that the use of stem cell derived cardiomyocytes and hepatocytes will enable better prediction of these toxicities during preclinical drug development. The number of published protocols for the differentiation of various stem cell lines into specific cell types is constantly increasing however, there is a lack of standardization between protocols. The use of different stem cell lines, differentiation inducing agents and culture conditions has resulted in variability between protocols. A contributing factor to the difficulty in standardizing differentiation protocols between various stem cell lines is that different lines respond variably to the same differentiating conditions (Allegrucci and Young, 2007).

There are more reported methods for differentiating human ES (hES) cells than mES and conditions used for the differentiation hES into cardiomyocytes and hepatocytes do not always induce the same changes in mES cells (Ginis et al., 2004). Furthermore, methods for producing a population of undifferentiated

pluripotent ES cells vary between human and mouse cell lines. Maintenance of pluripotency of mES cells *in vitro* can be achieved through supplementation of culture media with FCS and LIF. In comparison, supplementing culture media with LIF does not maintain hES cells in a pluripotent state (Hoffman and Merrill, 2007). LIF induced Stat3 signalling is vital for maintenance of pluripotency in mES cells however, activation of Stat3 signalling in hES cells is not sufficient enough to sustain self-renewal and to inhibit differentiation (Daheron et al., 2004).

Differentiation of ES cells is most commonly achieved through the formation of EBs as it is believed that this *in vitro* cell aggregation mimics the cell-cell interactions that occur during embryo development *in vivo* (Doetschman et al., 1985). The formation of EBs in LIF free medium has been shown to induce spontaneous differentiation of ES cells along the three germ layer lineages, mesoderm, endoderm and ectoderm (Leahy et al., 1999).

Directing differentiation of mES cells along a certain germ layer and towards a particular cell type can be achieved through supplementing cell culture medium with chemicals and protein growth factors (Manuilova et al., 2001). The use of chemicals is a less expensive method of directing differentiation of ES cells compared with the use of growth factors. Often one chemical is sufficient to direct differentiation whereas with growth factors a mixture of several factors is often required and typically growth factors can be 10 to 100 times more expensive than chemicals.

Although the use of chemicals provides a cost effective method for differentiating ES cells there are varying reports in the literature regarding their effect on promoting differentiation even when used with the same ES cell line. For example, differentiation of the D3 mES cell line via EB formation using medium

supplemented with retinoic acid promotes neural differentiation whilst simultaneously inhibiting mesoderm formation (Bain et al., 1996). However, these same conditions have been reported elsewhere to enhance mesoderm development and cardiomyocyte differentiation (Wobus et al., 1997).

Various protocols for the differentiation of numerous different mES cells lines have been reported and data from individual laboratories is often contrasting. The lack of standardization amongst protocols indicates that culture conditions for the differentiation of ES cells towards a desired phenotype have to be optimized on an individual cell line basis. It is also important to ensure that the developed protocols are reproducible in order to minimize the variance between different batches of differentiated cells.

3.2 Chapter Aims

The aim for this chapter was to develop reproducible methods for the differentiation of pluripotent E14Tg2a.4 mES cells into cardiomyocytes and hepatocytes, generating cells that could be used in *in vitro* assays to evaluate TRO toxicity. An important criterion was for differentiated cells to express key cardiac and hepatic marker genes.

3.3 Results

All experiments undertaken in this chapter were designed to support the development of reproducible protocols for the culture of pluripotent E14Tg2a.4 mES cells and their differentiation into cardiomyocytes and hepatocytes. To minimise costs alternatives to the use of expensive growth factors for culture and differentiation of mES cells were sought.

3.3.1 Production of Leukaemia Inhibitory Factor

Maintenance of self-renewal and pluripotency of mES cells is of utmost importance for cultures which are to be used in differentiation protocols. To develop standardized and reproducible protocols for differentiation of ES cells into cardiomyocytes and hepatocytes the starting cell population must consist of a homogenous culture of pluripotent stem cells. Supplementing cell culture medium with leukaemia inhibitory factor (LIF), a 20 kDa protein that is a key regulator of mES cell pluripotency, maintains mES cells in an undifferentiated state *in vitro*. Cell culture protocols provided with the E14Tg2a.4 mES cell line advised a daily change of medium supplemented with LIF. The volume of medium that was anticipated to be required over the course of this project and the quantity of commercial LIF that would be required made it more financially viable to produce LIF in-house than to purchase commercially available LIF. Murine LIF (mLIF) was purified from an E.coli culture transfected with the construct pGEX-2T-MLIF. To confirm production of mLIF the purified peptide was analysed by SDS-PAGE and mass spectrometry and compared against commercially available LIF and LIF sourced from collaborative laboratories, who had also produced LIF using the same vector. SDS-PAGE analysis (Figure 3.1) identified a common band at 20 kDa that was present in in-house derived, commercial and

sourced LIF samples. In the commercial LIF sample a large band at 65 kDa was also observed which was absent from in-house and sourced LIF samples. This band corresponded to bovine serum albumin (BSA), which was used as a carrier protein for commercial LIF. Mass spectrometry identified that the purified in-house peptide and the commercial and sourced samples were mLIF (Figure 3.2). Furthermore, the in-house purified peptide was found to have 79.8% sequence homology with human LIF (Figure 3.3). Sequence homology between murine and human LIF has previously been cited as 78% and both murine and human LIF can keep mES cells in an undifferentiated state in *in vitro* culture (Gough et al., 1988). Proteomic analysis of the in-house purified peptide confirmed that it was mLIF.

The concentration of in-house purified mLIF was measured using a protein quantification assay. BSA used to produce a standard curve from which the concentration of in-house LIF was calculated. The concentration of in-house LIF was calculated to be 0.046 mg/ml. Commercial LIF is recommended for use at a concentration of 100,000 Units of LIF per 100 ml of media. It was calculated that 21.83 µl of in-house purified LIF would be required per 100 ml of cell culture medium to provide activity that is equivalent to 100,000 Units of commercial LIF. The potency of in-house LIF was assessed with a cell growth assay wherein growth of E14Tg2a.4 mES cells, supplemented with varying concentrations of LIF, was observed over 24 hours (Figure 3.4). The recommended concentration for commercial LIF is 1000 Units of LIF per ml and this equivalent concentration of in-house LIF showed optimum cell growth. At lower concentrations of 0, 250 and 500 Units/ml, less cell proliferation was observed whereas higher concentrations of 1500 and 2000 units/ml LIF induced cell death resulting in cells

lifting off from cell culture plates and these dead cells were visible as debris in the cell culture medium.

Collectively the proteomic analysis and cell growth observations showed that the in-house purified LIF was equivalent to commercially available LIF both by sequence homology and potency and thus was suitable for use in maintaining cultures of undifferentiated E14Tg2a.4 mES cells.
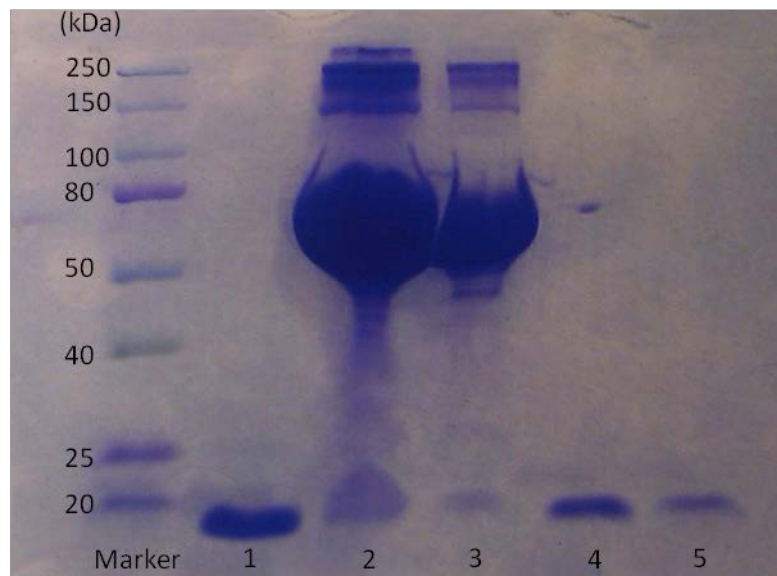
Figure 3.1 – SDS-PAGE gel of in-house purified peptide, commercially available LIF and sourced LIF. SDS-PAGE gel stained with Coomassie Blue, sample designations are: Lane 1: 10 µl In-house produced LIF, Lane 2: 10 µl Commercial LIF, Lane 3: 5 µl Commercial LIF, Lane 4: 10 µl Sourced LIF, Lane 5: 5 µl Sourced LIF. The bands at 20 kDa corresponds to murine LIF protein and the large bands at 65 kDa correspond to bovine serum albumin, which is used as a carrier protein for the commercial LIF.
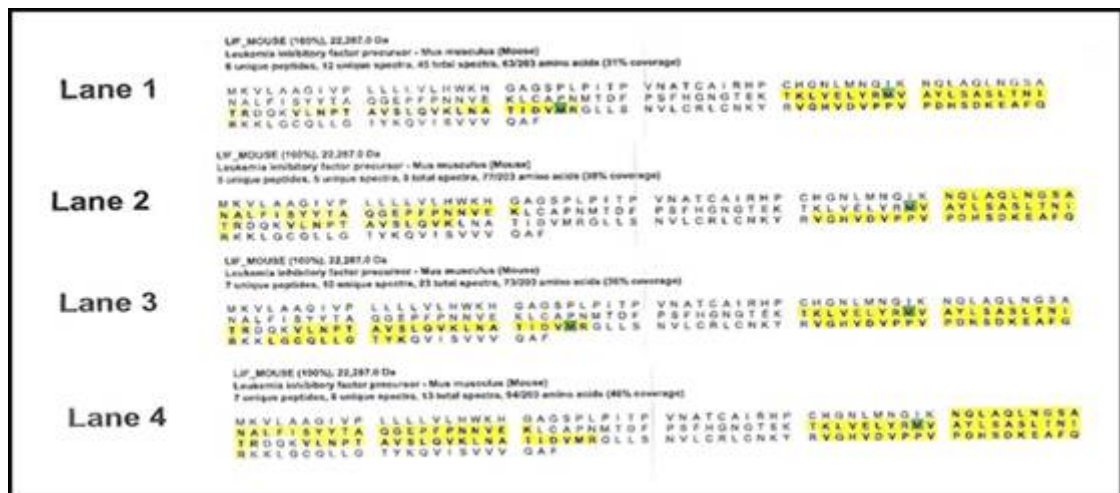
Figure 3.2 – Identification of in-house purified peptide, commercially available LIF and sourced LIF by mass spectrometry. The In-house purified peptide (lane 1), commercial LIF (lanes 2 and 3) and sourced LIF (lane 4) were identified as murine LIF samples. Residues that were detected by mass spectrometry are highlighted in yellow.
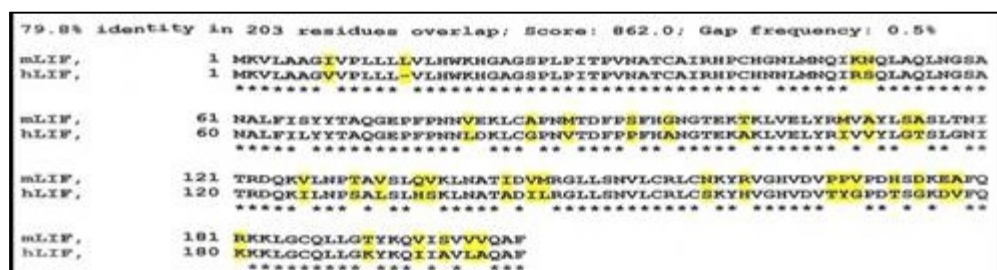
Figure 3.3 – Sequence homology between human and murine LIF. Mass spectrometry analysis showed there was 79.8% sequence homology between the in-house purified LIF and the known sequence of human LIF. This supported confirmation of the identity of the in-house purified peptide as the sequence homology between murine and human LIF has previously been cited at 78% by Gough et al (1988).

Observation at 2 hours after plating of cells

Observation at 26 hours after plating of cells

0 units/ml

250 units/ml

500 units/ml

1000 units/ml

1500 units/ml
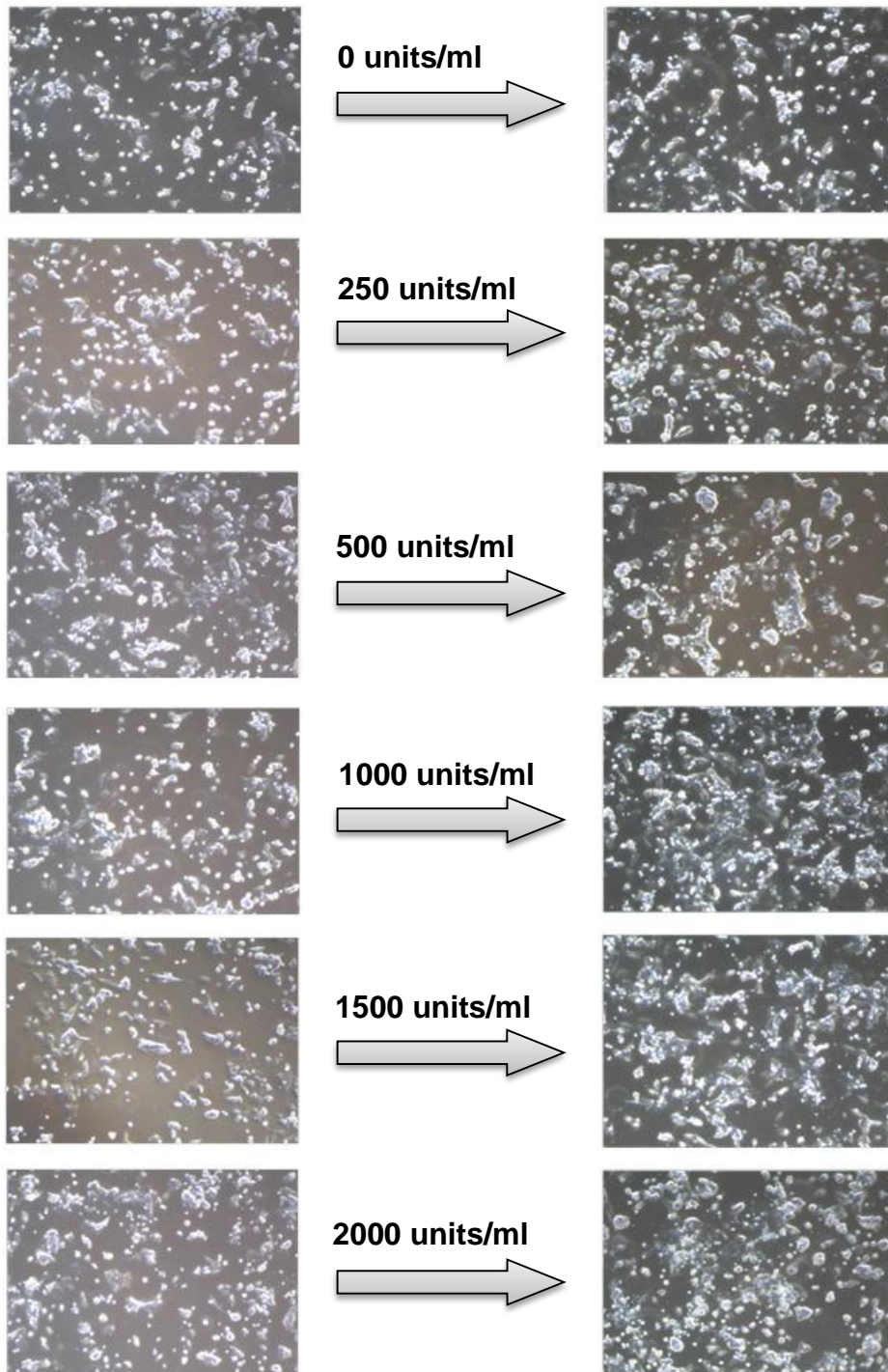
2000 units/ml

Figure 3.4 – Observation of E14Tg2a.4 mES cell growth over 24 hours in the presence of varying concentrations of in-house purified LIF. The greatest cell growth was found in cultures supplemented with 1000 units LIF/ml. At lower concentrations less cell proliferation was observed and at 1500 and 2000 units/ml cell death and these dead cells were observed as debris in the cell culture medium.

3.3.2 Post Thaw Expression of Pluripotency Markers in E14Tg2a.4 mES Cells

Pluripotent ES cells are preserved in freezing medium containing 10% DMSO, a compound that has been shown to induce differentiation (Wobus, 2001, Boheler et al., 2002). Stable expression of the key pluripotency regulator genes Nanog and Pou5f1 is representative of a pluripotent ES cell culture. For efficient and reproducible differentiation of ES cells into a particular cell type, a starting population of homogenous pluripotent ES cells is required. The effects of freeze-thaw processes and exposure to DMSO on the pluripotency of E14Tg2a.4 mES cells was assessed using RT-PCR. E14Tg2a.4 cells were thawed and cultured in LIF containing medium for seven passages. At each point of passage, a sample of cells was taken for RNA extraction following which RT-PCR was performed using primers for Nanog and Pou5f1. In RT-PCR, the concentration of a target gene, relative to the expression of an endogenous housekeeping gene, is defined by the delta threshold cycle (ΔC_t) value. Thus consistent C_t values for a given gene in multiple samples is indicative of the same level of gene expression across the samples. The C_t values for Nanog and Pouf51 were measured for seven passages post thaw. Significant differences were observed in the expression of Nanog in E14Tg2a.4 mES cells during the first 3 passages post thaw. After the fourth passage the ΔC_t value and thus expression of Nanog stabilised (Figure 3.5A). Significant differences were also observed in the ΔC_t values of Pou5f1 in E14Tg2a.4 mES cells during the first 5 passages post thaw, after which values stabilised (Figure 3.5B). Consistent ΔC_t values for Nanog and Pou5f1 were observed in E14Tg2a.4 mES cells that had been passaged at least five times post-thaw. Stable expression of Nanog and Pou5f1 was used as an indicator of

a homogenous pluripotent population of E14Tg2a.4 mES cells and thus cells were not used in differentiation protocols until they had been passaged at least 5 times post thaw.
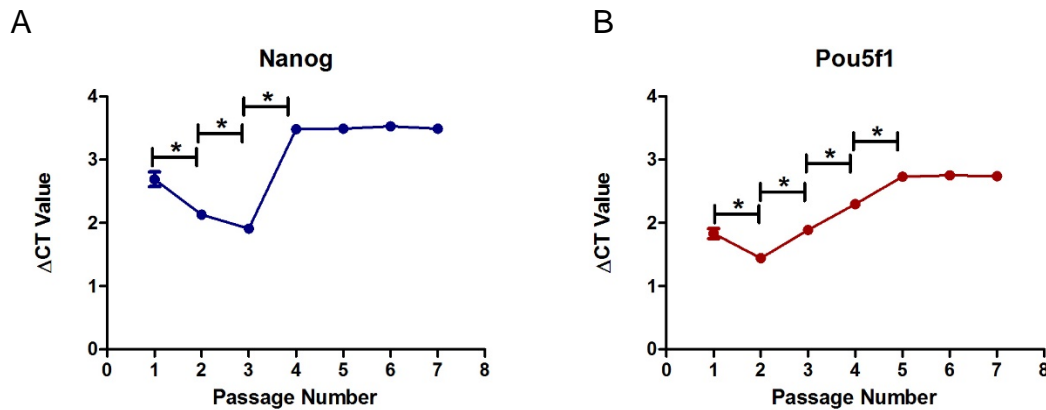
Figure 3.5 – Expression of pluripotency markers Nanog and Pou5f1 for 7 passages post thaw in E14Tg2a.4 mES cells. (A) Delta Ct (ΔCt) values for Nanog varied significantly for the first four passages post thaw. (B) ΔCt values for Pou5f1 varied significantly during the first five passages after cells were thawed. After five passages the expression of Nanog and Pou5f1 stabilised and significant differences in ΔCt values were not detected (data are mean ± SD (n=3) with results statistically significant at *$p < 0.05$ between passages).

3.3.3 Optimising Embryoid Body Formation

In many protocols the formation of EBs is the first critical step of differentiation. The production of EBs of a uniform shape and size and the use of consistent numbers of EBs per culture vessel, is required for the development of reproducible differentiation protocols. EBs were formed using three different

protocols as described in section 2.3.5 and as illustrated in Figure 3.6. The suspension culture method consisted of seeding E14Tg2a.4 mES cell suspension in bacteriological grade Petri dishes and incubating for 3 days. After 3 days EBs had formed however, they were not of uniform size and contained varying numbers of cells. Thus, this method was deemed unsuitable as it could not be utilised for the reproducible production of standardised EBs of a given shape and size. Utilization of the 'hanging drop' method (Wobus et al., 1997) resulted in the production of EBs consisting of the same size and cell number. Many groups that have utilized this method to form EBs and have started with seeding 500 cells in small droplets onto the lids of Petri dishes (Shiroi et al., 2002, Kumar and Sun, 2005, Takaki et al., 2006, Wang and Yang, 2008). Utilization of this method produced a single EB per droplet with all EBs in a culture consisting of the same spherical shape and diameter. The 'hanging drop' protocol was better than the suspension culture protocol at generating standardised EBs in a reproducible manner. However, it was a time consuming process, sensitive to disruption and would not be suitable for scaled-up or automated processes that are utilised during pre-clinical drug development in the pharmaceutical industry. With the 'hanging drop' protocol approximately 205 drops were seeded in close proximity onto one large Petri dish lid (15 cm diameter) (Figure 3.7), lids were inversed quickly and smoothly to minimize disruption of the drops and cells. Plates were incubated for 3 days during which disturbances to the plates or incubators caused drops to fall.

In order to standardize differentiation protocols the same number of EBs were seeded into each plate during differentiation. After formation using the 'hanging drop' method, EBs were collected and transferred into gelatin coated plates. This

was a time consuming task and subject to variance with regards to the number of EBs being collected and plated. Thus a third method of EBs formation was developed, which involved seeding defined numbers of cells in suspension into ultra-low attachment 'U' and 'V' microwell plates. The principle of this method was the same as that of the 'hanging drop' protocol with 500 cells being used to form each EB and with cell aggregation occurring as a result of the effect of gravity. With the ultra-low attachment U/V microwell plate method one EB was formed per well and it was possible to collect and transfer exact numbers of EBs using multi-channel pipettes. This method also reduced the time taken to set-up cultures for further differentiation and made it easier to track the number of EBs being plated. Further benefits of this method included the reduction of incubator space required as the 96-well plates could be stacked on top of each other. This protocol was more resistant to disturbances from incubator door/shelf movements and could easily be scaled-up and utilised with automated cell culture faculties. No difference was observed in the generation of EBs with either 'U' or 'V' shaped wells thus, both plates could be used interchangeably. Figure 3.7 illustrates EB formation by 'hanging drop' and ultra-low attachment multi-well formats. The ultra-low attachment U/V-bottomed 96-well plate method allowed for reproducible formation of EBs of a specific shape and size, allowed for consistent numbers of EBs to be seeded for further differentiation and could be utilised in scaled-up and automated cell culture processes.

Pluripotent E14Tg2a.4 mES cells
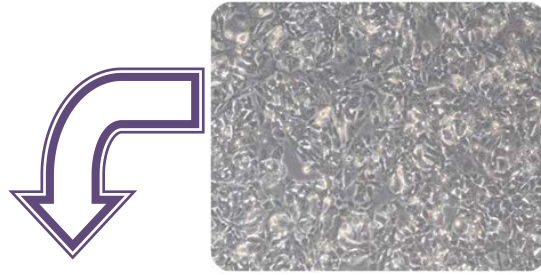
1. Suspension EB Formation

 After 3 days

2. Hanging Drop EB Formation

 After 3 days

3. Ultra-Low Attachment 'U' Well EB Formation

 After 3 days

4. Ultra-Low Attachment 'V' Well EB Formation

 After 3 days

Figure 3.6 – Methods trialled for forming EBs. (1) Culturing mES cells in suspension resulted in the formation of EBs. However, the EBs formed were not of uniform shape and size. (2) The 'Hanging Drop' method resulted in the formation of EBs of uniform shape and size but the plate set-up was sensitive to disruption and disturbances to the plates caused the drops to fall leading to loss of EBs. The principle of the Hanging Drop method was adapted using (3) 'U' and (4) 'V' bottomed ultra-low attachment 96-well plates. Uniform shape and sized EBs were produced using this method and no EBs were lost as a result of disturbances to the microwell plates.
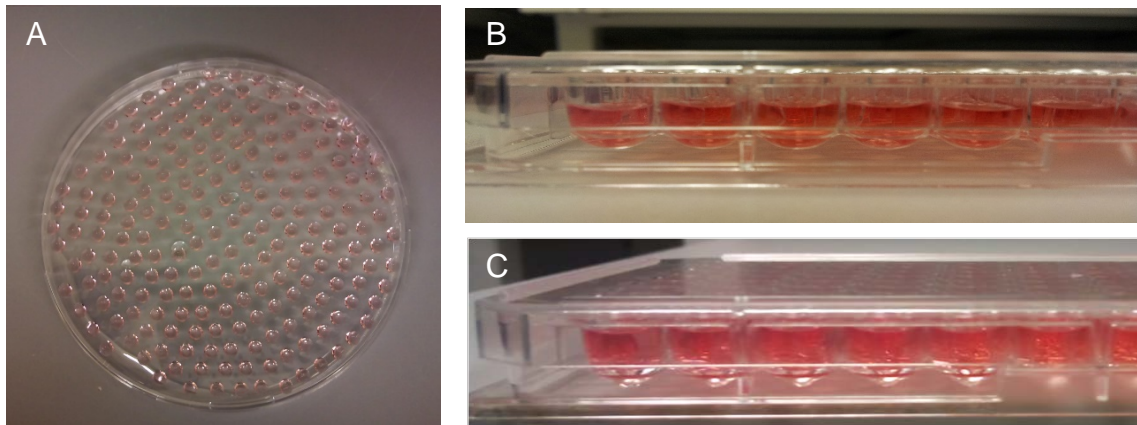
Figure 3.7 – Embryoid body formation by (A) 'hanging drop' or in (B) 'U' and (C) 'V' bottom microwell plates. With all 3 methods the initial number of cells used to produce EBs could be controlled and allowed for formation of uniform shaped EBs. One EB was formed in each droplet with the 'hanging drop' method and in each well of the ultra-low attachment microwell plates.

3.3.4 Attachment Culture of Embryoid Bodies for Differentiation

Following formation in suspension, EBs were transferred into gelatin coated tissue culture plates to allow them to attach and differentiate further. The reported length of time for which EBs must be kept in suspension before being plated for attachment culture varies and is typically cited as being between 3-7 days (Wobus and Guan, 1998). A marked difference was observed in the structural integrity between EBs that were plated on day 3 and day 6 of differentiation (Figure 3.8). EBs that were seeded for attachment culture on day 3 flattened out after attachment, lost their structural integrity and further outgrowth from the parental cell cluster was not observed. Thus seeding EBs on day 3 of differentiation was not a viable option for furthering differentiation as continuation of cell growth post attachment was not observed. In contrast, EBs that were

plated on day 6 of differentiation retained their structural integrity and spherical shape after attachment and outward growth of cells from the central EB was observed. This illustrated that seeding EBs onto tissue culture plates on day 6 of differentiation supported continued growth and differentiation of mES cells. Thus, in all further experimentations requiring differentiation of E14Tg2a.4 mES cells, EBs were seeded for attachment culture on day 6.
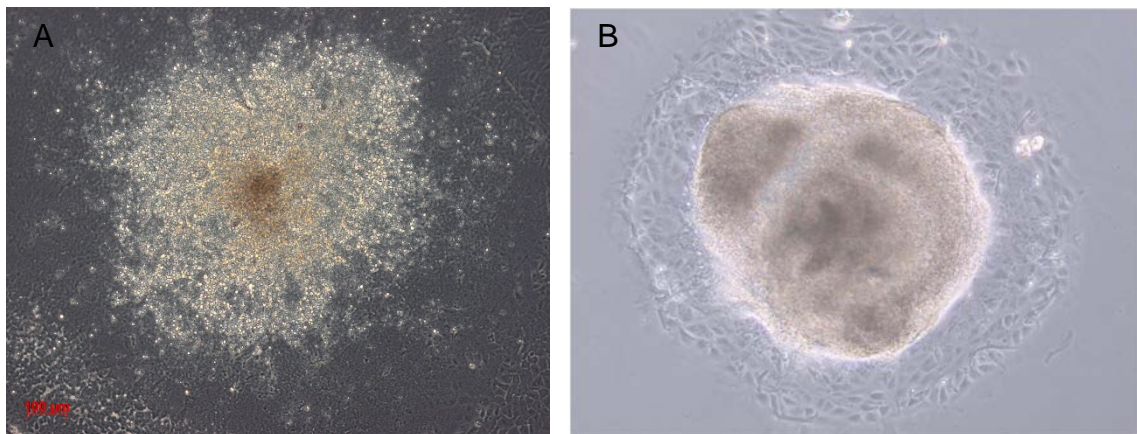
Figure 3.8 – Morphology of EBs 24 hours after being seeded onto gelatin coated tissue culture plates. (A) EBs seeded onto gelatin coated plates on day 3 of differentiation flattened out after attaching, lost structural integrity and cultures did not grow further. (B) EBs plated on day 6 of differentiation retained their structural integrity and cells were observed growing outwards from the central cell mass.

3.3.5 Development of Protocols for Differentiation of E14Tg2a.4 mES Cells into Cardiomyocytes

3.3.5.1 Spontaneous Differentiation

During experimentations to optimise EB formation it was observed that removal of LIF from cell culture medium resulted in the formation of spontaneously

contracting clusters within EBs. To verify that the cells were spontaneously differentiating into cardiomyocytes, EBs were produced in LIF free medium using ultra low attachment U/V bottom 96-well plates and seeded for attachment culture on day 6 of differentiation. On day 12 of differentiation RNA was extracted and RT-PCR was used to assess the expression of pluripotency and cardiac genes in these cultures. The expression of Nanog and Pou5f1 was used as a marker of pluripotency and the expression of cardiac structural genes (Myh6 and Myl2), genes encoding cardiac ion channels (Atp2a2 and Slc8a1) and a mesoderm transcription factor (Gata4) were used to assess cardiomyocyte differentiation. These cardiac gene markers were chosen from the recommendations of the Stem Cells for Safer Medicine (SC4SM) consortium, which was set-up to support, provide guidance on and encourage standardisation in developing stem cell based models for use in drug development (SC4SM, 2008). The expression of pluripotency and cardiac genes in differentiated cells compared with undifferentiated E14Tg2a.4 mES cells was used to assess induction of cardiomyocyte differentiation. Decreased expression of Nanog and Pou5f1 and increased expression of Myh6, Myl2, Atp2a2, Slc8a1 and Gata4 was observed in differentiated cultures (Figure 3.9). This showed a decrease in the presence of undifferentiated mES cells and illustrated spontaneous differentiation of E14Tg2a.4 mES cells towards a cardiomyocyte phenotype.

3.3.5.2 Directed Differentiation

Supplementing cell culture medium with small molecules has been reported to aid in promoting differentiation along a particular lineage and towards a specific cell type (Zaret, 2009). The use of ascorbic acid and DMSO has been reported

to promote differentiation of ES cells into cardiomyocytes (Boheler et al., 2002, Takahashi et al., 2003).
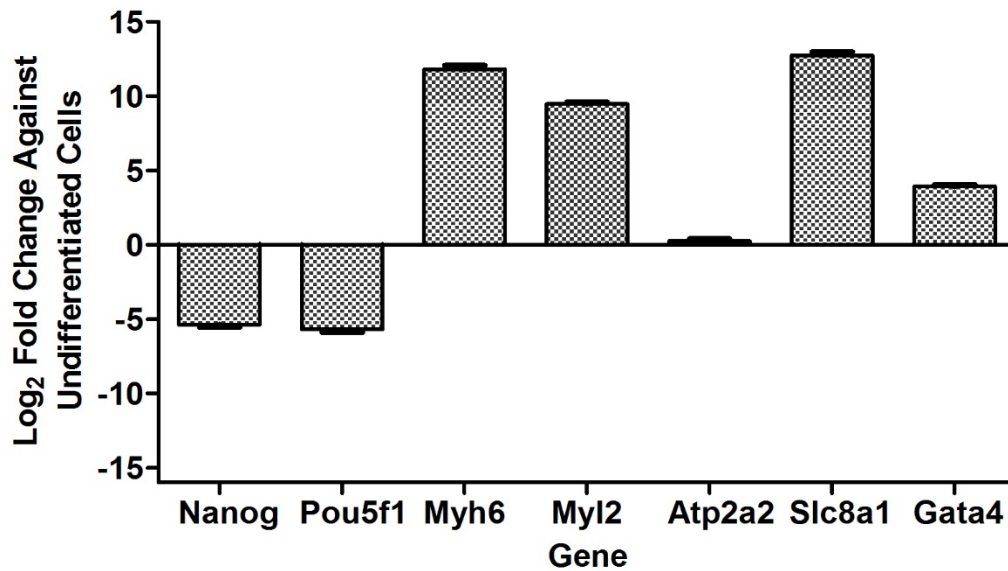
Figure 3.9 – Expression of pluripotency and cardiac marker genes in E14Tg2a.4 mES cells cultured in LIF free medium for 12 days. Formation and culture of EBs in the absence of LIF resulted in the development of spontaneously contracting clusters of cells. RT-PCR analysis of 12 day old cultures showed decreased expression of the pluripotency genes Nanog and Pou5f1 and increased expression of the cardiac structural genes Myh6 and Myl2, the cardiac ion channel Slc8a1 and the mesoderm transcription factor Gata4 in differentiated cultures compared with undifferentiated cells. A significant difference in the expression of Atp2a2 in differentiated cells compared with undifferentiated cells was not observed (data are mean ± SD (n=3), with results statistically significant at $p < 0.05$ against undifferentiated cells for all genes except Atp2a2).

To observe the effect of ascorbic acid and DMSO on differentiation of E14Tg2a.4 mES cells into cardiomyocytes, cells were differentiated for 12 days in LIF free

medium with either no additional supplement, ascorbic acid (10 µM), DMSO (1% v/v) or a combination of both ascorbic acid (10 µM) and DMSO (1% v/v). Expression of pluripotency and cardiac marker genes was assessed for each differentiation condition (Figures 3.10 and 3.11). The expression of each gene from cells differentiated using the four different medium compositions was compared with expression of that same gene in undifferentiated cells. The expression of the target gene in cultures differentiated with ascorbic acid (10 µM), DMSO (1% v/v) or a combination of both ascorbic acid (10 µM) and DMSO (1% v/v) was compared with cultures differentiated without additional supplements by one-way ANOVA with post hoc Dunnett's test. This analysis was used to observe if small molecules could be used to further direct and increase the differentiation of mES cells into cardiomyocytes compared with the spontaneous differentiation that had been observed when LIF had been removed from culture medium. The use of ascorbic acid, DMSO and a combination of the two supressed the expression of Nanog and Pou5f1 to a greater degree than that observed in cultures differentiated without additional supplements (Figure 3.10). The use of ascorbic acid and a combination of ascorbic acid and DMSO resulted in greater suppression of Nanog and Pou5f1 than that observed with the use of DMSO alone. The use of ascorbic acid and a combination of ascorbic acid and DMSO resulted in similar levels of Nanog suppression however a combination of ascorbic acid and DMSO produced the greatest suppression of Pou5f1. The decreased expression of the pluripotency regulator genes Nanog and Pou5f1 in cultures differentiated using DMSO (1% v/v), ascorbic acid (10 µM) and a combination of ascorbic acid (10 µM) and DMSO (1% v/v) illustrated that the use of these small molecules increased the differentiation of E14Tg2a.4 mES cells.
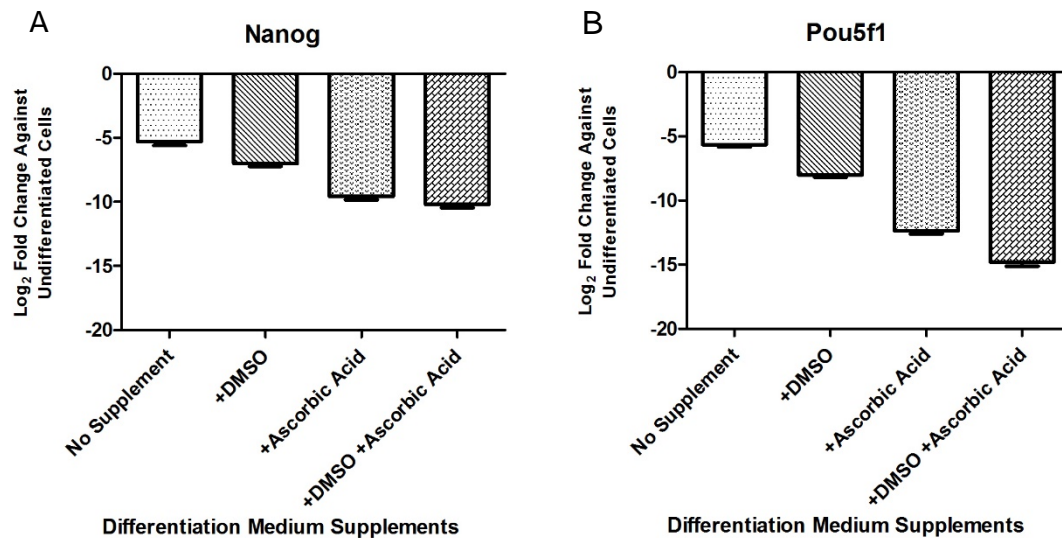
Figure 3.10 – Effect of ascorbic acid and DMSO on the expression of pluripotency genes in E14Tg2a.4 mES cells differentiated for 12 days. E14Tg2a.4 mES cells were cultured for 12 days in LIF free medium without additional supplements, with 10 µM ascorbic acid, 1% v/v DMSO and with a combination of 10 µM ascorbic acid and 1% v/v DMSO. RT-PCR analysis of cultures for the expression of the key pluripotency genes (A) Nanog and (B) Pou5f1. Supplementing medium with either ascorbic acid, DMSO or both resulted in greater suppression of Nanog and Pou5f1 compared to cultures differentiated without additional supplements. The greatest suppression of Nanog was observed in cultures differentiated using ascorbic acid and a combination of ascorbic acid and DMSO. The greatest suppression of Pou5f1 was seen in cultures differentiated with a combination of ascorbic acid and DMSO (data are mean ± SD (n=3), with results statistically significant at $p < 0.05$ for each medium supplement compared with no supplement by one-way ANOVA with post hoc Dunnett's test).

The use of ascorbic acid, DMSO and a combination of both resulted in greater expression of Myh6 than that which had been observed in cultures differentiated without additional supplement. The greatest expression was observed in cultures differentiated using both ascorbic acid (10 µM) and DMSO (1% v/v) (Figure

3.11A). Significantly greater induction of Myl2 was only observed with the use of ascorbic acid alone. In cultures differentiated using DMSO or a combination of ascorbic acid and DMSO, the expression of Myl2 was not increased above that observed in cultures differentiated without the use of additional supplements (Figure 3.11B). Significantly increased expression of Slc8a1 was observed in spontaneously differentiated cultures compared to undifferentiated cells. The use of ascorbic acid did not affect the expression of Slc8a1 resulting in similar levels of expression in these cultures compared with cultures allowed to spontaneously differentiate in LIF free medium. The use of DMSO alone and in combination with ascorbic acid resulted in a significant decrease in Slc8a1 expression compared to that observed in cultures differentiated without the use of additional supplements (Figure 3.11C).   Expression of Atp2a2 in spontaneously differentiated cultures and in cultures differentiated with DMSO was the same as that observed in undifferentiated cells. The use of ascorbic and a combination of ascorbic acid and DMSO resulted in a significant induction in the expression of Atp2a2 compared to spontaneously differentiated cultures. The greatest increase in Atp2a2 expression was observed in cultures differentiated using ascorbic acid (10 µM) (Figure 3.11D). Significantly increased expression of Gata4 was observed in cultures differentiated using ascorbic acid and a combination of ascorbic acid and DMSO compared with cultures differentiated without the use of additional supplements. The use of ascorbic acid alone and a combination of ascorbic acid and DMSO resulted in similar levels of increased Gata4 expression. The use of DMSO alone did not induce an increase in the expression of Gata4 beyond that observed in spontaneously differentiated cultures (Figure 3.11E). These data illustrated that the use of ascorbic acid (10 µM), DMSO (1% v/v) or a

combination of both ascorbic acid (10 µM) and DMSO (1% v/v) increased differentiation of mES cells towards a cardiomyocyte phenotype compared with cultures differentiated without the use of additional supplements. The use of DMSO (1% v/v) induced an increase in the expression of Myh6 but did not significantly increase the expression of Myl2, Atp2a2 or Gata4 beyond the expression levels that were observed in cultures differentiated without the use of additional supplements. Furthermore, the use of DMSO reduced the expression of Slc8a1, a gene that encodes for a sodium/calcium ion exchanger that plays an important role in the generation of action potentials in contracting cardiomyocytes (Quednau et al., 2004). A decrease in Slc8a1, compared with spontaneously differentiated cultures, was also observed in cultures differentiated using a combination of both ascorbic acid (10 µM) and DMSO (1% v/v). In addition, a decrease in the expression of Myl2 was also observed with use of the dual supplemented medium. The use of ascorbic acid (10 µM) resulted in increased expression of Myh6, Myl2, Atp2a2 and Gata4 compared to cultures differentiated without additional supplements. This illustrated that ascorbic acid could be used to direct the spontaneous differentiation towards a cardiomyocyte phenotype that had first been observed in cultures differentiated in LIF free medium without additional supplements.
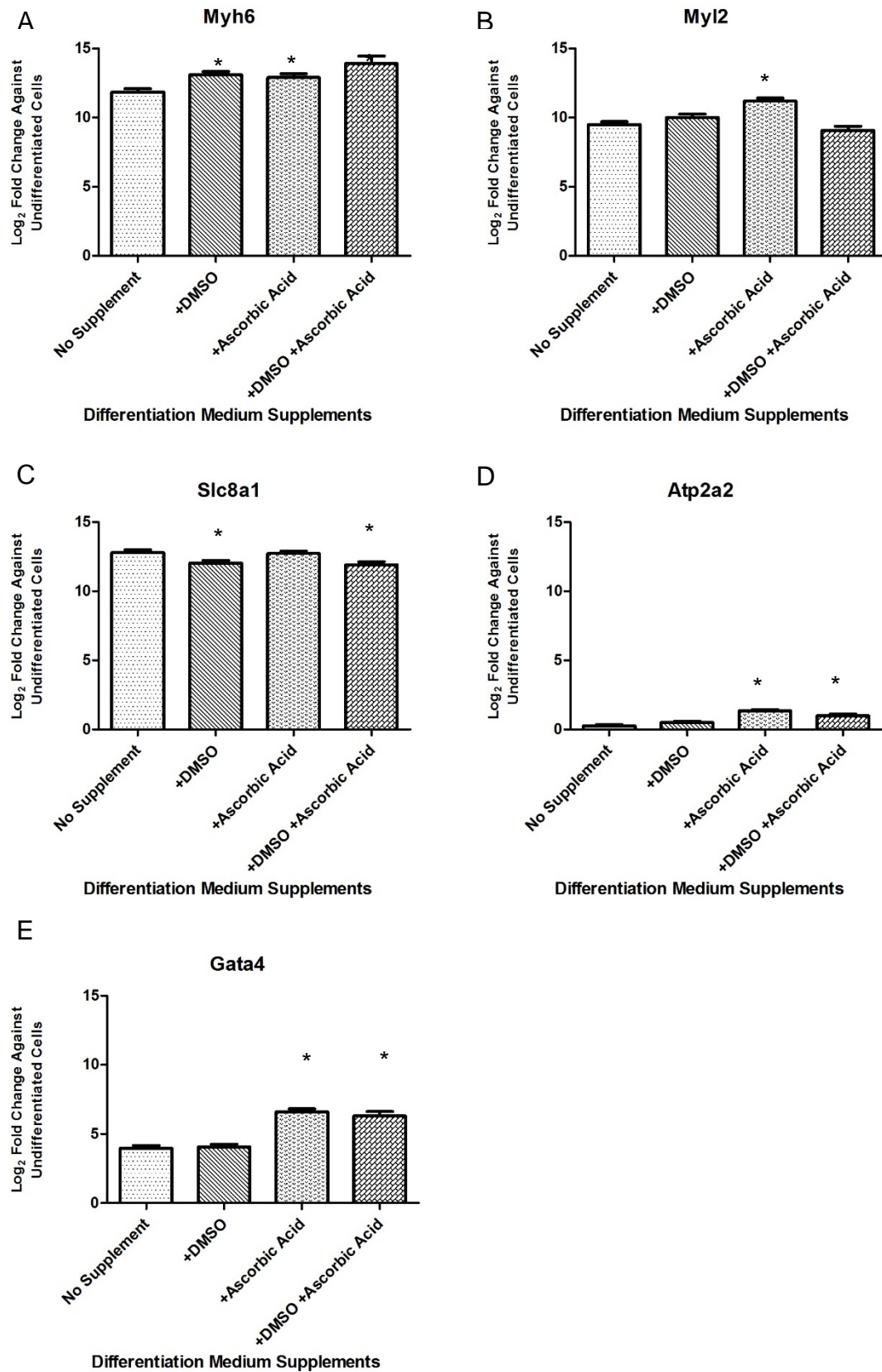
Figure 3.11 – Effect of ascorbic acid and DMSO on the expression of cardiac marker genes in E14Tg2a.4 mES cells differentiated for 12 days.

Please see next page for figure legend.

Figure 3.11 – Effect of ascorbic acid and DMSO on the expression of cardiac marker genes in E14Tg2a.4 mES cells differentiated for 12 days. E14Tg2a.4 mES cells were differentiated for 12 days in LIF free medium either spontaneously without additional supplements or with 10 µM ascorbic acid, 1% v/v DMSO and with a combination of 10 µM ascorbic acid and 1% v/v DMSO. RT-PCR analysis was used to assess the expression of the cardiac structural genes (A) Myh6 and (B) Myl2, the cardiac ion channels (C) Slc8a2 and (D) Atp2a2 and the mesoderm transcription factor (E) Gata4. In comparison with spontaneously differentiated cultures the use of DMSO increased expression of Myh6, did not induce significant change in expression of Myl2, Atp2a2 and Gata4 and decreased expression of Slc8a1. Decreased expression of Slc8a1 was also observed in cultured differentiated with a combination of ascorbic acid and DMSO. However, this combination medium did increase the expression of Myh6, Atp2a2 and Gata4 to higher levels than that which had been observed in spontaneously differentiated cultures. Compared with spontaneously differentiated cultures the use of ascorbic acid increased the expression of Myh6, Myl2, Atp2a2 and Gata4. In contrast to effects observed with the use of DMSO, either as a single agent or in combination with ascorbic acid, the use of ascorbic acid alone did not decrease the expression of Slc8a1. Expression levels of Slc8a1 were comparable between cultures differentiated without the use of additional supplements and those differentiated using ascorbic acid alone (data are mean ± SD (n=3), with results statistically significant at *$p < 0.05$ for each medium supplement compared with no supplement by one-way ANOVA with post hoc Dunnett's test).

3.3.5.3 Effect of Increasing Ascorbic Acid Concentration on Differentiation of E14Tg2a.4 mES Cells into Cardiomyocytes

Ascorbic acid was shown to promote differentiation of E14Tg2a.4 mES cell into cardiomyocyte-like cells. Initial experiments had been carried out using 10 µM ascorbic acid for 12 days and this caused an increase in expression of Myh6, Myl2, Atp2a2, Slc8a1 and Gata4 in comparison to undifferentiated cells (Figure 3.11). Differentiation was undertaken using 0, 10, 20, 50 and 100 µM ascorbic acid to ascertain if there was a correlation between concentration of ascorbic acid and induction of differentiation towards a cardiomyocyte phenotype. Expression of the pluripotency genes Nanog and Pou5f1 and the cardiac genes Myh6, Myl2, Mef2c, Slc8a1, Tnni3, Gata4, Ryr2, Atp2a2 and Bmp4 was assessed by RT-PCR. These cardiac marker genes were taken from the recommendations listed by the SC4SM consortium (SC4SM, 2008). The expression of target genes in cultures differentiated with 0, 20, 50 and 100 µM ascorbic acid was compared with cultures differentiated with 10 µM ascorbic acid by one-way ANOVA with post hoc Dunnett's test. The use of ascorbic acid resulted in decreased suppression of Nanog and Pou5f1 compared to cultures differentiated without additional supplements (Figure 3.12). The use of ascorbic acid concentrations above 10 µM did not result in significantly greater suppression of the pluripotency regulator genes Nanog and Pou5f1. These data showed that the use of ascorbic acid increased the degree of differentiation occurring in the cultures however, increasing the ascorbic acid concentration above 10 µM did not induce further differentiation. The use of 10 µM ascorbic acid increased the expression of the cardiac marker genes Myh6, Myl2, Mef2c, Slc8a1, Tnni3, Gata4, Ryr2, Atp2a2 and Bmp4 compared with cultures differentiated without ascorbic acid. However,

the use of ascorbic acid at 20, 50 and 100 µM did not significantly increase the expression of these cardiac genes beyond that observed in cultures differentiated using 10 µM ascorbic acid (Figure 3.13). These data illustrated that ascorbic acid could be used to promote differentiation of E14Tg2a.4 mES cells towards a cardiomyocyte phenotype, however, increasing the concentration above 10 µM did not result in increased differentiation of the cultures. Thus, all further experimentations requiring differentiation of E14Tg2a.4 mES cells into cardiomyocytes were undertaken using 10 µM ascorbic acid.
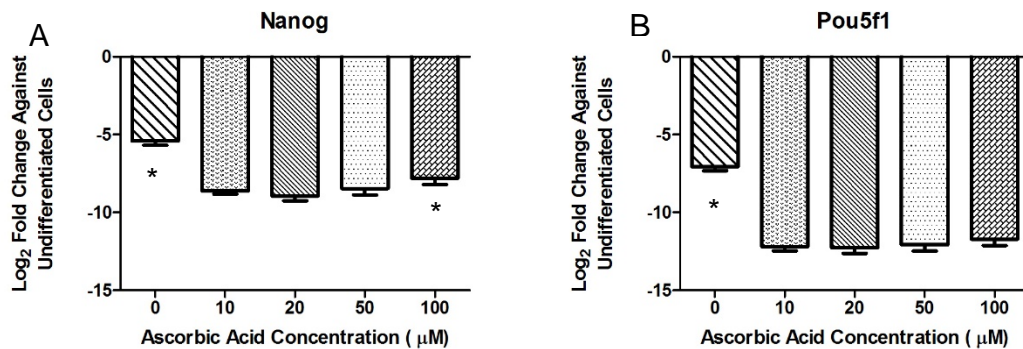
Figure 3.12 – Effect of ascorbic acid concentration on the expression of pluripotency genes in E14Tg2a.4 mES cells differentiated for 12 days. E14Tg2a.4 mES cells were differentiated in LIF free medium supplemented with 0, 10, 20, 50 and 100 µM ascorbic acid for 12 days. RT-PCR analysis was used to assess the expression of the key pluripotency genes (A) Nanog and (B) Pou5f1. In comparison to spontaneously differentiated cultures, cells differentiated using ascorbic acid had lower levels of Nanog and Pou5f1 expression. Increasing the ascorbic acid concentration above 10 µM did not result in further suppression of Nanog and Pou5f1 (data are mean ± SD (n=3), with results statistically significant at *$p < 0.05$ for that given concentration of ascorbic acid compared with 10 µM as by one-way ANOVA with post hoc Dunnett's test).
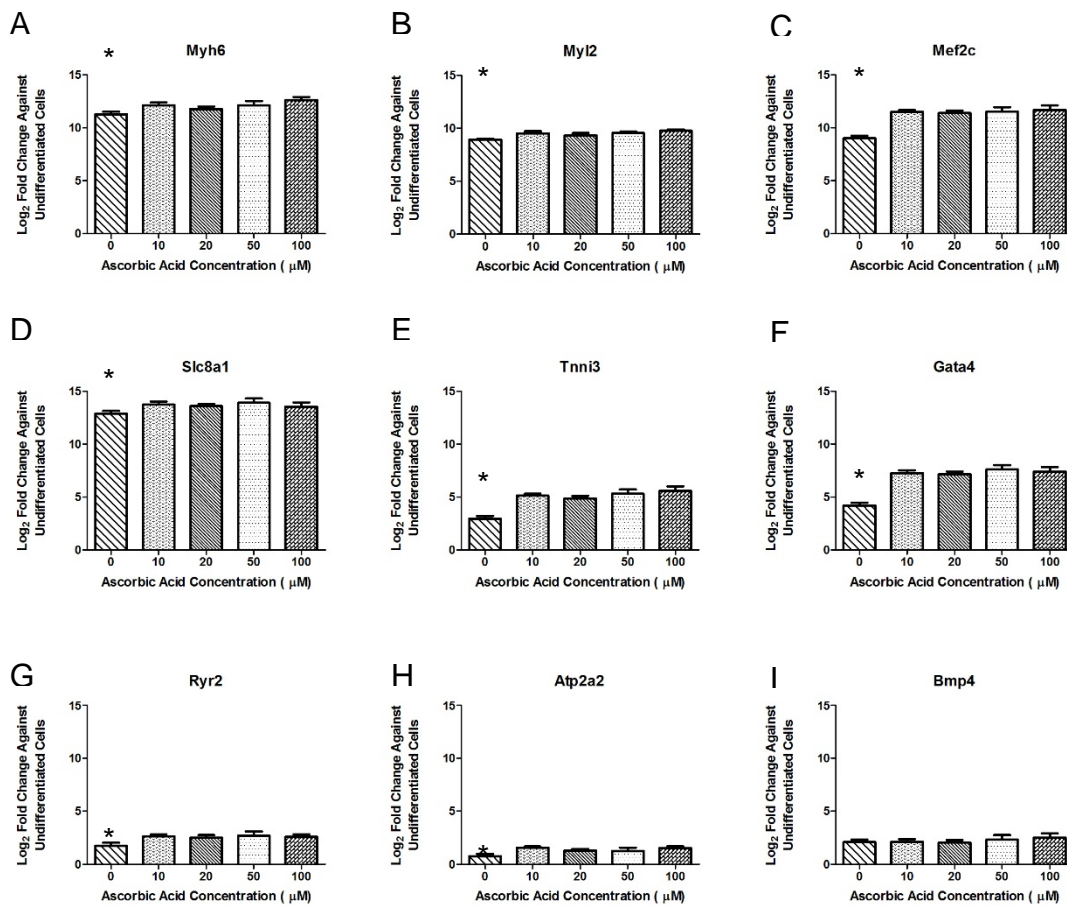
Figure 3.13 – Effect of ascorbic acid concentration on the expression of cardiac marker genes in E14Tg2a.4 mES cells differentiated for 12 days. E14Tg2a.4 mES cells were differentiated in LIF free medium supplemented with 0, 10, 20, 50 and 100 µM ascorbic acid for 12 days. RT-PCR analysis was used to assess the expression of the cardiac structural genes (A) Myh6, (B) Myl2, (E) Tnni3, the cardiac ion channels (D) Slc8a1, (G) Ryr2, (D) Atp2a2, the mesodermal transcription factors (E) Gata4 (I) Bmp4 and the cardiac transcription factor (C) Mef2c. In comparison to spontaneously differentiated cultures, cells differentiated using ascorbic acid had higher levels of Myh6, Myl2, Mef2c, Slc8a1, Tnni3, Gata4, Ryr2 and Atp2a2 expression. Increasing the ascorbic acid concentration above 10 µM did not further increase the expression of these genes. Ascorbic acid did not increase Bmp4 expression beyond that observed in spontaneously differentiated cultures (data are mean ± SD (n=3), with results statistically significant at *p < 0.05 for 0 µM compared with 10 µM ascorbic acid by one-way ANOVA with post hoc Dunnett's test).

3.3.5.4 Decreased Alkaline Phosphatase Activity

Alkaline phosphatase (AP) activity is a marker of pluripotency; during differentiation of mES cells this enzymatic activity is lost. Therefore AP activity can be used to trace differentiation of mES cells. AP activity was measured in the starting undifferentiated stem cell population (day 0) and at days 3, 6 and 9 of cardiomyocyte differentiation using 10 µM ascorbic acid (Figure 3.14). AP activity in differentiated cultures at day 3, 6 and 9 was compared with day 0 undifferentiated cultures by one-way ANOVA with post hoc Dunnett's test. As differentiation progressed AP activity significantly decreased. This illustrated loss of pluripotency and increased differentiation in the cultures in a time dependent manner.
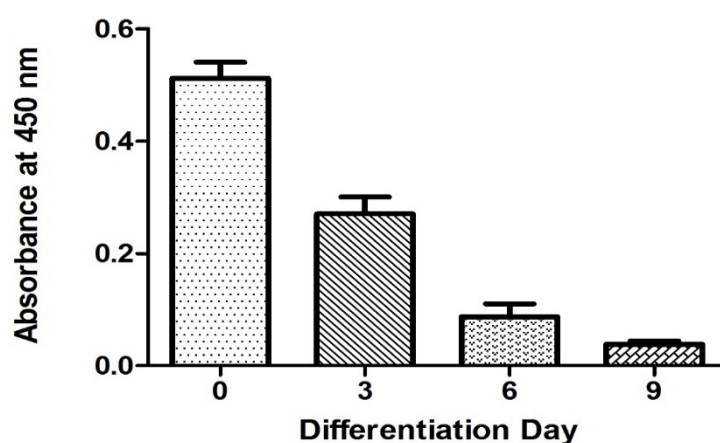
Figure 3.14 – Decrease in alkaline phosphatase activity during differentiation of E14Tg2a.4 mES cells using 10 µM ascorbic acid. Culturing E14Tg2a.4 mES cells in LIF free medium supplemented with 10 µM ascorbic acid resulted in a time dependent decrease in the presence of pluripotent cells within the treated cultures. AP activity at days 3, 6 and 9 of differentiation was significantly lower than the activity measured in the undifferentiated starting population of E14Tg2a.4 mES cells at day 0 (data are mean ± SD (n=3), with results statistically significant at *$p < 0.05$ for each time point compared with day 0 by one-way ANOVA with post hoc Dunnett's test).

3.3.5.5 Contracting Embryoid Bodies during Cardiomyocyte Differentiation

The ability to spontaneously contract is a unique property of cardiomyocytes and one which can be observed in *in vitro* cultures of primary cardiomyocytes. Visualization of contracting EBs within differentiating ES cell cultures is an early indicator of cardiac differentiation. Contracting clusters of cells were first observed in cultures of cells differentiated in LIF free medium without the use of additional supplements. The use of 10 μM ascorbic acid increased differentiation towards the formation of cardiomyocytes, which was illustrated by increased expression of cardiac marker genes. The effect of ascorbic acid on the number of contracting EBs was also measured. EBs were cultured in LIF free medium without additional supplements and with 10 μM ascorbic acid. The number of contracting EBs in each culture was recorded up to day 12 of differentiation (Figure 3.15). The first observation of contracting EBs was noted at day 3 in cultures supplemented with ascorbic acid and later at day 6 in EBs cultured without additional supplements. In cultures supplemented with ascorbic acid, 100% of the EBs were contracting by day 6, whereas in cultures without additional supplement a maximum of 88% of the EBs were contracting at day 12. The use of 10 μM ascorbic acid resulted in earlier development of contracting EBs and induction of contraction of all the EBs in each culture compared to EBs differentiated without additional supplements. For both cultures, differentiated with and without ascorbic acid, the average rate of contraction of the EBs was 60 beats/minute. The rate of contraction was found to be temperature dependent and within 30 minutes of cells being kept at room temperature the contractions ceased. However returning culture plates to incubators and re-warming them to 37°C resulted in revival of spontaneous contractions. This was significant for later

experimentations involving measurement of calcium ions during cell contractions as the occurrence of contractions was found to be temperature dependent.
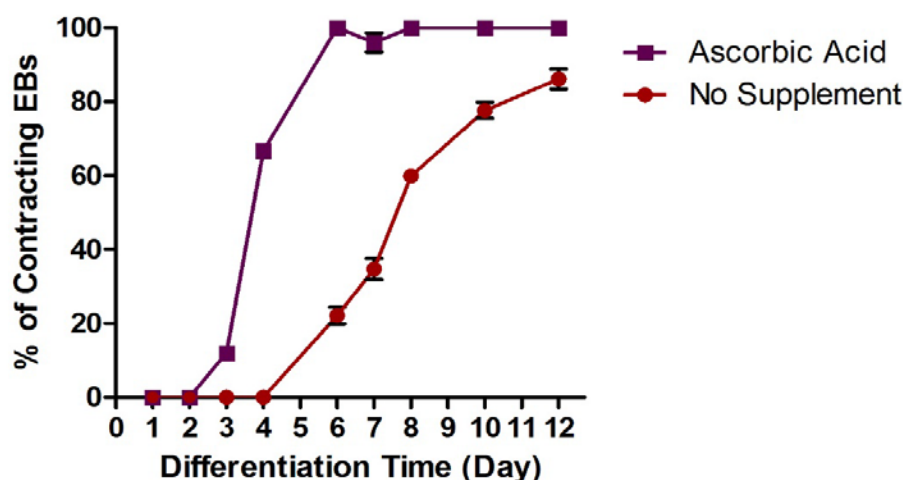
Figure 3.15 – Percentage of contracting embryoid bodies during cardiac differentiation. E14Tg2a.4 mES cells were differentiated using LIF free medium supplemented with and without 10 µM ascorbic acid and the number of contracting EBs were noted for 12 days of differentiation. Contractions in EBs were first noted at day 3 in cultures using ascorbic acid compared with day 6 in cultures differentiated without the use of additional supplements. In addition, by day 12 100% of EBs differentiated using ascorbic acid were observed to be contracting compared with 88% in cultures differentiated without additional supplements (data are mean ± SD (n=3), $p < 0.05$ between ascorbic acid and no supplement differentiation conditions).

3.3.5.6 Embryoid Body Morphology

The size and shape of EBs during cardiomyocyte differentiation using ascorbic acid was noted (Figure 3.16). Each EB was formed from a starting number of 500 cells and EBs were imaged on days 1, 2, 4 and 6, during suspension culture in U/V bottomed 96-well plates and on day 7 after they had been seeded onto gelatin coated tissue culture plates for attachment culture. EBs were approximately spherical in shape and rapidly grew from 200 to 1000 µm in diameter from day 1 to 7. After attachment cells were observed to be growing outwards from the central EB.
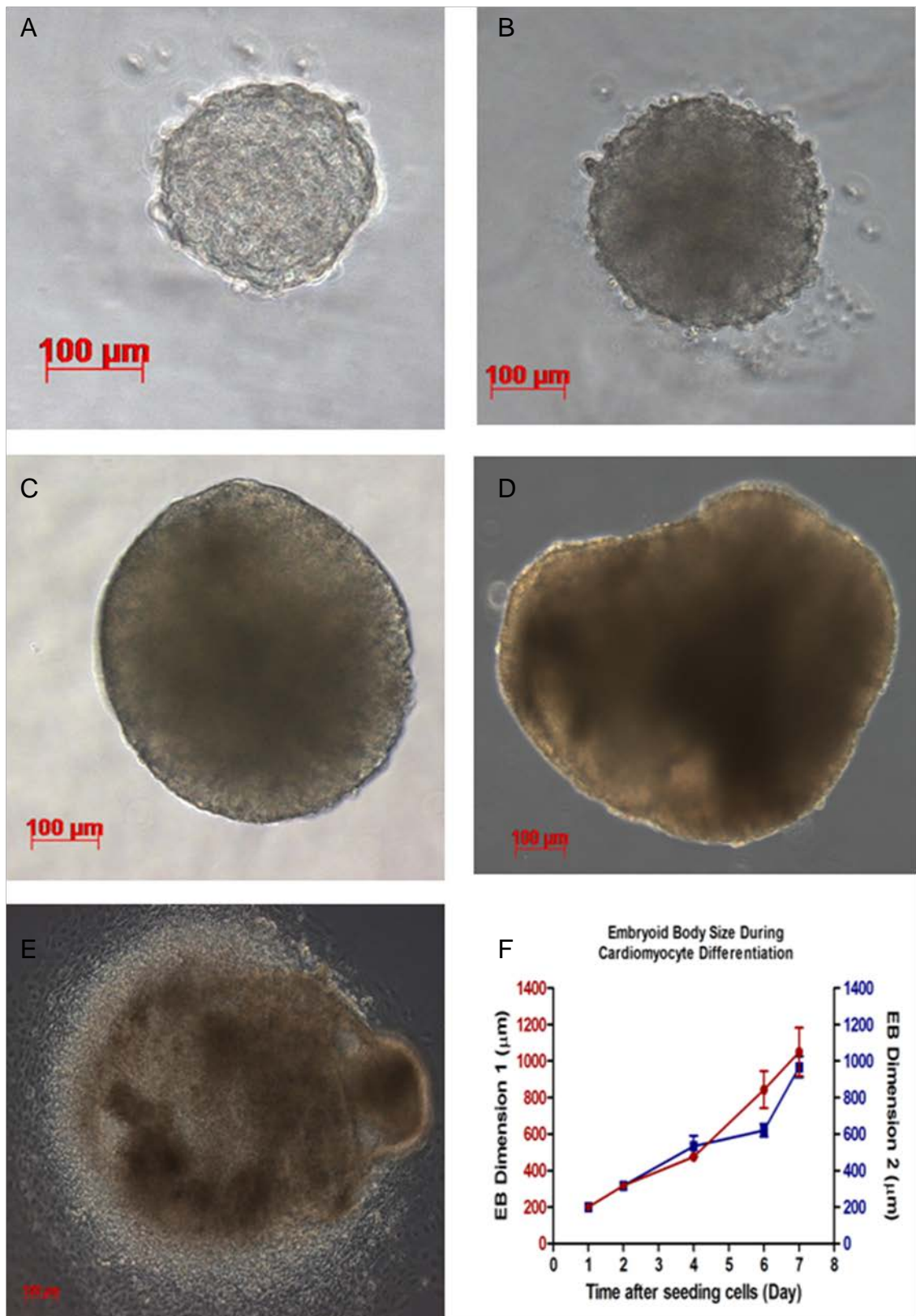
Figure 3.16 – Increasing EB size during cardiomyocyte differentiation. EB size in suspension culture at (A) day 1, (B) day 2, (C) day 4, (D) day 6 and after plating on (E) day 7. (F) Changes in EB 2-dimensional xy-plane dimensions (data are ± SD, (n= 72)).

3.3.5.7 Expression of Cardiac Marker Genes During Differentiation

Differentiation of E14Tg2a.4 mES cells in to cardiomyocytes was assessed by expression of genes encoding for cardiac structural proteins Myh6, Tnni3, Tcap and Myl2, transcription factors Mef2c, Tbx2, Nkx2.5 and Gata4, ion channels Slc8a1, Ryr2 and Atp2a2 and Phase I metabolizing enzyme Cyp1b1. Cultures were differentiated using 10 µM ascorbic acid, RNA was extracted on day 10, 12, 15, 20 and 24 of differentiation and cardiac gene expression was assessed by RT-PCR. The expression of target genes in cultures differentiated for 10, 12, 15 and 20 days was compared with cultures differentiated for 25 days by one-way ANOVA with post hoc Dunnett's test (Figures 3.17 and 3.18). The expression of Nkx2.5 (Figure 3.18B) and Tbx2 (Figure 3.18C) stabilised after 12 days of differentiation with no significant difference being observed between cultures differentiated for 12, 15, 20 and 24 days. No significant increase in the expression of Slc8a1 (Figure 3.17B), Myl2 (Figure 3.17F) and Ryr2 (Figure 3.18D) was observed between cultures that had been differentiated for 15, 20 and 24 days. Expression of Myh6 (Figure 3.17A), Mef2c (Figure 3.17C), Tnni3 (Figure 3.17D), Tcap (Figure 3.17E), Cyp1b1 (Figure 3.18E) and Atp2a2 (Figure 3.18F) increased until day 20 of differentiation with no significant difference in expression being observed between cultures differentiated for 20 and 24 days. At day 10 of differentiation the expression of Atp2a2 was similar to expression levels found in in undifferentiated cells. The expression of Gata4 (Figure 3.18A) increased during early differentiation but then began to decrease after day 12 of differentiation. Expression of Gata4 between cultures differentiated for 20 and 24 days did not differ significantly. These data illustrated that expression of cardiac marker genes increased until day 20 of differentiation and between days 20 and 24, expression

of all 12 genes stabilised. Post EB attachment differentiation of E14Tg2a.4 mES cultures was undertaken in 10 cm gelatin coated tissue culture plates with 72 EBs being plated into each dish. By day 24 of differentiation cultures were highly confluent and the lack of space for cell growth began to have detrimental effects on the cells resulting in cells peeling off from the culture plates. For all further experimentations cultures were differentiated using ascorbic acid and used between days 20 and 24 of differentiation as significant differences in cardiac gene expression and cell health were not observed between these time points.

3.3.5.8 Morphology of E14Tg2a.4 mES Cells Differentiated into Cardiomyocytes

EBs were differentiated into cardiomyocytes for a period of 24 days using 10 µM ascorbic acid. Differentiation cultures consisted of 72 EBs that were seeded into 10 cm gelatin coated tissue culture plates on day 6 of differentiation. It was observed that the proximity of attached EBs to each other influenced the morphology of the cells that grew out from the parental EBs. Outgrowth of cells from single EBs, which did not directly neighbour other EBs, was predominantly unidirectional with cells growing in a multi-layer (Figure 3.19A). By day 24 of differentiation, the site of attachment of original the EB was still visible and contracting cells were observed within this area. When two EBs attached in proximity to each, cells grew outwards from each EB, in the direction of the other EB (Figure 3.19B). These cells also grew in a multi-layer but formed myofibril like structures. With these cultures, contracting cells were observed in both the parental EBs and the fibre like structures that had formed between the two EBs.
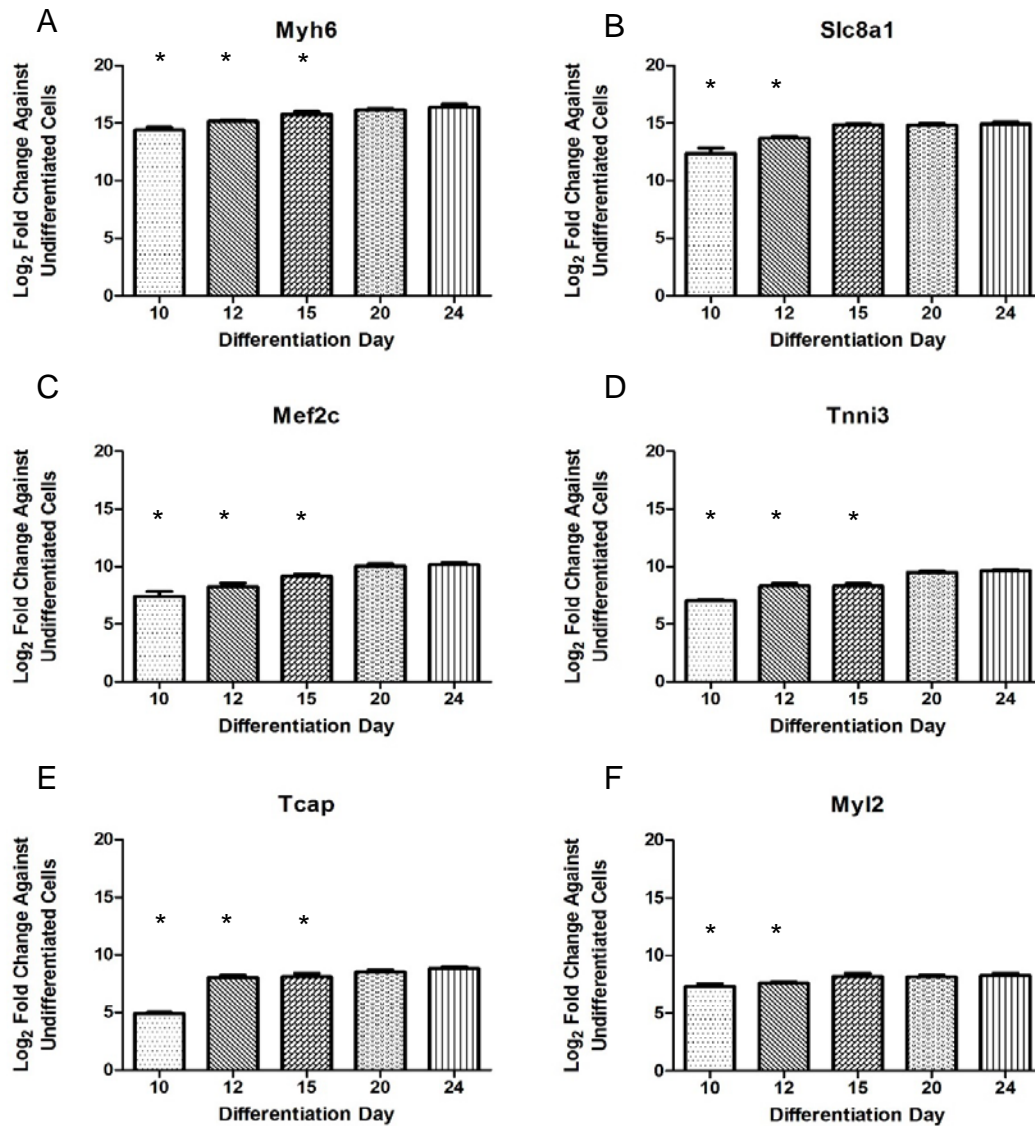
Figure 3.17 – Changes in cardiac gene expression during differentiation of E14Tg2a.4 mES cells into cardiomyocytes. E14Tg2a.4 mES cells were differentiated into cardiomyocytes using medium supplemented with 10 µM ascorbic acid. RT-PCR analysis was used to assess the expression of the cardiac structural genes (A) Myh6, (D) Tnni3, (E) Tcap and (F) Myl2, the cardiac ion channel (B) Slc8a1 and the cardiac transcription factor (C) Mef2c after 10, 12, 15, 20 and 24 days of differentiation. Expression of cardiac marker genes increased in a time dependent manner with no significant difference observed in expression levels between 20 and 24 day old cultures(data are mean ± SD (n=3), with results statistically significant at $*p < 0.05$ for each time point compared with day 24 cells by one-way ANOVA with post hoc Dunnett's test).
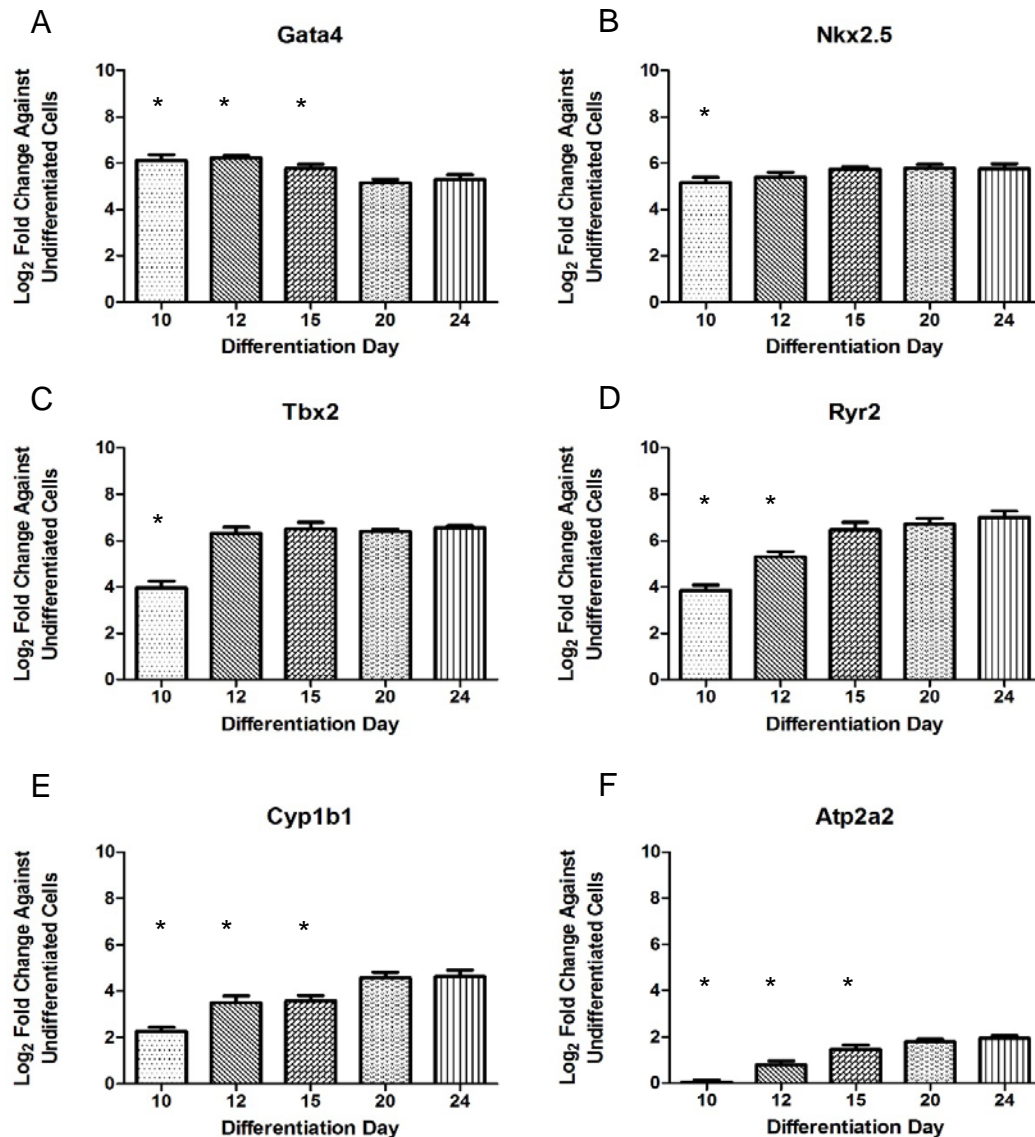
Figure 3.18 – Changes in cardiac gene expression during differentiation of E14Tg2a.4 mES cells into cardiomyocytes. Cardiac differentiation of E14Tg2a.4 was induced using medium supplemented with 10 µM ascorbic acid. RT-PCR analysis was used to assess the expression of the mesodermal transcription factors (A) Gata4, (C) Tbx2, cardiac transcription factor (B) Nkx2.5, cardiac ion channels (D) Ryr2, (F) Atp2a2 and Phase I metabolising enzyme (E) Cyp1b1 after 10, 12, 15, 20 and 24 days of differentiation. Expression of cardiac marker genes increased in a time dependent manner with no significant difference observed in expression levels between 20 and 24 day old cultures (data are mean ± SD (n=3), with results statistically significant at *$p < 0.05$ for each time point compared with day 24 cells by one-way ANOVA with post hoc Dunnett's test).
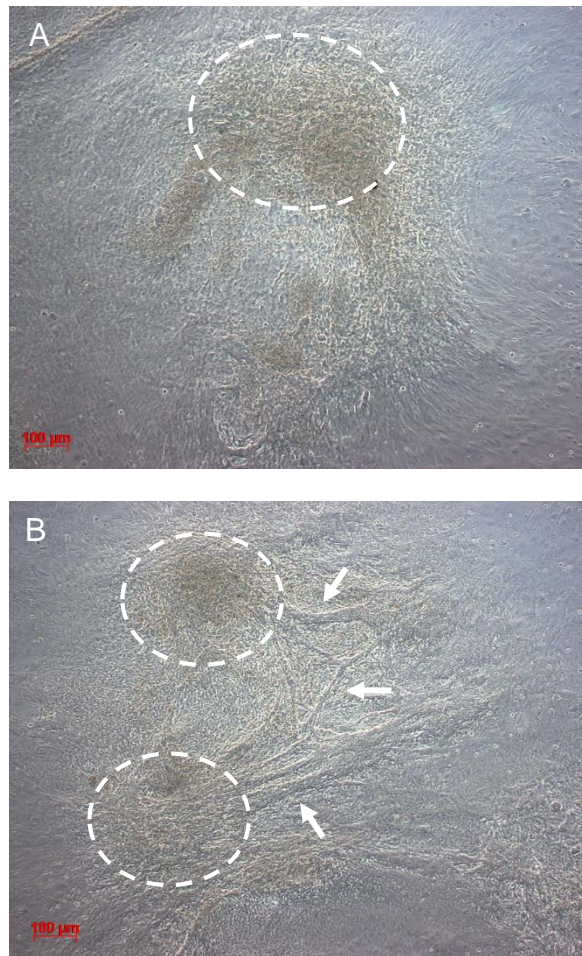
Figure 3.19 – Morphology of E14Tg2a.4 mES cells after 24 days of differentiation in medium supplemented with ascorbic acid. Differentiation of E14Tg2a.4 mES cells was initiated via EB formation in LIF free medium supplemented with 10 µM ascorbic acid. On day 6 of differentiation 72 EBs were seeded into each 10 cm gelatinised cell culture plate. After 24 hours EBs attached to the plates and continued to grow and contract (contracting areas enclosed by the dashed border) for up to 24 days. Growth of cells outwards from the EBs was influenced by proximity of attached EBs to each other. (A) Single EBs that did not neighbour other EBs on the plate remained compact and over 24 days unidirectional outgrowth of cells from the central EB was observed. (B) Where EBs attached in close proximity to each other outgrowth of cells form each EB occurred in the direction of the other EB. This lead to the formation of myofibril like structures (→), which contracted for the duration they were kept in culture.

3.3.5.9 Visualization of Cardiac Structural Proteins in Differentiated Cells

E14Tg2a.4 mES cells were differentiated into cardiomyocytes for 22 days via EB formation using medium supplemented with 10 µM ascorbic acid. EBs are 3-dimensional spherical structures, which upon attachment to cell culture surfaces, flatten out but continue to grow as a multi-layer of cells. Cells were isolated from EB cultures after 23 days of differentiation and seeded onto gelatin coated glass coverslips. The cells that attached to the coverslips (cells were then at day 24) were stained for the presence of cardiac structural proteins using the Millipore Cardiomyocyte Characterization kit. Expression of tropomyosin (Figure 3.20), actinin, atrial natueric peptide (ANP), troponin I and desmin (Figure 3.21) was detected in these cells. Varying levels of tropomyosin were detected in the cell cultures, indicating different degrees of differentiation amongst the cells by day 24. Three different intensities of tropomyosin staining are visible in Figure 3.20. Cell 1, contained very little expression of tropomyosin and this was localized to the nucleus border. Increased expression was observed in cell 2, which again bordered the nucleus but had begun to expand outwards. The intensity of tropomyosin in cell cluster 3 was much greater and cross-linking of tropomyosin between neighbouring cells was observed. The differences in staining intensity indicate that cells within a culture differentiated at different rates and cross-linking of tropomyosin staining in cell cluster 3 indicates that these cells were more differentiated than cells 1 and 2. Localization of actinin, ANP, troponin I and desmin staining within the cells varied. Staining of actinin (Figure 3.21A) and ANP (Figure 3.21B) was elongated whereas desmin (Figure 3.21C) and troponin I (Figure 3.21D) expression was localised around the nucleus. Staining of ANP was also detected within the nucleus of the cells. These results illustrated that in

addition to expression of cardiac marker genes, cells differentiated for 24 days using 10 µM ascorbic acid also expressed structural cardiac proteins.
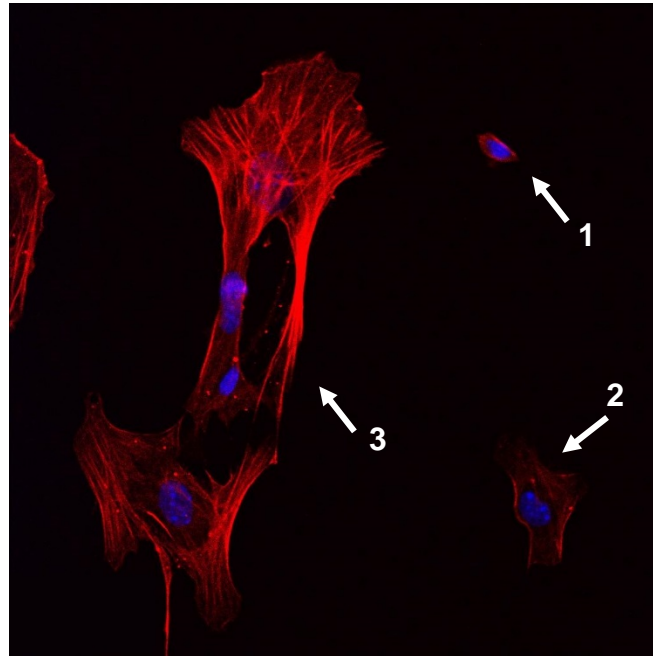
Figure 3.20 – Immunostaining of E14Tg2a.4 mES cell derived cardiomyocytes for the presence of tropomyosin. E14Tg2a.4 mES cells were differentiated via EB formation for 22 days using 10 µM ascorbic acid. Cultures were then disaggregated and cells were seeded on to gelatin coated glass cover slips. Cells were 24 days old when they were fixed stained for the presence of tropomyosin (red) and Hoechst 33342 was used for nuclear staining (blue). Variances in the expression of tropomyosin illustrated that individual cells within the EB were at different stages of differentiation. (1) Very little tropomyosin expression indicates the cell is at an early stage of cardiac differentiation. (2) Localisation of tropomyosin around the nucleus shows a partially differentiated cell. (3) Presence of elongated tropomyosin staining and cross-linking of tropomyosin between multiple cells illustrated the presence of mature differentiated cardiomyocytes.
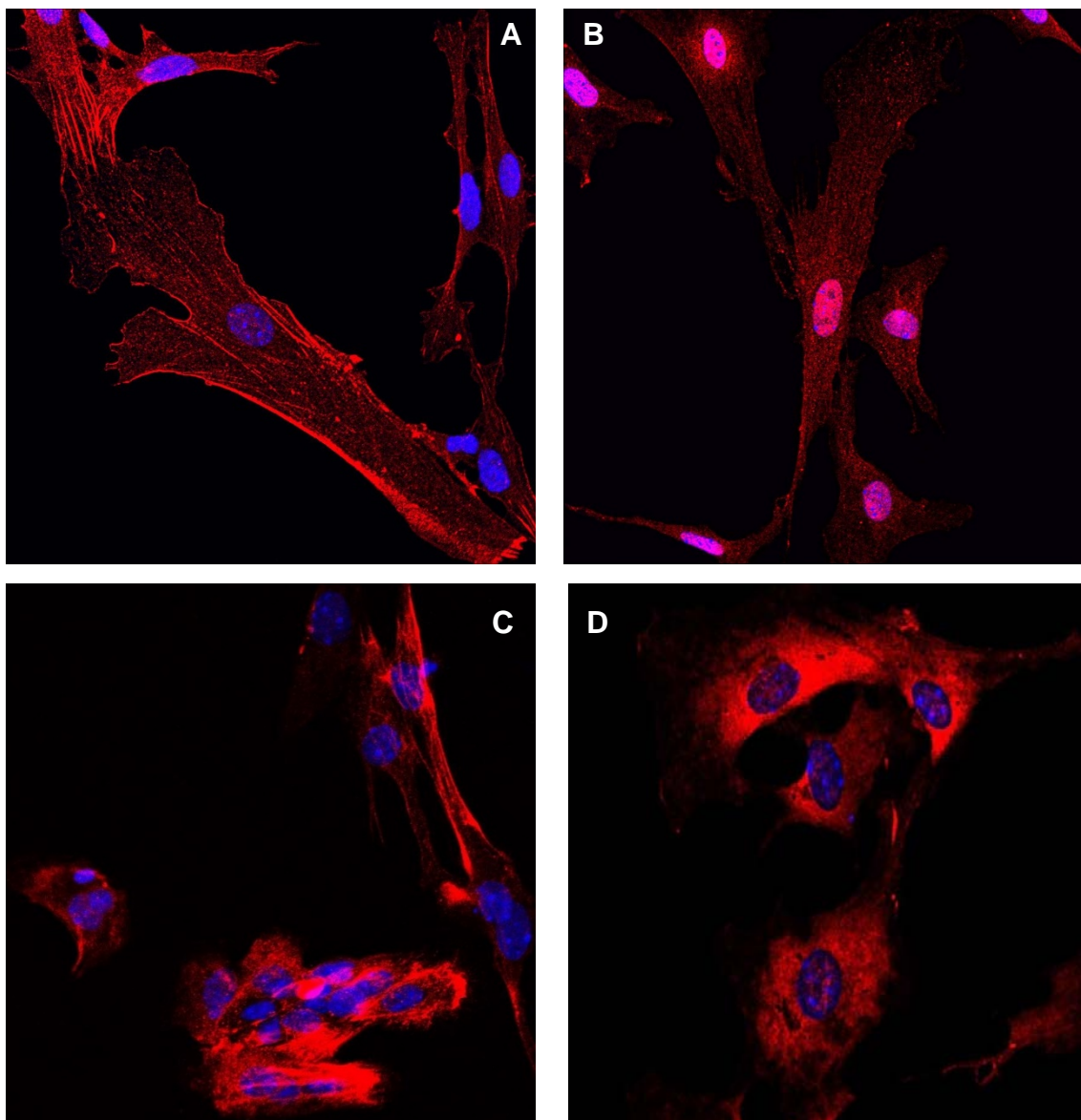
Figure 3.21 – Immunostaining of E14Tg2a.4 mES cell derived cardiomyocytes for the presence of (A) actinin, (B) atrial natriuretic peptide (ANP), (C) desmin and (D) troponin I. E14Tg2a.4 mES cells were differentiated via EB formation for 22 days using 10 µM ascorbic acid. Cultures were then disaggregated and cells were seeded on to gelatin coated glass cover slips. Cells were 24 days old when they were fixed stained for the presence of (A) actinin (red), (B) ANP (red) (C) desmin (red) and (D) troponin I (red) with Hoechst 33342 used for nuclear staining (blue). Localization of actinin, ANP, troponin I and desmin within the cells varied. Staining of (A) actinin and (B) ANP was elongated across the cells and presence of ANP was also found in the nucleus. Expression of (C) desmin and (D) troponin I was localised around the nucleus.

3.3.5.10 Identification & Isolation of Pure Cardiomyocytes Based on Mitochondrial Content

The earliest observation of contracting cells, during differentiation of E14Tg2a.4 mES cells into cardiomyocytes using medium supplemented with 10 µM ascorbic acid, was observed in 3 day old EBs. By day 12 of differentiation all EBs contained spontaneously contracting clusters of cells. These clusters continued to increase in size as differentiation progressed. Staining differentiated cells with cardiac structural proteins such as tropomyosin indicated that after 22 days of differentiation the cells within the cultures were at different stages of maturation. This indicated that differentiation of stem cells into cardiomyocytes using ascorbic acid resulted in a heterogeneous cell population consisting of mature and immature cells of the desired phenotype but potentially other cell types too. It has been reported that differentiation of stem cells results in a heterogeneous population of cells (Keller, 2005). The ability to isolate fully differentiated cells from stem cell cultures is highly desirable especially for the use of differentiated stem cells as regenerative therapies and as *in vitro* models for use during drug development. There is a potential for cell sorting to be utilised for isolation of desired cell populations however advances in this field are restricted by an absence of cell specific surface antigens. Although cell specific markers are available they are all intracellular markers, meaning that the cells are not viable for further culture and use post isolation (Mummery, 2010). In 2010 a novel technique for the isolation of differentiated cardiomyocytes was reported by Hattori et al (2010). This method involved selection of electrically active cardiomyocytes from differentiated stem cell cultures based on the fluorescence intensity of the mitochondrial specific dye TMRM. The principle of this technique

119

was based on observations of increased mitochondrial content in contracting primary mouse cardiomyocytes. When stained with TMRM, the cells with the most mitochondrial content had the highest fluorescence intensity and thus this criterion was utilized to isolate contracting cardiomyocytes from differentiated stem cell cultures. This technique was utilized to isolate a population of mature contracting cardiomyocytes from cultures of E14Tg2a.4 mES cells that had been differentiated using 10 µM ascorbic acid for 24 days. Differentiated cultures were dispersed to generate a cell suspension consisting of single cells, which was stained with TMRM and cells were sorted based on TMRM fluorescence by FACS (Figure 3.22). The cell suspension passed through a two–step sorting process, in sort 1 viable cells were selected from the parental cell population, this filtered out 14.1% of the cells. In sort 2, cells that had the highest TMRM fluorescence intensity were selected. These cells only accounted for 1.7% of the sort 1 cell population and 1.4% of the parental cell population. The collected cells were re-plated and after attachment some cells continued to spontaneously contract. Each EB was formed using 500 cells and 72 EBs were plated into 10 cm cell culture dishes on day 6 of differentiation. Pooling six culture plates on day 24 of differentiation produced a cell suspension consisting of an average of 2,200,000 cells and of this population approximately 30,000 cells were identified as having the highest mitochondrial content. Following the method published by Hattori et al (2010) it was possible to select a sub-population of differentiated cardiomyocytes, which had the highest mitochondrial content, however, this sub-population was very small and not all of the cells continued to spontaneously contract in culture and those that did contracted at different rates. Furthermore, it was observed that isolated cells did not proliferate, indicating a terminally

differentiated cardiomyocyte phenotype as adult cardiomyocytes *in vivo* do not proliferate.

The yield of pure cardiomyocytes after FACS isolation was very small and it was not possible to generate sufficient number of cells for use in drug treatment assays. Typically, 30,000 cells were isolated from a pool of six 10 cm cell culture plates containing a total of 432 EBs, thus providing only enough cells to seed into one well of 96-well plate. The yield of isolated cells was also lower than expected following observation of differentiated EB cultures, wherein large areas of contracting cells were observed implying that cultures contained a larger number of contracting cardiomyocytes. Expression of cardiac marker genes in cultures of differentiated EBs and in cells isolated from EBs by FACS was assessed by RT-PCR (Figure 3.23). Expression of genes encoding for cardiac structural proteins Myh6, Tnni3, Tcap and Myl2, transcription factors Mef2c, Tbx2, Nkx2.5 and Gata4, ion channels Slc8a1, Ryr2 and Atp2a2 and Phase I metabolizing enzyme Cyp1b1 did not differ between the intact EB cultures and the FACS isolated cells. It was therefore more practical and time and cost effective to use cultures of differentiated EBs in drug treatment assays than cultures of isolated cells.

Bright field and florescent images were taken of spontaneously contracting areas of differentiated EBs (Figure 3.24). It was observed that the highest florescence of TMRM was found in cells located within spontaneously contracting areas.

(A) Sort 1

(B) Sort 2

Cells were selected by highest TMRM fluorescence intensity and re-plated

C

D

E
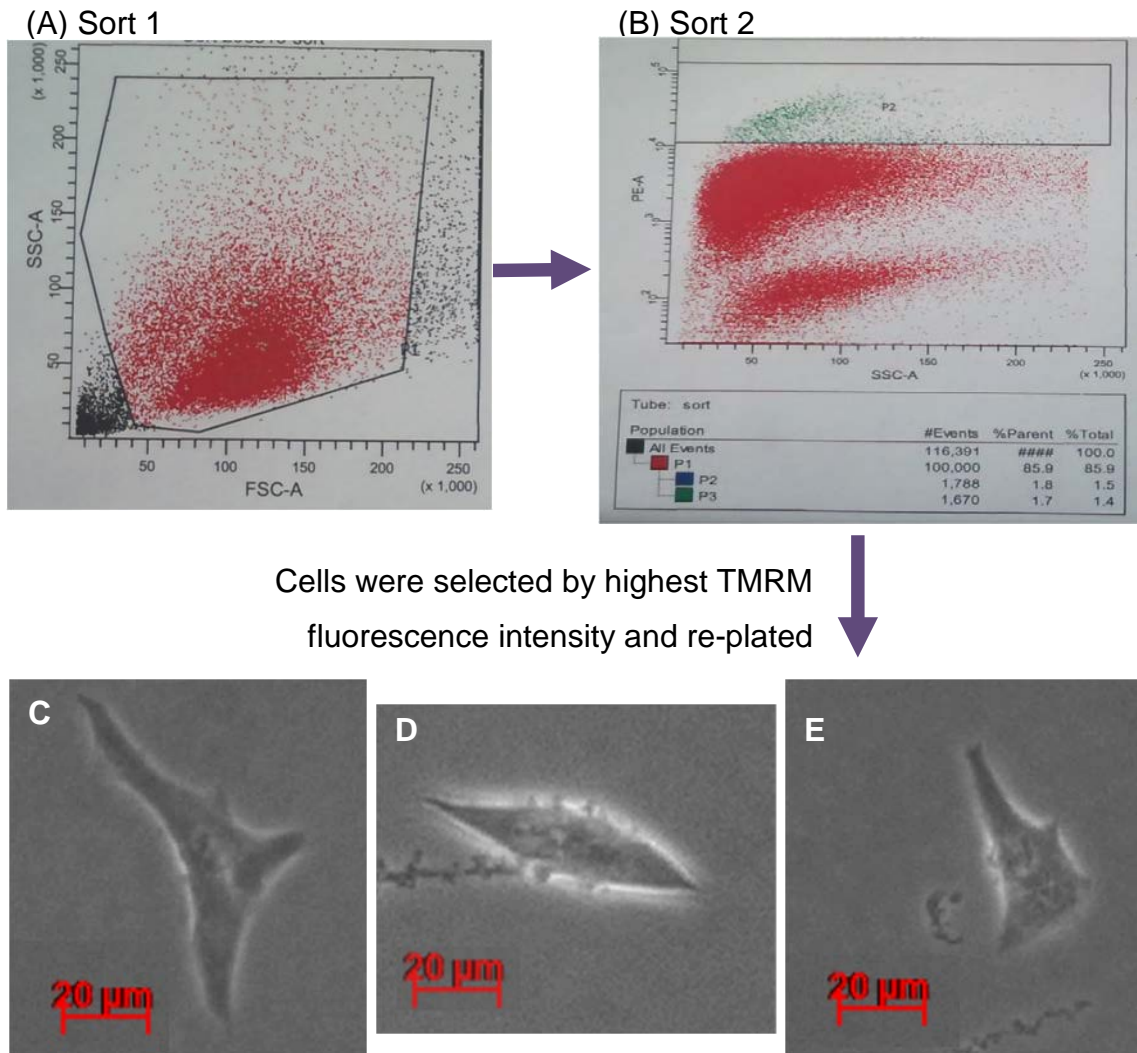
Figure 3.22 – Selection of contracting mES derived cardiomyocytes by fluorescence activated cell sorting. E14Tg2a.4 mES cells were differentiated via EB formation for 22 days using 10 μM ascorbic acid. Cultures were then disaggregated to generate a suspension of single cells containing 2-2.2 x 10^6 cells, cells were loaded with 10 nM TMRM, a mitochondrial specific dye and isolated by FACS. (A) Sort 1 selected viable cells from the whole population. (B) Sort 2 isolated the cells with the highest TMRM fluorescence from the viable population. Cells were collected and seeded into gelatin coated plates. (C-E) Post attachment morphology of the cells varied. Some cells lost the ability to contact and cells that continued to contract in culture did so at varying rates. No cell proliferation was observed in cultures of isolated cells. Isolation of differentiated cardiomyocytes using FACS was undertaken on three separate occasion and on average 1.8% of the parental population was isolated based on these cells having the highest TMRM fluorescence.
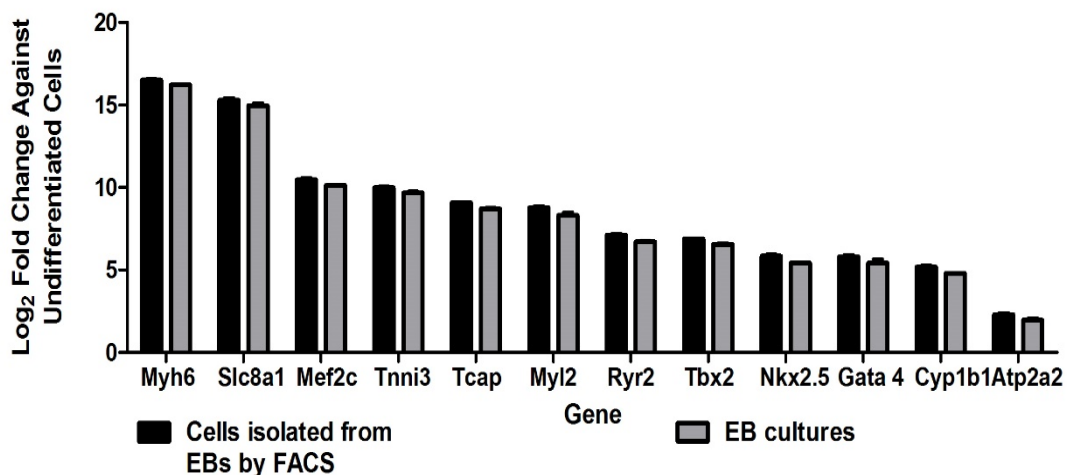
Figure 3.23 – Comparison of cardiac marker gene expression between cells isolated from EBs by FACS and intact EB cultures. E14Tg2a.4 mES cells were differentiated into cardiomyocytes via EB formation using 10 µM ascorbic acid. RNA was extracted from EB cultures that had been differentiated for 24 days and from cells that had been isolated from 22 day old EB cultures using FACS. These cells were sorted by FACS on day 22 of differentiation, re-plated and RNA was extracted on day 24. RT-PCR analysis was used to assess the expression of the cardiac structural genes Myh6, Tnni3, Tcap, Myl2, the cardiac ion channels Slc8a1, Ryr2, Atp2a2, the cardiac transcription factors Mef2c, Nkx2.5 the mesodermal transcription factors Tbx2, Gata4 and the Phase I metabolising enzyme Cyp1b1. Expression of all 12 cardiac marker genes was equivalent between the two cell populations (data are mean ± SD (n=3), results are not statistically significant with p >0.05 for comparison of gene expression across both cell populations).
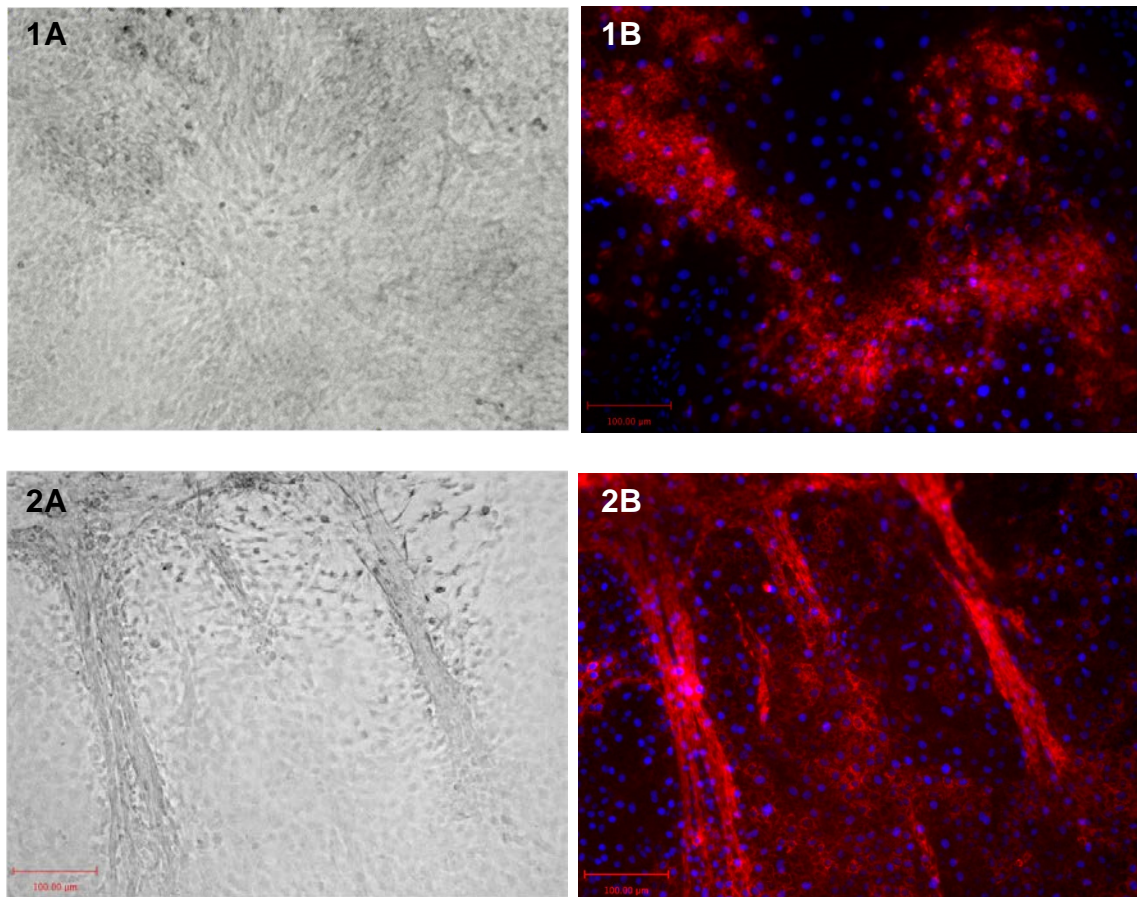
Figure 3.24 – Visualisation of cells containing the most mitochondria in cultures of mES cell derived cardiomyocytes. E14Tg2a.4 mES cells were differentiated into cardiomyocytes using 10 µM ascorbic acid. On day 24 of differentiation cultures of contracting EBs were stained with TMRM (red) and Hoechst 33342 (nuclear stain – blue). (A) Bright field and (B) fluorescent images were obtained for the same field. The morphology of contracting cell clusters was observed as being either (1) large areas of multilayer cell growth or (2) myofibril like structures on top of a monolayer of cells. Comparison of brightfield and fluorescent images of the same viewing field illustrated that the contracting cells within differentiated cultures had the greatest TMRM fluorescence and thus these cells contained the highest number of mitochondria.

3.3.5.11 Intracellular Calcium Fluctuations in Spontaneously Contracting Differentiated Cardiomyocytes

Contraction of cardiomyocytes is controlled by action potentials, which are generated via intracellular calcium fluctuations (Fleckenstein, 1977). Intracellular calcium fluctuations were measured in differentiated cardiomyocytes that had been isolated from EBs using FACS. Isolated cells were plated on to gelatin coated glass coverslips and loaded Fura-2 AM, a calcium specific dye. Movement of calcium ions within the cells was measured by fluorescence microscopy. It had previously been noted that the contractions of differentiated cultures was temperature dependent with contractions becoming slower as cell temperature dropped below $37^{\circ}C$. To minimise the effect of temperature change on cell contractions and subsequently intracellular calcium fluctuations, calcium imaging was done using a microscope with a stage heated to $37^{\circ}C$. After isolation of cells by FACS it had been observed that the beating rate of the isolated cardiomyocytes varied and some cells did not contract at all, even when cultures were kept at $37^{\circ}C$. This variance between cells was reflected in the recorded intracellular calcium oscillations in the isolated cells (Figure 3.25). Some cells displayed rhythmic rises and falls in intracellular calcium levels (Figure 3.25A), some had more sporadic changes and in some cells the concentration of intracellular calcium remained constant (Figure 3.25B). The data showed that the spontaneous contraction of the differentiated cells corresponded to changes observed in intracellular calcium levels.
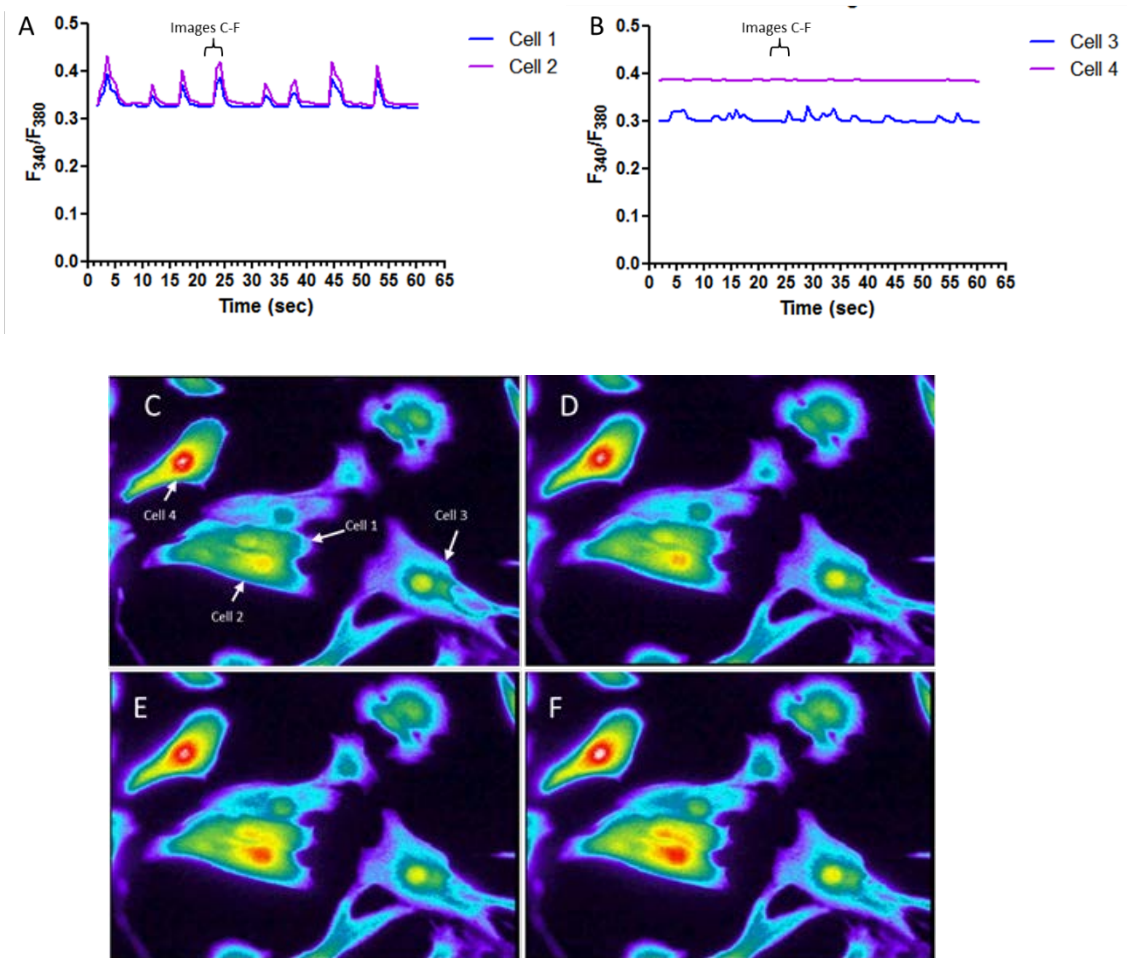
Figure 3.25 – Intracellular calcium oscillations in cardiomyocytes isolated from EBs. Spontaneous intracellular Ca^{2+} fluctuations in day 24 mES cell derived cardiomyocytes were measured using the calcium specific dye Fura-2 AM. Intracellular calcium levels varied amongst cells with some cells displaying rhythmic rises and falls in Ca^{2+} levels (A) whilst other cells had irregular or no changes (B). Images C-F are pseudo-colour images of the changes in calcium over a 5 sec period, as marked on graphs A and B. The cells numbered in image C correspond to the cells on graphs A and B.

3.3.5.12 Comparison of Cardiac Marker Gene Expression in Differentiated Cardiomyocytes and in Neonatal and Adult Heart Tissue

E14Tg2a.4 mES cells were differentiated into cardiomyocytes for 24 days using 10 µM ascorbic acid. The expression of cardiac marker genes in differentiated cells was compared to gene expression in heart tissue from neonatal and adult mice. Expression of genes encoding for cardiac structural proteins Myh6, Tnni3, Tcap and Myl2, transcription factors Mef2c, Tbx2, Nkx2.5 and Gata4, ion channels Slc8a1, Ryr2 and Atp2a2 and Phase I metabolizing enzyme Cyp1b1 in differentiated cells and heart tissue was assessed by RT-PCR. In comparison to heart tissue from a 2 day old mouse (Figure 3.26A) and from a 8 week old mouse (Figure 3.26B), differentiated cardiomyocytes had significantly lower levels of expression of Myh6, Myl2, Atp2a2, Slc8a1, Gata4, Tcap, Ryr2 and Tnni3. Differentiated cardiomyocytes had significantly greater expression of Cyp1b1 compared to heart tissue from a 2 day old mouse but had similar Cyp1b1 expression levels to those found in heart tissue from an 8 week old mouse.
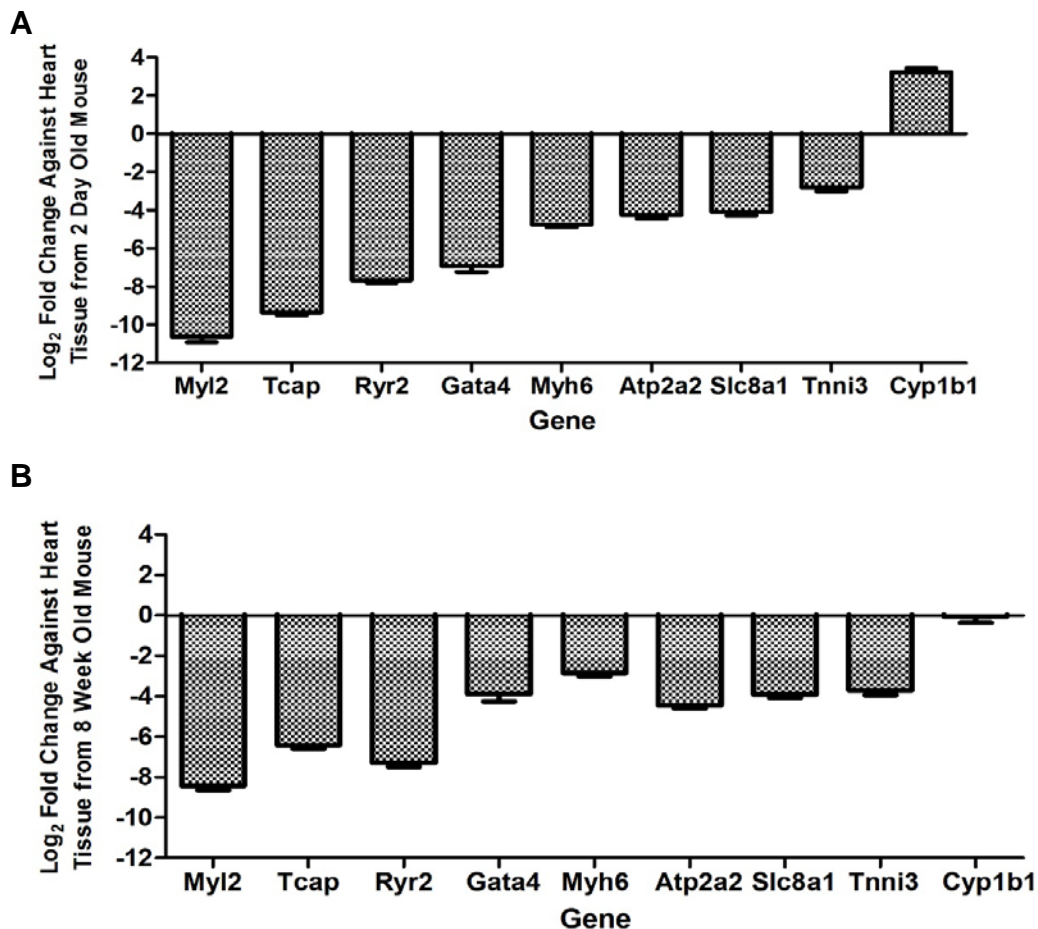
Figure 3.26 – Comparison of cardiac gene expression of mES cell derived cardiomyocytes and heart tissue from neonatal and adult mice. E14Tg2a.4 mES cells were differentiated into cardiomyocytes using 10 µM ascorbic acid for 24 days. RT-PCR analysis was used to compare the expression of the cardiac structural genes Myh6, Myl2, Tcap Tnni3, the cardiac ion channels Atp2a2, Slc8a1, Ryr2, the mesodermal transcription factor Gata4 and the Phase I metabolising enzyme Cyp1b1 in differentiated cardiomyocytes and heart tissues from a (A) 2 day old mouse and (B) 8 week old mouse. Differentiated cardiomyocytes had significantly lower levels of genes encoding for cardiac structural proteins, transcription factors and ion channels compared to expression levels found in neonatal and adult heart tissue. Expression of the gene encoding for the Phase I metabolising enzyme Cyp1b1 was significantly higher in differentiated cardiomyocytes than in neonatal tissue. However, the expression level of Cyp1b1 in stem cell derived cardiomyocytes was similar to levels found in adult heart tissue (data are mean ± SD (n=3), results are statistically significant at $p < 0.05$ for comparison of all genes except Cyp1b1 in 8 week old mice).

3.3.6 Development of Protocols for Differentiation of E14Tg2a.4 mES Cells into Hepatocytes

3.3.6.1 Optimising Medium Composition for Differentiation

Several LIF free medium compositions were trialled to induce differentiation of E14Tg2a.4 mES cells into hepatocytes via EB formation. Hep-basal medium (composed of IMDM medium, l-glutamine (1x), sodium pyruvate (1x), non-essential amino acids (1x) and β-mercaptoethanol (0.1 mM)) was supplemented with different concentrations and combinations of FCS, sodium butyrate, dexamethasone (Dex) and insulin-transferrin-selenium (ITS) supplement to induce differentiation of E14Tg2a.4 mES cells into hepatocytes (Table 3.1).

Medium Terminology	Medium Components in addition to Hep-basal medium
Hep-medium 1	15% FCS
Hep-medium 2	5% FCS
Hep-medium 3	4% FCS, 1% ITS and 10^{-7} M Dex
Hep-medium 4	15% FCS and 1 mM sodium butyrate

Table 3.1: Hep-medium compositions. Supplements added to Hep-basal medium (composed of IMDM medium, l-glutamine (1x), sodium pyruvate (1x), non-essential amino acids (1x) and β-mercaptoethanol (0.1 mM) for use in differentiation of E14Tg2a.4 mES cells into hepatocytes.

The first medium trialled for hepatocyte differentiation was termed Hep-medium 1 and was composed of Hep-basal medium supplemented with 15% FCS. EBs formed with Hep-medium 1 were cultured in suspension until day 6 after which

they were seeded into gelatinised plates and kept in culture till day 25. At this point RNA was extracted from the differentiated cultures and RT-PCR was used to assess the expression of the pluripotency genes Nanog and Pou5f1, the endoderm transcription factors Sox17 and Hnf4a, the foetal liver marker Afp and the genes Alb, Foxa2, Ttr, Slco1b2, Cyp7a1 and Cyp3a11, which are markers of metabolically active hepatocytes. The student's t-test was used to determine significant differences in gene expression between differentiated and undifferentiated cells (Figure 3.27). Cells differentiated using Hep-medium 1 had significantly lower levels of Pou5f1 and Nanog expression compared to undifferentiated cells, indicating loss of pluripotency with use of Hep-medium 1. Hep-medium 1 induced increased expression of the hepatic marker genes Afp, Alb, Hnf4a, Foxa2, Ttr and Sox17. Differentiated cultures were also assessed for the expression of Cyp7a1, Cyp3a11 and Slco1b2, however expression of these genes were not detected in cultures differentiated using Hep-medium 1. Although there was increased expression of hepatic marker genes in cultures differentiated using Hep medium 1, these cultures also contained clusters of contracting cells, indicating that a sub-population of cells had differentiated along the mesoderm lineage towards a cardiomyocyte phenotype.

To reduce the formation of the mesoderm germ layer and to enhance formation of the endoderm germ layer the concentration of FCS was reduced from 15 to 5%; this medium was termed Hep-medium 2. This method was adapted from protocols using low FCS concentrations for the differentiation of hES cells into hepatocytes (D'Amour et al., 2005, Agarwal et al., 2008). It was observed that the EBs formed using Hep-medium 2 were much smaller than the EBs that had been produced using Hep-medium 1. Furthermore, after being seeded into gelatinised

tissue culture plates on day 6 of differentiation, these smaller EBs failed to attach. This implied that components of FCS were critical for the formation of viable EBs from mES cells and that low FCS concentration inhibited proliferation of the cells hence the reduced size of the EBs. Hep-medium 2 was discarded because the EBs produced using this medium did not attach to tissue culture plates for further growth and differentiation.
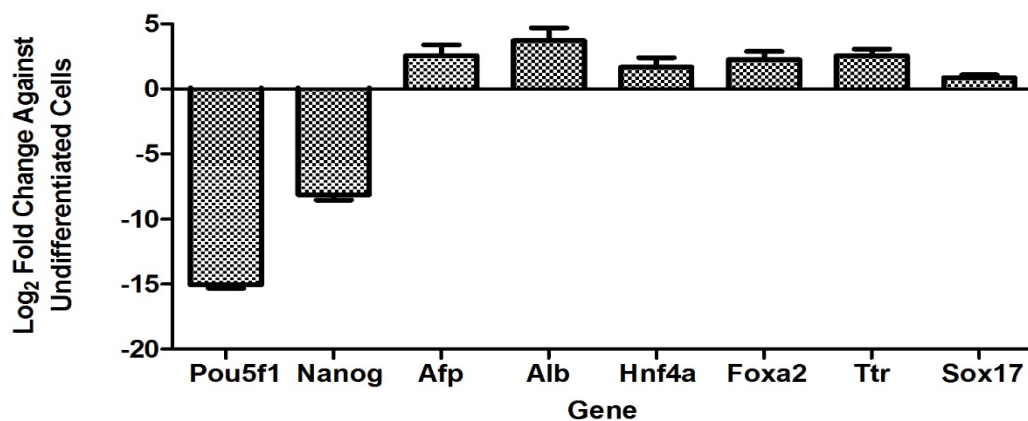
Figure 3.27 – Expression of pluripotency and hepatic marker genes in E14Tg2a.4 mES cells differentiated in Hep-medium 1. E14Tg2a.4 mES cells were differentiated into via EB formation using Hep-medium 1 for 25 days. RT-PCR analysis of 25 day old cultures showed decreased expression of the pluripotency genes Nanog and Pou5f1 and increased expression of the endoderm transcription factors Sox17 and Hnf4a, the foetal liver marker Afp and the genes Alb, Foxa2 and Ttr, which are markers of metabolically active (data are mean ± SD (n=3), with results statistically significant at $p < 0.05$ for all genes).

To enhance differentiation of E14Tg2a.4 mES cells into hepatocytes a two medium protocol was designed. Firstly EBs were formed using Hep-medium 1 and were seeded into gelatinised tissue culture plates on day 6 using this medium. EBs attached within 24 hours after being seeded following which the differentiation medium was changed to Hep-medium 3. EB cultures were

maintained in Hep-medium 3 till day 25 after which RNA was extracted and expression of pluripotency and hepatocyte marker genes was assessed by RT-PCR (Figure 3.28). Cells differentiated using Hep-medium 3 had significantly lower levels of Pou5f1 and Nanog expression compared to undifferentiated cells, indicating loss of pluripotency with use of Hep-medium 3. Hep-medium 3 induced increased expression of the hepatic marker genes Afp, Alb, Hnf4a, Foxa2, Ttr, Sox17, Cyp7a1 and Cyp3a11. Expression of Slco1b2 was tested for but not detected in cultures differentiated using Hep-medium 3.
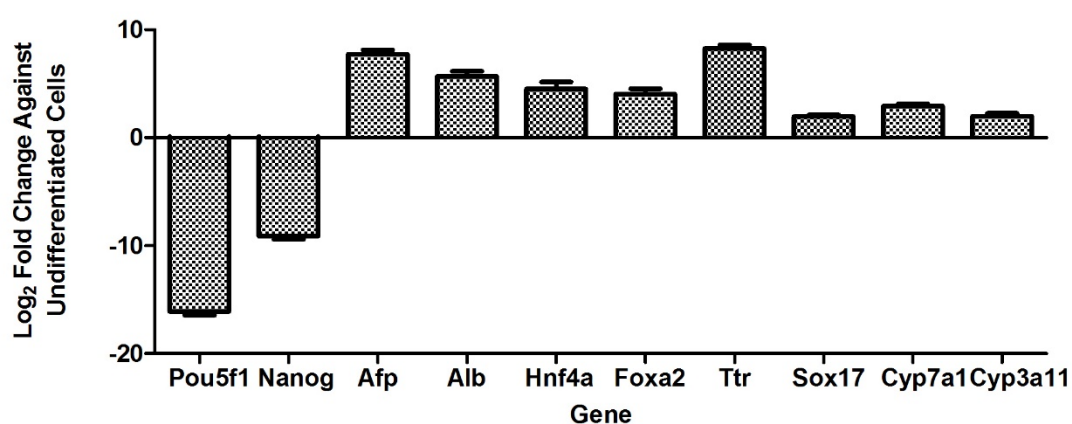
Figure 3.28 – Expression of pluripotency and hepatic marker genes in E14Tg2a.4 mES cells differentiated in Hep-medium 1 and 3. E14Tg2a.4 mES cells were formed into EBs using Hep-medium 1. On day 6 of differentiation EBs were seeded into gelatinised culture plates in Hep-medium 3. Cultures were kept in HEP-medium 3 till day 25. RT-PCR analysis of 25 day old cultures showed decreased expression of the pluripotency genes Nanog and Pou5f1 and increased expression of the endoderm transcription factors Sox17 and Hnf4a, the foetal liver marker Afp and the genes Alb, Foxa2, Ttr, Cyp7a1 and Cyp3a11, which are markers of metabolically active (data are mean ± SD (n=3), with results statistically significant at p < 0.05 for all genes).

Sodium butyrate has been reported to enhance hepatocyte differentiation of mES cells (Zhou et al., 2010). E14Tg2a.4 mES cells were seeded into ultra-low attachment U/V bottom 96-well plates in Hep-medium 4, which was composed of

15% FCS and 1 mM sodium butyrate. By day 3 of differentiation EBs were not visible and thus had failed to form indicating that sodium butyrate interfered with the process of cell aggregation. Therefore, Hep-medium 4 was not suitable for use in differentiation E14Tg2a.4 mES cells into hepatocytes.

Subsequently, differentiation cultures were set-up wherein Hep-medium 1 was used for the first 3 days of differentiation to promote EB formation. On day 4 of differentiation, Hep-medium 1 was replaced with Hep-medium 4 and cells were cultured in suspension until day 6, when they were transferred into gelatinised tissue culture plates for further growth and differentiation. However, after 72 hours EBs did not attach to the gelatinised plated and thus this differentiation attempt was unsuccessful at differentiating E14Tg2a.4 mES cells into hepatocytes. The presence of sodium butyrate may have prevented EBs from attaching to gelatinised plates. To investigate this, EBs were cultured in Hep-medium 1 for 3 days, then in Hep-medium 4 until day 6 of differentiation. At this point EBs were transferred into Hep- medium 3 and seeded into gelatinised tissue culture plates. EBs attached to the plates within 24 hours and were maintained in this medium until day 25 when RNA was extracted from the differentiated cultures. RT-PCR analysis showed decreased expression of the pluripotency genes in these cultures compared with expression in undifferentiated cells (Figure 3.29). Furthermore, increased expression of the hepatic marker genes Afp, Alb, Hnf4a, Foxa2, Ttr, Sox17, Cyp7a1, Cyp3a11 and Slco1b2 was also observed in these differentiated cultures.

Three of the tested protocols produced cells that were viable for up to 25 days and which expressed a number of hepatic marker genes. Cultures were not kept beyond 25 days because the differentiated cultures became too confluent and

cells began to detach from the tissue culture plates. Attempts were made to passage cultures, however, after trypsin treatment few cells re-attached and thus it was not a viable option to passage differentiating cultures.
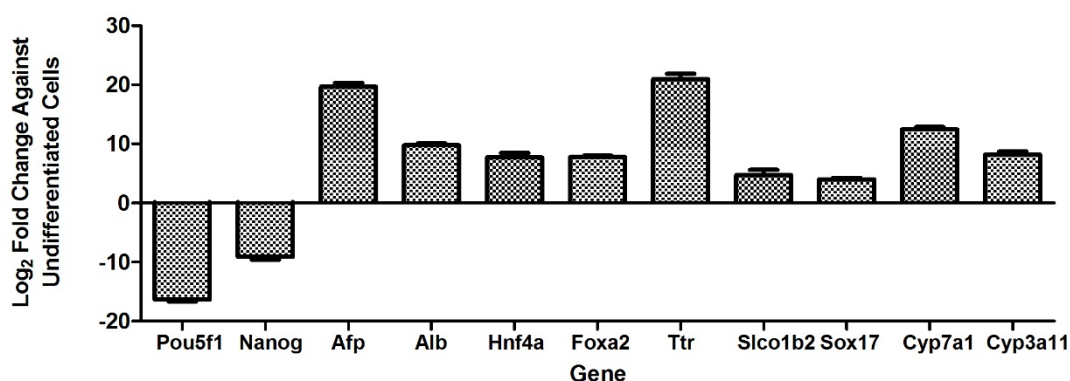
Figure 3.29 – Expression of pluripotency and hepatic marker genes in E14Tg2a.4 mES cells differentiated using a combination of Hep-medium 1, 3 and 4 for 25 days. E14Tg2a.4 mES cells were formed into EBs using Hep-medium 1. On day 3 medium was changed to Hep-medium 4 to support EB maturation. On day 6 of differentiation EBs were seeded into gelatinised culture plates in Hep-medium 3. Cultures were kept in Hep-medium 3 till day 25. RT-PCR analysis of 25 day old cultures showed decreased expression of the pluripotency genes Nanog and Pou5f1 and increased expression of the endoderm transcription factors Sox17 and Hnf4a, the foetal liver marker Afp and the genes Alb, Foxa2, Ttr, Slco1b2, Cyp7a1 and Cyp3a11, which are markers of metabolically active hepatocytes (data are mean ± SD (n=3), with results statistically significant at $p < 0.05$ for all genes).

Cultures were set up using the three successful differentiation protocols to deduce which combination of supplements induced the greatest differentiation of E14Tg2a.4 mES cells into hepatocytes (Table 3.2). The first protocol utilised Hep-medium 1 from day 0 to 25 of differentiation. The second protocol involved forming EBs using Hep-medium 1 and then changing to Hep-medium 3 after EBs had attached to gelatinised plates and maintaining cultures in this medium until

day 25. The third protocol involved forming EBs from day 0 to 3 using Hep-medium 1 followed by maturing the EBs from day 3 to 6 in Hep-medium 4. Before seeding cells into gelatinised plates the medium was changed to Hep-medium 4 and differentiated cultures were maintained in this medium until day 25.

Differentiation		Medium used for hepatocyte differentiation		
Days	Stage	Protocol 1	Protocol 2	Protocol 3
0 – 3	EB Formation	Hep-medium 1	Hep-medium 1	Hep-medium 1
3 – 6	EB Maturation	Hep-medium 1	Hep-medium 1	Hep-medium 4
6 - 25	EB attachment and outgrowth	Hep-medium 1	Hep-medium 3	Hep-medium 3

Table 3.2: Hep-medium combinations utilised for differentiation of E14Tg2a.4 mES cells into hepatocytes. Differentiation of E14Tg2a.4 mES cells was divided into 3 stages; EB formation occurred during days 0-3, EB maturation occurred during days 3-6 and EB attachment and growth occurred from day 6-25. The composition of each Hep-medium is detailed in table 3.1.

RNA was extracted from each of the differentiated cultures on day 25 and RT-PCR analysis was used to assess the expression of hepatic marker genes. Expression of target genes that were expressed with use of all three protocols were compared to expression in undifferentiated E14Tg2a.4 mES cells using one way ANOVA analysis. Where a target gene was only detected with two of the protocols, expression of the gene with use of the two protocols was compared using the student's t-test. Slco1b2 was only detected in cultures differentiated

using protocol 3 and its expression in undifferentiated and differentiated cells was compared using the student's t-test. All three differentiation protocols induced the same degree of suppression in the expression of the pluripotency regulator genes Nang and Pou5f1 (Figure 3.30). The use of FCS alone (protocol 1) increased the expression of the hepatic markers Ttr, Afp, Alb, Foxa2, Hnf4a, and Sox17 in comparison to undifferentiated cells (Figure 3.31). Decreasing the FCS concentration to 4% and supplementing differentiation medium with 1% ITS and 10^{-7}M Dex (protocol 2) on day 7 of differentiation enhanced expression of Ttr, Afp and Hnf4a in comparison to cells differentiated using protocol 1. In addition, protocol 2 induced expression of Cyp7a1 and Cyp3a11, which was not observed in cultures differentiated using protocol 1 (Figure 3.32). Protocol 3 induced the greatest expression of the hepatic marker genes Ttr, Afp, Alb, Foxa2, Hnf4a, Sox17, Cyp7a1 and Cup3a11. Furthermore, expression of the liver specific anion transporter Slco1b2 was only detected in cells differentiated using protocol 3. Protocol 3 was utilised for all further hepatocyte differentiation experiments because it induced the greatest expression of hepatic marker genes in differentiated E14Tg2a.4 mES cells.
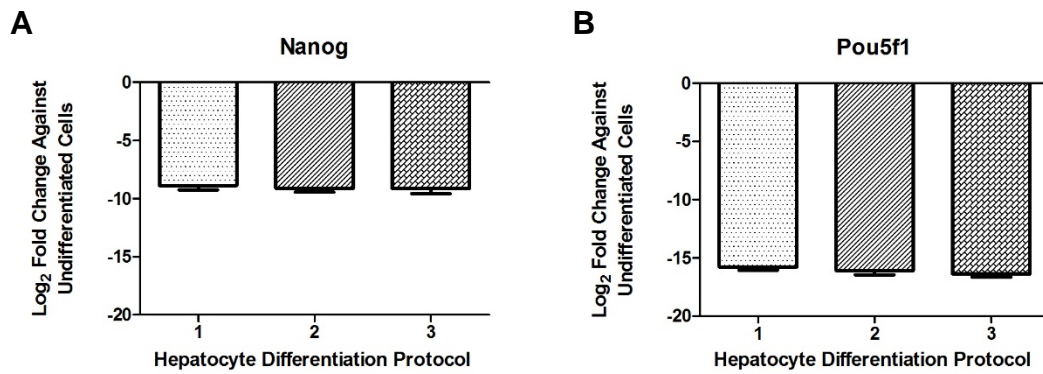
Figure 3.30 – Effect of differentiation protocols 1, 2 and 3 on the expression of pluripotency marker genes in differentiated E14Tg2a.4 mES cells. E14Tg2a.4 mES cells were differentiated for 25 days using protocols 1, 2 and 3. RT-PCR analysis of 25 day old cultures showed that all three differentiation conditions induced the same degree of suppression of the pluripotency genes (A) Nanog and (B) Pou5f1 (data are mean ± SD (n=3), results are not statistically significant with $p > 0.05$ by one-way ANOVA).
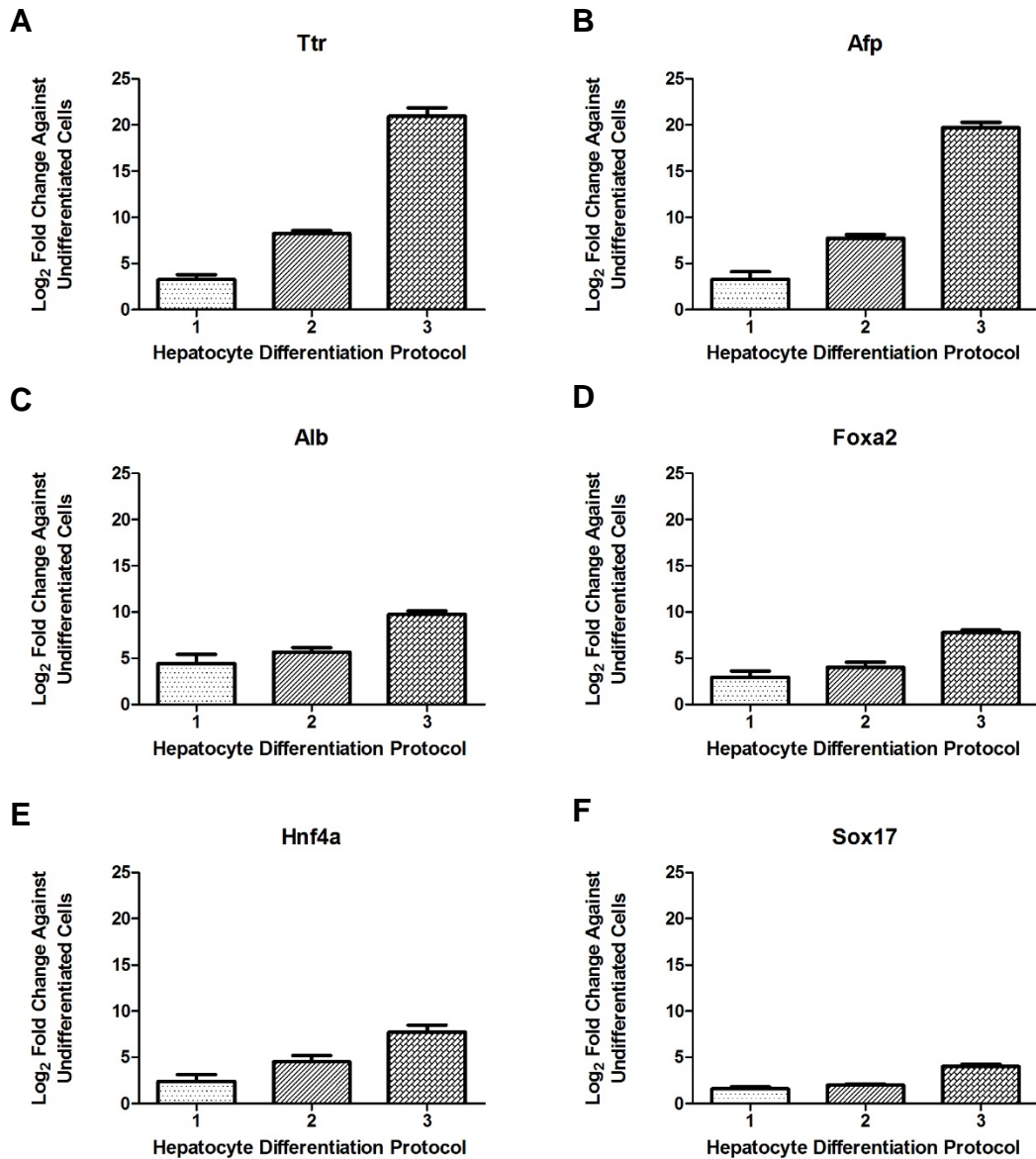
Figure 3.31 – Effect of differentiation protocols 1, 2 and 3 on the expression of pluripotency marker genes in differentiated E14Tg2a.4 mES cells. E14Tg2a.4 mES cells were differentiated for 25 days using protocols 1, 2 and 3. RT-PCR analysis was used to assess the expression of hepatic marker genes. The most significant and highest expression of Ttr, Afp, Alb, Foxa2, Hnf4a and Sox17 was measured in E14Tg2a.4 mES cells that had been differentiated using protocol 3 (data are mean ± SD (n=3), results are statistically significant at $p < 0.05$ by one-way ANOVA).
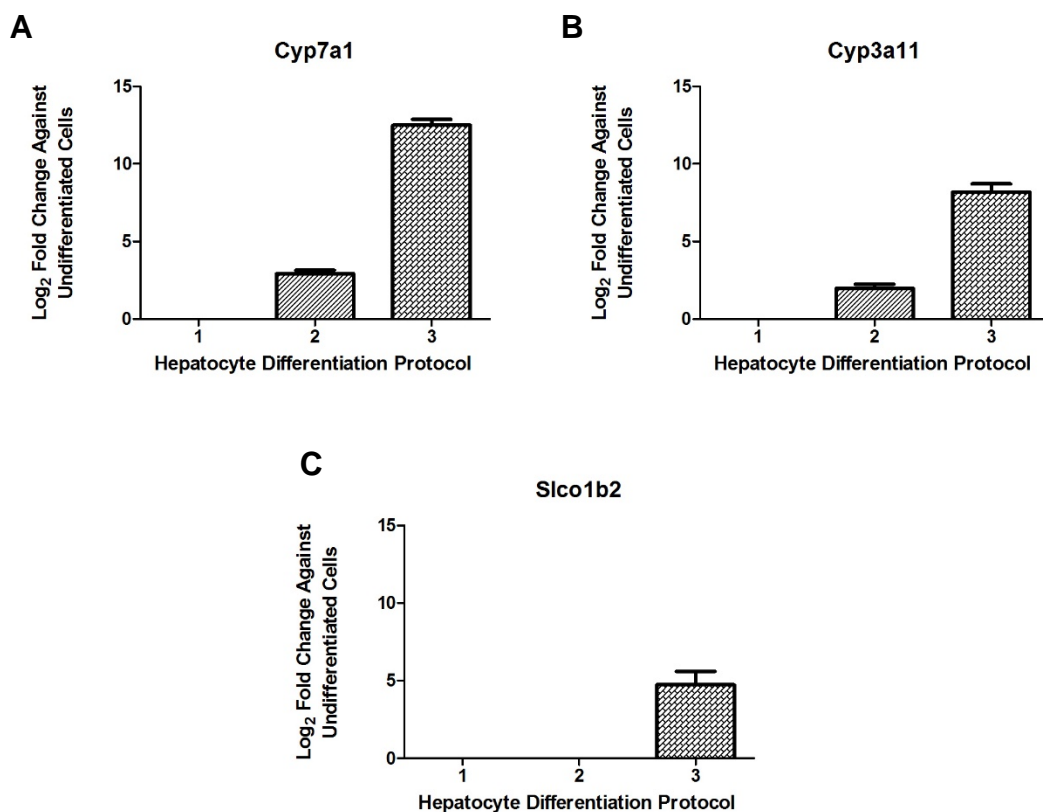
Figure 3.32 – Effect of differentiation protocols 1, 2 and 3 on the expression of pluripotency marker genes in differentiated E14Tg2a.4 mES cells. E14Tg2a.4 mES cells were differentiated for 25 days using protocols 1, 2 and 3. RT-PCR analysis was used to assess the expression of hepatic marker genes. Hepatocyte differentiation protocol 1 did not induce expression of Cyp7a1, Cyp3a11 and Slco1b2. Protocols 2 and 3 induced expression of Cyp7a1 and Cyp3a11 with the most significant up regulation of these genes measured in cells differentiated using protocol 3. Increased expression of Slco1b2 in comparison with undifferentiated cells was only observed in cultures differentiated using protocol 3 (data are mean ± SD (n=3), $p < 0.05$ for comparison of protocol 2 and 3 for Cyp7a1 and Cyp3a11 expression and for Slco1b2 expression in differentiated cells compared with undifferentiated cells).

3.3.6.2 Decreased Alkaline Phosphatase Activity

During differentiation mES cells lose AP enzymatic activity and thus AP activity was used to trace differentiation of E14Tg2a.4 mES cells. AP activity was measured in the starting undifferentiated stem cell population (day 0) and at days 3, 6 and 9 of hepatocyte differentiation using protocol 3 (Figure 3.33). AP activity in differentiated cultures at day 3, 6 and 9 was compared with day 0 undifferentiated cultures by one-way ANOVA with post hoc Dunnett's test. As differentiation progressed AP activity significantly decreased. The most significant decrease in AP activity was observed between days 3 and 6 of differentiation. This corresponds with the EB maturation stage of differentiation wherein EBs were exposed to sodium butyrate (1 mM); this indicates that sodium butyrate is a potent inducer of stem cell differentiation.
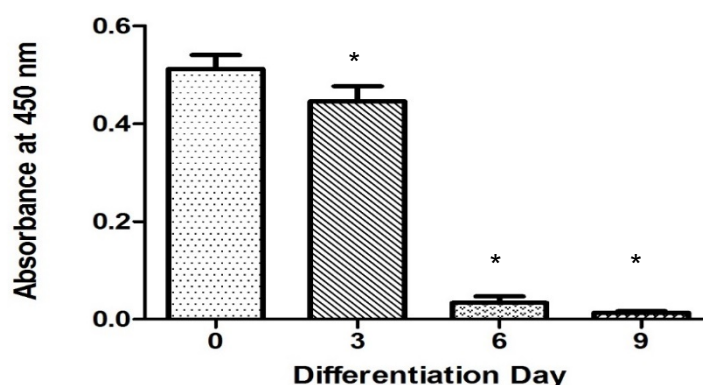
Figure 3.33 – Decrease in alkaline phosphatase activity during differentiation of E14Tg2a.4 mES cells using hepatocyte differentiation protocol 3. Differentiation of E14Tg2a.4 mES cells using hepatocyte differentiation protocol 3 resulted in a time dependent decrease in the presence of pluripotent cells within the differentiated cultures. AP activity at days 3, 6 and 9 of differentiation was significantly lower than the activity measured in the undifferentiated starting population of E14Tg2a.4 mES cells at day 0 (data are mean ± SD (n=3), *$p < 0.05$ for each time point compared with day 0 by one-way ANOVA with post hoc Dunnett's test).

3.3.6.3 *Increasing EB size during differentiation of mES cells into Hepatocyte-like cells*

Pluripotent E14Tg2a.4 cells were differentiated into hepatocytes via EB formation using protocol 3. The size and shape of EBs during hepatocyte differentiation using noted (Figure 3.34). Each EB was formed from a starting number of 500 cells and EBs were imaged on days 1, 2, 4 and 6, during suspension culture in multi-well plates and on day 7 after they had been seeded onto gelatin coated plates for attachment culture. EBs were approximately spherical in shape and steadily grew in diameter from 200 to 400 µm from day 1 to 6. Removal of sodium butyrate and seeding the EBs onto gelatinized plates led to a further increase of 200 µm in diameter. After plating EBs continued to expand in size, with cells growing outward from the central EB. EB formation for both cardiomyocyte and hepatocyte differentiation protocols started with 500 cells. However, it was noted that there was less outgrowth of cells from plated EBs during hepatocyte differentiation compared with cardiomyocyte differentiation. Subsequently, for hepatocyte differentiation 96 EBs were plated into each 10 cm cell culture dish as opposed to 72 EBs that were plated during cardiomyocyte differentiation.
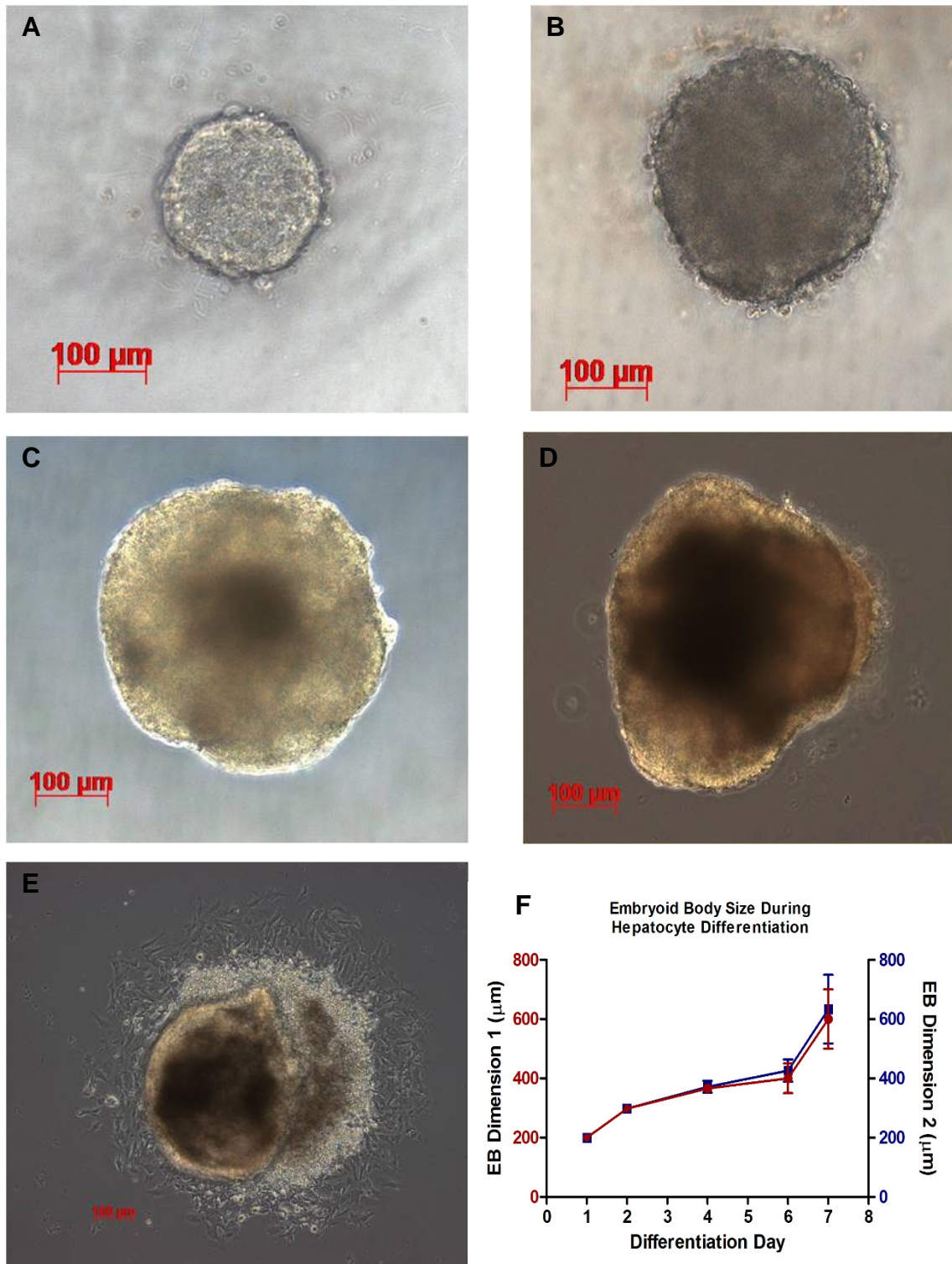
Figure 3.34 – Increasing EB size during differentiation of E14Tg2a.4 mES cells using hepatocyte protocol 3. EB size in suspension culture at (A) day 1, (B) day 2, (C) day 4, (D) day 6 and after plating on (E) day 7. (F) Changes in EB 2-dimensional xy-plane dimensions (data are ± SD, (n= 72)).

3.3.6.4 EBs Differentiated into Hepatocyte-like Cells Remain as Compact Clusters during 25 Days of Differentiation

From observations of EBs in culture it was noted that once EBs had attached to cell culture plates, cells began to grow outwards from the central EB. In addition to this growth, proliferation also was observed within EBs, with the compact cluster increasing in size as differentiation progressed. By day 25 cell cultures consisted of highly compact EBs, in which cells were growing in a 3D manner and flat monolayers of cells surrounding the EB (Figure 3.35)
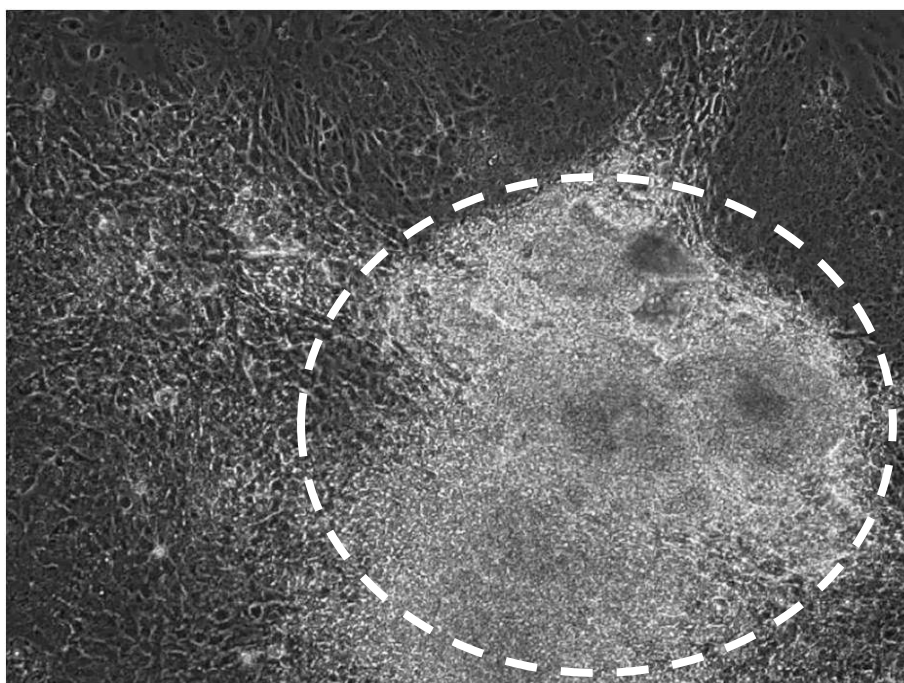
Figure 3.35 – Morphology of E14Tg2a.4 mES cells after 25 days of differentiation using hepatocyte protocol 3. Differentiation of E14Tg2a.4 mES cells was undertaken via EB formation using 3 different medium. EBs were formed using Hep-medium 1, matured using Hep-medium 4 and then seeded into gelatinised plates and maintained in Hep-medium 3. 96 EBs were seeded into each 10 cm gelatinised cell culture and cultures continued to grow post attachment. However, most proliferation appeared to occur within the EB generating highly condensed clusters of cells (encircled).

3.3.6.5 Expression of Hepatic Marker Genes in Differentiating mES Cells

To profile the differentiation of E14Tg2a.4 mES cells into hepatocytes, cells were differentiated via EB formation using the medium compositions outlined in protocol 3. RNA was extracted from undifferentiated cells and from differentiation cultures at days 6, 9, 12, 15, 18, 21 and 25 and RT-PCR was used to assess the expression of, the endoderm transcription factors Sox17 and Hnf4a, the foetal liver marker Afp and the genes Alb, Foxa2, Ttr, Slco1b2, Cyp7a1 and Cyp3a11, which are markers of metabolically active hepatocytes. These hepatic marker genes were taken from the recommendations listed by the SC4SM consortium (SC4SM, 2008) The expression of target genes in cultures differentiated for 6, 9, 12, 15, 18 and 21 days was compared with expression levels in cells differentiated for 25 days by one-way ANOVA with post hoc Dunnett's test. It was found that the expression of all 9 marker genes increased in a time dependent manner (Figures 3.36 and 3.37). Expression of the genes Afp, Sox7, Cyp3a11 and Slco1b2 were not found to be significantly different between cultures differentiated for 21 and 25 days. Likewise the expression levels of Hnf4a and Foxa2 were similar between cultures differentiated for 18, 21 and 25 days and the expression levels of Ttr did not differ significantly between cultures differentiated for 15, 18, 21 and 25 days. The expression levels of Alb and Cyp7a1 continued to increase with time and the highest levels were measured in cultures differentiated for 25 days. Unlike with the other 7 genes, the expression of Alb and Cyp7a1 was significantly different between cultures differentiated for 21 and 25 days.
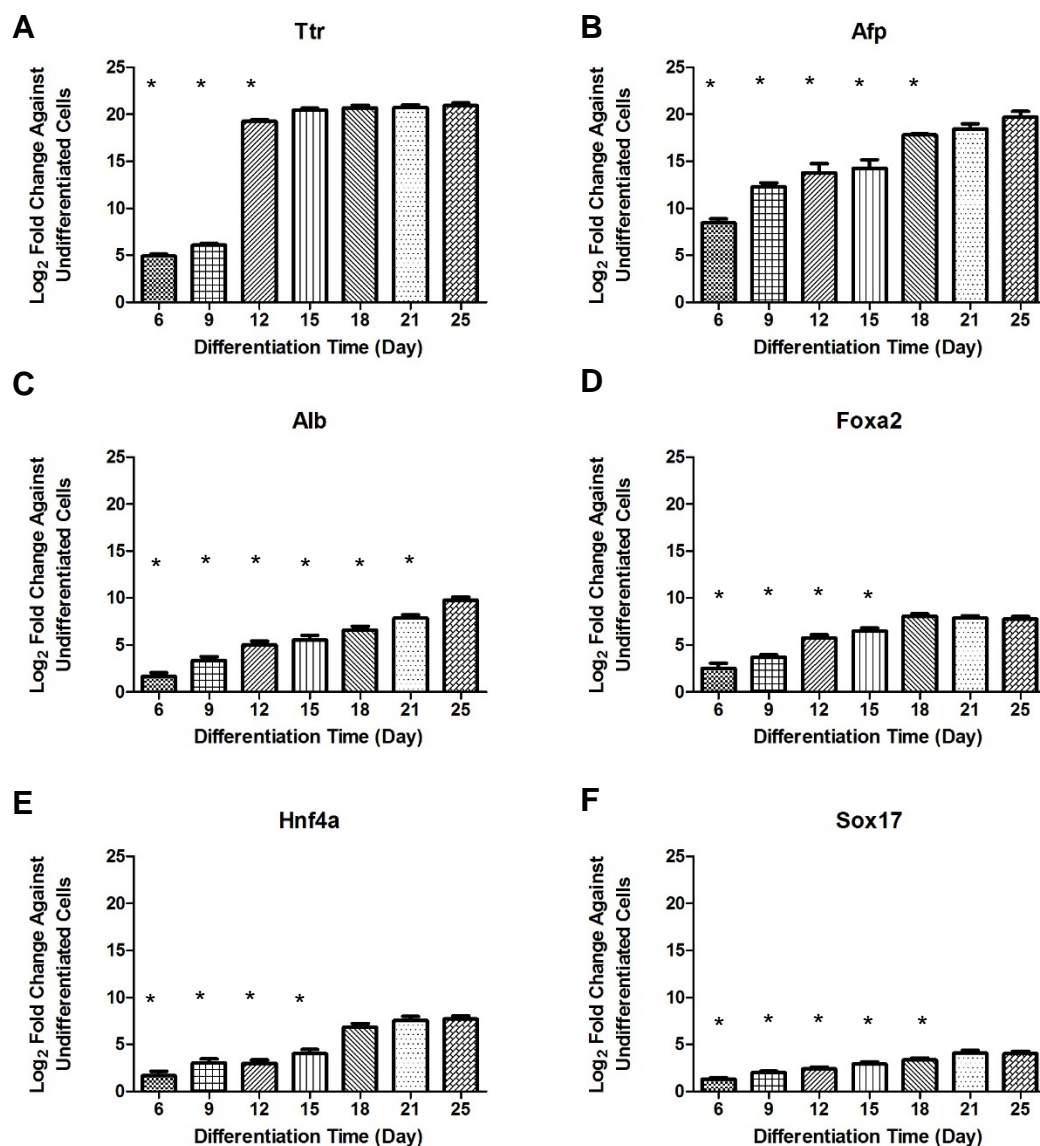
Figure 3.36 – Changes in hepatic gene expression during differentiation of E14Tg2a.4 mES cells into hepatocytes. E14Tg2a.4 mES cells were differentiated into hepatocytes using protocol 3. RT-PCR analysis was used to assess the expression of markers of metabolically active hepatocytes (A) Ttr, (C) Alb, (D) Foxa2, foetal liver marker (B) Afp and endoderm transcription factors (E) Hnf4a and (F) Sox17 after 6, 9, 12, 15, 18, 21 and 25 days of differentiation. Expression of hepatic marker genes increased in a time dependent manner. Similar expression levels were observed between 21 and 25 day old cultures of all genes except Alb. Expression of Alb did not stabilise during 25 days of differentiation (data are mean ± SD (n=3), *p < 0.05 for time points compared with day 25 cells by one-way ANOVA with post hoc Dunnett's test).
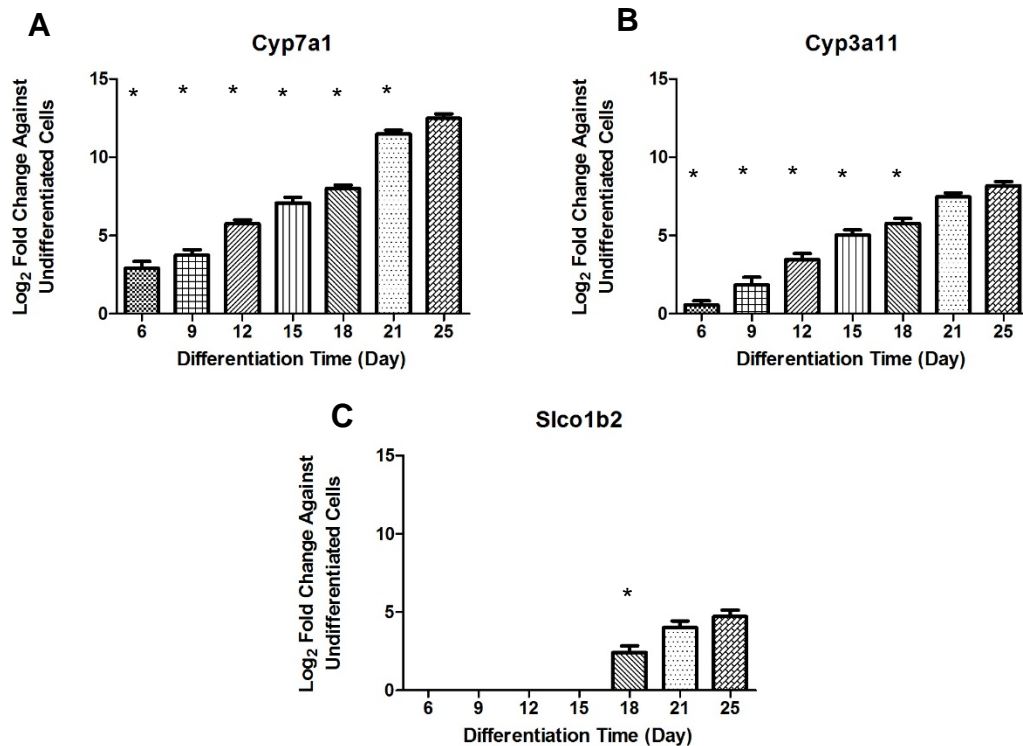
Figure 3.37 – Changes in hepatic gene expression during differentiation of E14Tg2a.4 mES cells into hepatocytes. E14Tg2a.4 mES cells were differentiated into hepatocytes using protocol 3. RT-PCR analysis was used to assess the expression of markers of metabolically active hepatocytes (A) Cyp7a1, (B) Cyp3a11 and (C) Slco1b2 after 6, 9, 12, 15, 18, 21 and 25 days of differentiation. (A) Expression of Cyp7a1 increased in a time dependent manner and levels did not stabilise during 25 days of differentiation. (B) Cyp3a11 expression increased with differentiation time and comparable levels were measured in 21 and 25 day old cultures. (C) Expression of Slco1b2 was not detected until day 18 of differentiation and expression in 21 and 25 day old cultures did not differ significantly (data are mean ± SD (n=3), *p < 0.05 for time points compared with day 25 cells by one-way ANOVA with post hoc Dunnett's test).

3.3.6.6 Differentiation of E14Tg2a.4 mES cells into Hepatocytes Generates a Heterogeneous Culture Containing Contracting EBs

During hepatocyte differentiation using protocol 3 it was noted that some EBs, post attachment to gelatinised plates, contained clusters of spontaneously contracting cells. This indicated that the cultures contained a sub-population of cells that were differentiating along the mesoderm lineage towards a cardiomyocyte phenotype. The onset of spontaneous contraction and the percentage of EBs containing these clusters was observed in cultures of E14Tg2a.4 mES cells undergoing differentiation into cardiomyocytes using 10 µM ascorbic acid and into hepatocytes using protocol 3. During hepatocyte differentiation the percentage of EBs containing contracting clusters increased from 5 to 35% from day 7 to 12 of differentiation but did not increase further for up to day 25 (Figure 3.38). With the use of protocol 3, contracting segments were first noticed at day 7 whereas with the use of ascorbic acid for cardiomyocyte differentiation, beating clusters were observed earlier at day 3. By day 8 of ascorbic acid directed differentiation 100% of the EBs contained beating clusters, whereas with protocol 3 a maximum of 35% of the EBs contained areas of contracting cells by day 25. These data illustrated that both ascorbic acid and protocol 3 induced the formation of contracting cells however, the percentage of contracting EBs was much lower in cultures differentiated into hepatocytes using protocol 3 than in cultures differentiated in to cardiomyocytes using ascorbic acid.
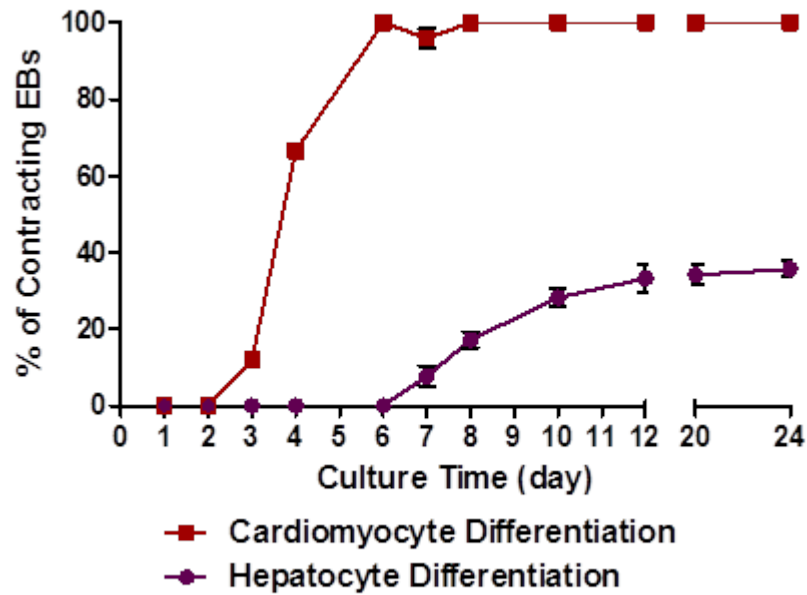
Figure 3.38 – Percentage of contracting embryoid bodies during E14Tg2a.4 mES cell differentiation into hepatocytes and cardiomyocytes. E14Tg2a.4 mES cells were differentiated using LIF free medium supplemented with 10 μM ascorbic acid for production of cardiomyocytes and using hepatocyte differentiation protocol 3 for production of hepatocytes. The number of contracting EBs were noted in each culture for 24 days for 12 days of differentiation. Contractions in EBs were first noted at day 3 in cultures using ascorbic acid compared with at day 7 in cultures differentiated using hepatocyte protocol 3. 100% of EBs being induced to differentiate into cardiomyocytes were observed to be contracting by day 24 compared with maximum of 35% of EBs in cultures undergoing differentiation into hepatocytes (data are mean ± SD (n=3), $p < 0.05$ between cardiomyocyte and hepatocyte differentiation conditions).

3.3.6.7 Expression of Cardiac Marker Genes in Hepatocyte Cultures

Cultures of E14Tg2a.4 mES cells undergoing differentiation using hepatocyte protocol 3 were observed to contain clusters of contracting cells. Expression of genes encoding for cardiac structural protein, ion channels and transcription factors were measured during 25 days of differentiation (Figures 3.39 and 3.340). Expression of the structural genes Myh6, Myl2, Tnni3, Tcap, cardiac transcription factor Mef2c and mesodermal transcription factors Gata4 and Tbx2 were detected at day 6 of Differentiation. Expression of Myh6, Tnni3 and Tcap stabilised after 12 days, Myl2, Gata4 and Tbx2 levels increased till day 15 after which levels plateaued and expression of Mef2c stabilised after 18 days of differentiation. Expression of Ryr2 increased from day 9 to 18 of differentiation and then stabilised. Expression of Slc8a1 increased from day 12 to 18 after which levels did not increase further. Increased expression of Atp2a2 was detected at day 12 of differentiation and levels did not increase further for the duration the cells were kept in culture. These data confirmed the presence of a heterogeneous culture of differentiated mES cells.

To deduce if cultures differentiated using hepatocyte protocol 3 contained more hepatocytes or cardiomyocytes, E14Tg2a.4 mES cells were differentiated using protocol 3 for 25 days. RNA was extracted and RT-PCR analysis was used to assess the fold increase in hepatic and cardiac marker gene expression in differentiated cultures (Figure 3.41). Expression of hepatic marker genes in differentiated cultures compared with undifferentiated cultures was increased by 4 - 21 fold with a medium fold change increase of 8. In comparison, increased expression of cardiac marker genes in these cultures ranged from 2 to 8 fold with a medium fold change increase of 3. The increased expression of hepatic marker

gens compared with cardiac marker genes illustrated that the cultures contained more hepatocytes than cardiomyocytes.

Ascorbic acid had been found to direct differentiation of E14Tg2a.4 mES cells into cardiomyocytes and had induced increased expression of cardiac marker genes. E14Tg2a.4 mES cells were differentiated using 10 µM ascorbic acid and as according to hepatocyte differentiation protocol 3 for 24 days. Expression of cardiac marker genes was assessed in cultures differentiated using both condition using RT-PCR. Gene levels were compared to ascertain which method induced the greatest up-regulation of cardiac marker genes. Figure 3.42 illustrates that the use of ascorbic acid (10 µM) produced cultures that had significantly higher expression levels of the genes encoding for cardiac structural proteins Myh6, Tnni3, Tcap, Myl2, cardiac ion channels Slc8a1, Ryr2, Atp2a2, cardiac transcription factor Mef2c and mesodermal transcription factors Tbx2 and Gata4. Thus ascorbic acid was better than hepatocyte differentiation protocol 3 at inducing differentiation of E14Tg2a.4 mES cells into cardiomyocytes. The production of cardiomyocytes was an unintended by-product of hepatocyte differentiation using small molecules.
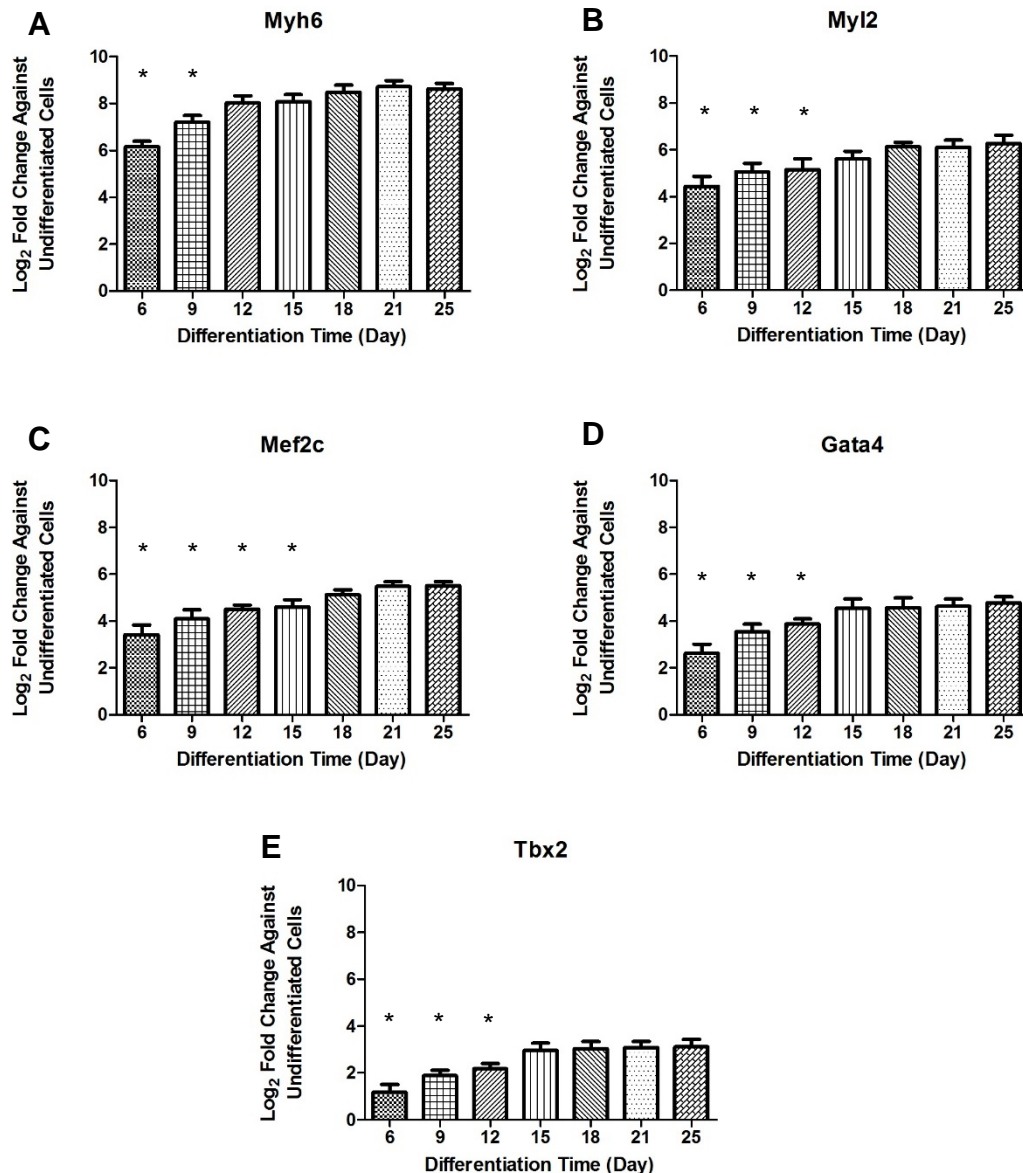
Figure 3.39 – Expression of cardiac genes in E14Tg2a.4 mES differentiated using hepatocyte protocol 3. E14Tg2a.4 mES cells were differentiated into hepatocytes using protocol 3. Cultures contained segments of contracting cells indicating differentiation of some cells into cardiomyocytes. RT-PCR analysis was used to assess the expression of cardiac structural genes (A) Myh6, (B) Myl2, cardiac transcription factor (C) Mef2c and mesodermal transcription factors (D) Gata4, (E) Tbx2 after 6, 9, 12, 15, 18, 21 and 25 days of differentiation. Expression of these cardiac marker genes increased up to day 18 of differentiation after which expression levels stabilised and no further increase in expression was observed for up to 25 days (data are mean ± SD (n=3), *p < 0.05 for each time point compared with day 25 cells by one-way ANOVA with post hoc Dunnett's test).
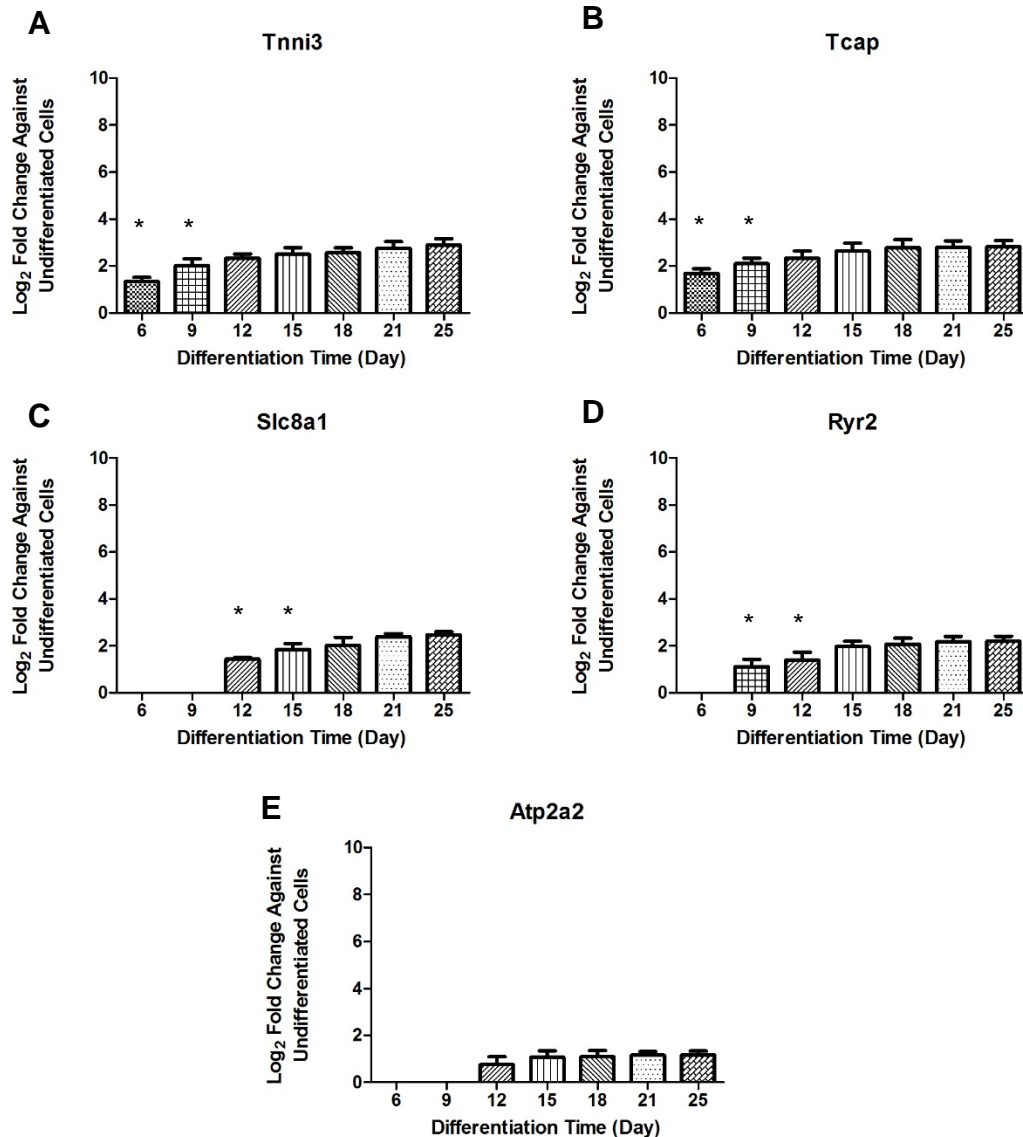
Figure 3.40 – Expression of cardiac genes in E14Tg2a.4 mES differentiated using hepatocyte protocol 3. E14Tg2a.4 mES cells were differentiated into hepatocytes using protocol 3. RT-PCR analysis was used to assess the expression of cardiac structural genes (A) Tnni3, (B) Tcap and cardiac ion channels (C) Slc8a1 (D) Ryr2, (E) Atp2a2, after 6, 9, 12, 15, 18, 21 and 25 days of differentiation. Expression of Tnni3 and Tcap stabilised after 12 days of differentiation. Expression of Ryr2 was not detected until day 9 of differentiation and after day 12 levels plateaued. Expression of Slc8a1 and Atp2a2 was not detected till day 12 of differentiation. Slc8a1 expression increased till day 18 and then levels stabilised. Expression of Atp2a2 was first detected at day 12 and further induction of expression was not observed up to day 25 (data are mean ± SD (n=3), *$p < 0.05$ for each time point compared with day 25 cells by one-way ANOVA with post hoc Dunnett's test).
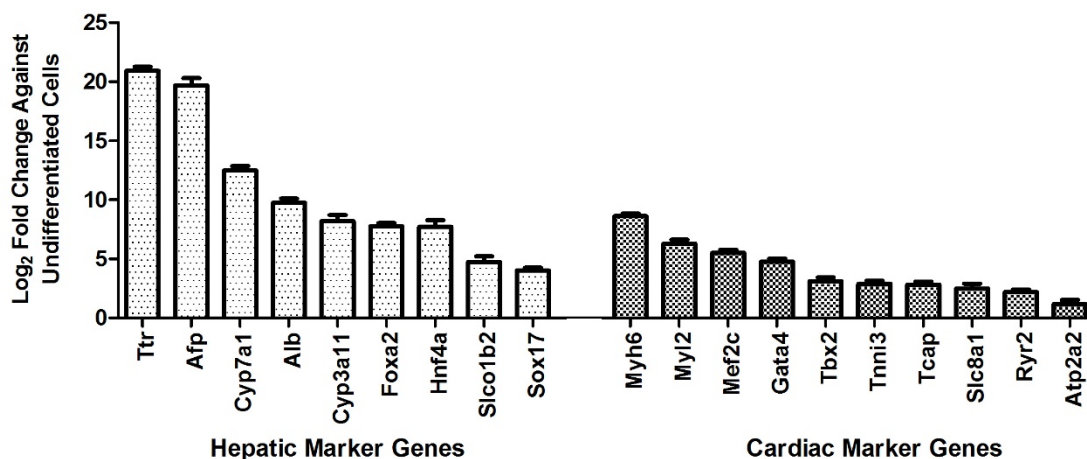
Figure 3.41 – Expression of hepatic and cardiac genes in E14Tg2a.4 mES differentiated using hepatocyte protocol 3. E14Tg2a.4 mES cells were differentiated into hepatocytes using protocol 3. RT-PCR analysis was used to assess the expression of hepatic and cardiac marker genes in 25 day old cultures. Expression levels of hepatic marker genes were higher than expression of cardiac genes in differentiated cultures (data are mean ± SD (n=3), results are statistically significant at $p < 0.05$ expression of increased expression of hepatic maker genes in comparison with cardiac marker genes).
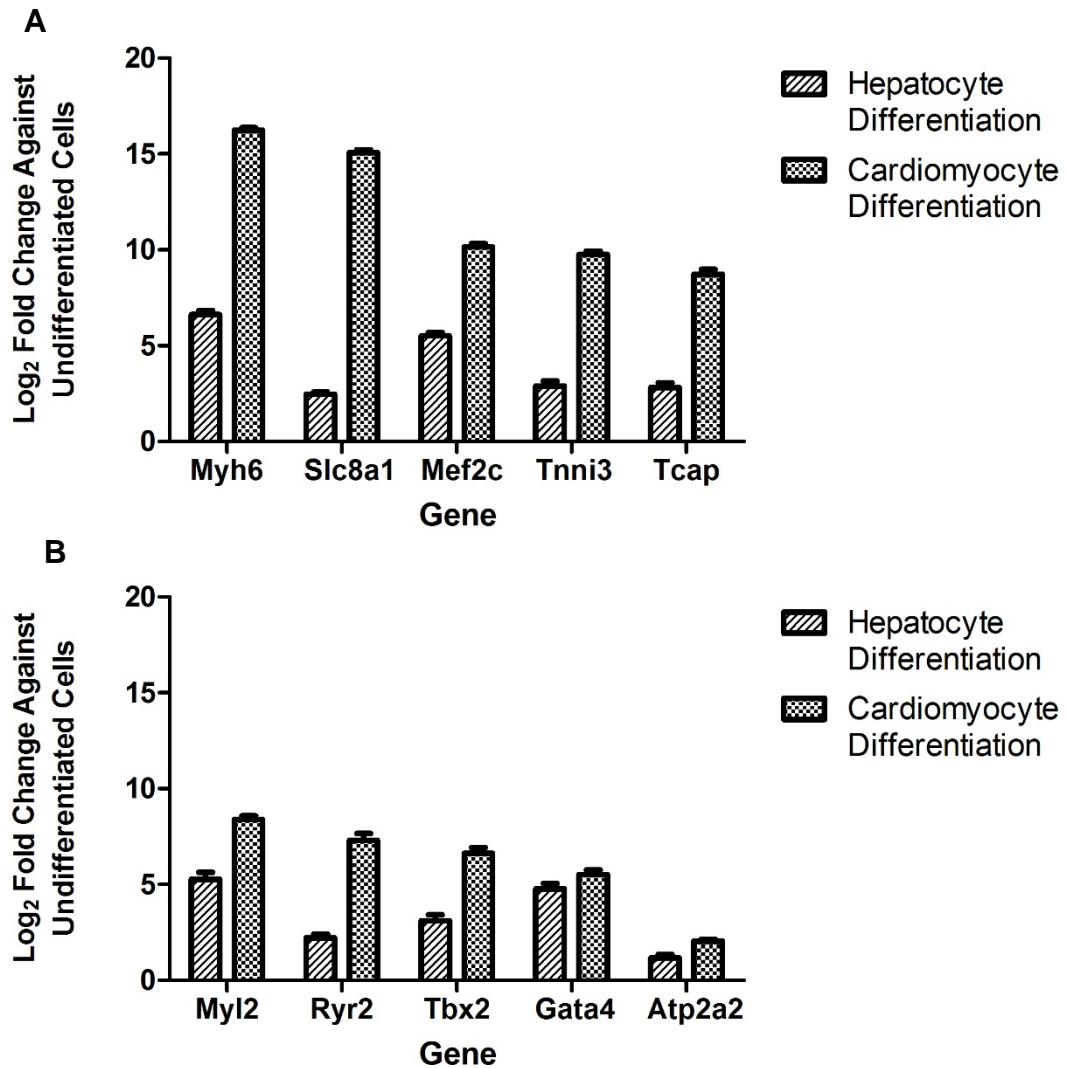
Figure 3.42– Expression of cardiac marker genes in E14Tg2a.4 mES cells differentiated into hepatocytes and cardiomyocytes. E14Tg2a.4 mES cells were differentiated for 24 days using LIF free medium supplemented with 10 µM ascorbic acid for production of cardiomyocytes and using hepatocyte differentiation protocol 3 for production of hepatocytes. (A-B) RT-PCR analysis was used to assess the expression at day 24 of cardiac structural genes Myh6, Tnni3, Tcap, Myl2, cardiac ion channels Slc8a1, Ryr2, Atp2a2, cardiac transcription factor Mef2c and mesodermal transcription factors TBx2 and Gata4. Cultures differentiated for the production of cardiomyocytes using 10 µM ascorbic acid had significantly greater expression levels of cardiac marker genes than cultures differentiated for the production of hepatocytes (data are mean ± SD (n=3), p < 0.05 between cardiomyocyte and hepatocyte differentiation conditions).

3.3.6.8 Comparison of Hepatic Marker Gene Expression in mES Derived Hepatocytes and Liver Tissue

E14Tg2a.4 mES cells were differentiated into hepatocytes for 25 days using hepatocyte protocol 3. RT-PCR analysis was used to compare the expression of foetal liver marker Afp, markers of metabolically active hepatocytes Alb, Foxa2, Ttr, Slco1b2, Cyp7a1, Cyp3a11 and endoderm transcription factors Hnf4a and Sox17 in differentiated hepatocytes with liver tissue from a 2 day old and 8 week old mouse (Figure 3.43). Differentiated hepatocytes had significantly lower levels of hepatic marker genes compared with neonatal liver tissue. In comparison with adult liver tissue differentiated hepatocytes still had significantly lower levels of Alb, Foxa2, Ttr, Slco1b2, Cyp7a1 and Cyp3a11. However, mES cell derived hepatocytes expressed Hnf4a and Sox17 at similar levels to those found in adult liver tissue and had significantly higher levels of Afp.
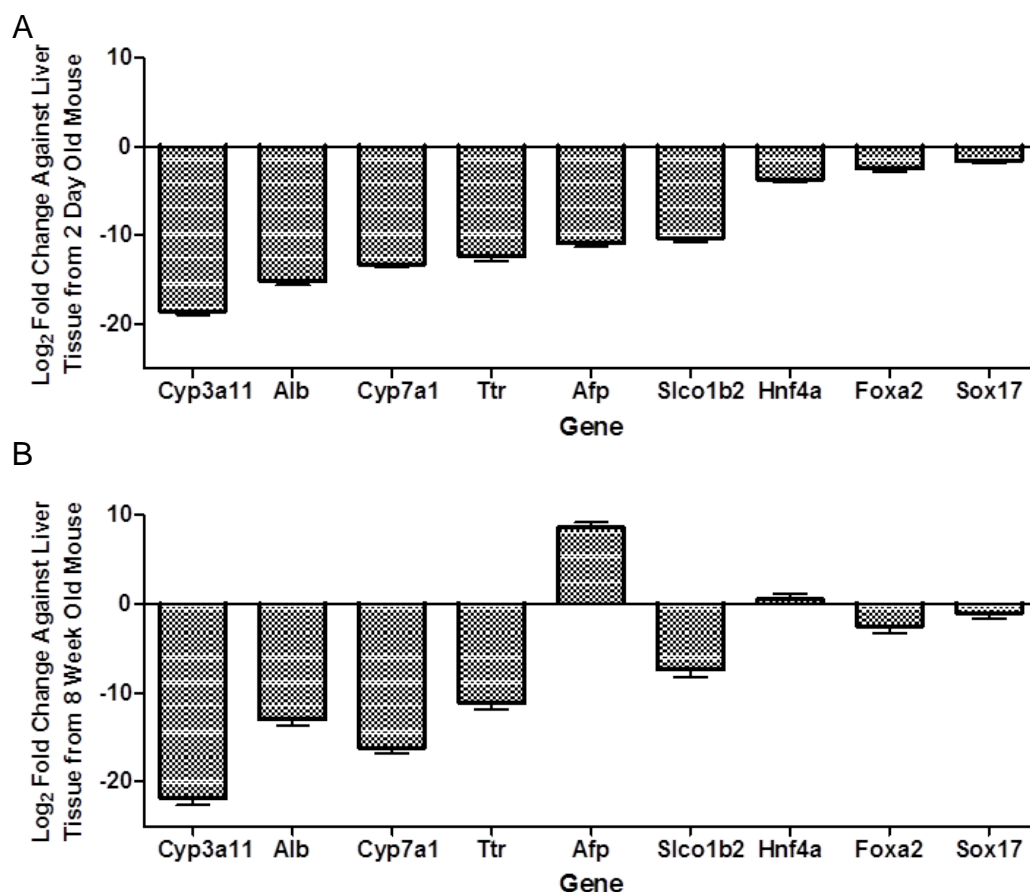
Figure 3.43 – Comparison of hepatic gene expression of mES cell derived hepatocytes and liver tissue from neonatal and adult mice. E14Tg2a.4 mES cells were differentiated into hepatocytes using differentiation protocol 3 for 25 days. RT-PCR analysis was used to compare the expression of foetal liver marker Afp, markers of metabolically active hepatocytes Alb, Foxa2, Ttr, Slco1b2, Cyp7a1, Cyp3a11 and endoderm transcription factors Hnf4a and Sox17 in differentiated hepatocytes and liver tissue from a (A) 2 day old mouse and (B) 8 week old mouse. (A) Differentiated hepatocytes had significantly lower levels hepatic marker genes compared with neonatal liver tissue. (B) In comparison with adult liver tissue, differentiated cells had much higher levels of Afp and comparable levels of Hnf4a and Sox17. Significantly lower levels of Alb, Foxa2, Ttr, Slco1b2, Cyp7a1 and Cyp3a11 were found in mES differentiated hepatocytes compared with adult liver tissue (data are mean ± SD (n=3), $p < 0.05$ for comparison of differentiated cells with 2 day old liver and for all genes except Hnf4a and Sox17 in comparison with 8 week old liver.)

3.3.7 Maintaining mES Cell Differentiated Cardiomyocytes and Hepatocytes in FCS Free Medium

The differentiated cardiomyocytes and hepatocytes produced in this project were developed for use in *in vitro* assays for profiling of TRO induced transcriptomic changes and to potentially provide information regarding mechanisms of TRO induced toxicity. Both cell types were differentiated using medium that contained FCS, which contains a significant amount of the protein BSA and TRO is known to be >99% protein bound (FDA, 1999). Treatment of differentiated cells with TRO using medium containing FCS would have affected the concentration of free TRO available for uptake by the cells. Furthermore, the medium would have to be free of any compounds that were used to differentiate the cells to prevent cross-reaction of TRO and the differentiation inducing compounds. Expression of cardiac marker genes in differentiated cardiomyocytes and expression of hepatic marker genes in differentiated hepatocytes had been shown to be stable between days 20 – 25 of differentiation. Both cell types were differentiated till day 22 following which cultures were either kept in differentiation medium or treatment medium, which consisted of KO-DMEM (for cardiomyocytes) or IMDM (for hepatocytes) supplemented with ITS supplement (5%), l-glutamine (1X), sodium pyruvate (1X), non-essential amino acids (1X) and β-mercaptoethanol (0.1 mM). Cultures were maintained for 48 hours after which RNA was extracted and RT-PCR was preformed to assess changes in gene expression between cultures maintained in medium supplemented with and without FCS. RT-PCR analysis showed that removing FCS and differentiation inducing compounds from cell culture medium on day 22 for 48 hours did not alter the expression of cardiac or hepatic marker genes in differentiated cardiomyocytes and hepatocytes (Figures

3.44 and 3.45). These data illustrated that it was possible to remove FCS from culture medium prior to treatment of differentiated cells with TRO, thus maximising availability of free unbound TRO.
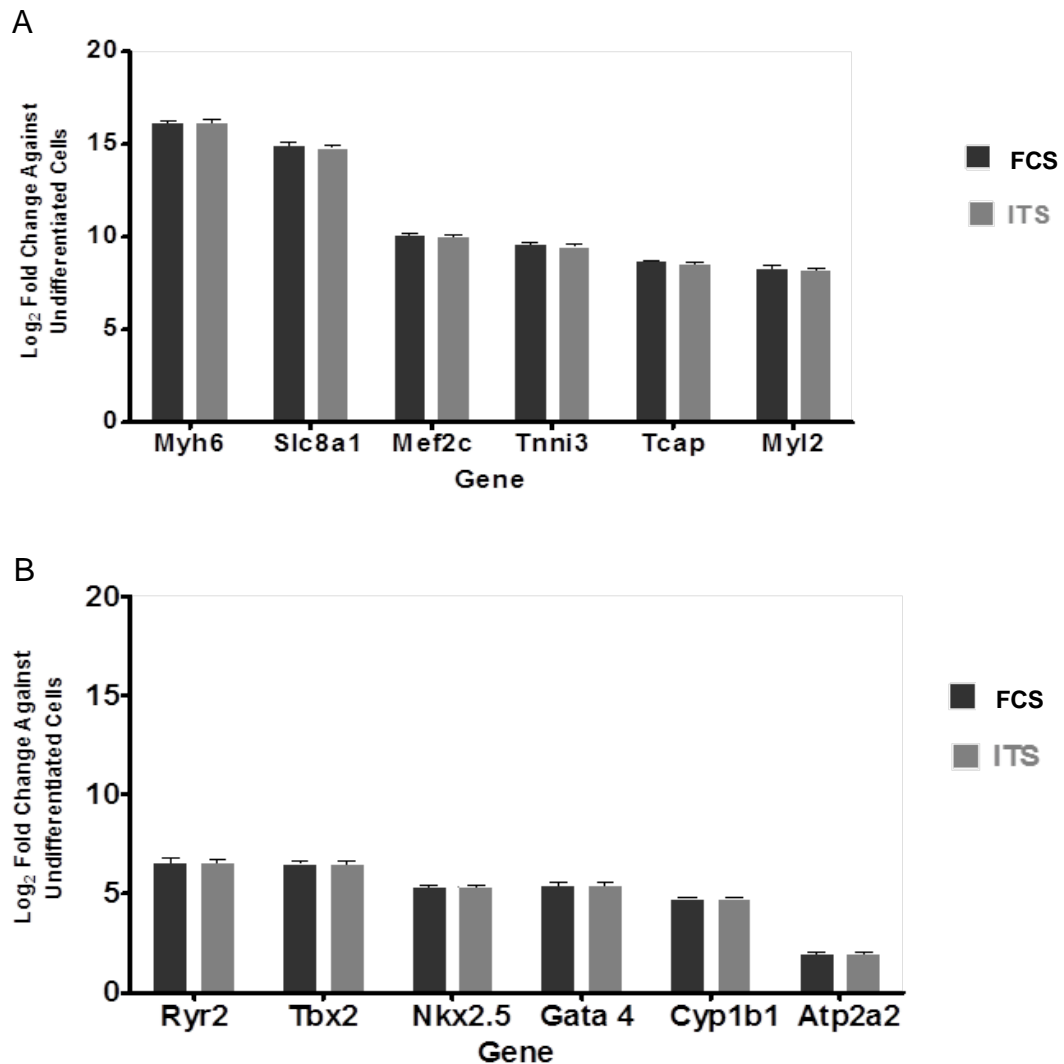
Figure 3.44 – Comparison of cardiac gene expression of mES cell derived cardiomyocytes maintained in medium supplemented with and without FCS for 48 hours. E14Tg2a.4 mES cells were differentiated into cardiomyocytes 22 days. On day 22 cells were either kept in medium containing FCS or in FCS free medium which contained with ITS supplement. After 48 hours RNA was extracted and cardiac marker gene expression was assessed by RT-PCR. (A - B) Expression of cardiac marker genes was similar in cells maintained with FCS or ITS (data are mean $\pm$ SD (n=3), results are not statistically significant at $p > 0.05$ for comparison of cells maintained in FCS or ITS medium for 48 hours).
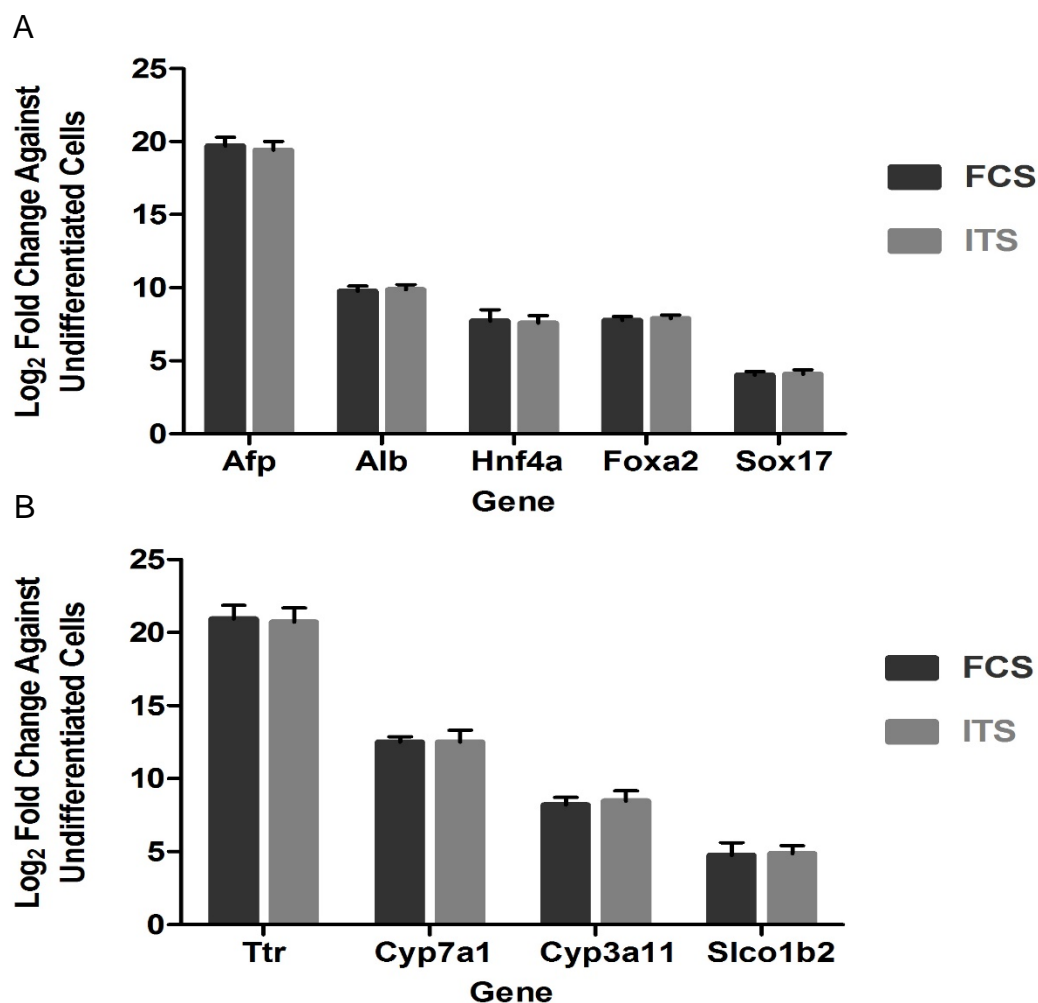
Figure 3.45 – Comparison of hepatic gene expression of mES cell derived hepatocytes maintained in medium supplemented with and without FCS for 48 hours. E14Tg2a.4 mES cells were differentiated into cardiomyocytes 22 days. On day 22 cells were kept in medium either containing FCS or ITS. After 48 hours RNA was extracted and cardiac marker gene expression was assessed by RT-PCR. (A - B) Expression of hepatic marker genes was similar in cells maintained with FCS or ITS (data are mean ± SD (n=3), results are not statistically significant at $p > 0.05$ for comparison of cells maintained in FCS or ITS medium for 48 hours).

3.4 Discussion

The aims of this chapter were to optimize protocols for the culture and differentiation of the E14Tg2a.4 mES cell line with a focus on producing cardiomyocytes and hepatocytes for use in drug treatment assays.

3.4.1 Maintaining E14Tg2a.4 mES Cell Pluripotency

The first important step in developing reproducible protocols for stem cell differentiation is to ensure that the starting stem cell population is pluripotent. Supplementing cell culture medium with LIF maintains mES cells in a pluripotent and proliferative state. Murine LIF was produced in house and was shown to be equivalent to more expensive commercially available LIF at supporting proliferation of E14Tg2a.4 mES cells (Figure 3.4). It was observed that the expression of the key pluripotency regulator genes Nanog and Pou5f1 in E14Tg2a.4 mES cells varied for the first five passages post thaw after which levels stabilised (Figure 3.5). Stable expression of Nanog and Pou5f1 marks the presence of a pluripotent ES cell population and thus cells were passaged at least five times post thaw before they were utilised in differentiation assays.

3.4.2 Embryoid Body Formation

Differentiation of ES cells is most commonly initiated via the formation of 3D cell aggregates termed EBs in LIF free medium. EBs are 3D structures that resemble post-implantation embryos and support the development of the three germ layers during differentiation (Desbaillets et al., 2000). The two most commonly utilised protocols for EB formation are via suspension culture or 'hanging drop' formation. The reproducible formation of EBs of specific size is a prerequisite for standardization of ES cell differentiation. Culture of ES cells in suspension, without LIF, leads to uncontrolled cell aggregation resulting in the formation of

EBs of varied size. A highly cited method for the standardized generation of EB is the 'hanging drop' method (Wobus, 2001). This method involves seeding 20 µl droplets containing fixed numbers of cells on to the inside of a Petri dish lid followed by inverting the lid onto a dish and incubating the dishes. Drawbacks of this procedure are that it can be time consuming especially when large numbers of EBs are required and hanging drops are vulnerable thus disturbances to the plate can cause the drops to merge or fall. The principle of the hanging drop method was used to develop a robust, scalable system for the production of EBs. Ultra low attachment 'U' and 'V' bottomed 96-well plates mimicked the environment of the hanging drop with one EB forming in each well. These plates were resistant to incubator disturbances and reduced the time needed to produce large batches of EBs (Figure 3.6). Commercially available AggreWell plates from StemCell Technologies work on a similar principle however; it is a more costly procedure. The cost of producing one EB via the U/V ultra-low attachment 96-well plate method developed in this project was 1.04p/EB compared with 17.5p/EB, which is the approximate cost of the AggreWell system.

EBs are formed in suspension however furthering differentiation requires attachment of EBs to coated cell culture plates. The reported length of time for which EBs must be cultured in suspension before they are plated varies from 3 – 7 days (Wobus, 2001). We found that plating EBs on day six of differentiation resulted in optimal conditions for further differentiation with EBs retaining their structural integrity and ability to proliferate post attachment (Figure 3.8).

To determine if the U/V ultra-low attachment 96-well plate method was suitable for the reproducible production of EBs the size of EBs during the first 7 days of cardiomyocyte and hepatocyte differentiation was recorded (Figure 3.16 and

3.34). For time point, 8 EBs were measures per 96-well plate, 3 plates were measured for each differentiation experiment and differentiation was undertaken on 3 separate occasions. Variances in EB size for each time point across the 3 different differentiation experiments was non-significant. This illustrated that the U/V ultra-low attachment 96-well plate method was suitable for the reproducible production of uniform size and shaped EBs.

3.4.3 Ascorbic Acid Directed Differentiation of E14Tg2a.4 mES Cells into Cardiomyocyte-like Cells

Removal of LIF results in spontaneous differentiation of mES cell in to cells of the three germ layers (Smith et al., 1988). Directed differentiation of pluripotent mES cells can be achieved via supplementing media with small molecules (Chen et al., 2006). Differentiation of E14Tg2a.4 mES cells was assessed by measuring expression of cardiomyocyte specific genes as approved by the Stem Cells 4 Safer Medicine consortium (SC4SM, 2008). Removing LIF from cell culture medium induced the formation of spontaneously contracting clusters and RT-PCR analysis showed that there was up regulation of cardiac specific genes in these cultures (Figure 3.9). This spontaneous differentiation along the mesoderm lineage towards a cardiomyocyte phenotype was enhanced via supplementation of differentiation medium with 10 µM ascorbic acid. Ascorbic acid has been cited to induce cardiac differentiation in embryonic stem cells and its ability to induce cardiomyogenesis is thought to be unrelated to its antioxidant properties as other antioxidants such as N-acetylcysteine and vitamin E, have no effect on cardiomyocyte differentiation (Takahashi et al., 2003). The precise mechanism by which ascorbic acid promotes cardiac differentiation is not yet known. Use of ascorbic acid over a period of 24 days produced cultures of spontaneously

contracting cells that expressed genes encoding for the mesodermal transcription factors Gata4 and Tbx2, the cardiac transcription factors Nkx2.5 and Mef2c, the cardiac structural proteins Myh6, Myl2, Tnni3 and Tcap, the cardiac ion channels Slc8a1, Ryr2 and Atp2a2 and the Phase I metabolising enzyme Cyp1b1 (Figures 3.17 and 3.18). The cells also expressed the cardiac structural proteins tropomyosin, actinin, atrial natriuretic peptide and desmin (Figures 3.20 and 3.21). Differentiation undoubtedly produces a heterogeneous cell culture consisting of cells at various stages of differentiation and non-invasive systems for isolating pure cell types are highly sought after. An absence of cardiac specific cell surface antigens on cardiomyocytes makes it difficult to isolate a pure population of mature cardiomyocytes (Mummery, 2010). For isolation of differentiated cardiomyocytes a novel technique was recently derived by Hattori et al (2010), which selects electrically active cardiomyocytes based on fluorescence intensity of a mitochondrial specific dye. The method is based on higher mitochondrial content, thus increased fluorescence in contracting differentiated cardiomyocytes. Isolation of differentiated cardiomyocytes using this method produced a very low yield of pure cardiomyocytes (Figure 3.22). The number of cells collected post sorting, approximately 30,000 cells from a parental population of 2 million cells, was insufficient for use in drug treatment assays however would be sufficient for certain *in vitro* assays such as single cell electrophysiology or microelectrode array assays (Caspi et al., 2009). It was observed that cardiomyocytes differentiated using ascorbic acid were able to spontaneously contract in culture and that these contractions corresponded with changes in intracellular calcium levels (Figure 3.23). Contractions of cardiomyocytes *in vivo* are controlled by cardiac action potentials that are

generated from cycling increases and decreases in intracellular calcium levels. In cardiomyocytes, release of calcium from the sarcoplasmic reticulum (SR) is mediated by the ryanodine receptor Ryr2. The released calcium interacts with the sarcomeric components myosin, actin and troponin resulting in a shortening of the cardiomyocyte. Relaxation of the cell occurs through the removal of cytosolic calcium by its re-uptake into the SR, a process mediated by the sarco-endoplasmic reticulum calcium channel, Atp2a2. The increase and decrease in intracellular calcium results in contraction and relaxation of cardiomyocytes (Niggli, 1999). Increased expression of the cardiac calcium channels Ryr2 and Atp2a2, several cardiac structural genes and proteins and fluctuations in intracellular calcium levels were observed in cardiomyocytes differentiated from pluripotent E14Tg2a.4 mES cells using ascorbic acid. Comparison of the cardiac gene signature of differentiated E14Tg2a.4 mES cells to heart tissue from 2 day and 8 week old mice showed that the *in vitro* cells had much lower expression levels of mesodermal and cardiac transcription factors, cardiac ion channels and structural markers. In contrast, the expression of the phase I metabolising enzyme Cyp1b1 was found to be comparable between differentiated cardiomyocytes and heart tissue from an 8 week old mouse.

These data illustrated that the differentiated mES cells shared some functional and structural similarities to cardiomyocytes found *in vivo.*

3.4.4 Differentiation of E14Tg2a.4 mES Cells into Hepatocyte-like Cells Required a Multi-Medium Protocol

Removal of LIF from cell culture medium induces differentiation of mES cells. With the E14Tg2a.4 mES cell line spontaneous differentiation in LIF free medium was more directed along the mesoderm lineage than towards the endoderm germ

layer. Within 12 days of being cultured in LIF free medium E14Tg2.4 mES cells had a 5 – 10 old increase in key cardiac marker genes (Figure 3.9). In comparison, after 25 days of differentiation in LIF free medium expression of hepatic marker genes was upregulated by 2 to 5 fold (Figure 3.27). Several medium compositions (Tables 3.1 and 3.2) were trialled to induce differentiation along the endoderm lineage towards the production of hepatocytes. The most successful differentiation conditions tested involved the use of different medium to support EB formation, maturation and attachment culture of attached EBs. The greatest induction of hepatic marker genes was observed in cultures where LIF free Hep-basal medium supplemented with 15% FCS was used to form EBs, these EBs were then exposed to 1 mM sodium butyrate to promote maturation of the EBs following which EBs were seeded for attachment culture in hep-basal medium supplemented with 4% FCS, 1% ITS and 10^{-7}M Dex (Figures 3.31 and 3.32). E14Tg2a.4 mES cells had shown a preference for mesoderm differentiation and clusters of contracting cells were observed in cultures differentiated for the production of hepatocytes (Figure 3.38). Analysis of cultures differentiated for the production of hepatocytes showed increasing expression of cardiac marker genes up to day 15 of differentiation after which gene levels plateaued (Figures 3.39 and 3.40). However, these differentiated cultures had higher expression levels of hepatic marker genes than cardiac marker genes (Figure 3.41). This illustrated that there was greater differentiation within the cultures towards the production of hepatocytes and the formation of cardiomyocytes was an unintended by-product. Ascorbic acid was shown to be a greater inducer of cardiomyocyte differentiation than the three medium hepatocyte differentiation protocol (Figure 3.42).

3.4.5 Summary

These data illustrated the difficulty of differentiating E14Tg2a.4 mES cells into cardiomyocytes and hepatocytes; highlighting that differentiation results in a heterogeneous cell population. The most commonly used method for inducing differentiation is via the formation of EBs. The intended purpose of EBs is to mimic embryo development as it occurs *in vivo* and thus support differentiation of ES cells. However, during *in vitro* differentiation attempts are made to promote formation of a particular germ layer and specific cell type; in contrast during embryo development *in vivo* germ layers and cell types form concurrently. Therefore it's not surprising that differentiated ES cell cultures *in vitro* are heterogeneous. Attempts to differentiate mES cells into hepatocytes resulted in cultures containing a sub-population of cardiomyocytes. During development *in vivo* formation of the endoderm and mesoderm germ layers is believed to stem from one precursor cell population termed the mesoendoderm. These cells then sub-divide to produce two distinct yet interconnecting layers which become the mesoderm and endoderm germ layers. Moreover, further development of the endoderm germ layer is believed to be dependent on cell-cell interactions and signalling from the mesoderm germ layer (Zorn and Wells, 2009). Therefore it is likely that for differentiation and development of hepatocytes from ES cells *in vitro* the formation of mesoderm is also required. This correlated with the observation in this project wherein 30% of the cells in cultures of differentiated hepatocytes were cardiomyocytes.

Differentiated cardiomyocytes and hepatocytes expressed cardiac and hepatic marker genes however, gene expression in mES derived cells was much lower than levels observed in tissue. Contributing factors to this are the use of small

molecules in place of growth factors and the length of time for which the cells were differentiated. Experimenting with combinations of growth factors for the differentiation of E14Tg2a.4 mES cells was not a financially viable option for this project. Differentiated cardiomyocytes expressed cardiac genes and proteins and contracted spontaneously in culture. The hepatocytes expressed key hepatic genes including genes encoding for enzymes involved in metabolic function such as phase I metabolising enzyme Cyp3a11 and Cyp7a1, which encodes for the rate limiting enzyme in the biosynthesis of bile acids from cholesterol. It was illustrated that differentiated cardiomyocytes and hepatocytes could be maintained in FCS free medium for 48 hours without any effects being observed on cardiac and hepatic marker gene expression. TRO is a highly protein bound drug thus addition of it to cell culture medium containing FCS greatly affects the availability of free TRO.

The aims of this chapter were met through the development of differentiation methods that were standardised and reproducible, generated cells that expressed key cardiac and hepatic marker genes, resembled developing cardiomyocytes and hepatocytes and could be maintained in FCS free medium allowing treatment with highly protein bound drugs such as TRO.

Chapter 4: Transcriptomic Analysis of an *In Vivo* Troglitazone Normal Mouse Model

4.1 Introduction

TRO was an oral anti-diabetic drug that was used for the treatment of T2D. It was prescribed for daily administration at doses between 200-1000 mg/day (discussions with GSK) and was effective at increasing tissue sensitivity to insulin in patients with T2D resulting in a decrease in blood glucose levels (Petersen et al., 2000). TRO was first marketed in January 1997 by Sankyo in Japan followed by Parke-Davis Warner-Lambert in the USA in April of that year and was subsequently launched in the UK by GSK in October 1997 (Gale, 2001). By November 1997 an estimated 600,000 T2D patients in the USA, 200,000 in Japan and 5000 in the UK had been prescribed TRO and 35 cases of TRO induced hepatotoxicity, including one death, had been reported to the FDA (Ault, 1997, Mitchell, 1997). Initial reports of adverse reactions to TRO prompted GSK to withdraw it from the UK market in December 1997. TRO was withdrawn from worldwide sale in March 2000 following 61 reported cases of TRO induced fatal liver failure (Gale, 2001). TRO induced hepatotoxicity was defined as being idiosyncratic as it affected a small percentage of the patient population and there was an absence of a common factor that could be used to predict patient susceptibility (Smith, 2003). In addition to reports of TRO induced hepatotoxicity, there were registered cases of TRO induced cardiotoxicity. In 1999, 50 spontaneous adverse reaction cases of TRO induced heart failure, including six fatalities, were reported by the Endocrinologic and Metabolic Drugs Advisory Committee to the FDA. The committee also noted that in a particular patient trial 4% of the test group developed peripheral oedema and one patient developed pulmonary oedema, whereas no adverse cardiovascular effects were reported in the placebo group (FDA, 1999a). Although cardiotoxicity was not a factor in the

withdrawal of TRO it has been a major safety issue for the other members of the TZD compound family. This was emphasized by the withdrawal of rosiglitazone (ROSI), which was removed from the market in September 2010 due to increased risk of adverse cardiovascular events occurring in patients using the drug (MHRA, 2010). Furthermore, the development of muraglitazar, another member of TZD compound class was halted after the completion of phase III clinical trials due to increased incidence of heart failure in clinical patients (Nissen et al, 2005). Interestingly, between 1999 and 2006, 21 cases of ROSI and pioglitazone (another member of the TZD family) associated liver failure were reported to the FDA with 81% of cases resulting in fatality. During post-mortem pathological liver assessment of these patients, signs of necrosis and inflammation were detected (Floyd, Barbehenn et al. 2009). These reports imply that there is adverse cardio- and hepato- toxicity associated with the TZD compound family. All members of the TZD family are PPARγ agonists and it is through this signalling pathway that they exert their pharmacological effects. Activation of PPARγ by TRO and ROSI *in vitro* has shown that there is some degree of overlap between the gene sets that both compounds regulate (Camp et al., 2000). Altered gene expression in response to TRO dosing may provide insight into transcriptional changes that precede development of toxicity and thus may help to identify transcriptomic biomarkers of toxicity.

4.2 Chapter Aims

The aim of this chapter was to ascertain an *in vivo* transcriptomic signature of TRO induced gene changes in heart and liver tissue using a normal mouse model. The data acquired from the *in vivo* study would be used to evaluate the utility of *in vitro* mES cell derived cardiomyocytes and hepatocytes as model

systems for the evaluation of drug induced toxicity, with reference to TRO. In addition, transcriptomic data would be reviewed to deduce if it could inform on possible mechanisms of TRO induced toxicity in the heart and liver.

4.3 Results

4.3.1 Choice of *In Vivo* Model

Adult male 129P2/OlaHsd mice were chosen for this study, which was undertaken as described in section 2.4. The transcriptomic data acquired from this study was to be compared with data from treatment of E14Tg2a.4 mES cell derived cardiomyocytes and hepatocytes. This mES cell line was derived from 129P2/OlaHsd strain mice and thus to enable a direct comparison of *in vitro* and *in vivo* data mice of the same strain were chosen for this study.

4.3.2 Dose Administration and Calculated TRO Intake

During preclinical development of TRO mice were administered the drug in varying doses up to a maximum of 1600 mg/kg/day (unpublished GSK data). Other published studies have utilised doses ranging up to 1200 mg/kg/day (Breider et al., 1999, Herman et al., 2002, Jin et al., 2007). The doses used in this study reflected those used in early preclinical studies. Mice were administered TRO via the diet at intended doses of 0 (control), 200, 400, 800 and 1200 mg/kg/day for 7 and 14 days. Six mice were utilised for each dose group at both 7 and 14 day time points resulting in a total of 60 mice being used; this was undertaken to provide statistical significance to the results. TRO was administered via the diet to the mice as TRO was taken orally by patients and it had been reported that administering TRO with food increases its absorption by 30-85% (FDA, 1999b). Thus administering TRO via the diet mirrored the method of intake that was observed in the patient population and allowed for maximum absorption of the ingested dose.

The average diet consumption for a mouse is reported to be 3-5 g (Lloyd and Wolfensohn, 2003). The maximum diet consumption guideline of 5 g/day was

used to mix TRO with the diet. This equated to the maximum dose of TRO being delivered per dose group if the mice consumed 5 g of diet per day. Each dose group contained six mice, fresh diet containing TRO was administered to the mice daily and the total consumed diet weight was measured and divided by six to give an average individual mouse diet consumption value for each dose group (Table 4.1). Average diet consumption in the 7 day study ranged from 3.50 – 4.45 g/day, with the highest consumption observed in the intended 800 mg/kg/day TRO dose group. On average all of the TRO dosed mice in the 7 day study consumed more diet than the control mice. In the 14 day study the average diet consumed ranged from 3.82 – 5.63 g/day and again the highest diet consumption was observed in the intended 800 mg/kg/day TRO dose group. On average all of the TRO dosed mice, except the 400 mg/kg/day group, in the 14 day study consumed more diet than the control mice.

TRO had been mixed with the diet to provide the maximum dose for each group upon the consumption of 5 g/day. All of the mice in the 7 day study consumed less than 5 g/day of diet and subsequently the calculated average TRO doses that they received were less than the intended doses (Table 4.2). Excluding the control group, the intended TRO doses were 200, 400, 800 and 1200 mg/kg/day and the ingested doses were 159, 326, 712 and 925 mg/kg/day. In the 14 day study the control, 200 and 400 mg/kg/day dose groups consumed less than 5 g/day diet and the 800 and 1200 mg/kg/day groups consumed 5.63 and 5.33 g/day diet, respectively.

Subsequently, the lower dose groups ingested lower than intended TRO doses and the higher does groups were administered more TRO than planned. The intended doses for 14 day mice were, excluding control, 200, 400, 800 and 1200

mg/kg/day and the ingested doses were 170, 279, 901, 1280 mg/kg/day.

(A) Average Diet Consumption per mouse (g/day)				
Day Number	**TRO Dosing Group (mg/kg/day)**			
	0 (Control)	**200**	**400**	**800**	**1200**
1	3.50	3.83	3.67	4.00	3.83
2	3.00	3.33	4.33	4.50	3.83
3	3.33	4.33	4.17	4.50	3.83
4	3.33	3.67	3.67	5.00	3.67
5	3.83	4.50	4.83	4.67	4.00
6	3.83	4.50	3.83	4.33	4.00
7	3.67	3.67	4.00	4.17	3.83
Average =	3.50	3.98	4.07	4.45	3.86

(B) Average Diet Consumption per mouse (g/day)				
Day Number	**TRO Dosing Group (mg/kg/day)**			
	0 (Control)	**200**	**400**	**800**	**1200**
1	3.33	3.83	3.33	5.00	4.50
2	3.33	3.67	3.17	4.17	5.67
3	3.50	3.83	3.17	5.17	4.83
4	3.17	4.33	3.33	6.33	5.67
5	3.67	4.33	3.67	4.33	4.83
6	3.67	4.67	3.50	5.17	6.33
7	3.33	3.83	3.67	5.83	5.50
8	3.67	4.33	3.50	5.83	4.33
9	4.17	5.33	3.83	5.83	5.50
10	4.17	4.00	3.17	5.83	6.17
11	4.67	3.83	3.33	6.33	6.00
12	4.83	5.00	3.67	6.50	5.83
13	3.67	4.17	3.83	6.33	4.50
14	4.33	4.50	3.67	6.17	5.00
Average =	3.82	4.26	3.49	5.63	5.33

Table 4.1 – Average diet consumption during 7 and 14 day *in vivo* mouse studies. For each TRO dose group 6 male mice were caged together and provided with 35 g of diet/TRO mix per day. Average diet consumption per mouse (g/day) was calculated for mice in (A) 7 day and (B) 14 day studies. During both studies the highest diet consumption was observed in the 800 mg/kg/day dose groups and with the exception of the 14 day 400 mg/kg/day dose group, the TRO dosed mice consumed more diet than the control mice.

(A) Average Achieved TRO Dose Per Mouse (mg/kg/day)					
Day Number	TRO Dosing Group (mg/kg/day)				
	0 (Control)	200	400	800	1200
1	0	153	294	640	919
2	0	133	346	720	919
3	0	173	334	720	919
4	0	147	294	800	881
5	0	180	386	747	960
6	0	180	306	693	960
7	0	147	320	667	919
Average =	0	159	326	712	925

(B) Average Achieved TRO Dose Per Mouse (mg/kg/day)					
Day Number	TRO Dosing Group (mg/kg/day)				
	0 (Control)	200	400	800	1200
1	0	153	266	800	1080
2	0	147	254	667	1361
3	0	153	254	827	1159
4	0	173	266	1013	1361
5	0	173	294	693	1159
6	0	187	280	827	1519
7	0	153	294	933	1320
8	0	173	280	933	1039
9	0	213	306	933	1320
10	0	160	254	933	1481
11	0	153	266	1013	1440
12	0	200	294	1040	1399
13	0	167	306	1013	1080
14	0	180	294	987	1200
Average =	0	170	279	901	1280

Table 4.2 – Average achieved TRO dose during 7 and 14 day *in vivo* mouse studies. For each TRO dose group 6 male mice were caged together and provided with fresh diet/TRO mix per day. TRO was mixed with the diet to provide delivery of the group dose to each mouse upon consumption of 5 g/day. Using average diet consumption values (Table 4.1) the average achieved TRO doses were calculated. (A) All the mice in the 7 day study consumed less than the intended TRO doses. (B) During the 14 day study, mice in the lower two dose groups, 200 and 400 mg/kg/day, consumed less TRO than intended and mice in the higher 800 and 1200 mg/kg/day groups consumed more than the intended dose.

4.3.3 Effect of TRO on Body Weight in Mice Dosed for 7 and 14 Days

Increases in body weights were observed in both 7 and 14 day studies in control and treated mice (Figures 4.1 and 4.2). In the 7 day study there was a significant increase in body weight gain compared with control for mice dosed with 159 and 712 mg/kg/day. In contrast, in the 14 day study the greatest weight gain was observed in the control group and mice dosed with 279 mg/kg/day had significantly less weight gain in comparison to control mice.
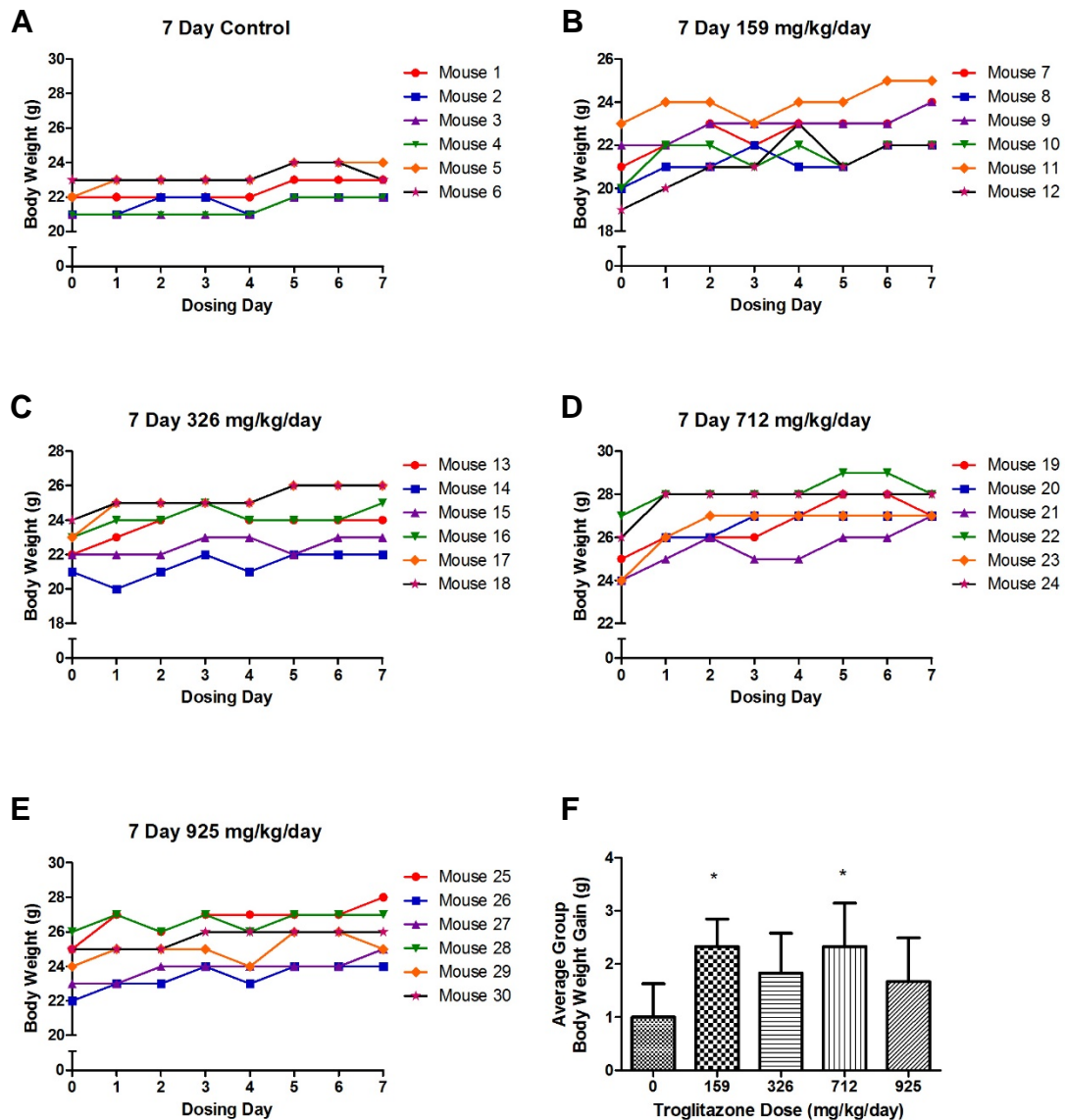
Figure 4.1 – Changes in body weight during 7 day administration of TRO via the diet. Body weights were measured daily for each mouse in the (A) control group and in the groups with average achieved TRO doses of (B) 159, (C) 326, (D) 712 and (E) 925 mg/kg/day. (F) All mice gained weight during the 7 day study. In comparison with the control group, mice administered 159 and 712 mg/kg/day TRO gained significantly more weight (data are mean ± SD (n=6) *p < 0.05 for TRO dose group compared with control (0 mg/kg/day).
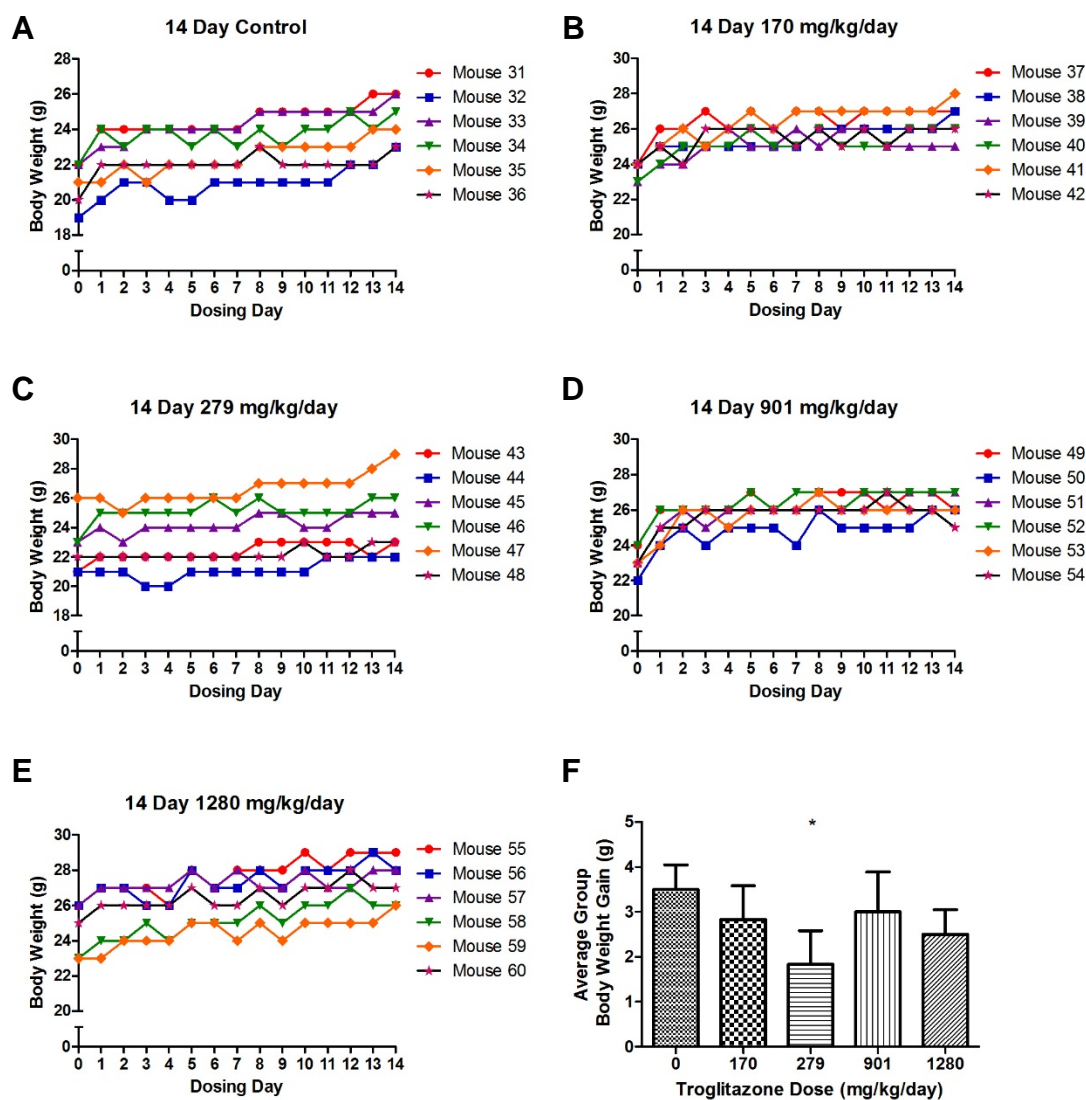
Figure 4.2 – Changes in body weight during 14 day administration of TRO via the diet. Body weights were measured daily for each mouse in the (A) control group and in the groups with average achieved TRO doses of (B) 170, (C) 279, (D) 901 and (E) 1280 mg/kg/day. (F) Increased average weight gain was observed in all dose groups. Mice administered 279 mg/kg/day TRO gained significantly less weight than the control group (data are mean ± SD (n=6) *p < 0.05 for 279 mg/kg/day dose group compared with control (0 mg/kg/day).

4.3.4 Effect of TRO on Heart Tissue

For mice in the 7 day study the average achieved TRO doses per group were 0, 159, 326, 712 and 925 mg/kg/day and in the 14 day study the average achieved TRO doses per group were 0, 170, 279, 901 and 1280 mg/kg/day. At the point of necropsy heart tissue was excised from each mouse, flash frozen in liquid nitrogen and stored at -80°C until RNA was extracted. Qualitative and quantitative analysis of extracted RNA was undertaken before it was used for microarray and RT-PCR analysis.

In-house printed mouse whole genome microarrays were used to assess differential expression of genes between heart tissue from control mice and mice dosed with 925 mg/kg/day TRO for 7 days. ArrayTrack was used to analyse microarray data and identify genes that were differentially expressed between control and TRO dose groups. Genes were selected that had Log_2 fold change values of >0.5 or <-0.5 with significance of $p<0.05$. This produced a gene list consisting of 61 up-regulated genes and 167 down-regulated genes (Figure 4.3). Most log_2 gene expression change values were found to be between -1 – -0.5 and 0.6 – 1 indicating slight changes in gene expression. Ingenuity Pathway Analysis (IPA) was used to assess the involvement of these 228 differentially expressed genes in biological and toxicological pathways however no significant connections were found.

TRO Induced Gene Expresion Changes
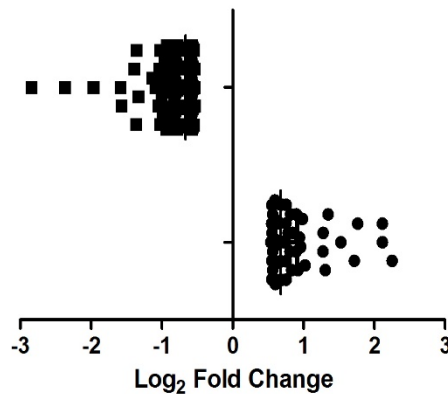
Figure 4.3 – Gene expression changes in heart tissue from mice dosed with 925 mg/kg/day TRO for 7 days. Microarray analysis identified 61 up-regulated genes and 167 down-regulated genes, with $\log_2$ fold changes <-0.5 or >0.5, in heart tissue from mice dosed with 925 mg/kg/day TRO for 7 days.

Illumina MouseWG-6 v2.0 microarrays were used to assess the differential expression of genes between heart tissue from control mice and mice dosed with 1280 mg/kg/day TRO for 14 days. ArrayTrack was used to analyse microarray data and identify genes that were differentially expressed between control and TRO dose groups. Genes were selected that had Log_2 fold change values of >0.6 or <-0.6 with significance of $p<0.05$. This produced a gene list consisting of 42 up-regulated genes and 23 down-regulated genes (Figure 4.4). Pathway analysis of these 65 differentially expressed genes identified three sub groups of genes than have been reported to interact with each other forming networks that have been associated with cardiovascular development and function, glycerol metabolism and transport and regulation of circadian rhythm (Figures 4.5).

TRO Induced Gene Expresion Changes
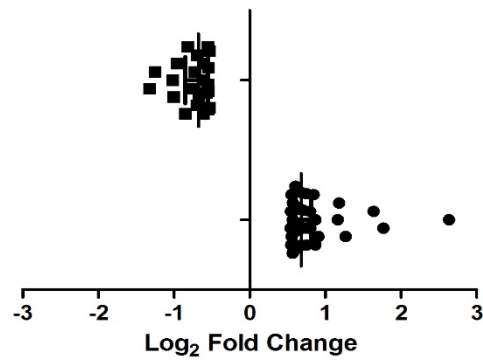
Figure 4.4 – Gene expression changes in heart tissue from mice dosed with 1280 mg/kg/day TRO for 14 days. Microarray analysis identified 42 up-regulated genes and 23 down-regulated genes, with $\log_2$ fold changes <-0.5 or >0.5, in heart tissue from mice dosed with 1280 mg/kg/day TRO for 14 days.

A Cardiovascular development and function network

B Glycerol metabolism and transport

C Circadian rhythm regulation
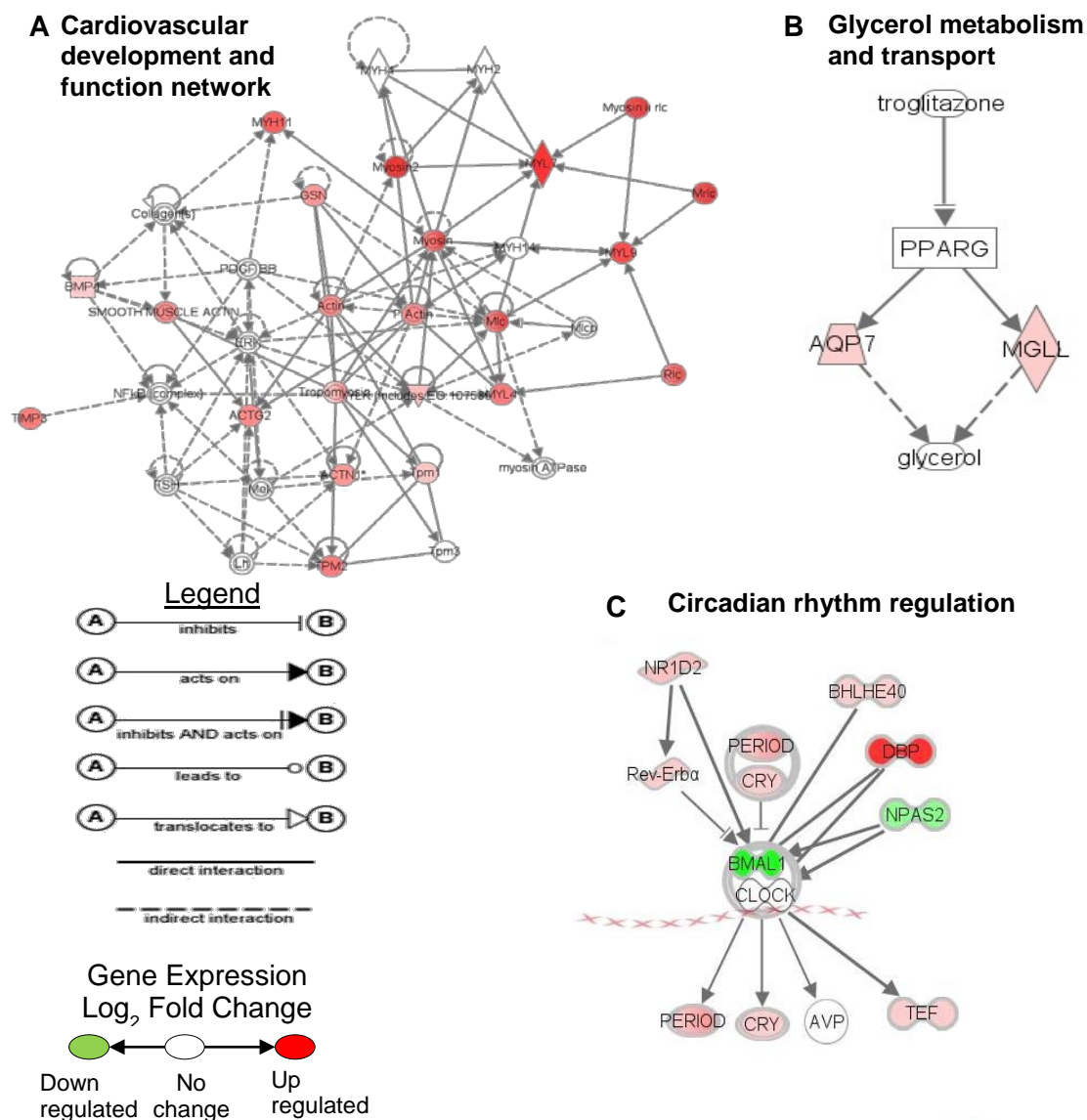
Figure 4.5 – Gene networks identified from microarray data analysis of heart tissue from mice administered 1280 mg/kg/day TRO for 14 days. Pathway analysis of microarray data from heart tissue of mice administered 1280 mg/kg/day TRO for 14 days identified that a sub-group of genes that were up-regulated by TRO interact with each other. These genes have been reported to be involved in (A) cardiovascular development and function, (B) glycerol metabolism and transport and (C) regulation of circadian rhythm Genes identified from microarray data are coloured red and green with the colour intensity representing the degree of up or down regulation of the gene in heart tissue from mice dosed with 1280 mg/kg/day TRO for 14 days compared with control mice.

The genes identified in the cardiovascular development and function network were members of the myosin gene family (Myl7, Myh11, Myl9, Mylk and Myl4), the tissue inhibitor of metalloproteinase family (Timp3 and Timp4), the actin gene family (Actg2 and Actn1), the tropomyosin gene family (Tpm2 and Tpm1), the bone morphogenetic protein family (Bmp4) and an actin depolymerizing factor (Gsn). In addition, to these genes, which had been identified by pathway analysis, Tcap, a gene that encodes for the sarcomeric telethonin protein, was also found to be up-regulated in heart tissue from mice dosed with 1280 mg/kg/day for 14 days. The microarray data from analysis of heart tissue from the top TRO dose groups in both the 7 and 14 day studies were compared to observe the expression changes of the genes Tcap, Myl7, Myh11, Timp3, Actg2, Tpm2, Gsn, Actn1, Myl9, Bmp4, Timp4, Mylk, Tpm1 and Myl4 (Figure 4.6). The expression of all 14 genes was up-regulated in the heart tissue from mice that had been administered 1280 mg/kg/day TRO for 14 days. In comparison, only Tcap was found to be up-regulated in heart tissue from mice administered 925 mg/kg/day TRO for 7 days. The 14 genes that were found to be up-regulated in heart tissue from mice dosed with 1280 mg/kg/day were cross-checked with toxicity gene lists in IPA to identify genes involved in the development of cardiac pathophysiology. A sub-set of 7 genes consisting of Myh11, Actg2, Tpm2, Timp3, Timp4, Tcap and Bmp4 were identified that have been cited in the literature as being involved in adverse cardiac events such as dilated cardiomyopathy, abnormal ventricle morphology and increased blood pressure (Figure 4.7).
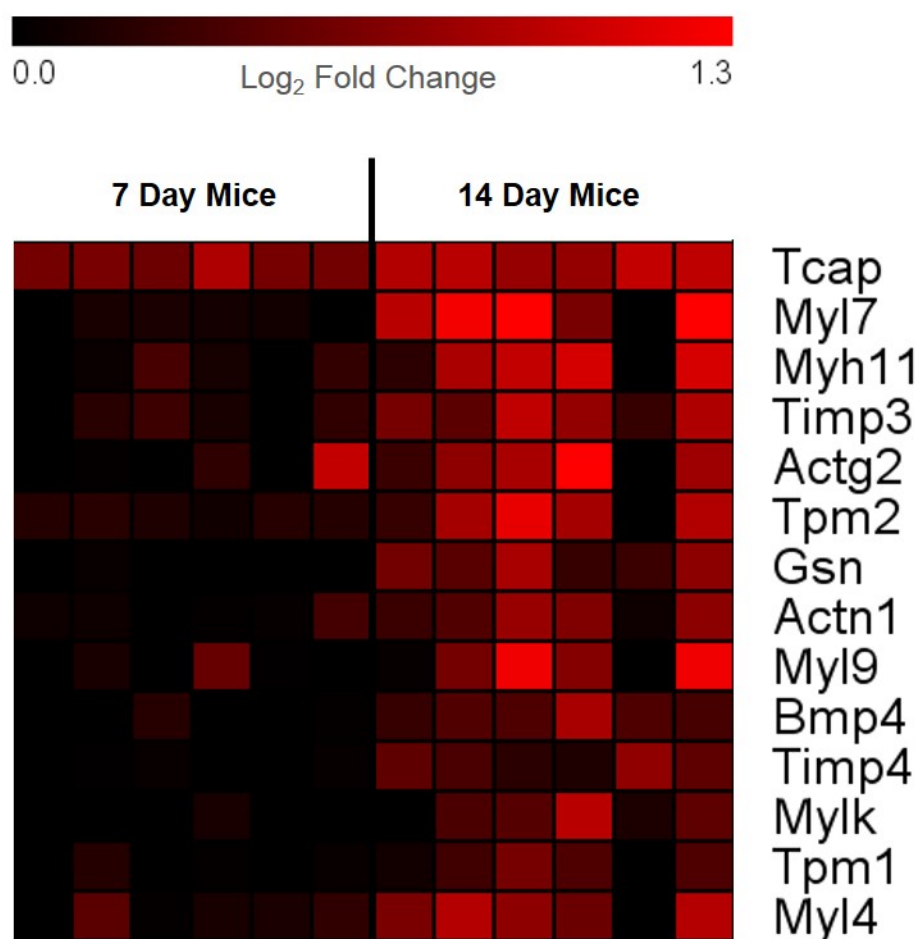
Figure 4.6 – Changes in expression of genes involved in cardiac structure and function in response to TRO treatment. Microarray analysis of heart tissue from mice dosed with 1280 mg/kg/day TRO for 14 days and 925 mg/kg/day TRO for 7 days identified a number of gene expression changes. The above genes were identified by pathway analysis and literature mining as being involved in the regulation of cardiac structure and function. Only increased expression of Tcap was observed in heart tissue after 7 days of TRO treatment however, after 14 days increased expression of all genes was observed (data are $\log_2$ fold changes of gene expression in each mouse (each column represents an individual mouse) in the top TRO dose groups at day 7 and 14 in comparison with their respective controls. Results are statistically significant at $p<0.05$ by Welch's t-test for all genes at day 14 and for Tcap at day 7 in comparison with control).
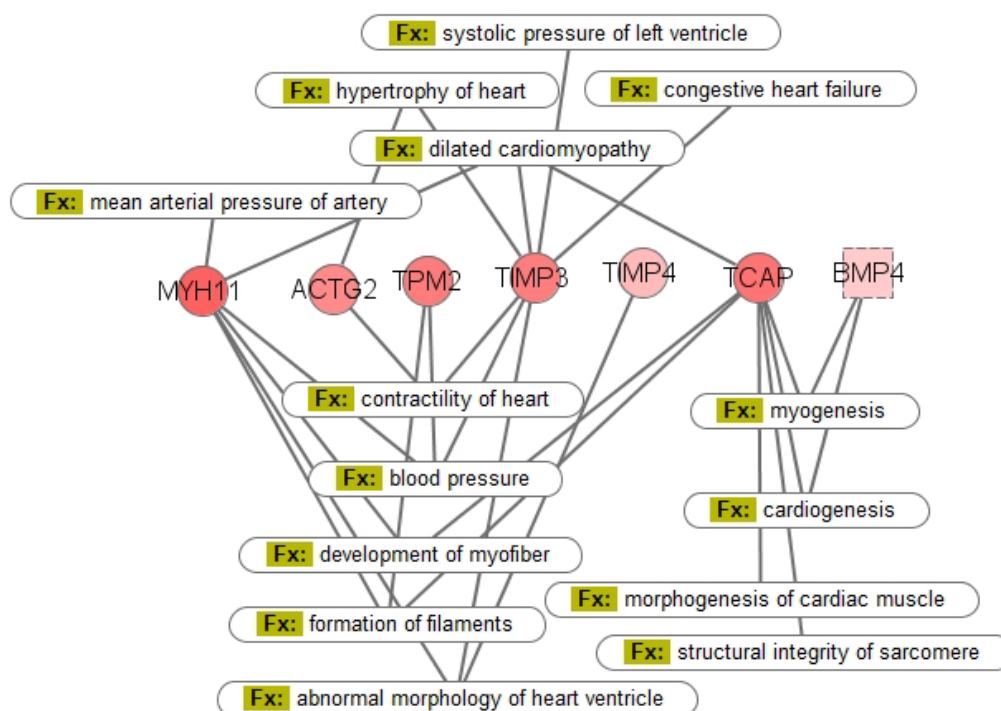
Figure 4.7 – TRO treatment increased expression of genes involved in development of cardiac pathophysiology. Administering 1280 mg/kg/day TRO for 4 days resulted in up-regulation of genes involved in regulating cardiac structure and function. Seven of these genes were identified by pathway analysis as being involved in the development of adverse cardiac events such as dilated cardiomyopathy, abnormal ventricle morphology and increased blood pressure. Expression of these genes was first identified by microarray analysis (Figure 4.6) and then confirmed by RT-PCR (Figure 4.8).

RT-PCR analysis was used to confirm the increased expression of these genes, which had been initially identified by microarray analysis, in heart tissue from mice dosed with 1280 mg/kg/day TRO. Furthermore, RT-PCR was used to assess the expression of these 7 genes in heart tissue from mice dosed with 170, 279 and 901 mg/kg/day TRO (compared with controls) for 14 days and in all mice from the 7 day study. Significantly increased expression of Bmp4, Tcap, Timp4 and Tpm2 was observed in heart tissue from mice dosed with 279, 901 and 1280 mg/kg/day TRO for 14 days compared with control mice, whereas TRO induced expression of Myh11, Actg2 and Timp3 was only observed with mice administered 901 and 1280 mg/kg/day TRO for 14 days (Figure 4.8). RT-PCR analysis of heart tissue from mice in the 7 day study identified only changes in the expression of Tcap, which was significantly higher in heart tissue from mice that had been administered 712 and 925 mg/kg/day for 7 days compared with control mice (Figure 4.10). The RT-PCR data confirmed the gene expression changes that had been identified by microarray analysis of heart tissue from mice administered the highest TRO doses for 7 and 14 days. These data also illustrated that similar increases in the expression levels of genes involved in the development of cardiac pathophysiology were induced in mice dosed with 901 and 1280 mg/kg/day TRO for 14 days. These data identified that administration of TRO could induce expression of Myh11, Actg2, Tpm2, Timp3, Timp4, Tcap and Bmp4, which have been associated with the development of cardiac pathophysiology.
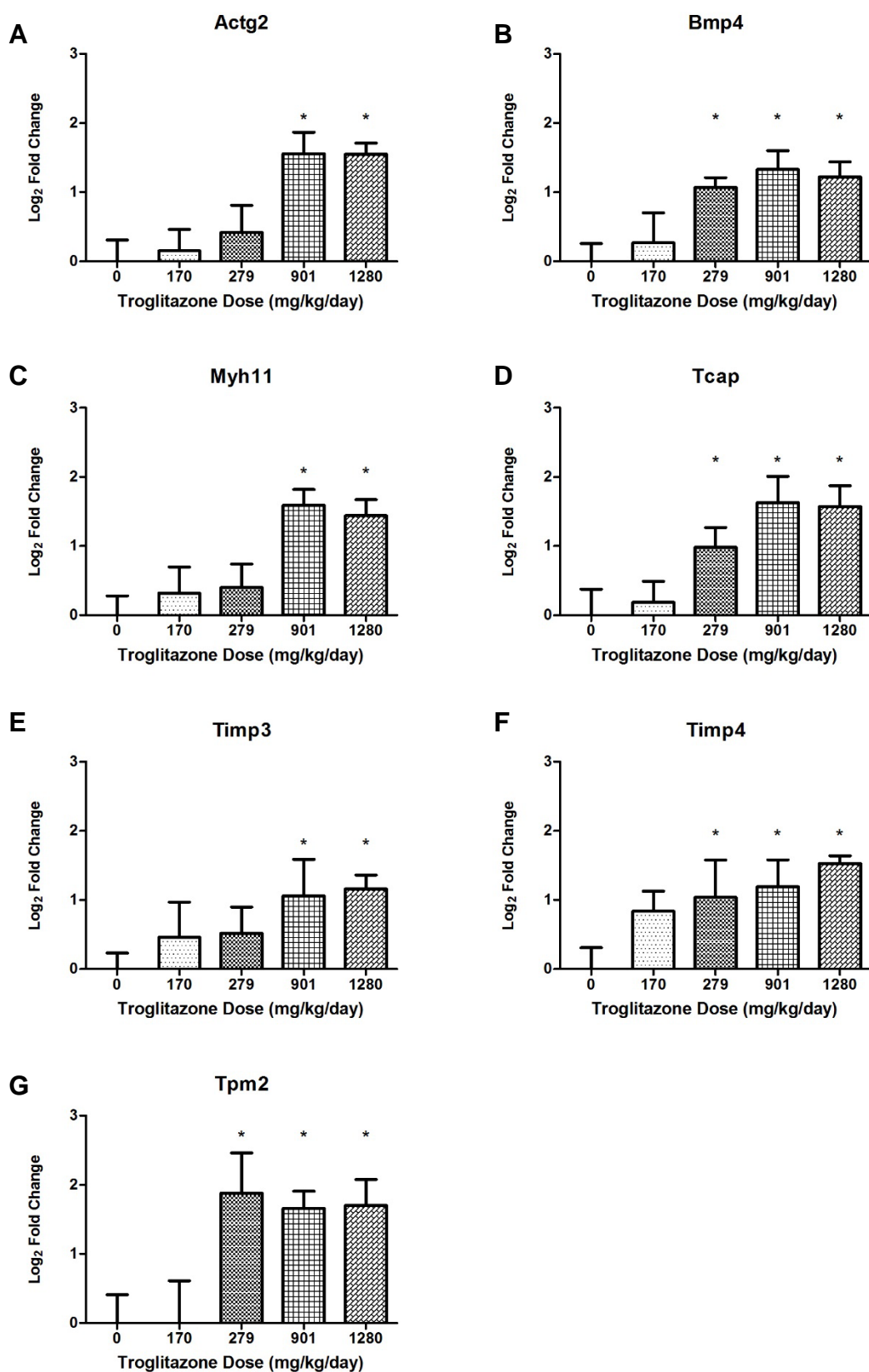
Figure 4.8 – TRO induced gene expression changes in heart tissue of mice administered TRO for 14 days. Please see next page for figure legend.

Figure 4.8 – TRO induced gene expression changes in heart tissue of mice administered TRO for 14 days. Expression of genes identified as being involved in the development of cardiac pathophysiology were assessed by RT-PCR. Heart tissue from mice dosed with 0, 170, 279, 901 and 1280 mg/kg/day TRO for 14 days was analysed for the expression of (A) Actg2, (B) Bmp4, (C) Myh11, (D) Tcap, (E) Timp3, (F) Timp4 and (G) Tpm2. Mice dosed with 901 and 1280 mg/kg/day TRO for 14 days had significantly higher levels of Actg2, Bmp4, Myh11, Tcap, Timp3, Timp4 and Tpm2 gene expression than control mice (0 mg/kg/day dose group). Expression of Bmp4, Tcap, Timp4 and Tpm2 was also up-regulated in mice administered 279 mg/kg/day TRO compared with controls (data are mean ± SD (n=6), results are statistically significant at $p<0.05$ for given dose compared with control by one-way ANOVA with post hoc Dunnett's test).
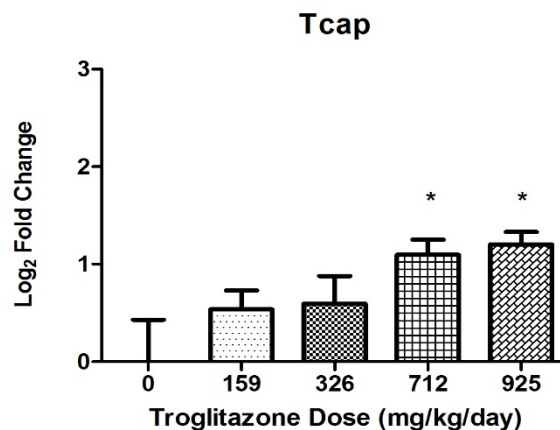
Figure 4.9 – Expression of Tcap gene in heart tissue of mice administered TRO for 7 days. Expression of Tcap in heart tissue from mice administered 0 (control), 159, 326, 712, 925 mg/kg/day TRO for 7 days was assessed by RT-PCR. Mice dosed with 712 and 925 mg/kg/day TRO had significantly higher levels of Tcap expression compared with control mice. Significant differences between the expression of Tcap in control mice and mice dosed with 159 and 326 mg/kg/day TRO were not observed (data are mean ± SD (n=6), results are statistically significant at $p<0.05$ for given dose compared with control by one-way ANOVA with post hoc Dunnett's test).

Pathway analysis of microarray data from mice dosed with 1280 mg/kg/day TRO for 14 days identified that increased expression of the genes encoding for aquaporin 7 (Aqp7) and monoglyceride lipase (Mgll) were consequences of TRO induced Ppary activation. Furthermore, Aqp7 and Mgll were associated with transport and metabolism of glycerol. Expression of Aqp7 and Mgll in heart tissue of mice dosed with 0 (control), 170, 279, 901 and 1280 mg/kg/day for 14 days was assessed by RT-PCR (Figure 4.10). Increased expression of Aqp7 and Mgll was observed in the heart tissue of mice administered 901 and 1280 mg/kg/day compared with controls. Administering 159 and 326 mg/kg/day TRO for 7 days did not induce changes in expression of Aqp7 and Mgll. Expression of both genes in heart tissue from mice administered 0 (control), 159, 326, 712, 925 mg/kg/day TRO for 7 days was also assessed by RT-PCR however, no differences in expression were observed between the control and dosed mice.
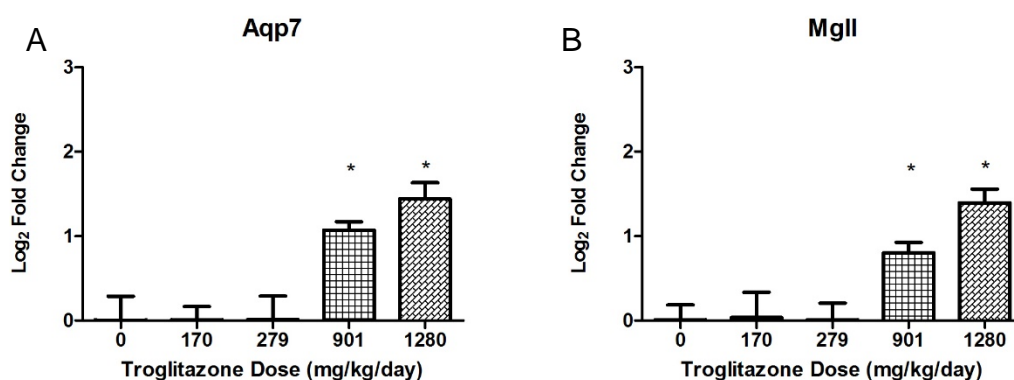
Figure 4.10 – Expression of Aqp7 and Mgll in heart tissue of mice administered TRO for 14 days. Expression of (A) Aqp7 and (B) Mgll in heart tissue of mice administered 0 (control), 170, 279, 901 and 1280 mg/kg/day TRO for 14 days was assessed by RT-PCR. In comparison with controls, mice administered 901 and 1280 mg/kg/day had increased cardiac expression of Aqp7 and Mgll (data are mean ± SD (n=6), results are statistically significant at $p < 0.05$ for given dose compared with control by one-way ANOVA with post hoc Dunnett's test).

Pathway analysis of microarray data from mice dosed with 1280 mg/kg/day TRO for 14 days identified differential expression of genes involved in regulation of circadian rhythm. The genes Dbp, Per2, Nr1d2, Tef, Nr1d1, Bhlhb2, Cry2 and Per1 were up-regulated and the genes Npas2 and Arntl were down-regulated in the hearts of mice administered 1280 mg/kg/day TRO for 14 days. Cross reference of these 10 genes with microarray data generated from analysis of heart tissue from mice dosed with 925 mg/kg/day TRO for 7 days revealed that some of the genes were also up-regulated after 7 days of TRO treatment. However, the expression of Npas2, which was down-regulated in heart tissue of mice dosed with 1280 mg/kg/day TRO for 14 days was up-regulated in the hearts of mice administered 925 mg/kg/day for 7 days (Figure 4.11). The $\log_2$ fold changes in gene expression observed at day 7 were smaller than the changes measured at day 14. Pathway analysis did not link changes in expression of circadian genes with development of adverse cardiac events.

Administering TRO to mice at various doses for 7 and 14 days induced expression changes in a small sub-set of genes. The greatest changes were detected in mice administered 1280 mg/kg/day TRO for 14 days. The gene changes were not associated with overt toxicity however, increased expression of several genes that encode for sarcomeric proteins implies that adaptive changes at the transcriptomic level were occurring after 14 days of TRO treatment. The transcriptomic signature of TRO on heart tissue includes changes in expression of genes involved in cardiovascular function, glycerol transport and metabolism and regulation of circadian rhythm.
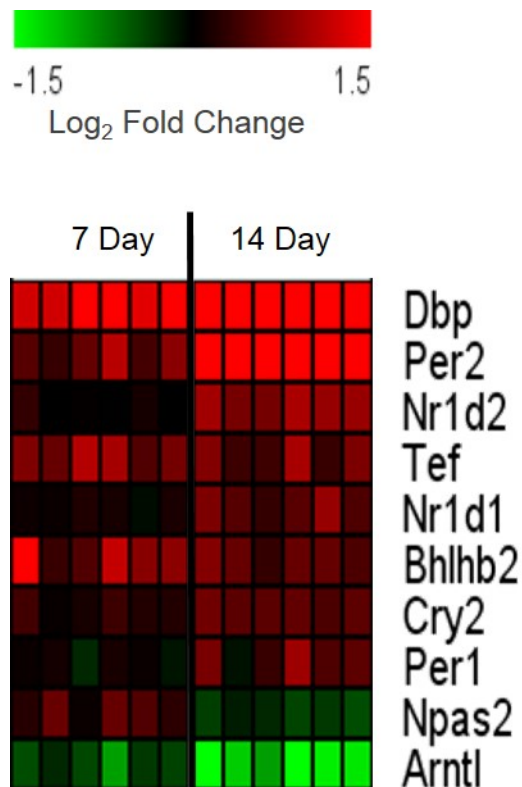
Figure 4.11 – Changes in expression of circadian clock genes in heart tissue of mice dosed with TRO for 7 and 14 days. Microarray analysis of heart tissue from mice dosed with 1280 mg/kg/day TRO for 14 days and 925 mg/kg/day TRO for 7 days identified changes in expression of genes involved in regulation of circadian rhythm (data are $\log_2$ fold changes of gene expression in each mouse (each column represents a mouse) in the top TRO dose groups at day 7 and 14 in comparison with their respective controls. Results are statistically significant at $p<0.05$ by Welch's t-test for all genes at day 14 and for Dbp, Per2, Tef, Bhlb2 and Arntl at day 7 in comparison with control).

4.3.5 Effect of TRO on Liver Tissue

4.3.5.1 Histopathological Analysis of Liver Tissue

At the point of necropsy in both the 7 and 14 day studies, small tissue sections were taken from the livers of 3 mice per dose group. Samples were sent to GSK for histopathological assessment by GSK pathologists; the reported observations are listed in Table 4.3. No abnormalities were observed in any of the liver samples from the control mice (0 mg/kg/day TRO groups). In the 7 day study centrilobular hypertrophy, ranging from minimal to mild, was observed in 2 of the 3 mice in the 326 mg/kg/day dose group and in all 3 mice in the 712 and 925 mg/kg/day dose groups. In addition, in the liver tissue of one mouse in the 326 mg/kg/day group minimal increased mitotic activity was observed. No abnormalities were observed in the livers of mice dosed with 159 mg/kg/day. In the 14 day study all TRO doses induced some degree of centrilobular hypertrophy. In the 170 and 279 mg/kg/day groups one mouse had minimal and two mice had mild centrilobular hypertrophy. In the 901 mg/kg/day group the three tested mice each had different degrees of centrilobular hypertrophy, minimal, mild and moderate. In the top 1280 mg/kg/day dose group one mouse had mild and two mice had moderate centrilobular hypertrophy. One mouse in each of the 279, 901 and 1280 mg/kg/day groups had minimal increased mitotic activity. The results indicate that TRO caused centrilobular hypertrophy in a time and dose dependent manner.

(A) 7 Day Study	Troglitazone Dose Group (mg/kg/day)				
Liver Observation	0 (control)	159	326	712	925
No Abnormality Detected	3 mice	3 mice	1 mouse		
Centrilobular Hypertrophy			1 mouse - minimal 1 mouse - mild	3 mice - mild	3 mice - mild
Minimal Increased Mitotic Activity			1 mouse - some abnormally shaped figures observed		

(B) 14 Day Study	Troglitazone Dose Group (mg/kg/day)				
Liver Observation	0 (control)	170	279	901	1280
No Abnormality Detected	3 mice				
Centrilobular Hypertrophy		1 mouse - minimal 2 mice - mild	1 mouse - minimal 2 mice - mild	1 mouse - minimal 1 mouse - mild 1 mouse - moderate	1 mouse - mild 2 mice - moderate
Minimal Increased Mitotic Activity			1 mouse - some abnormally shaped figures observed	1 mouse - some abnormally shaped figures observed	1 mouse - some abnormally shaped figures observed

Table 4.3 – Histopathological observations of liver tissue from mice dosed with TRO for 7 and 14 days. Liver tissue samples were sent to GSK for histopathological analysis from 3 of the 6 mice in each dose group at both time points.(A) In the 7 day study centrilobular hypertrophy was observed in 2 mice from the 326 mg/kg/day group and in all 3 tested mice in the 712 and 925 mg/kg/day groups (B) In the 14 day study centrilobular hypertrophy was detected in all 3 mice examined from each dose group with moderate hypertrophy being detected in 2 mice from the highest TRO dose group.

4.3.5.2 Transcriptomic Analysis of Liver Tissue

In-house printed mouse whole genome microarrays were used to assess differential expression of genes between liver tissue from control mice and mice dosed with 1280 mg/kg/day TRO for 14 days. ArrayTrack was used to analyse microarray data and identify genes that were differentially expressed between control and TRO dose groups. Genes were selected that had Log_2 fold change values of >0.5 or <-0.5 with significance of $p<0.05$. This produced a gene list consisting of 297 up-regulated genes and 473 down-regulated genes (Figure 4.12). Most log_2 gene expression change values were found to be between -1.2 – -0.5 and 0.6 – 1.1 indicating slight changes in gene expression. The circadian clock gene Dbp was the most up-regulated gene and the most down-regulated gene was Chka, which encodes for the protein choline kinase alpha. IPA was used to assess the involvement of these 770 differentially expressed genes in biological and toxicological pathways.

TRO Induced Gene Expresion Changes
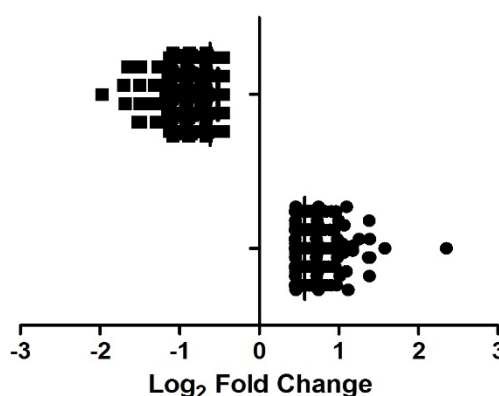
Figure 4.12 – Gene expression changes in liver tissue from mice dosed with 1280 mg/kg/day TRO for 14 days. Microarray analysis identified 297 up-regulated genes and 473 down-regulated genes, with log_2 fold changes <-0.5 or >0.5, in liver tissue from mice dosed with 1280 mg/kg/day TRO for 14 days.

Pathway analysis identified a sub-group of 29 genes that were up or down regulated in the livers of mice administered 1280 mg/kg/day TRO for 14 days compared with controls. The genes encoded for enzymes involved in the metabolism of fatty acids (Figure 4.13). Microarray analysis of liver tissue identified that administration of 1280 mg/kg/day TRO for 14 days caused an increase in the expression of genes involved in fatty acid (FA) metabolism (Figure 4.14). The genes Aadac, Lipf, Lpl, Prdx6, Mgll and Gpd2 encode for enzymes involved in the degradation of triglycerides and glycerol, a process that produces fatty acids (FAs) for use in the production of energy. Mitochondrial β-oxidation of long chain FAs is regulated by carnitine palmitoyltransferase, which is encoded for by the gene Cpt1a and located in the outer mitochondrial membrane. This enzyme controls the rate-limiting step in the transport of FAs across the mitochondrial membrane into the mitochondrial matrix where FAs are metabolised further. The genes Aldh5a1, Acat1, Hadha, Hmgcs1, Hmgcl and Acox2 encode for enzymes involved in the production of Acetyl-CoA, a substrate produced during FA β-oxidation which feeds into the tricarboxylic acid (TCA) cycle enabling production of NADH (nicotinamide adenine dinucleotide). NADH and $FADH_2$ (flavin adenine dinucleotide), which is produced during FA β-oxidation, are used in the electron transport chain for production of ATP (adenosine triphosphate) (Berg et al., 2002, Jogl et al., 2004). Several of the up-regulated genes involved in FA metabolism are downstream targets of Pparγ and TRO is a Pparγ agonist (Berger and Moller, 2002, Rakhshandehroo et al., 2010). This implies that increased expression of genes involved in FA metabolism is an effect of TRO mediated activation of Pparγ and is reflective of the pharmacological activity of TRO.

Figure 4.13 TRO administration increases expression of genes involved in fatty acid metabolism in the liver. Genes identified from pathway analysis of microarray data from mice dosed with 1280 mg/kg/day TRO for 14 days were associated with processes involved in metabolism of fatty acids in the liver. Red and green colouring of gene symbols represents up and down regulation, respectively, of gene expression.

Figure 4.14 – TRO treatment effected expression of genes involved in hepatic fatty acid metabolism. Microarray analysis of liver tissue from mice dosed with 1280 mg/kg/day TRO for 14 identified a number of gene expression changes. These genes were identified by pathway analysis and literature mining as being involved in hepatic FA metabolism (data are $\log_2$ fold changes of gene expression in each mouse (each column represents a mouse) in the top TRO dose groups at day 7 and 14 in comparison with their respective controls. Results are statistically significant at $p < 0.05$ for comparison of mice dosed with 1280 mg/kg/day TRO for 14 days compared with control mice by Welch's t-test).

Microarray analysis did not reveal any differences in the expression of Pparγ and Pparα between control mice and mice administered 1280 mg/kg/day for 14 days. However, increased expression of hepatic Pparγ and Pparα in mice dosed with TRO was detected using RT-PCR (Figure 4.15). Significantly increased expression of Pparγ and Pparα was detected in the livers of mice administered 901 and 1280 mg/kg/day TRO for 14 days, compared with controls. Liver tissues from all mice in the 7 day study were also analysed using RT-PCR however, significant differences in gene expression between control and TRO dosed mice were not observed.
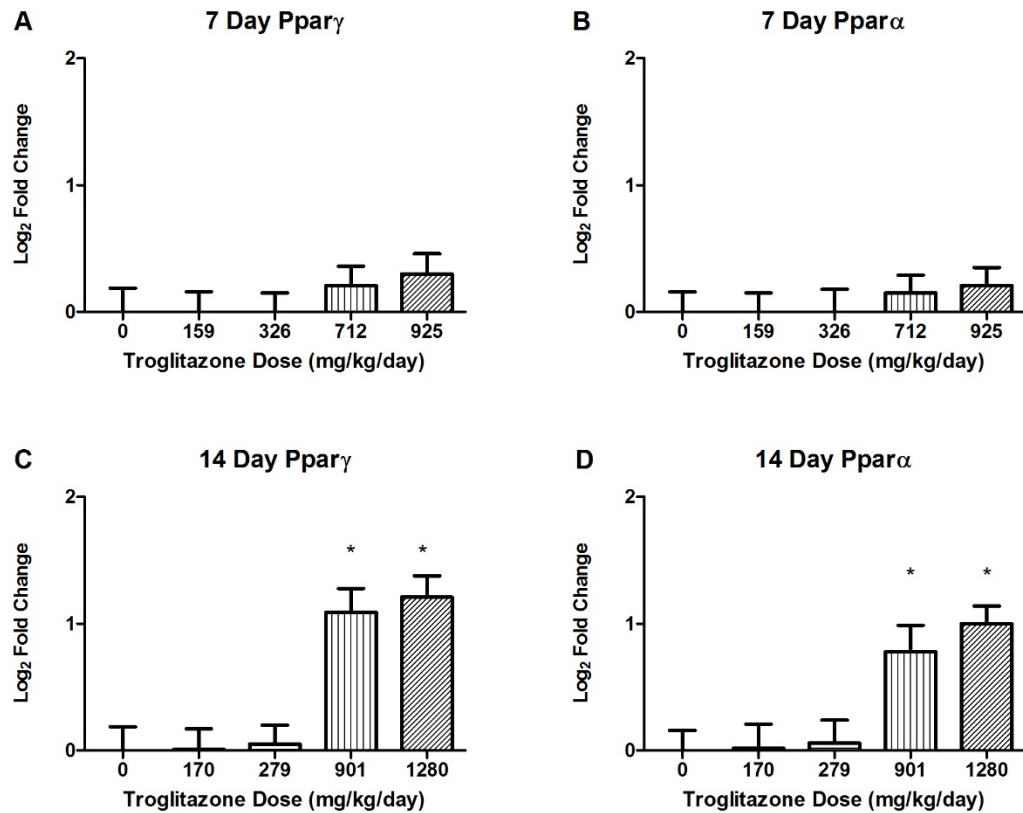
Figure 4.15 – Expression of Pparɣ and Pparα in liver tissue of mice administered TRO for 7 and 14 days. Expression of (A) Pparɣ and (B) Pparα in liver tissue of mice administered 0 (control), 159, 326, 712 and mg/kg/day TRO for 7 days and expression of (C) Pparɣ and (D) Pparα in liver tissue of mice administered 0 (control), 170, 279, 901 and 1280 mg/kg/day TRO for 14 days was assessed by RT-PCR. In comparison with controls, mice administered 901 and 1280 mg/kg/day TRO had increased cardiac expression of hepatic Pparɣ and Pparα. Administering TRO for 7 days did not significantly affect expression of hepatic Pparɣ and Pparα (data are mean ± SD (n=6), results are statistically significant at $p<0.05$ for given dose compared with control by one-way ANOVA with post hoc Dunnett's test).

Pathway analysis identified increased expression of the genes Cyp7a1 and Scp2 in the livers of mice dosed with 1280 mg/kg/day TRO for 14 days. These two genes encode for enzymes involved in the neutral bile acid synthesis pathway (Figure 4.16). In addition, reviewing microarray data identified increased expression of Cyp7b1, which encodes for an enzyme involved in the acidic bile acid synthesis pathway and increased expression of Abcc2, which encodes for a bile salt exporter pump. These four genes are involved in the production and transport of bile acids and their expression in the livers of control and TRO dosed mice was assessed by RT-PCR. Analysis of liver tissue from mice administered 159, 326, 712 and 925 mg/kg/day TRO for 7 days in comparison with controls did not identify changes in the expression of Cyp7a1, Cyp7b1, Abcc2 and Scp2. Thus administering TRO for 7 days at various doses did not alter bile acid production or transport. Analysis of liver tissue from mice dosed with TRO for 14 days illustrated, in comparison to controls, identified increased expression of Cyp7a1, Cyp7b1, Abcc2 and Scp2 in mice administered 279, 901 and 1280 mg/kg/day TRO (Figure 4.17). A significant increase in the expression of these four genes was not observed in the livers from mice dosed with 170 mg/kg/day for 14 days. The data illustrate that TRO induced up-regulation of Cyp7a1, Cyp7b1, Abcc2 and Scp2 occurred in a dose dependent manner.
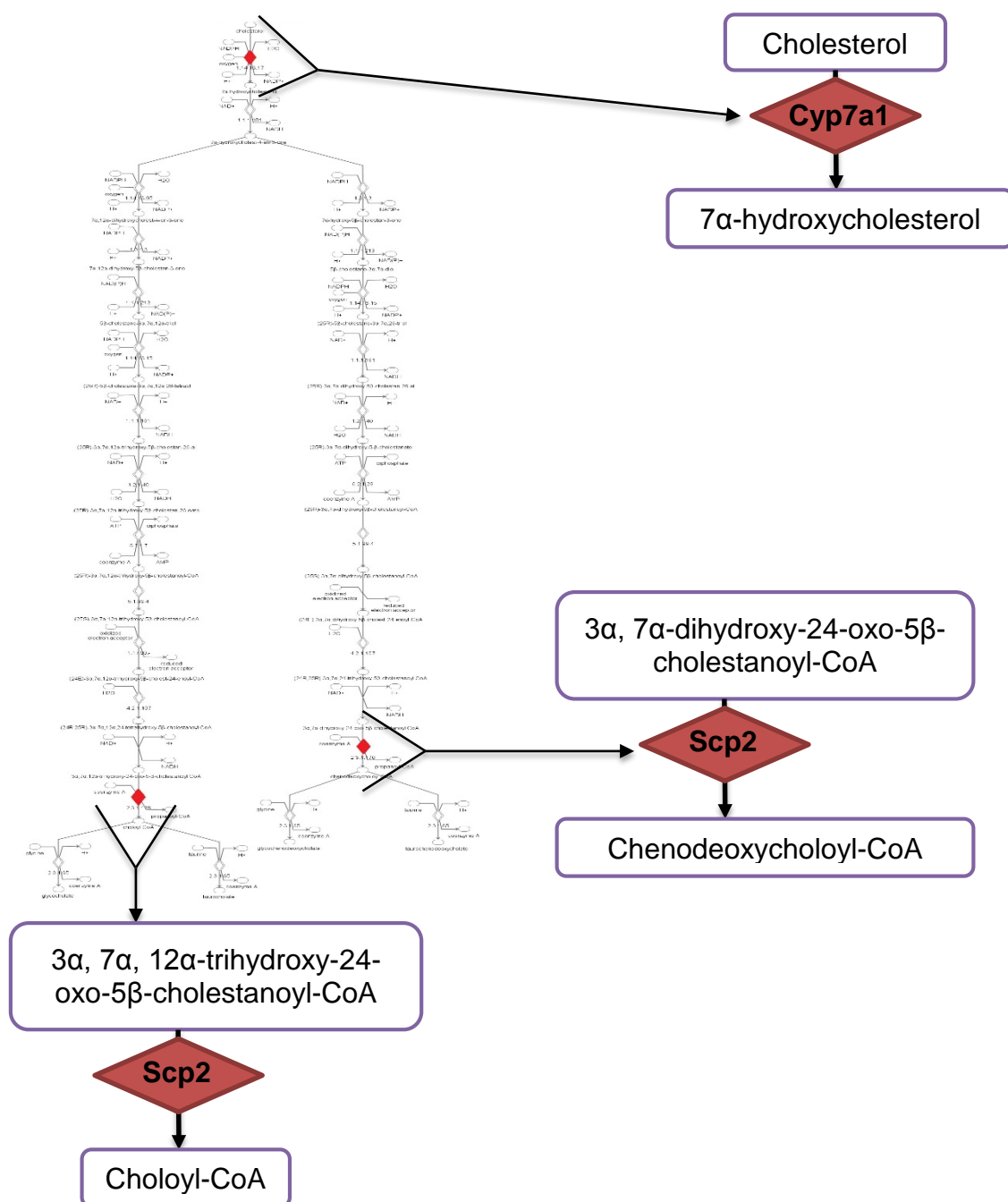
**Figure 4.16 – Bile acid synthesis pathway identified from microarray data analysis of liver tissue from mice administered 1280 mg/kg/day TRO for 14 days.** Pathway analysis of microarray data from liver tissue of mice administered 1280 mg/kg/day TRO for 14 days identified increased expression of Cyp7a1 and Scp2 in comparison with controls (symbols coloured red). Cyp7a1 encodes for the first and rate-limiting enzyme in the process of converting cholesterol into bile acids.
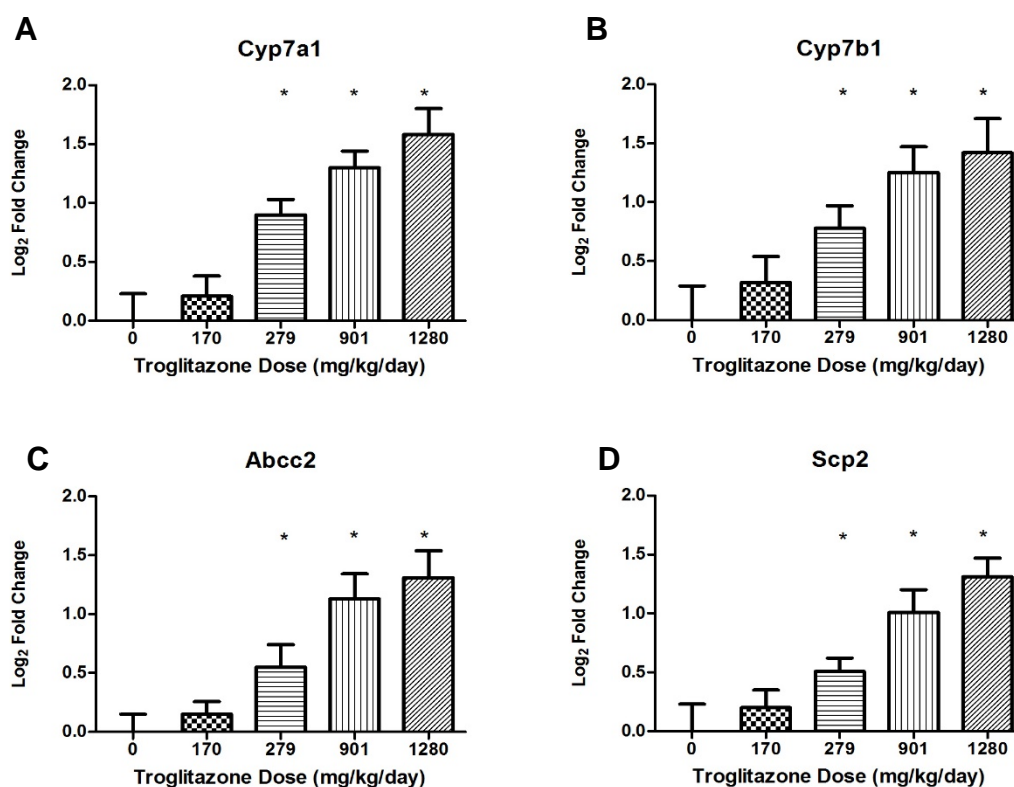
Figure 4.17 – Expression of genes involved in bile acid synthesis and transport in liver tissue of mice administered TRO for 14 days. Expression of (A) Cyp7a1, (B) Cyp7b1, (C) Abcc2 and (D) Scp2 in liver tissue of mice administered 0 (control), 170, 279, 901 and 1280 mg/kg/day TRO for 14 days was assessed by RT-PCR. In comparison with controls, mice administered 279, 901 and 1280 mg/kg/day had increased expression of the genes Cyp7a1 and Scp2, which encode for enzymes involved in the neutral bile acid synthesis pathway, increased expression of the gene Cyp7b1, which encodes for an enzyme involved in the acidic bile acid synthesis pathway and up-regulation of Abcc2, which encodes for a bile salt exporter pump (data are mean $\pm$ SD (n=6), results are statistically significant at $p < 0.05$ for given dose compared with control by one-way ANOVA with post hoc Dunnett's test).

Analysis of microarray data derived from the liver tissue from mice administered 1280 mg/kg/day TRO for 14 days identified increased expression of genes reported to be involved in the response of the liver to xenobiotic metabolism and cellular stress. These genes were not detected by pathway analysis, they were identified by reviewing literature. Expression of Dbp and Tef, two of the three members of the PAR bZip transcription factor family, are regulated by the circadian clock and are involved in regulating the expression of genes involved in xenobiotic metabolism including PPARα (Paschos et al., 2010). Expression of Dbp was up-regulated in liver tissue of mice administered 279, 901 and 1280 mg/kg/day TRO for 14 and expression of Tef was upregulated in livers of mice dosed with 901 and 1280 mg/kg/day TRO (Figure 4.18). Increased expression of Dbp was also detected in livers of mice dosed with TRO for 7 days but only in the 925 mg/kg/day dose group. Increased expression of hepatic Tef was not detected at any TRO dose in the 7 day study. Thrsp mRNA levels in the liver are increased when *de novo* fatty acid synthesis is chemically induced. Up-regulation of Thrsp was only observed in the livers of mice administered 1280 mg/kg/day TRO for 14 days; increased expression was not detected in the livers of mice from the other TRO dose groups in the 14 day study and nor at any TRO dose level in the 7 day study (Figure 4.19). Activation of Thrsp has been linked to fat accumulation in animal models (Breuker et al., 2010). Expression of Atf4 and Ddit3 and their downstream target Trib3 is induced by endoplasmic reticulum (ER) stress (Han et al., 2013). In mice from the 14 day study, increased expression of Atf4, Ddit3 and Trib3 was detected in the livers of mice dosed with 1280 mg/kg/day. Up-regulation of Ddit3 was also seen in livers from mice dosed with 901 mg/kg/day and increased expression of hepatic Trib3 was measure in mice administered

279, 901 and 1280 mg/kg/day. Increased expression of Atf4 and Ddit3 was not observed in the livers of mice dosed with TRO for 7 days and up-regulation pf Trib3 was only observed in mice administered 925 mg/kg/day. Furthermore, increased expression another ER stress marker, Dnajb9, was detected in livers of mice administered 901 and 1280 mg/kg/day for 14 days (Figure 4.20).
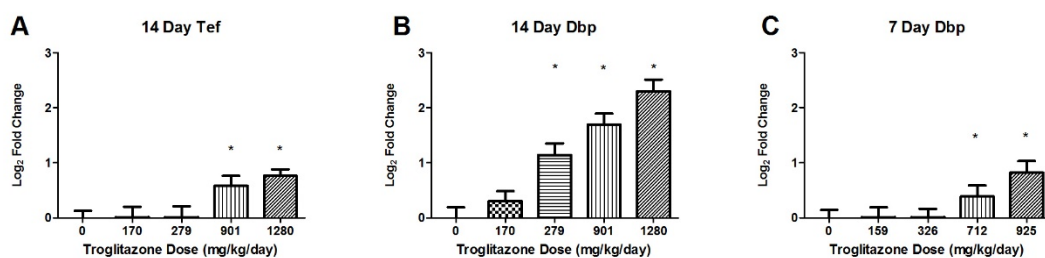
Figure 4.18 – Expression of circadian clock output in liver tissue of mice administered TRO for 7 and14 days. Expression of (A) Tef and (B) Dbp in the livers of mice dosed with TRO for 14 days and expression of hepatic (C) Dbp in mice administered TRO for 7 days was assessed by RT-PCR. In comparison with controls, Tef was up-regulated in mice that had been administered 901 and 1280 mg/kg/day for 14 days. Expression of Dbp was ALSO up-regulated in mice from these two dose groups and also in mice administered 279 mg/kg/day TRO for 14 days. Expression of Tef was not different been control and dosed mice in the 7 day study however, increased expression of Dbp was detected in mice administered 712 and 925 mg/kg/day TRO for 7 days (data are mean ± SD (n=6), results are statistically significant at *$p < 0.05$ for given dose compared with control by one-way ANOVA with post hoc Dunnett's test).
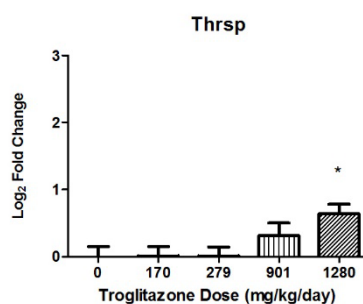
Figure 4.19 – Expression of hepatic Thrsp in mice administered TRO for 14 days. Expression of Thrsp in the livers of mice dosed with TRO for 14 days was assessed by RT-PCR. In comparison with controls, Thrsp was significantly up-regulated in mice that had been administered 1280 mg/kg/day for 14 days (data are mean ± SD (n=6), *p<0.05 for given dose compared with control by one-way ANOVA with post hoc Dunnett's test).
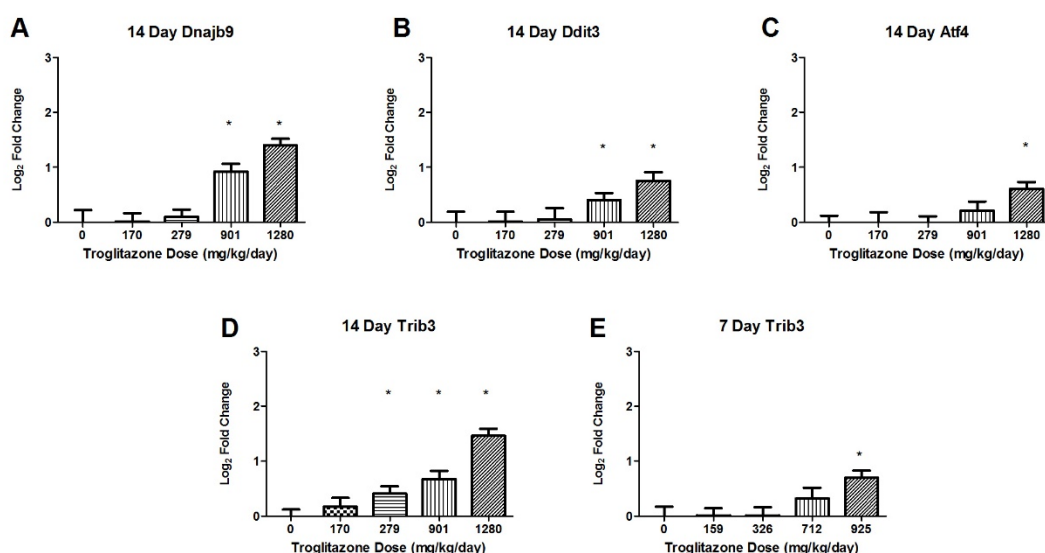
Figure 4.20 – Expression of ER stress associated genes in liver tissue of mice administered TRO for 7 and14 days. Expression of (A) Dnajb9, (B) Ddit3, (C) Atf4 and (D) Trib3 in the livers of mice dosed with TRO for 14 days and expression of hepatic (C) Trib3 in mice administered TRO for 7 days was assessed by RT-PCR. In comparison with controls, Dnajb9 and Ddit3 were up-regulated in mice that had been administered 901 and 1280 mg/kg/day for 14 days and increased expression of hepatic Atf4 was found in mice administered 1280 mg/kg/day for 14 days. Trib3 was up-regulated in the livers of mice administered 279, 901 and 1280 mg/kg/day for 14 days and in mice dosed with 925 mg/kg/day for 7 days (data are mean ± SD (n=6), *p<0.05 for given dose compared with control by one-way ANOVA with post hoc Dunnett's test).

4.4 Discussion

The aim of this study was to identify changes at the transcriptomic level *in vivo* which could be compared with profiles generated *in vitro* using stem cell based models. In addition it was anticipated that transcriptomic changes in the heart and liver tissue would inform on potential mechanisms of TRO induced toxicity. *In vivo* mouse transcriptomic data was required to ascertain the suitability of using *in vitro* differentiated mES cell based models for the detection and understanding of TRO induced toxicity. The differentiated mES cells were anticipated to be similar to cardiomyocytes and hepatocytes *in vivo* from wild type mice. Therefore, to allow comparison of *in vitro* and *in vivo* data a profile of TRO induced transcriptomic changes in a normal mouse model was required.

4.4.1 TRO Induced Transcriptomic Changes in the Heart

Transcriptomic analysis of heart tissue from mice dosed with TRO for 7 and 14 days was undertaken using microarrays and RT-PCR. Pathway analysis and literature mining was used to link gene expression changes to physiological and toxicological pathways. Microarray analysis of heart tissue from mice administered 1280 mg/kg/day for 14 days showed increased expression of genes involved in cardiovascular development and function, glycerol metabolism and transport and circadian regulation. These gene sets formed the gene signature for the effects of TRO on the hearts of normal mice and gene expression changes were most prevalent in mice dosed with 1280 mg/kg/day for 14 days.

TRO induced changes in the expression of genes involved in the regulation of cardiac circadian rhythm are most likely a pharmacological rather than toxicological effect of the drug. The master circadian clock is found in the suprachiasmatic nuclei (SCN) of the anterior hypothalamus with peripheral clocks

206

found in tissues such as the heart, liver, kidneys and skeletal muscle (Reppert and Weaver, 2001). Circadian clocks control numerous processes such as, sleep-wake cycles, metabolism, blood pressure, body temperature and hormone secretion. Furthermore, disruption of the clock has been linked to the metabolic diseases obesity and diabetes (Bechtold et al., 2010). The master circadian clock in the SCN and those in peripheral tissues such as the heart contain the same molecular components. Circadian clocks consist of positive and negative transcriptional and translational feedback loops. Transcription is driven by binding of the transcription factor heterodimers Npas2:Bmal1 to the E-box enhancer elements located within the promoter regions of the genes, Per1, Per2, Cry2, Nr1d2 and Nr1d1. The subsequent Period and Cryptochrome proteins, encoded for by the Per and Cry genes respectively, heterodimerise, translocate to the nucleus and negatively regulate the Npas2:Bmal1 complex. Therefore Npas2 and Bmal1 genes are expressed in opposite phases to Per and Cry genes (Reppert and Weaver, 2001). Administration of 1280 mg/kg/day TRO for 14 days resulted in the up-regulation of Per and Cry genes and the down-regulation of Npas2 and Arntl. In addition, increased expression of the genes Nr1d2 and Nr1d1, which encode for the proteins Rev-Erbα and Rev-Erbß, was also observed (Levi and Schibler, 2007, Paschos et al., 2010). Expression of Dbp and Tef, two of the three members of the PAR bZip transcription factor family, are regulated by the circadian clock and are involved in regulating the expression of genes involved in regulating the heart's response to stresses such as pressure change, hypertrophy and xenobiotic metabolism (Gachon et al., 2006, Durgan and Young, 2010). Both genes were up-regulated in the hearts of mice administered for 7 and 14 days (Figure 4.11). The cardiac circadian clock regulates the heart's response

to changes in blood pressure. The use TRO has been shown to increase plasma volume and such an increase can cause an increase in blood pressure (Weir, 2010). Thus, it is possible that the differential expression of circadian genes in the heart was a compensatory mechanism employed in response to the potential TRO induced hypervolemia.

Increased expression of Mgll and Aqp7, which are involved in the formation and transport of glycerol, respectively, were also observed in response to TRO treatment. During increased energy demand triglycerides undergo hydrolysis to aid ATP formation; Mgll is the last enzyme of the lipolysis pathway and converts monoglycerides into glycerol and fatty acids. Fatty acids undergo β-oxidation forming acetyl CoA, which enters the TCA cycle and glycerol is converted into a substrate for glycolysis (Zimmermann et al., 2009). Aqp7 is the only cardiac glycerol transporter and facilitates transport of glycerol into the heart to increase energy production under stressful conditions (Hibuse et al., 2009). Up regulation of Mgll and Aqp7 indicates a TRO mediated increased energy demand in the heart, which may be due to the sarcomere remodelling undertaken to compensate for increased pressure in the heart.

Genes identified as having a role in cardiovascular development and function were further analysed to connect these changes in gene expression to potential mechanisms of TRO induced cardiotoxicity. Pathway analysis associated up-regulation of the genes Myh11, Actg2, Tmp2, Timp3, Timp4, Bmp4 and Tcap with cardiac pathophysiology. (Figure 4.7). These genes regulate structural changes in the heart to compensate for increased blood pressure and volume changes. TRO induced increases in plasma volume have been reported in animal studies and clinical trials in healthy human volunteers. Administration of TRO for 6 weeks

to 24 healthy individuals resulted in a 6-8% in increase in plasma volume (FDA 1999). Increased plasma volume can cause pressure overload in the heart. Sarcomere remodelling is a mechanism that is utilised to compensate for increased stress in the heart and protect against heart failure (Kehat and Molkentin, 2010). Changes in plasma volume were not measured in this study, however, increased expression of the genes that encode for some of the key sarcomere components myosin (Myl7, Myh11, Myl9, Myl4, Mylk), actin (Actg2), actinin (Actn1), tropomyosin (Tpm2, Tpm1) and titin-cap (Tcap) were up-regulated after 14 days of TRO treatment. This implies that adaptive changes to TRO induced cardiac stress were undertaken in the hearts of mice administered 1280 mg/kg/day TRO for 14 days (Figure 4.6). Increased expression of these genes was not observed in the hearts of mice administered 925 mg/kg/day TRO for 7 days, with the exception of Tcap, which was up-regulated. Tcap encodes for the titin-cap protein that has been reported to be up-regulated in *in vivo* and *in vitro* models of doxorubicin induced cardiac hypertrophy. Cardiac remodelling occurs as part of the stress response to toxic insult induced hypertrophy (Pointon et al., 2010). Tcap has been shown to be involved in sarcomere formation and is critical for maintenance of sarcomere integrity (Gregorio et al., 1998). The increased expression of Tcap after 7 days of TRO treatment and the subsequent up-regulation of sarcomeric genes at day 14 imply that Tcap is an early biomarker of adaptive structural changes in the heart in response to TRO.

Although TRO was withdrawn due to severe hepatotoxicity, there were reports of TRO induced heart failure in patients (FDA, 1999a). The cardiovascular safety of the TZD compound family members has been questioned, investigated and discussed many times (Chaggar et al., 2009) The increased risk of adverse

cardiovascular events occurring with the use of ROSI led to its withdrawal from the UK market in September 2010 (MHRA, 2010). Furthermore, the development of Muraglitazar, another member of the TZD compound class was halted after the completion of phase III clinical trials due to increased incidence of heart failure (Nissen et al, 2005). Thus, there is increasing evidence that the observed cardiotoxicity with members of the TZD compound family is a class effect. The mechanism of TZD induced heart failure is hypothesized to be a result of increased fluid retention leading to oedema, which can result in congestive heart failure (Lago et al., 2007). Oedema can increase the stress on the heart inducing compensatory mechanisms such as cardiac remodelling. Adaptive changes in sarcomeres can delay but not prevent heart failure; onset of such adverse cardiac events would be dependent on the degree of stress exerted on the heart (Kehat and Molkentin, 2010). Adaptive myocardial changes may not exert any adverse cardiac effect for the majority of patients prescribed TZDs; however for a subset with already existing underlying cardiomyopathies the stress placed on the heart as a result of TZD administration could result in heart failure. Cardiovascular disease is the main cause of morbidity and mortality in patients with T2D (Betteridge, 2004). It is possible that a patient and their physician may not be aware that they have an underlying cardiomyopathy, especially if they are asymptomatic. If such patients were to be prescribed TZDs such as TRO this could result in an adverse cardiovascular event. It is possible that the patients reported to have suffered from TRO induced cardiotoxicity may have had undiagnosed pre-existing heart conditions.

4.4.2 TRO Induced Transcriptomic Changes in the Liver

The hepatic gene signature from 129Ola/Hsd male mice treated with 1280 mg/kg/day TRO for 14 days included genes involved in FA metabolism, bile acid synthesis and ER stress. TRO was prescribed as an insulin sensitizer for the treatment of T2D. Patients with T2D have fasting hyperglycaemia as a result of tissue resistance to the action of insulin. The primary goal of anti-diabetic agents used in the treatment of T2D is to lower blood glucose levels. Pparγ is expressed predominantly in adipose but is also present at much lower levels in the liver. Administration of 901 and 1280 mg/kg/day TRO for 14 days significantly increased hepatic expression of Pparγ (Figure 4.15). Pparγ agonists have been shown to induce expression of the gene in liver tissue (Davies et al., 1999, Rogue et al., 2010). TRO is a Pparγ agonist, which upon binding to the receptor activates transcription of genes involved in glucose and lipid metabolism.

TRO induced hepatotoxicity was a rare event however the severity of the reactions lead to its withdrawal. There are many hypotheses regarding the mechanisms of TRO induced hepatotoxicity however there is no conclusive evidence (Smith, 2003). Pathway analysis identified that the largest network of differentially expressed genes in the liver, as a result of TRO administration, have a functional role in fatty acid metabolism. TRO caused increased expression of genes involved in triglyceride and glycerol degradation (Figure 4.12), fatty acid β-oxidation (Figure 4.13) and acetyl CoA production (Figure 4.14). Increased expression of the genes that encode for the 6 key steps in FA oxidation were up-regulated by TRO treatment (Table 4.4).

Third party content removed

Table 4.4 – Key steps in FA oxidation. Details of the six main reactions, the enzymes that catalyse the reactions and the genes that encode for the enzymes in FA oxidation (adapted from Berg et al., 2002).

Increased expression of enzymes involved in bile acid synthesis was also observed (Figure 4.17). Cholesterol is synthesized from acetyl CoA, which is a product of glycolysis and fatty acid β-oxidation. Accumulation of cholesterol within hepatocytes stimulates increased bile acid production (Russell, 2003). The rate limiting step in the conversion of cholesterol into bile acids is controlled by Cyp7a1, which was up-regulated in response to TRO treatment. Previous studies have reported that TRO decreases triglyceride levels and increases HDL cholesterol levels (Mudaliar and Henry, 2001). This data is indicative of the pharmacological action of TRO and supports earlier reports that TRO decreases

triglyceride levels. Analysis of microarray data from mice dosed with 1280 mg/kg/day TRO for 14 days highlighted increased expression of several genes that have previously been cited as having a role in the liver's response to stress and injury (Figure 4.16). In normal liver the expression of PPARγ is relatively low in comparison with adipose tissue in which PPARγ is abundantly expressed (Rogue et al., 2010). We found increased expression of hepatic PPARγ in response to 14 day treatment with 901 and 1280 mg/kg/day TRO. PPARγ controls the expression of Trib3, a novel marker of ER (endoplasmic reticulum) stress, which was up-regulated in the liver tissue of mice dosed for 14 days with 279, 901 and 1280 mg/kg/day and mice does for 7 days with 925 mg/kg/day. In addition to Trib3, increased expression of Ddit3 and Dnajb9 was also observed in 14 day 901 and 1280 mg/kg/day liver tissues and increased expression of Atf4 was observed in the 14 day highest dose group. Trib3, Ddit3 and Atf4 have been shown to be involved in the regulation of cellular responses to ER stress inducing agents (Hu et al., 2004). *In vitro* studies have shown that Ddit3 is induced by Atf4 and that Trib3 is a target gene of Ddit3 (Ohoka et al., 2005). Dnajb9 is involved in the refolding of unfolded proteins and is up-regulated during ER stress (Shen et al., 2002). Trib3 has previously been shown to be up-regulated *in vitro* in response to TRO treatment and it has been associated with increased lipolysis (Jousse et al., 2007, Cheon et al., 2009). Several genes that were up-regulated in the liver were shown to be downstream targets of Ppary and involved in hepatotoxic pathways, including the onset of hepatic steatosis.

4.4.3 Summary

There is indication here that TRO induced toxicity may be associated with ER stress and/or increased hepatic Ppary expression. T2D is a metabolic disease and as a result patients often have increased levels of cellular stress due to disturbances in metabolic pathways (Ozcan et al., 2004). In addition, these patients also have elevated expression of Ppary in the liver, compared with normal individuals (Reddy and Sambasiva Rao, 2006). TRO induced increased Ppary expression may promote the development of hepatic steatosis. It is also possible that TRO may exaggerate cellular stress leading to cell death through ER stress mediated mechanisms. This implies that the nature and occurrence of TRO induced toxicity is patient dependent and would help to explain why TRO only caused ADRs in a small sub set of the rather large patient population. Although there is a potential hint towards TRO induced ER stress in this model it is not conclusive. TRO toxicity is difficult to model in a normal animal model and this may be due to low levels of hepatic Ppary expression and the absence of increased cellular stress in this model in comparison with disease models. Ideally, a model is required that more accurately mimics the patient population. Therefore for the next study a high fat diet induced diabetes mouse model was utilized (Chapter 5).

Chapter 5: Transcriptomic Analysis of an *In Vivo* Troglitazone Diabetes Mouse Model

5.1 Introduction

The transcriptomic profile of the toxicity of TRO in a normal mouse model indicated a potential role of TRO in the activation of Pparγ mediated steatosis and ER stress toxicity pathways (Chapter 4). TRO was used in the treatment of T2D, a metabolic disease with complex pathophysiology (Stumvoll et al., 2005). Thus TRO induced gene changes observed in normal physiological conditions may be exaggerated in diseased states. A second *in vivo* study was undertaken to acquire a profile of TRO induced biochemical and transcriptomic changes in a mouse model that mimicked the physiological state of the patient population. The high fat diet (HFD) mouse model has been shown to be a robust model for T2D research (Winzell and Ahrén, 2004).

Obesity and overnutrition are highly prevalent risk factors for the development of T2D. It is reported that >60% of obese patients develop T2D and approximately 90% of all type 2 diabetics are overweight or obese (Hu et al., 2001, Stumvoll et al., 2005, Magkos et al., 2009). The link between obesity and T2D results from the increased production of free fatty acids, glycerol, hormones and pro-inflammatory cytokines in obese patients, which contributes to the development of insulin resistance, a key characteristic of T2D (Kahn et al., 2006). Accumulation of excess lipids as a result of overnutrition has been show to disrupt cellular mechanisms and cause ER stress. Disruption of ER homeostasis decreases insulin mediated tyrosine phosphorylation of insulin receptor substrate-1, resulting in reduced insulin signalling leading to the development of T2D (Ozcan et al., 2004). Improvement of ER stress using agents such as Buphenyl, which is known to improve ER function, has been shown to increase tissue sensitivity to insulin and normalize hyperglycaemia in diabetic mice (Ozcan et al., 2006).

Furthermore, in 2007 a clinical study was commissioned to investigate the effect of Buphenyl in T2D patients. The study was completed in 2010 however, no data has yet been reported (Health, 2010). Excess lipids are also stored as triglycerides in the liver and their accumulation results in hepatic steatosis (Videla, 2009). Several genes that were up-regulated in the normal mouse study were down stream targets of Pparγ and are involved in hepatic lipid storage pathways. Under normal physiological conditions low levels of Pparγ are found in the liver however expression can be induced by TRO, which is a Pparγ agonist. Compared with normal physiological conditions, the expression of hepatic Pparγ is increased in patients with insulin resistance and T2D (Pettinelli and Videla, 2011). Thus further induction by TRO in these patients may be a factor in the development of TRO mediated toxicity.

A HFD induced T2D mouse model was used to investigate TRO induced toxicity as the model mimics the development and characteristics of T2D in the patient population. Increased Pparγ expression has been observed in HFD models of T2D but has not been observed in genetic models (Vidal-Puig et al., 1996, Kim et al., 2004). The 'gold standard' mouse strain for HFD induced diabetic studies is the C57BL/6J strain, which was used in this study. This strain has been shown to be most responsive to the development of insulin resistance and glucose intolerance in response to being fed a 60% HFD (60% of calories in this diet were derived from fats) (Winzell and Ahrén, 2004).

5.2 Chapter Aims

The aim of this chapter was to develop a HFD induced mouse model of T2D for use in deducing a profile of TRO induced transcriptional changes in a model that represented that pathophysiological changes associated with the disease in the

patient population. The gene signatures of transcriptional changes in the heart and liver would be used to evaluate the utility of *in vitro* mES cell derived cardiomyocytes and hepatocytes as model systems for the evaluation of drug induced toxicity, with specific reference to TRO.

5.3 Results

5.3.1 Choice of *In Vivo* Model

For this study a mouse model of T2D that reflected the pathophysiology of the disease in the patient population was required. Overnutrition is a leading factor in the development of T2D, which is characterised by blood hyperglycaemia and impaired glucose tolerance (Pi-Sunyer, 2009). To mimic the effects of overnutrition in mice a HFD model was used. The 'gold standard' mouse strain for HFD induced diabetic studies is the C57BL/6J strain. It has been shown to be most responsive to the development of insulin resistance and glucose intolerance in response to being fed a 60% HFD (a diet in which 60% of calories are derived from fats) (Winzell and Ahrén, 2004). This study was undertaken using adult male and female strain C57BL/6J mice as described in section 2.4. Mice were fed a 60% HFD for 18 weeks before TRO dosing was commenced. The lean controls used in this study were adult male and female strain C57BL/6J mice fed on standard chow; a diet in which 17% of calories were derived from fats (information from diet product leaflet).

5.3.2 Effect of HFD on Body Weight

Thirty adult mice of each gender were caged in groups of 5, generating 6 cages of male and female mice. Mice were fed a HFD daily and the body weight of each mouse was measured weekly (Figures 5.1 and 5.2). Body weights increased with administration of the HFD. After 18 weeks of HFD administration, the average body weight was 40 ± 5 g for male mice and 38 ± 4 g for female mice. The average body weight gain over the 18 week period was 13.07 ± 4.50 g for male mice and 17.21 ± 3.59 g for female mice.
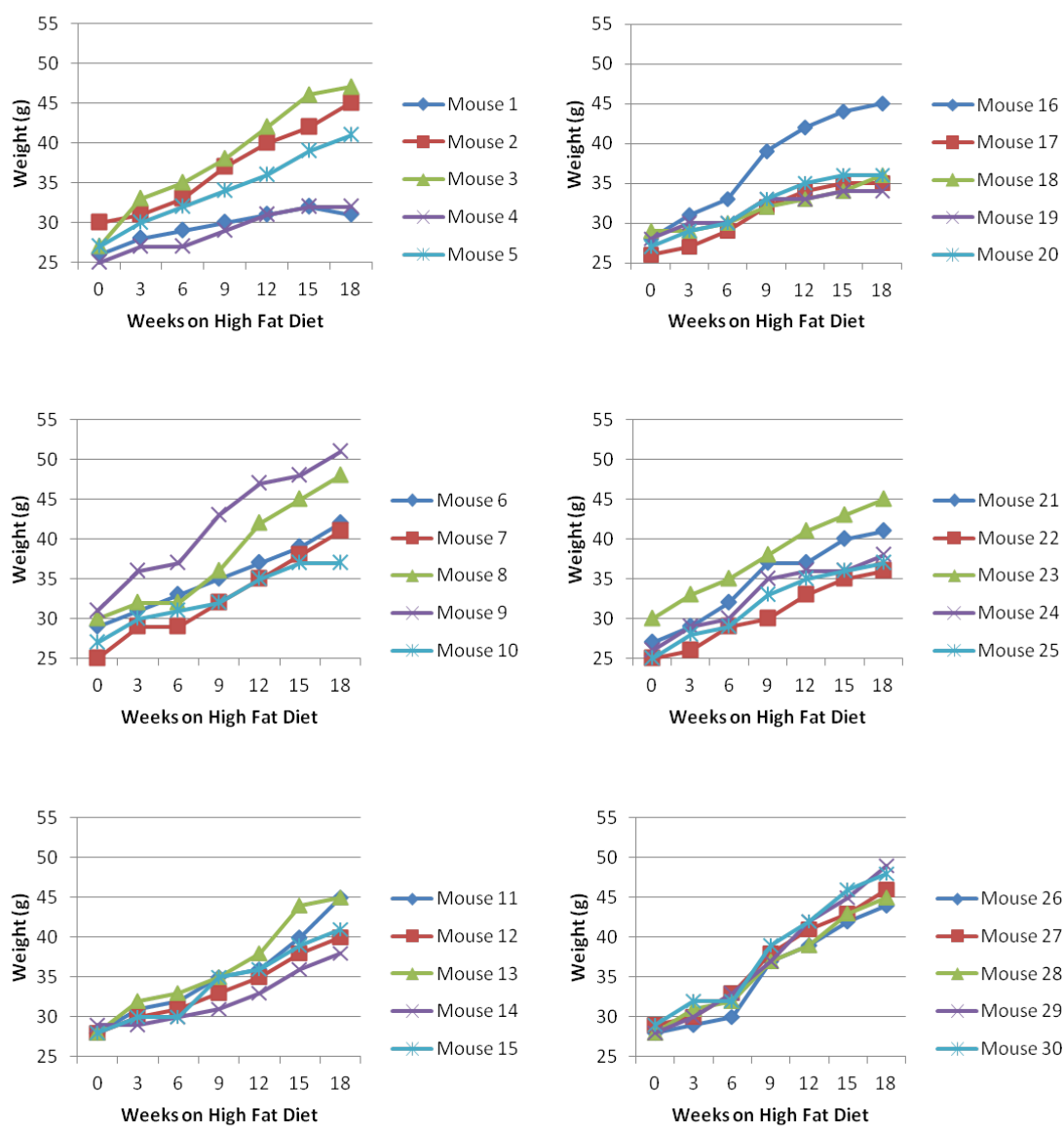
Figure 5.1 – Body weight changes of male mice fed a HFD for 18 weeks.

After being fed on a HFD for 18 weeks the average body weight gain for male mice was 13.07 ± 4.50 g.
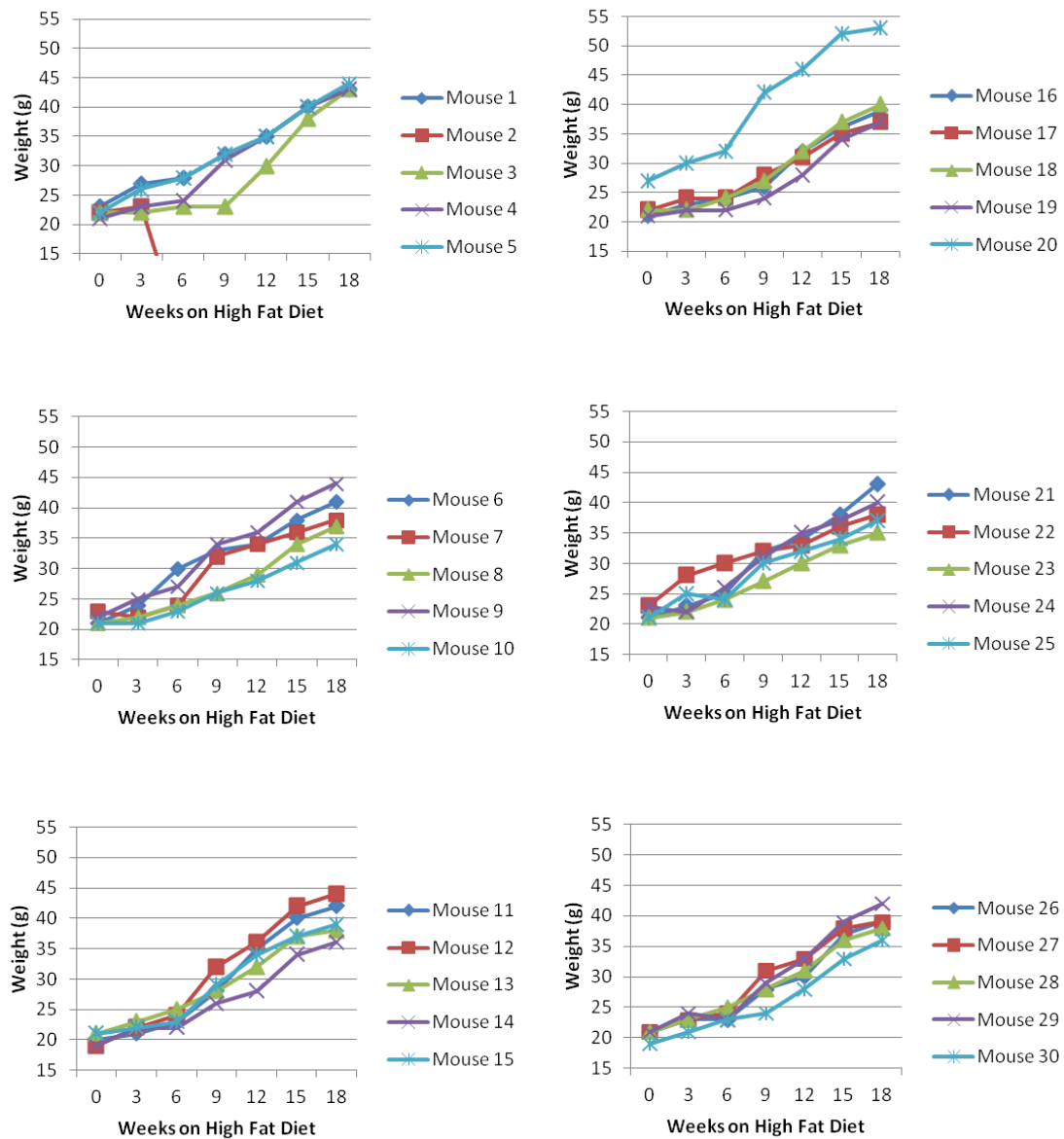
Figure 5.2 – Body weight changes of female mice fed a HFD for 18 weeks.

After being fed on a HFD for 18 weeks the average body weight gain for female mice was 17.21 ± 3.59 g. Mouse 2 died in week 3 during a blood sampling procedure.

5.3.3 Effect of HFD on Blood Glucose

Hyperglycaemia is a hallmark of T2D and is often the first parameter measured during diagnosis of T2D in the patient population. In this study blood glucose (BG) levels were measured after 3, 8 and 11 weeks of HFD administration and values were compared with BG levels in lean adult mice (Figure 5.3). Significant differences between BG levels in lean and HFD mice were not observed until week 11 of HFD administration. With the female mice 3 groups had significantly higher BG levels than lean mice and with the male mice 2 groups had significantly higher levels.

In the clinic, elevated BG levels are indicative of the onset of glucose intolerance however these results alone do not confirm its development. Some patients with T2D can be asymptomatic and will not have elevated BG levels (American Diabetes Association, 2004). Thus, using only BG levels to diagnose glucose intolerance would result in a misdiagnosis of these patients. To account for these factors The World Health Organization recommends the use of the oral glucose tolerance test (OGTT) to confirm the development of T2D in patients (WHO, 2006). The OGTT tests the efficiency with which glucose is metabolized and removed from the blood. OGTTs were undertaken after mice had been fed on a HFD for 16 weeks. Six mice of each gender were used, with one mouse taken from each group. Following a 6 hour fast, mice were administered a bolus of glucose (2 g/kg) by oral gavage. BG levels were measured prior to glucose administration and at 15, 30, 60, 90 and 120 minutes post dose. Administrating a bolus of glucose resulted in higher BG levels in both female and male mice compared to lean mice (Figure 5.4). For both genders, after 30 minutes post dose administration, BG levels were significantly higher in HFD mice than in lean mice.

After 60 minutes post dose, the BG levels of female HFD mice had returned to similar levels measured in lean mice but male HFD mice still had elevated BG levels. Two hours after glucose administration the BG levels of all the mice had returned to the levels measured before glucose was administered. Higher BG levels after 30 minutes for female and after 60 minutes for male HFD compared with lean mice is indicative of glucose intolerance in the HFD mice. This was also reflected in the AUC (area under the curve) measurements, which were significantly higher for male and female HFD mice compared with lean mice. These data illustrate impaired glucose tolerance and thus development of T2D pathophysiology in mice fed on a HFD for 16 weeks.
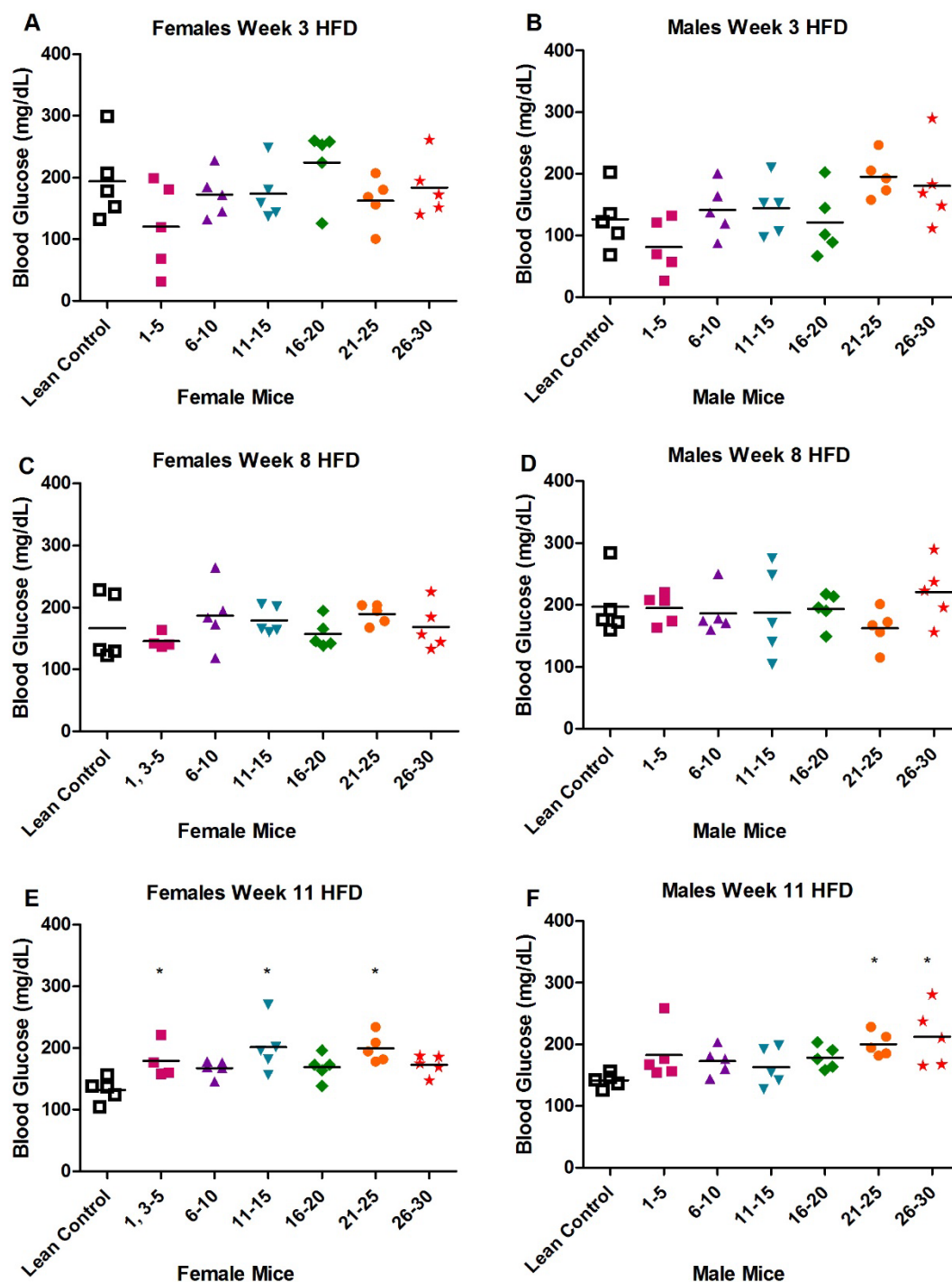
Figure 5.3 – Blood glucose levels of lean and HFD mice. BG levels were measured in female and male mice fed on a HFD (mice numbered 1-30) or on standard chow (lean controls) for (A-B) 3 weeks, (C-D) 8 weeks and (E-F) 11 weeks. Significant differences in BG levels of HFD and lean mice were observed after 11 weeks of HFD administration (Data plotted are values for each mouse plus group means , results are statistically significant at *p<0.05 for given mouse group compared with lean controls by one-way ANOVA with post hoc Dunnett's test).
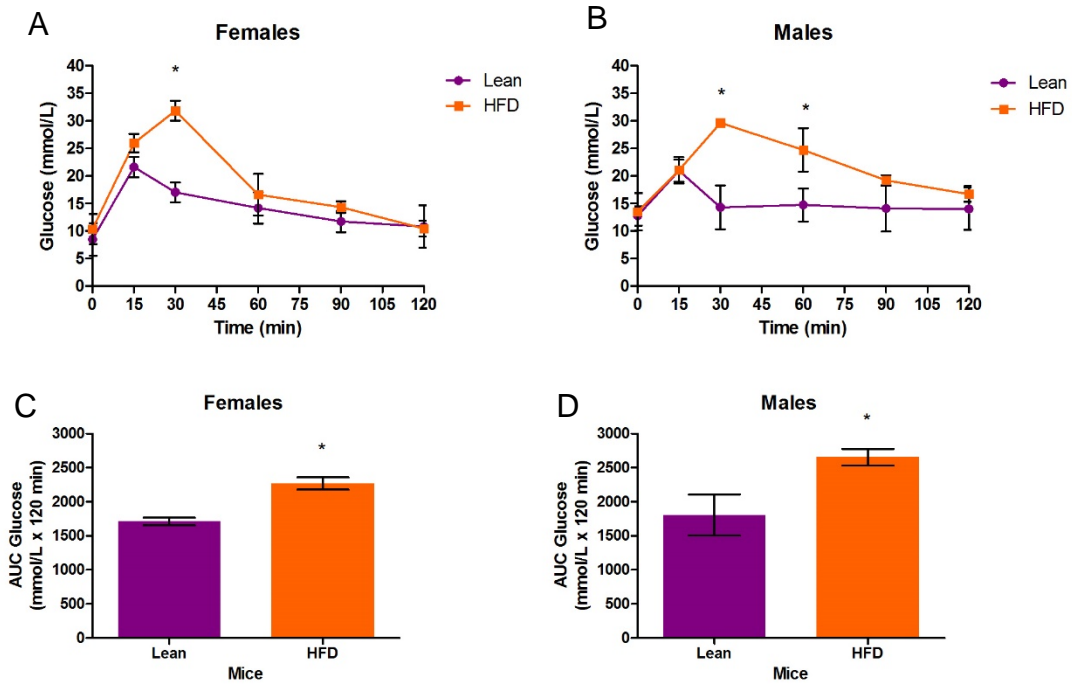
Figure 5.4 – Oral glucose tolerance test of lean and HFD mice. OGTT was performed on male and female lean mice and mice that had been fed a HFD for 16 weeks. Mice were fasted for 6 hours and then administered a bolus of glucose (2g/kg) by oral gavage. BG levels of (A) female and (B) mice were measured at T0, prior to dosing and at intervals post dosing for up to 2 hours. BG levels in lean mice increased for 15 minutes post dose and then began to decrease. In HFD mice, BG levels continued to rise for up to 30 minutes post glucose administration and these levels were significantly higher than those measured in lean mice. (C-D) AUC values for HFD female and male mice were significantly higher than those measured in lean mice (Data are mean ± SD (n=6), results are statistically significant at *p<0.05 for HFD mice compared with lean mice by t-test analysis).

5.3.4 Dose Administration and Calculated TRO Intake

High and mid-range intended doses of 400 and 1200 mg/kg/day, in addition to control (vehicle only), were selected from the dose range used in the previous study (Chapter 4). These two doses were selected because they had different effects on Ppary expression, which was hypothesized to be a factor in the development of TRO induced toxicity. TRO was administered via the diet, keeping the delivery method consistent between both *in vivo* studies. To ensure the mice would consume enough diet to ingest the target TRO doses the normal HFD diet consumption of 10 male and 10 female mice was measured during the week before TRO dosing was commenced. The mice were divided into groups of 5 and two pots containing 40 g of diet was placed in each cage. The weight of remaining diet was measured and the consumed diet was divided by five to give a measure of average diet consumed per mouse (Table 5.1). On average the female mice consumed 2 g HFD diet per day and the male mice consumed 2.5 g HFD per day. TRO was subsequently mixed with the HFD to ensure that the maximum dose of the drug would be ingested if the female mice ate 2 g diet/day and if the male mice ate 2.5 g diet/day.

The intended doses for male and female mice were 0 (control), 400 and 1200 mg/kg/day for 7 and 14 days. Each dose group contained 5 mice except the 7 day female control group, which contained 4 mice (one mouse died during blood sampling at week 3 of HFD administration). Fresh HFD containing TRO was administered to the mice daily and the total consumed diet weight for each group was measured and divided by the number of mice per group to give an average diet consumed value (Table 5.2). The male and female control mice consumed similar amounts of diet to the intended amount of 2.5 g for males and 2 g for

females. Male mice in the 7 day 400 mg/kg/day TRO group consumed similar amounts of diet per day to the control group. In contrast the female mice in the 7 day 400 mg/kg/day group only consumed 1.66 g diet/day, which was less than the expected consumption. Both male and female mice in the 7 day 1200 mg/kg/day group consumed less diet/TRO mix than expected. In the 14 day study the male and female controls, both 400 mg/kg/day groups and the male 1200 mg/kg/day group consumed similar amounts of the diet to the intended amounts. The female 1200 mg/kg/day group consumed 1.61 g diet/ day, which was less than the intended amount of 2 g diet/day.

The variances between expected consumption and average calculated consumption of diet subsequently affected the doses of TRO ingested by the mice (Table 5.3). For the 7 day 400 mg/kg/day dose groups male mice on average ingested 354 mg/kg/day and females ingested 316 mg/kg/day TRO and for the 1200 mg/kg/day dose group male mice on average ingested 810 mg/kg/day and females ingested 986 mg/kg/day TRO. The increased diet consumption of mice in the 14 day 400 mg/kg/day groups meant the males ingested 396 mg/kg/day and female mice ingested 387 mg/kg/day. For the 14 day top dose group the intended TRO dose was 1200 mg/kg/day but the achieved doses were 1049 mg/kg/day for male mice and 1006 mg/kg/day for females.

Cage Details	Day	Diet Given (g)		Diet Left after 24h (g)		Total Diet Eaten (g)	Diet Eaten Per Mouse (g)	Ave. Diet Eaten Per Mouse (g)	Ave. Diet Eaten Per Gender (g)
		Pot 1	Pot 2	Pot 1	Pot 2				
Cage No.5	1	40	40	38	35	7	**1.4**		
	2	40	40	36	35	9	**1.8**		
	3	40	40	35	36	9	**1.8**		
	4	40	40	35	35	10	**2.0**	2.0	
5	5	40	40	31	38	11	**2.2**		
Female	6	40	40	40	28	12	**2.4**		
Mice	7	40	40	37	32	11	**2.2**		2.0
Cage No.6	1	40	40	36	37	7	**1.4**		
	2	40	40	36	36	8	**1.6**		
	3	40	40	32	38	10	**2.0**		
	4	40	40	33	37	10	**2.0**	1.9	
5	5	40	40	32	40	8	**1.6**		
Female	6	40	40	37	30	13	**2.6**		
Mice	7	40	40	36	32	12	**2.4**		
Cage No.15	1	40	40	30	37	13	**2.6**		
	2	40	40	29	38	13	**2.6**		
	3	40	40	31	38	11	**2.2**		
	4	40	40	29	39	12	**2.4**	2.6	
5	5	40	40	28	39	13	**2.6**		
Male	6	40	40	28	37	15	**3.0**		
Mice	7	40	40	31	36	13	**2.6**		2.5
Cage No.16	1	40	40	37	31	12	**2.4**		
	2	40	40	38	32	10	**2.0**		
	3	40	40	38	31	11	**2.2**		
	4	40	40	40	29	11	**2.2**	2.3	
5	5	40	40	29	40	11	**2.3**		
Male	6	40	40	29	38	13	**2.6**		
Mice	7	40	40	39	28	13	**2.6**		

Table 5.1 – Average HFD diet consumption for male and female mice. Each dose group consisted of 5 mice, (4 mice in 7 day female control group) 35 g of diet was placed in each cage and changed daily. The amount of diet consumed per cage was average to give a value for diet consumed by each mouse per day. Female mice on average consumed 2 g diet/day and males consumed 2.5 g diet/day.

(A)	Average Diet Consumption Per Mouse (g/day)					
Day Number	Troglitazone Dosing Group (mg/kg/day)					
	0 (Control)		400		1200	
	Male	Female	Male	Female	Male	Female
1	2.00	2.25	1.80	1.60	2.00	1.20
2	2.00	2.25	2.00	1.80	1.20	1.60
3	2.60	2.25	2.40	1.60	1.20	1.40
4	2.80	2.00	3.40	1.80	1.60	2.00
5	2.40	2.50	2.60	1.80	1.80	1.80
6	2.60	2.25	2.00	1.40	1.60	1.60
7	2.80	2.25	2.40	1.60	2.00	1.60
Average =	2.46	2.25	2.37	1.66	1.63	1.60

(B)	Average Diet Consumption Per Mouse (g/day)					
Day Number	Troglitazone Dosing Group (mg/kg/day)					
	0 (Control)		400		1200	
	Male	Female	Male	Female	Male	Female
1	3.00	2.00	1.80	1.80	1.40	1.40
2	2.60	2.60	1.20	1.60	1.40	1.40
3	2.80	2.00	2.00	1.60	2.20	1.00
4	3.40	2.60	2.20	1.80	1.80	1.60
5	2.80	2.60	2.20	1.80	1.80	1.80
6	2.80	2.40	2.60	1.60	2.40	1.80
7	2.40	2.40	2.00	1.80	2.20	1.40
8	3.20	2.60	2.80	2.00	2.60	1.40
9	3.40	2.80	2.80	2.20	2.40	1.80
10	2.40	2.40	2.80	2.20	3.00	1.80
11	2.40	2.80	2.20	2.20	2.80	2.00
12	2.80	2.60	2.60	2.20	2.60	2.20
13	2.80	2.00	2.20	1.80	2.20	1.00
14	3.20	2.20	2.00	2.20	2.40	2.00
Average =	2.86	2.43	2.24	1.91	2.23	1.61

Table 5.2 – Average diet consumption during TRO dosing in 7 and 14 day studies. Each dose group consisted of 5 mice, (4 mice in 7 day female control group) 35 g of diet was placed in each cage and changed daily. Average diet consumption per mouse (g/day) was calculated for mice in (A) 7 day and (B) 14 day studies. The expected diet consumption was 2 g/mouse/day for females and 2.5 g/mouse/day for males. Male and female control mice consumed more diet than expected and female mice in the 1200 mg/kg/day consumed less diet than expected

(A)	Average Achieved Troglitazone Dose Per Mouse (mg/kg/day)					
Day Number	Troglitazone Dosing Group (mg/kg/day)					
	0 (Control)		**400**		**1200**	
	Male	**Female**	**Male**	**Female**	**Male**	**Female**
1	0	0	273	304	946	735
2	0	0	301	342	578	985
3	0	0	361	304	581	865
4	0	0	506	351	790	1229
5	0	0	385	342	922	1101
6	0	0	298	266	827	990
7	0	0	354	304	1028	994
Average =	0	0	354	316	810	986

(B)	Average Achieved Troglitazone Dose Per Mouse (mg/kg/day)					
Day Number	Troglitazone Dosing Group (mg/kg/day)					
	0 (Control)		**400**		**1200**	
	Male	**Female**	**Male**	**Female**	**Male**	**Female**
1	0	0	321	362	1853	856
2	0	0	215	325	597	846
3	0	0	350	328	944	611
4	0	0	392	363	769	979
5	0	0	387	367	789	1113
6	0	0	460	326	1042	1120
7	0	0	353	369	956	875
8	0	0	493	405	1130	874
9	0	0	500	446	1052	1136
10	0	0	497	446	1280	1130
11	0	0	386	439	1195	1257
12	0	0	460	436	1120	1376
13	0	0	387	363	943	632
14	0	0	350	441	1016	1279
Average =	0	0	396	387	1049	1006

Table 5.3– Average achieved TRO dose consumed via diet for 7 and 14 day studies. Each dose group consisted of 5 mice (4 mice in 7 day female control group). Using average diet consumption values (Table 5.2), the average achieved TRO doses were calculated. (A) Male and female mice in the 7 day study consumed less than the intended doses of 400 and 1200 mg/kg/day. (B) In the 14 day study the mice in the 400 mg/kg/day groups ingested TRO at doses very close to those intended. Male and female mice in the 1200 mg/kg/day groups only ingested 1049 and 1006 mg/kg/day TRO, respectively.

5.3.5 Effect of TRO on Body Weight in Mice Dosed for 7 and 14 Days

Administering TRO at 316 and 986 mg/kg/day to female mice for 7 days did not results in significant changes in body weight in these mice compared with controls (Figure 5.5). Significant changes were observed in male mice dosed for 7 days. Mice administered 354 mg/kg/day gained more weight than the control mice however, mice dosed with 810 mg/kg/day had significant weight loss in comparison with weight changes in control mice. In the 14 day study female control mice gained significantly more weight than mice dosed with 387 and 1006 mg/kg/day TRO. Mice in the 1006 mg/kg/day dose group lost weight whilst the weight of mice in the 387 mg/kg/day dose group was on average unchanged after 14 days of TRO treatment. Significant differences between weights of male mice dosed with 396 and 1049 mg/kg/day and control mice were not observed. Administering TRO at 810 mg/kg/day for 7 days had the greatest effect on the body weight of male mice, causing an average loss of 3.4 g whereas the greatest weight change in female mice was observed in the 14 day study wherein dosing with 1006 mg/kg/day resulted in an average loss of 1.6 g in weight.
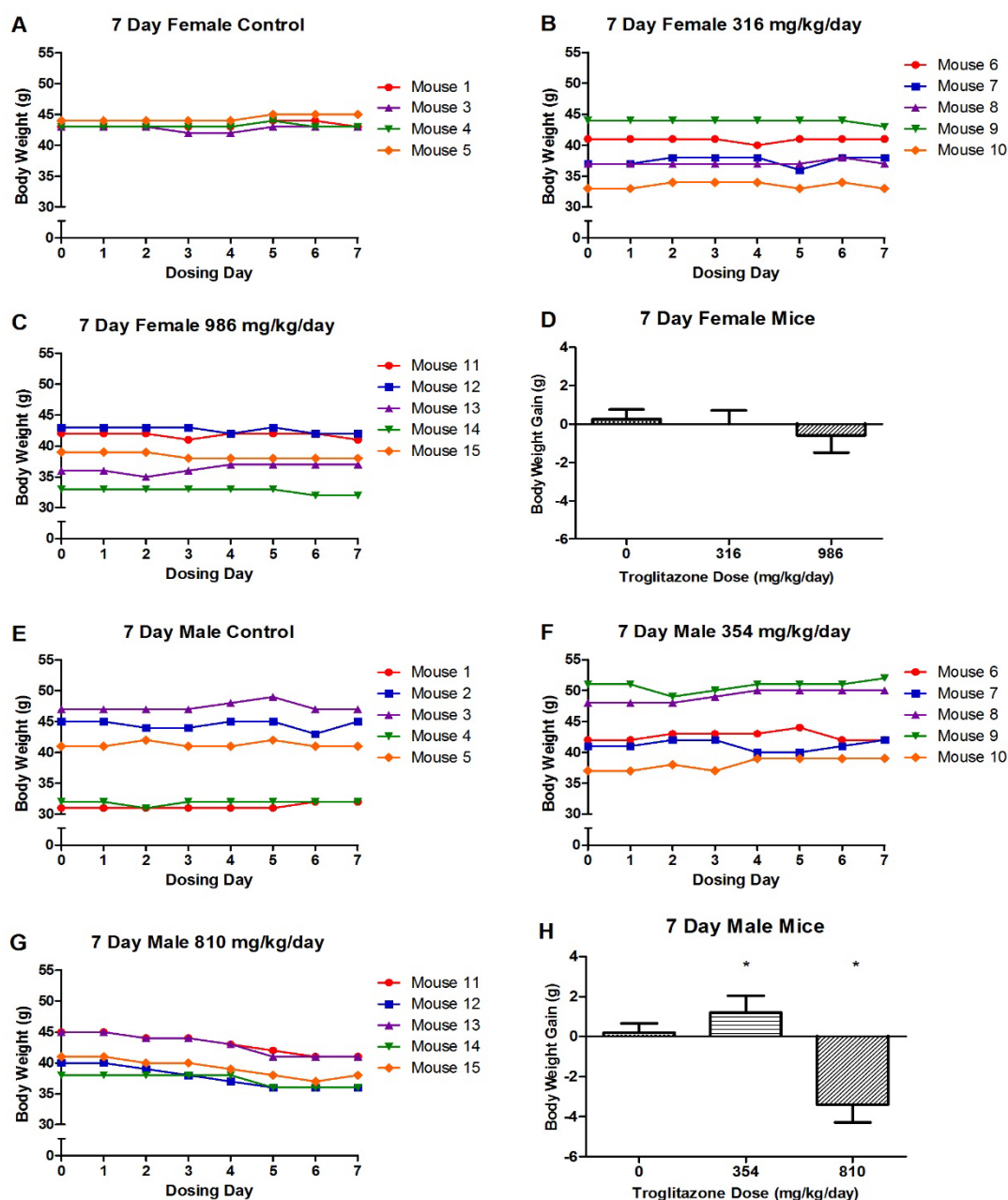
Figure 5.5 – Changes in body weight during 7 day TRO dosing in male and female mice. Body weights were measured daily for each mouse in the female (A) control (0 mg/kg/day), (B) 316 and (C) 986 mg/kg/day dose groups and for male mice in (E) control, (F) 354 and (G) 810 mg/kg/day dose groups. (D) Significant differences in body weight gain between control and TRO dosed female mice were not observed. (H) Male mice dosed with 354 mg/kg/day gained more weight than control mice and mice dosed with 810 mg/kg/day lost weight in comparison with controls (Data are mean ± SD (n=5, n=4 for female controls), *p<0.05 for given dose group compared with controls by one-way ANOVA with post hoc Dunnett's test).
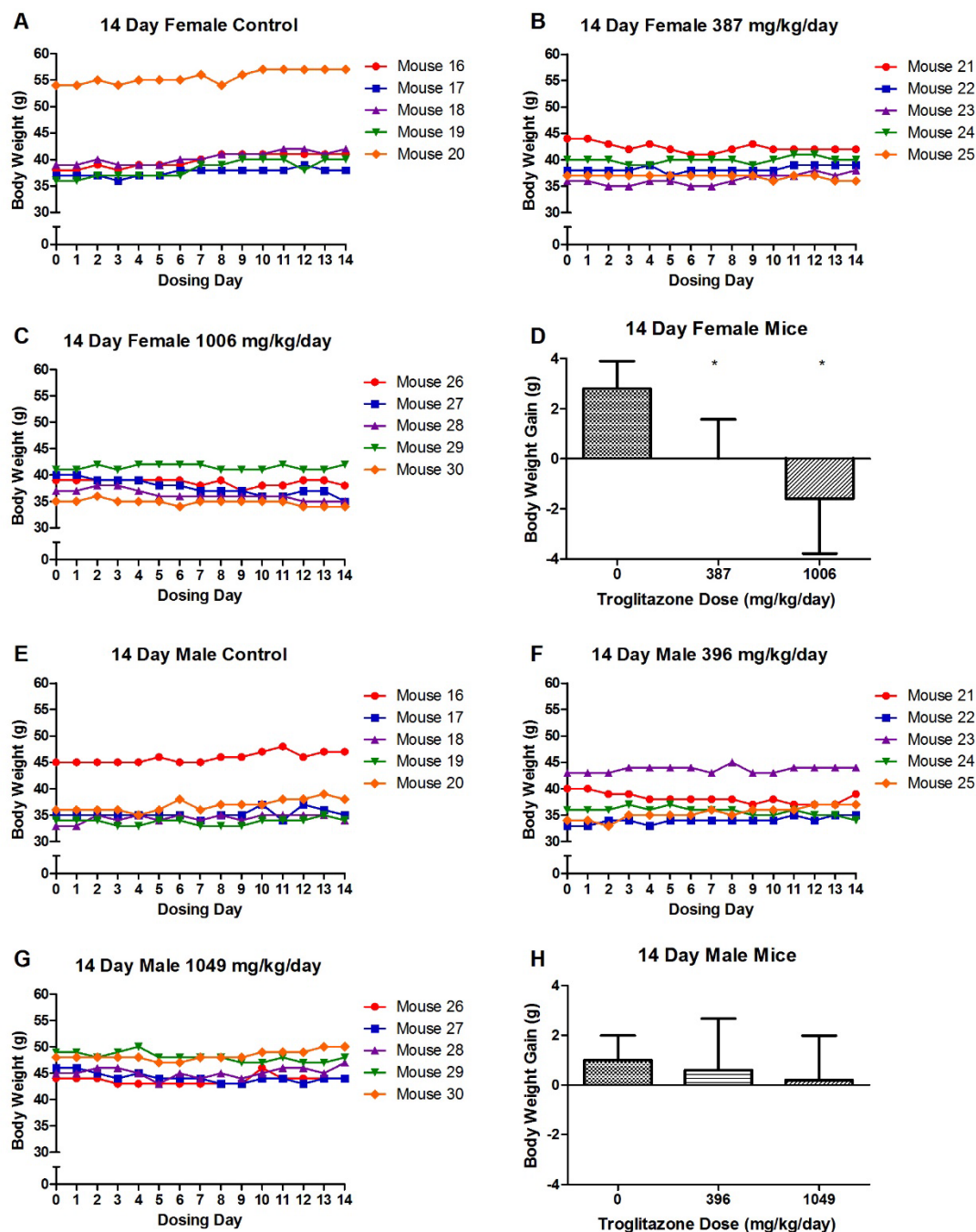
Figure 5.6 – Changes in body weight during 14 day TRO dosing in male and female mice. Body weights were measured daily for each mouse in the female (A) control (0 mg/kg/day), (B) 387 and (C) 1006 mg/kg/day dose groups and for male mice in (E) control, (F) 396 and (G) 1049 mg/kg/day dose groups. (D) Female control mice gained significantly more weight than TRO dosed mice. (H) Significant body weight gain differences were not observed between male control mice and mice dosed with 396 and 1049 mg/kg/day (Data are mean ± SD (n=5), *p<0.05 for given dose group compared with controls by one-way ANOVA with post hoc Dunnett's test).

5.3.6 Detection of TRO in Plasma

Plasma extracted from blood taken at necropsy was analysed by LC-MS for the detection of TRO. This was to confirm that the mice had absorbed the compound, which had been mixed into the diet. TRO was not detected in plasma from the female and male control mice but was detected in all of the TRO dosed mice, where sufficient volume of plasma was obtained for analysis (Figure 5.7). This illustrated that the mice had absorbed the drug from the diet.
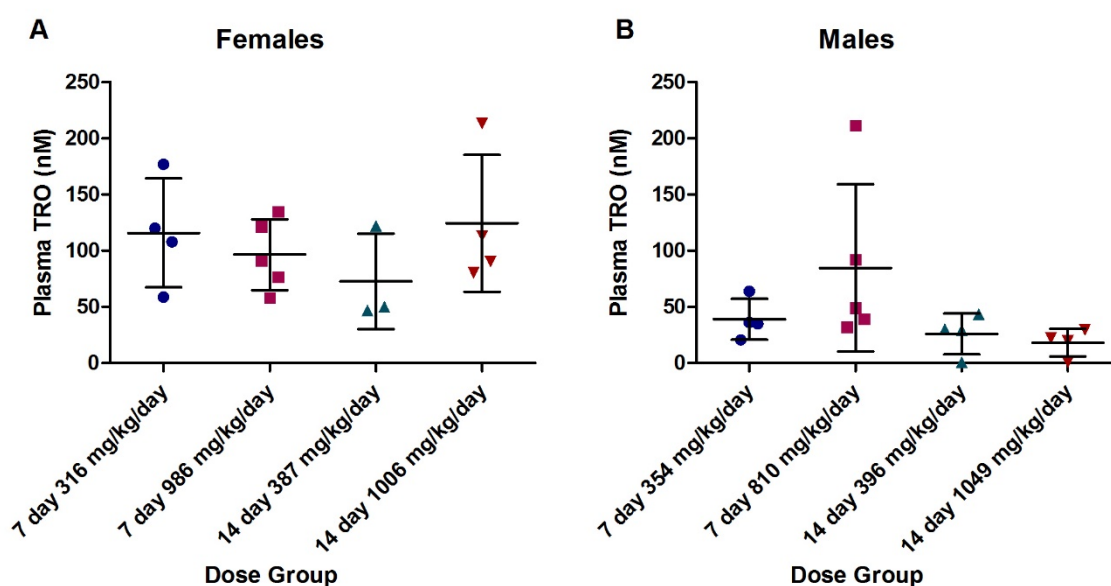
Figure 5.7 – LC–MS detection of TRO in plasma from 7 and 14 day dosed male and female mice. LC–MS analysis detected TRO in the plasma from (A) female and (B) male mice from both dose groups in the 7 and 14 day studies. TRO was not detected in control (vehicle only) mice (Data plotted mean ± SD).

5.3.7 Effect of TRO on Blood Glucose

TRO was used in the treatment of T2D, where its pharmacological action resulted in sensitization of tissues to the action of insulin. An effect of this was lowering of BG levels and improvement of glucose intolerance in patients. Administration of a HFD to female and male mice resulted in the development of impaired glucose clearance in these mice compared to lean control mice that had been fed on standard chow (Figure 5.4). An OGTT was performed on day 6 of the 7 day study and on day 13 of the 14 day study on male and female HFD control, TRO dosed and lean control mice. BG levels were measured at T0 and at 15, 30, 60, 90 and 120 minutes after administration of a bolus of glucose (2 g/kg) and compared between test groups at each time point. The AUC was calculated to compare glucose tolerance of the TRO dosed and lean control mice with the HFD controls. In the 7 day female study the HFD mice had significantly higher BG levels than lean control mice. Administering 316 and 986 mg/kg/day TRO reduced BG levels to the same concentration that was measured in lean control mice (Figure 5.8). Glucose tolerance of female mice dosed with TRO for 7 days and lean control mice was better than that of HFD mice, illustrated by lower AUC values for these mice. Results from the 7 day male study followed the same pattern as the 7 day females with HFD control mice having higher BG levels that remained elevated for longer (Figure 5.9). Again, administration of TRO, at doses of 354 and 810 mg/kg/day, lowered BG levels and improved glucose tolerance, resulting in no differences being detected between TRO dosed and lean control mice. Female mice that had been administered 387 and 1006 mg/kg/day TRO for 14 days had similar responses to the OGGT as the lean control mice (Figure 5.10). The 14 day female HFD control mice had higher BG levels than TRO dosed and lean

control mice. Male mice dosed with 396 mg/kg/day TRO for 14 days only had higher BG levels than HFD control mice 30 minutes after glucose had been administered, at other time points there was no significant difference between BG levels of the two groups (Figure 5.11). In contrast, male mice administered 1049 mg/kg/day for 14 days had lower BG levels than HFD controls at 15, 30 and 60 minutes after glucose administration. Furthermore, TRO dosed female and male mice in the 7 and 14 day studies had BG levels lower than HFD controls at least 3 time points. The minimal difference in BG levels between HFD control mice and mice dosed with 396 mg/kg/day TRO for 14 days resulted in no significant difference in AUC and thus glucose tolerance between these groups. Male mice dosed with 1049 mg/kg/day TRO for 14 days and lean control mice had lower AUC values than HFD control mice. During the OGTT mice dosed with 1049 mg/kg/day TRO for 14 days had lower BG levels than the lean mice at 15 minutes after glucose had been administered.

Overall the data illustrate that administering TRO to HFD mice resulted in lower peak BG levels and improved glucose tolerance in these mice.
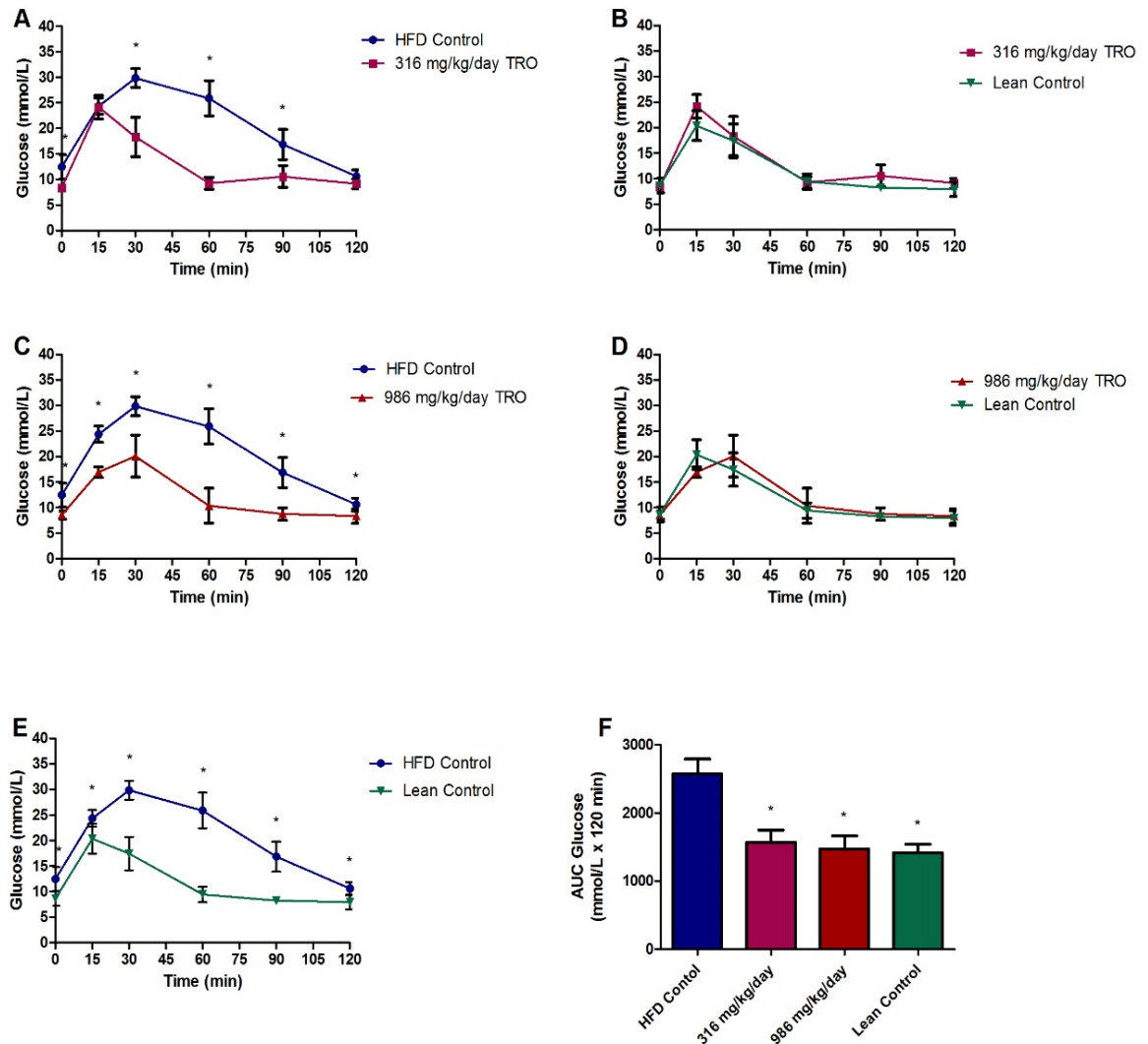
Figure 5.8 – OGTT results of female mice administered TRO for 7 days. Responses of mice dosed with 316 mg/kg/day TRO were compared with (A) HFD controls and (B) lean controls. Responses of mice dosed with 986 mg/kg/day TRO were compared with (C) HFD controls and (D) lean controls. (E) Responses of HFD mice were compared with lean mice. (F) Glucose clearance of TRO dosed and lean mice were compared with HFD controls. TRO administration improved glucose intolerance, reducing both the peak concentration of glucose levels and the time taken for elevated glucose levels to normalize (data are mean ± SD (n=5, n=4 for HFD controls); (A-E) *$p < 0.05$ for comparison between groups at each time point by t-test analysis; (F) *$p < 0.05$ for given group compared with HFD control by one-way ANOVA with post hoc Dunnett's test)
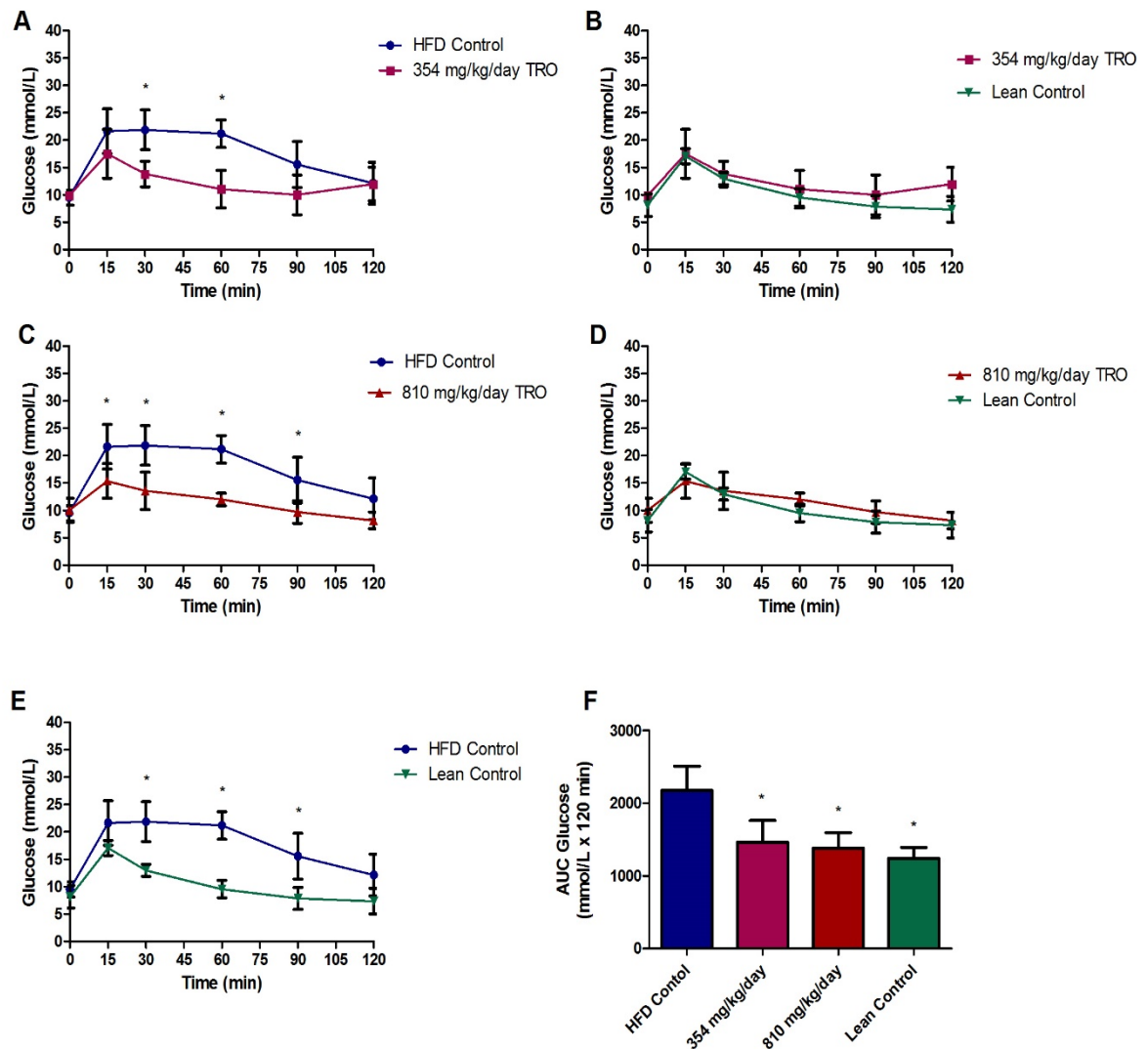
Figure 5.9 – OGTT results of male mice administered TRO for 7 days.
Responses of mice dosed with 354 mg/kg/day TRO were compared with (A) HFD
controls and (B) lean controls. Responses of mice dosed with 810 mg/kg/day TRO
were compared with (C) HFD controls and (D) lean controls. (E) Responses of HFD
mice were compared with lean mice. (F) Glucose clearance of TRO dosed and lean
mice were compared with HFD controls. TRO administration improved glucose
intolerance, reducing both the peak concentration of glucose levels and the time
taken for elevated glucose levels to normalize (data are mean ± SD (n=5); (A-E)
*$p < 0.05$ for comparison between groups at each time point by t-test analysis; (F)
*$p < 0.05$ for given group compared with HFD control by one-way ANOVA with post
hoc Dunnett's test)
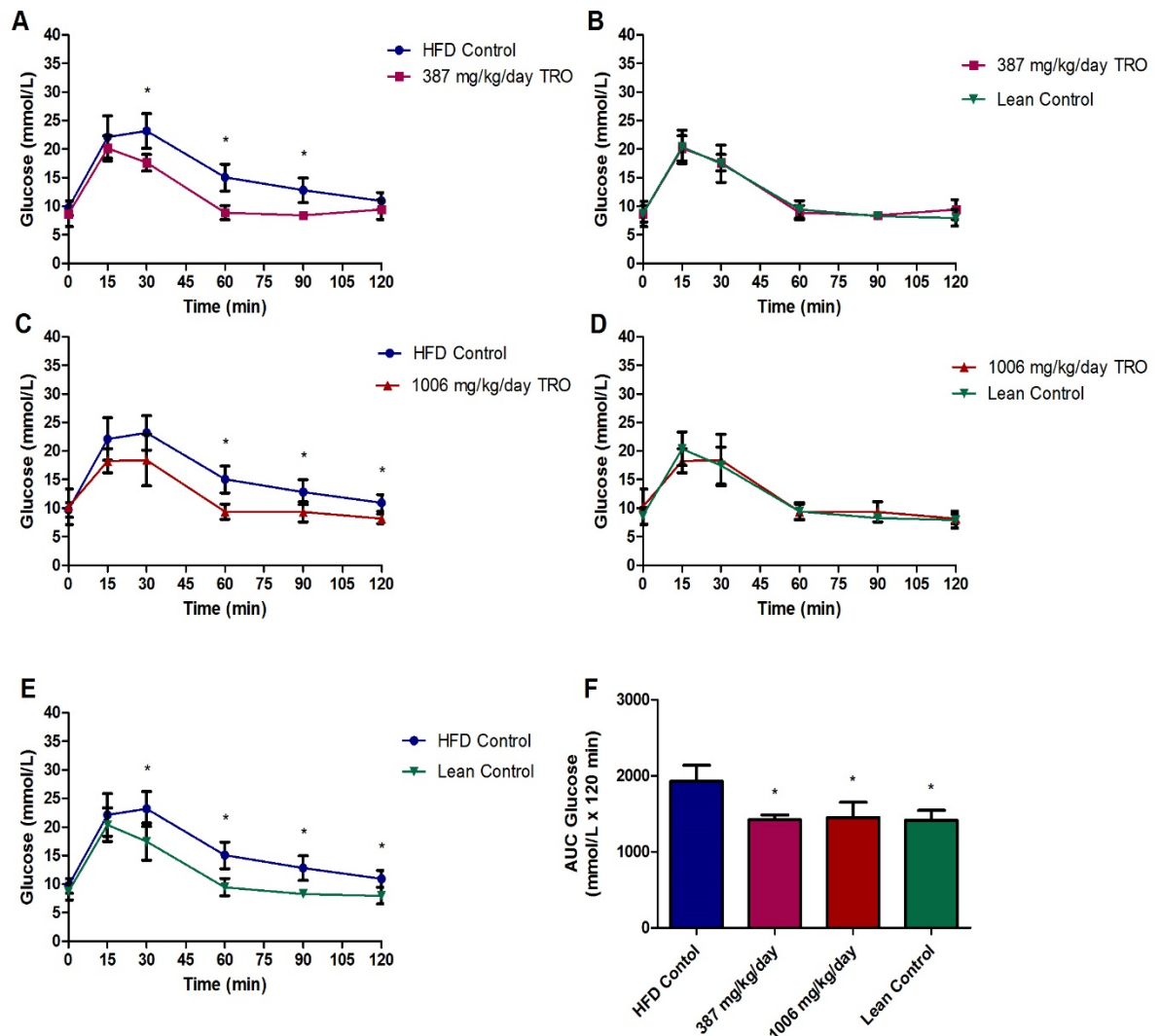
Figure 5.10 – OGTT results of female mice administered TRO for 14 days.
Responses of mice dosed with 387 mg/kg/day TRO were compared with (A) HFD controls and (B) lean controls. Responses of mice dosed with 1006 mg/kg/day TRO were compared with (C) HFD controls and (D) lean controls. (E) Responses of HFD mice were compared with lean mice. (F) Glucose clearance of TRO dosed and lean mice were compared with HFD controls. TRO administration improved glucose intolerance, reducing both the peak concentration of glucose levels and the time taken for elevated glucose levels to normalize (data are mean ± SD (n=5); (A-E) *p<0.05 for comparison between groups at each time point by t-test analysis; (F) *p<0.05 for given group compared with HFD control by one-way ANOVA with post hoc Dunnett's test)
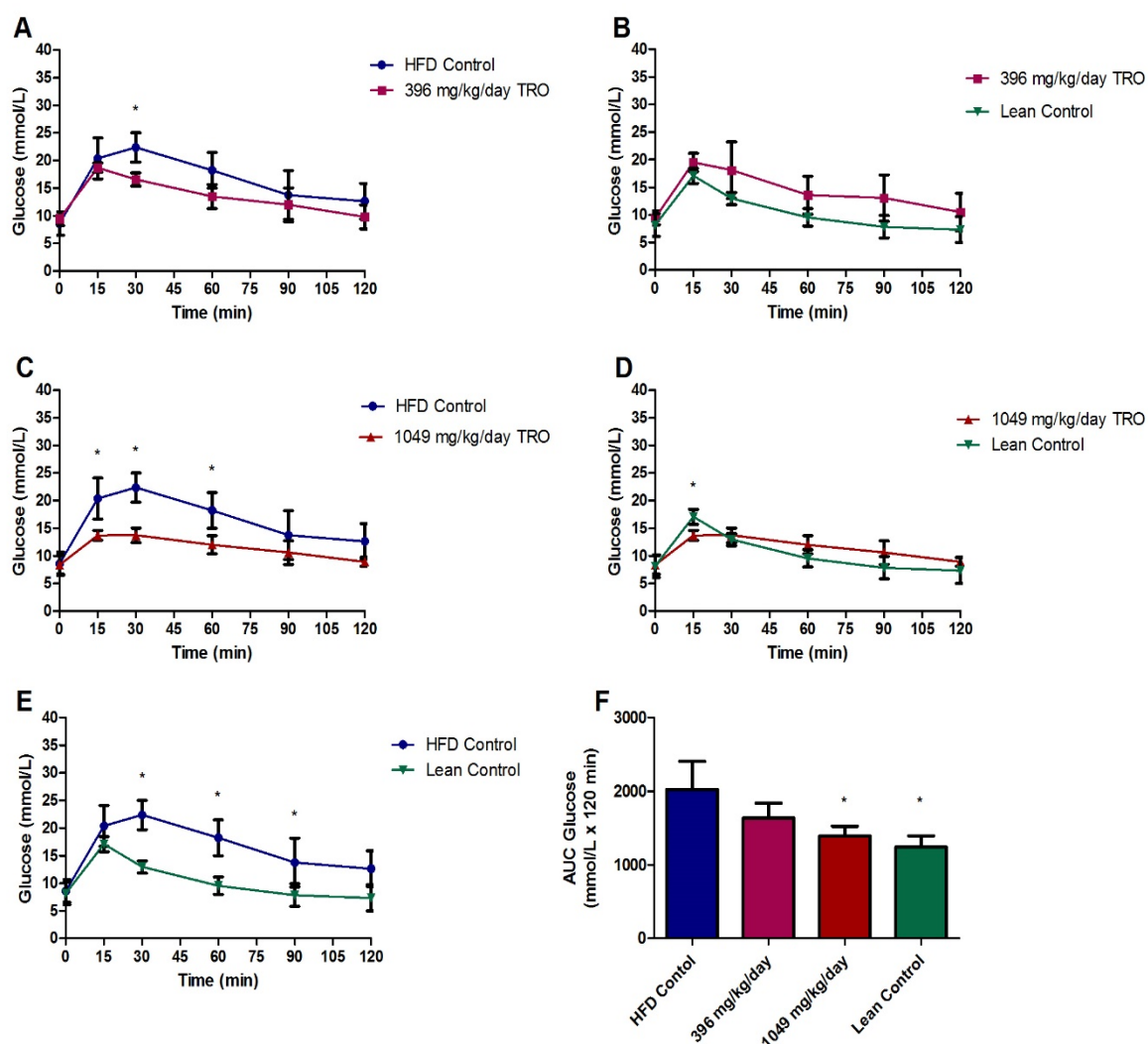
Figure 5.11 – OGTT results of male mice administered TRO for 14 days. Responses of mice dosed with 396 mg/kg/day TRO were compared with (A) HFD controls and (B) lean controls. Responses of mice dosed with 1049 mg/kg/day TRO were compared with (C) HFD controls and (D) lean controls. (E) Responses of HFD mice were compared with lean mice. (F) Glucose clearance of TRO dosed and lean mice were compared with HFD controls. TRO administration improved glucose intolerance, reducing both the peak concentration of glucose levels and the time taken for elevated glucose levels to normalize (data are mean ± SD (n=5); (A-E) *$p < 0.05$ for comparison between groups at each time point by t-test analysis; (F) *$p < 0.05$ for given group compared with HFD control by one-way ANOVA with post hoc Dunnett's test)

5.3.8 Effect of TRO on the Hearts of Diabetic Mice

Male and female mice were administered TRO via the diet for 7 and 14 days. At the point of necropsy heart tissue was excised from each mouse, flash frozen in liquid nitrogen and stored at -80°C until RNA was extracted. Qualitative and quantitative analysis of RNA was undertaken before it was used for microarray and RT-PCR analysis. Illumina mouse whole genome arrays were used to assess differential expression of genes between heart tissue from control and TRO dosed male and female mice in the 7 and 14 day studies. ArrayTrack was used to analyse microarray data and identify genes that were differentially expressed between the control and TRO dose groups. Genes that had $\log_2$ fold change values of >0.5 or <-0.5 with significance $p<0.05$ were selected to form the gene signature of TRO treatment for each dose group (Figures 5.12 and 5.13). The fewest changes in gene expression was observed in the hearts of male mice administered 316 mg/kg/day TRO for 7 days and the largest number of gene expression changes were observed in the hearts of female mice administered 1006 mg/kg/day TRO for 14 days. Increased expression of the genes Angptl4 and Car4 and decreased expression of Aqp1 and Kcna5 was observed in all TRO dosed mice in comparison with control mice. Pathway analysis of microarray data from heart tissue of HFD mice dosed with TRO did not associate the cardiac gene expression changes with any physiological or toxicological pathways. Microarray data was analysed for increased expression of genes involved in sarcomere remodelling, which was observed in the normal TRO mouse model. However, differences in the expression of Actg2, Bmp4, Myh11, Tcap, Timp3, Timp4 and Tpm2 in heart tissue of control and TRO dosed HFD mice were not detected by microarray analysis. RT-PCR was subsequently used as a secondary analysis

method to test for differences in the expression of these genes in heart tissue from control and TRO administered HFD mice. The RT-PCR data confirmed that there was no difference in the expression of these sarcomere remodelling genes between control and TRO dosed mice. The two other gene networks identified in heart tissue of normal mice dosed with TRO were differential expression of genes involved in regulation of circadian rhythm and glycerol transport and metabolism. Differential expression of genes involved in the circadian clock were not detected in the hearts of HFD mice dosed with TRO for 7 and 14 days. Increased expression of the genes Aqp7 and Mgll, which are involved in glycerol transport and metabolism, in heart tissue was observed in the normal TRO mouse study and was also detected by microarray analysis of heart tissue of HFD mice administered TRO for 7 and 14 days. These gene expression changes were confirmed using RT-PCR analysis of heart tissue from female and male mice administered TRO for 7 and 14 days (Figures 5.14 and 5.15). Pathway analysis connected increased Aqp7 and Mgll with transport and metabolism of glycerol and showed both genes to be downstream targets of Pparγ. This study provided a gene signature of the effects of TRO on the hearts of male and female mice, however these differentially expressed genes did not identify any mechanisms of TRO induced cardiotoxicity.
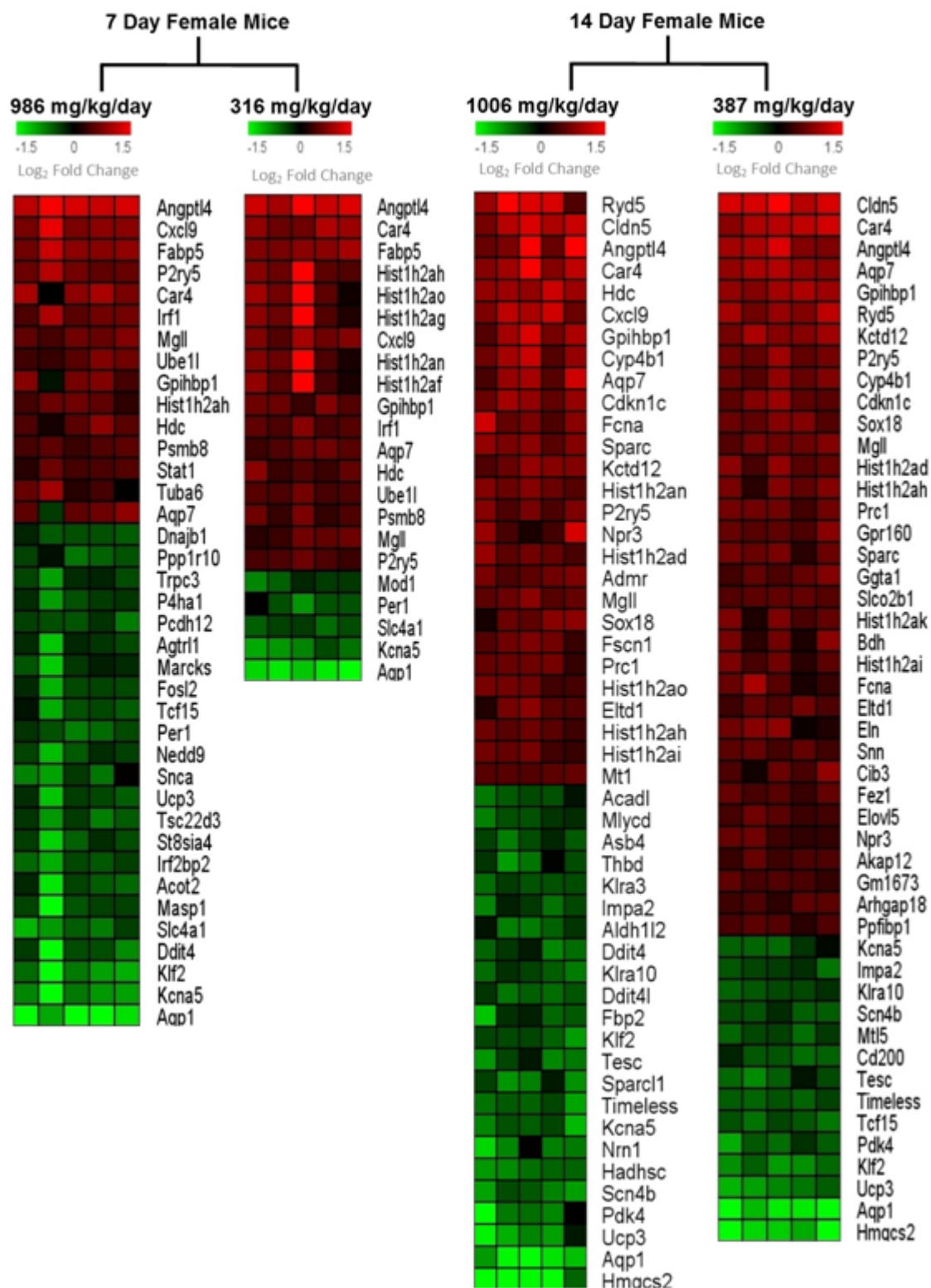
Figure 5.12 – Transcriptomic profiling of heart tissue from female mice administered TRO for 7 and 14 days. Microarray analysis identified genes differentially expressed in response to TRO treatment (Data shows -0.5< $\log_2$ fold change >0.5 of genes with results are statistically significant at p<0.05 compared with respective 7 and 14 day controls).
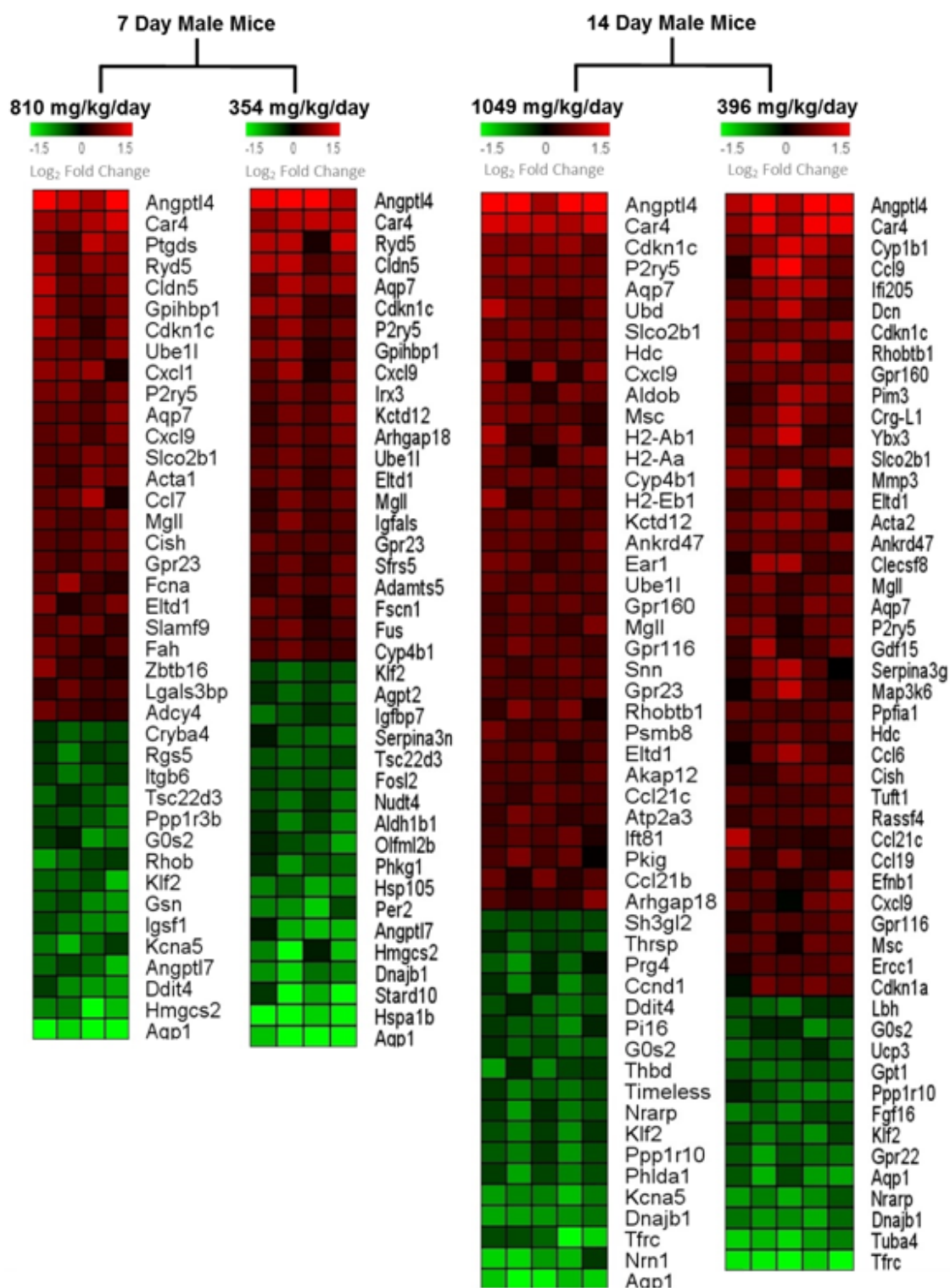
Figure 5.13 – Transcriptomic profiling of heart tissue from male mice administered TRO for 7 and 14 days. Microarray analysis identified genes differentially expressed in response to TRO treatment (Data shows -0.5< log$_2$ fold change >0.5 of genes with results are statistically significant at p<0.05 compared with respective 7 and 14 day controls).
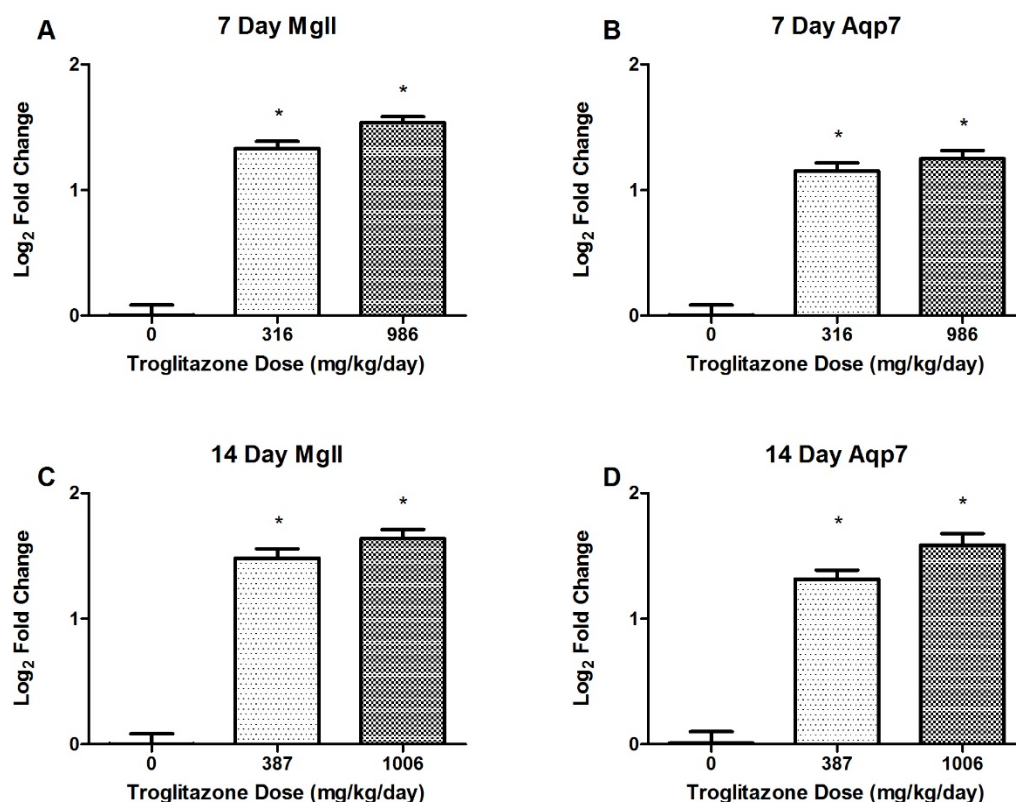
Figure 5.14 – Expression of Mgll and Aqp7 in hearts of female mice administered TRO for 7 and 14 days. Expression of the genes Mgll and Aqp7 was assessed by RT-PCR in the hearts of female mice administered 316 and 986 mg/kg/day TRO for 7 days and 387 and 1006 mg/kg/day TRO for 14 days. (A and C) Increased expression of Mgll was observed in the hearts of female mice dosed with TRO for 7 and 14 days. (B and D) Increased expression of Aqp7 was observed in the hearts of female mice dosed with TRO for 7 and 14 days (data are mean ± SD (n=5, n=4 for 7 day controls), results are statistically significant at *$p < 0.05$ for given dose compared with control by one-way ANOVA with post hoc Dunnett's test).
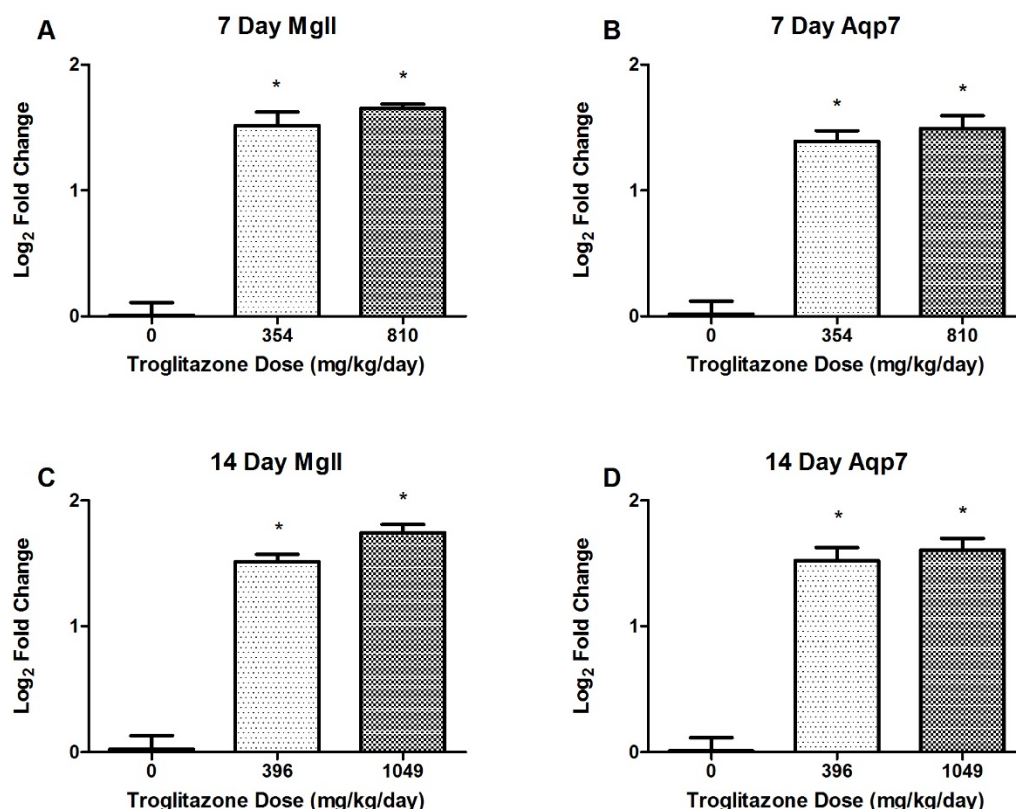
Figure 5.15 – Expression of Mgll and Aqp7 in hearts of male mice administered TRO for 7 and 14 days. Expression of the genes Mgll and Aqp7 was assessed by RT-PCR in the hearts of male mice administered 354 and 810 mg/kg/day TRO for 7 days and 396 and 1049 mg/kg/day TRO for 14 days. (A and C) Increased expression of Mgll was observed in the hearts of male mice dosed with TRO for 7 and 14 days. (B and D) Increased expression of Aqp7 was observed in the hearts of male mice dosed with TRO for 7 and 14 days (data are mean ± SD (n=5), results are statistically significant at *$p<0.05$ for given dose compared with control by one-way ANOVA with post hoc Dunnett's test).

5.3.9 Effects of TRO on the Livers of Diabetic Mice

Mice in this study were fed on a HFD to mimic the development of T2D in the same manner in which it occurs in the patient population. Administration of a HFD was expected to cause biochemical changes, such as the onset of glucose intolerance and this change was observed after the mice had been fed a HFD for 18 weeks. In addition, it was anticipated that feeding mice a HFD would lead to transcriptional changes in the liver. In particular, increased expression of hepatic Pparγ was anticipated and has been reported to occur in murine HFD models (Kim et al., 2004). RT-PCR analysis was used to detect the expression of Pparγ and Pparα in the livers of male and female lean control mice, HFD control mice and HFD TRO dosed mice from the 7 and 14 day studies (Figures 5.16 and 5.17). Administering a HFD resulted in increased expression of Pparγ in the livers of male and female mice with greater induction in gene expression being observed in the livers of male mice. Administering TRO for 7 and 14 days further increased the expression of Pparγ in the liver and again expression levels were higher in male mice. Administering a HFD also caused an increase in the expression of Pparα in the livers of male and female mice compared with lean mice. The degree of up-regulation was similar between both genders and the increase in Pparα expression was smaller than the increase in Pparγ. Administering TRO for 7 and 14 days did not affect the expression levels of Pparα in the livers of male and female mice.
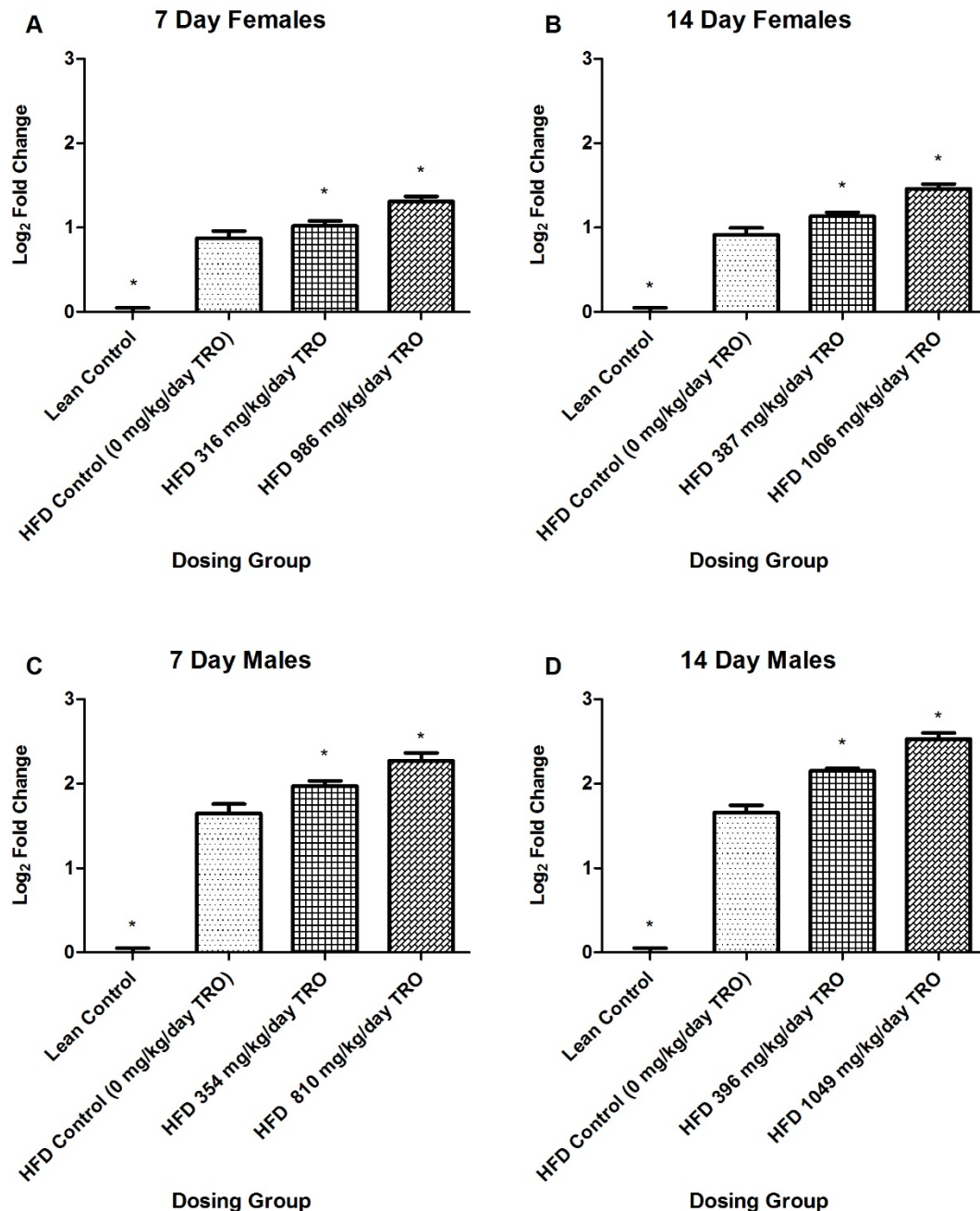
Figure 5.16 – Expression of Pparγ in livers of HFD male and female mice administered TRO for 7 and 14 days. (A-D) Expression of hepatic Pparγ was assessed by RT-PCR in the livers of male and female lean control mice, HFD control mice and HFD mice dosed with TRO for 7 and 14 days. Feeding a HFD to male and female mice resulted in increased expression of Pparγ in the liver. Administering TRO further increased the expression levels of hepatic Pparγ (data are mean ± SD (n=4/5), results are statistically significant at $*p < 0.05$ for given group compared with HFD controls by one-way ANOVA with post hoc Dunnett's test).
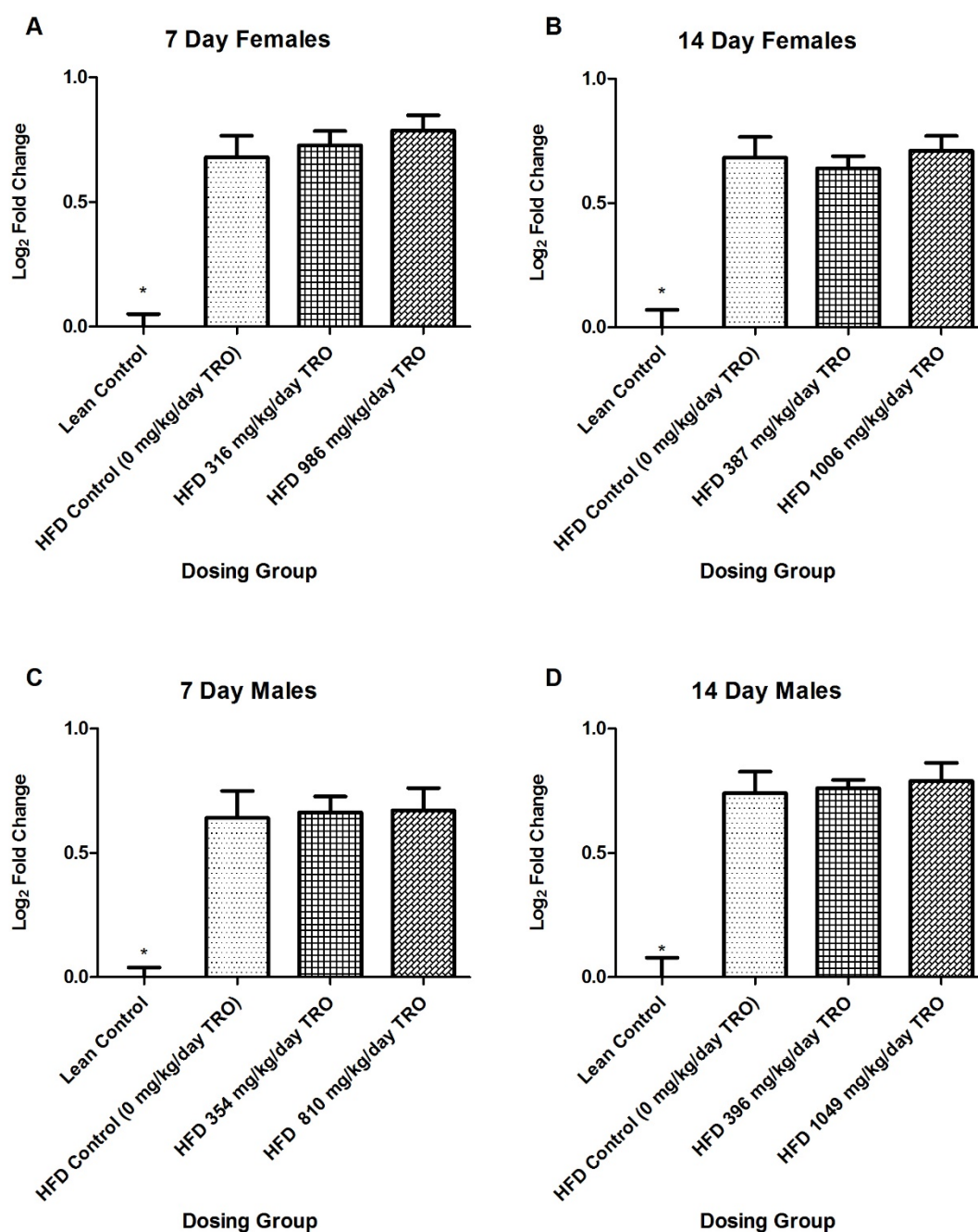
Figure 5.17 – Expression of Pparα in livers of HFD male and female mice administered TRO for 7 and 14 days. (A-D) Expression of hepatic Pparα was assessed by RT-PCR in the livers of male and female lean control mice, HFD control mice and HFD mice dosed with TRO for 7 and 14 days. Feeding a HFD to male and female mice resulted in increased expression of Pparα in the liver. Administering TRO did not affect the expression of hepatic Pparα, which was similar between HFD control and HFD TRO dosed mice (data are mean ± SD (n=4/5), *$p < 0.05$ for given group compared with HFD controls by one-way ANOVA with post hoc Dunnett's test).

Male and female mice were administered TRO via the diet for 7 and 14 days. At the point of necropsy liver tissue was excised from each mouse, flash frozen in liquid nitrogen and stored at -80°C until RNA was extracted. Qualitative and quantitative analysis of RNA was undertaken before it was used for microarray and RT-PCR analysis. Illumina mouse whole genome arrays were used to assess differential expression of genes between liver tissue from HFD control and HFD TRO dosed male and female mice in the 7 and 14 day studies. ArrayTrack was used to analyse microarray data and identify genes that were differentially expressed between the control and TRO dose groups. Genes that had $\log_2$ fold change values of >0.5 or <-0.5 with significance p<0.05 were selected to form the gene signature of TRO treatment for each dose group (Figures 5.18 and 5.19). The fewest changes in gene expression was observed in the livers of female mice administered 387 mg/kg/day TRO for 14 days and the largest number of gene expression changes were observed in the livers of female mice administered 1006 mg/kg/day TRO for 14 days. Pathway analysis of microarray data identified a sub-set of genes that were differentially expressed in all TRO dose groups and associated these genes with lipid metabolism. Increased expression of Slc27a1, Agpat6 and Mogat1 was observed in all male and female TRO dose groups compared with controls and these genes were shown to be involved in the synthesis of triglycerides in the liver (Figure 5.20). RT-PCR analysis was used to confirm gene expression changes in these 3 genes, which had been detected by microarray analysis. Increased expression of Slc27a1, Agpat6 and Mogat1 was detected in the livers of male and female mice administered TRO for 7 and 14 days (Figures 5.21 and 5.22). The greatest increase in the expression of these genes was observed in the livers of male mice administered 1049 mg/kg/day TRO

for 14 days and in female mice administered 1006 mg/kg/day TRO for 14 days. Expression of Slc27a1, Agpat6 and Mogat1 was higher in the livers of female mice than in the livers of male mice. In addition to increased expression of genes involved in triglyceride synthesis, expression of genes involved in triglyceride accumulation in the liver were also up-regulated in the livers of TRO dosed mice. Increased expression of the genes Cfd, Cidea, Cidec and S3-12 was detected by microarray analysis in the livers of male mice administered TRO for 7 and 14 days. Up-regulation of Cfd, Cidec and S3-12 was detected by microarray analysis in the livers of female mice but no changes were detected in the expression of Cidea in control and TRO dosed mice in the 7 and 14 day studies. RT-PCR analysis was used to confirm these gene changes and the data correlated with the changes that had been detected by microarray analysis (Figures 5.23 and 5.24).

At the point of necropsy it was noted that the appearance of livers from male mice administered 1049 mg/kg/day TRO for 14 days was notably different compared with all other mice from the study. The livers of mice from this group were yellowish-brown in colour and the colouring was speckled across the tissue. In contrast, the livers of all the other male and female control and TRO dosed mice reddish-brown in colour. Yellow discolouring of the liver is associated with intra-hepatic jaundice caused by liver damage. Microarray data from the livers of male mice administered 1049 mg/kg/day TRO for 14 days was analysed for differential expression of genes involved in bile acid synthesis and export. Increased expression of Cyp7a1 and Cyp8b1, which encode for enzymes involved in the synthesis of bile acids from cholesterol and decreased expression of Abcb11, which encodes for the bile salt export pump that transports bile acids from

hepatocytes into the bile canaliculi, were identified from the microarray data. RT-PCR was used to assess the expression of Cyp7a1, Cyp8b1 and Abcb11 in the livers of male and female mice dosed with TRO for 7 and 14 days (Figures 5.25 and 5.26). Administering TRO resulted in increased expression of Cyp7a1 and Cyp8b1 and decreased expression of Abcb11 in male and female mice in the 7 and 14 day studies. The differences between TRO dosed and control mice were significant although the $\log_2$ fold change values were predominantly >-0.5 and <0.5, indicating slight changes in gene expression. The largest $\log_2$ fold changes were observed in the 14 day top TRO dose male and female groups. For female mice the largest increase in Cyp7a1 and Cyp8b1 expression and the greatest degree of down-regulation of Abcb11 was observed in mice administered 1006 mg/kg/day TRO for 14 days. Likewise with the male mice the greatest changes in gene expression were observed in the livers of mice administered 1049 mg/kg/day TRO for 14 days. $\log_2$ fold change <-1 in expression of Abcb11 was only observed in the livers of male mice administered 1049 mg/kg/day TRO for 14 days. The 14 day male mice administered 1049 mg/kg/day TRO were observed to have yellow discolouring of the liver and these mice were shown to have the largest fold changes in the expression of genes involved in bile acid synthesis and secretion.
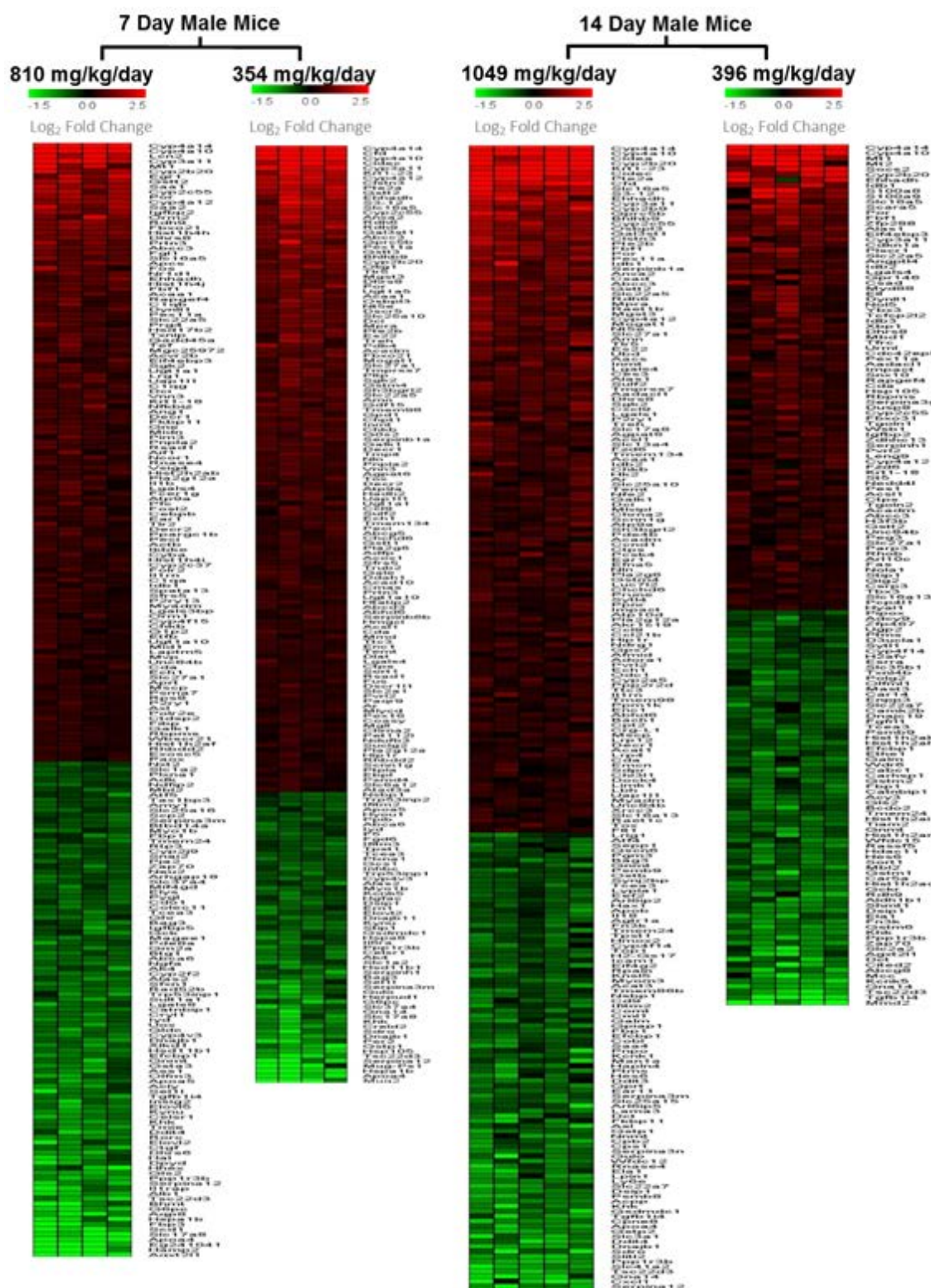
Figure 5.18 – Transcriptomic profiling of liver tissue from male mice administered TRO for 14 and 7 days. Microarray analysis identified genes differentially expressed in response to TRO treatment (Data shows -0.5< log$_2$ fold change >0.5 of genes with results statistically significant at p<0.05 compared with respective 7 and 14 day controls).
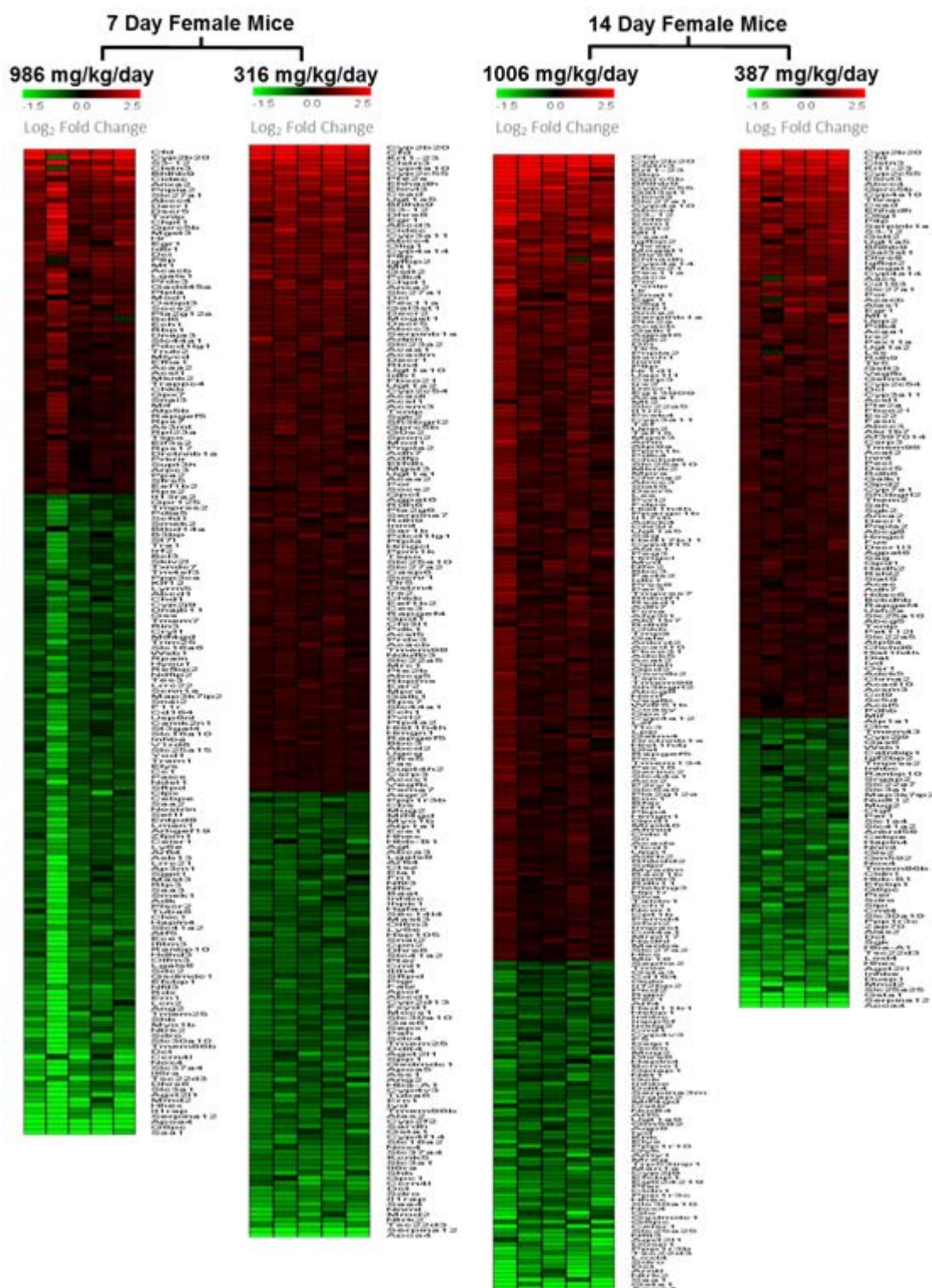
Figure 5.19 – Transcriptomic profiling of liver tissue from female mice administered TRO for 14 and 7 days. Microarray analysis identified genes differentially expressed in response to TRO treatment (Data shows -0.5< log$_2$ fold change >0.5 of genes with results statistically significant at p<0.05 compared with respective 7 and 14 day controls).
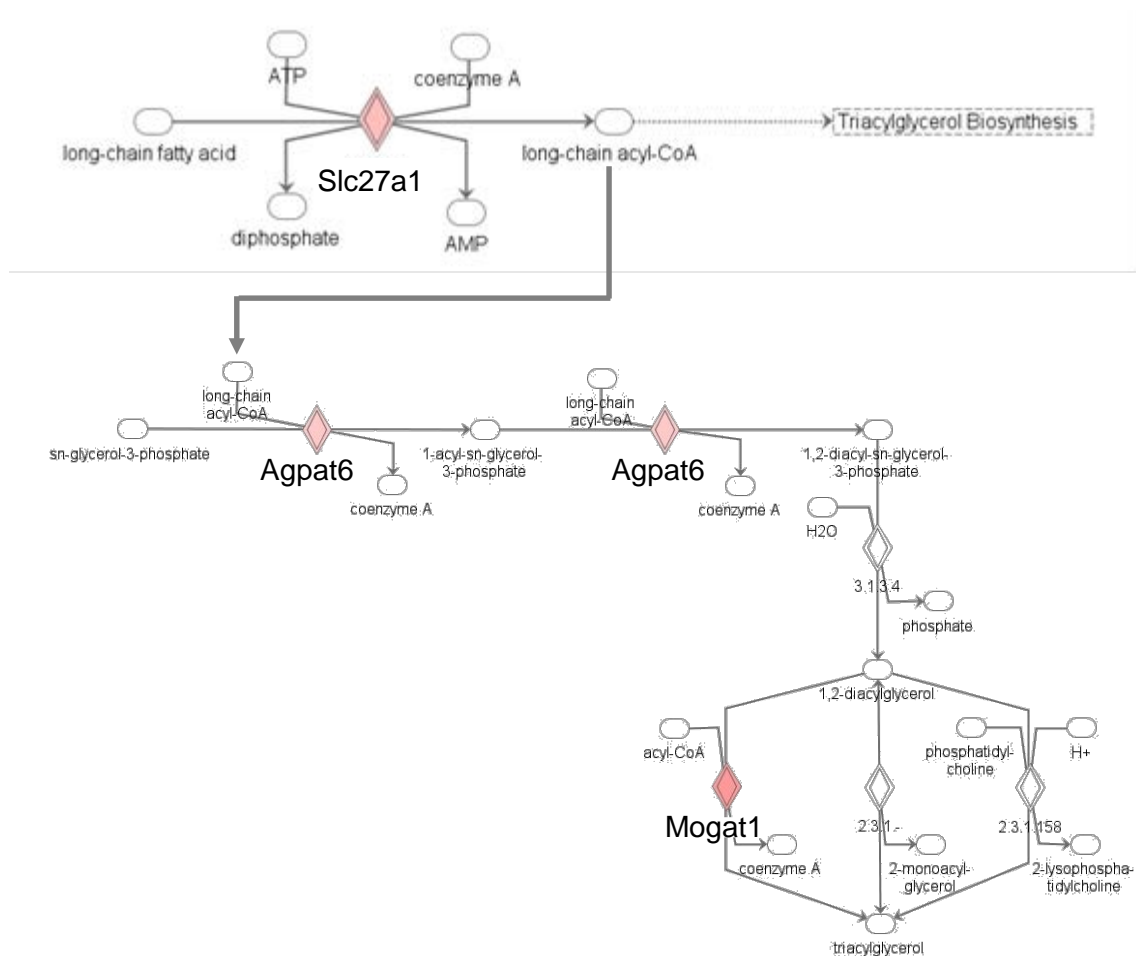
Figure 5.20 – TRO administration increased expression of genes involved in triglyceride synthesis in the liver. Pathway analysis of microarray data from male and female mice dosed with TRO for 14 days identified up-regulation of the genes Slc27a1, Agpat6 and Mogat1 in the livers of TRO dosed mice.
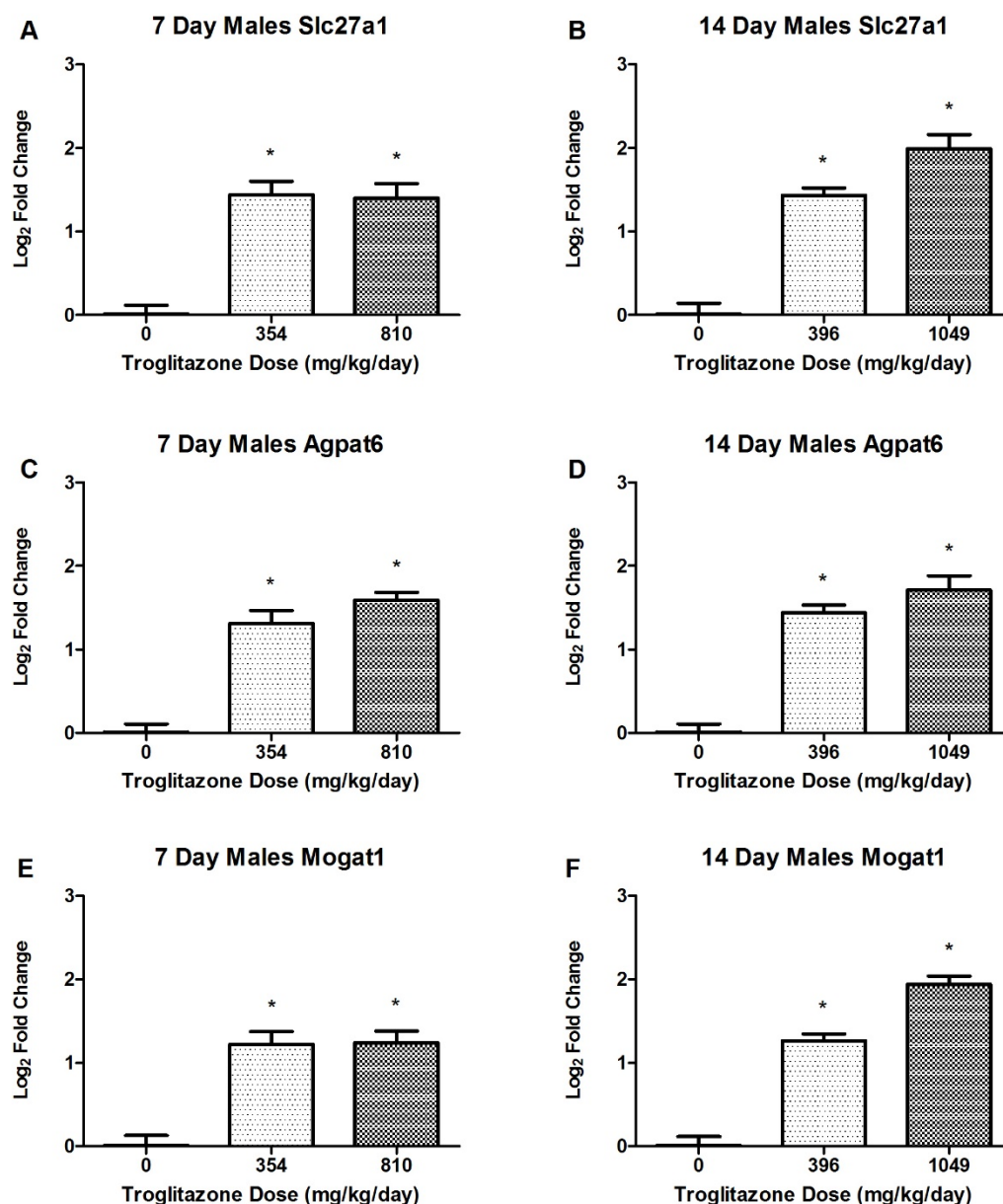
Figure 5.21 – Expression of genes involved in triglyceride synthesis in livers of HFD male mice administered TRO for 7 and 14 days. (A-F) Expression of hepatic Slc27a1, Agpat6 and Mogat1 was assessed by RT-PCR in the livers of control mice and mice dosed with TRO for 7 and 14 days. TRO treatment resulted in increased expression of hepatic Slc27a1, Agpat6 and Mogat1 with the greatest increases observed in mice administered 1049 mg/kg/day TRO for 14 days (data are mean ± SD (n=5), results are statistically significant at *$p < 0.05$ for given group compared with controls by one-way ANOVA with post hoc Dunnett's test).
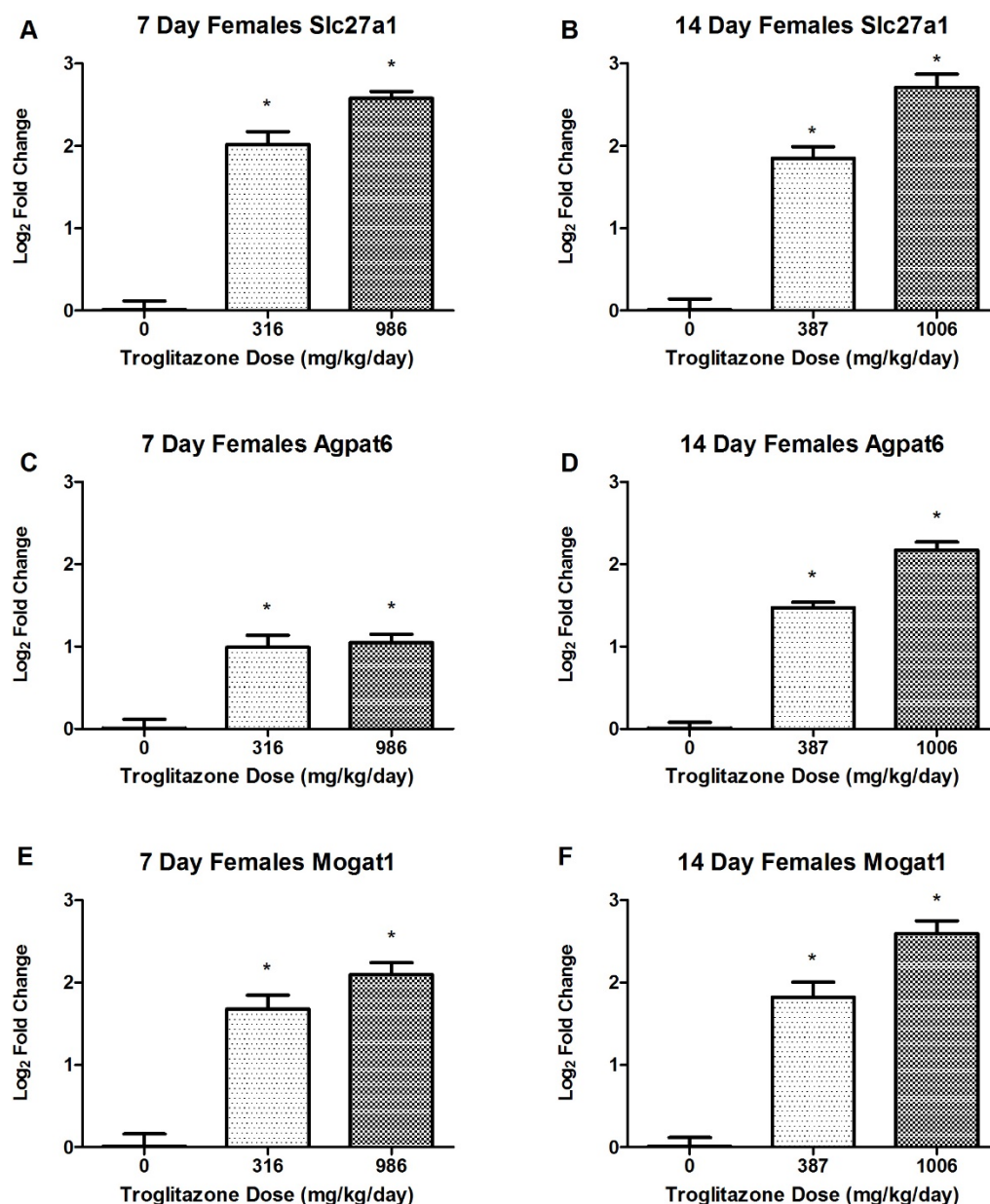
Figure 5.22 – Expression of genes involved in triglyceride synthesis in livers of HFD female mice administered TRO for 7 and 14 days. (A-F) Expression of hepatic Slc27a1, Agpat6 and Mogat1 was assessed by RT-PCR in the livers of control mice and mice dosed with TRO for 7 and 14 days. TRO treatment resulted in increased expression of hepatic Slc27a1, Agpat6 and Mogat1 with the greatest increases observed in mice administered 1006 mg/kg/day TRO for 14 days (data are mean ± SD (n=5, n=4 for 7 day controls), results are statistically significant at *$p < 0.05$ for given group compared with controls by one-way ANOVA with post hoc Dunnett's test).

Figure 5.23 – Expression of genes involved in triglyceride accumulation in livers of HFD male mice administered TRO for 7 and 14 days. Please see next page for legend.

Figure 5.23 – Expression of genes involved in triglyceride accumulation in livers of HFD male mice administered TRO for 7 and 14 days. Expression of hepatic Cfd, Cidea, Cidec and S3-12 was assessed by RT-PCR in the livers of control mice and mice dosed with TRO for 7 and 14 days. (A and B) Expression of Cfd in the livers of male mice dosed with TRO increased in a time and dose dependent manner with the greatest induction of gene expression being observed in the livers of mice administered 1049 mg/kg/day TRO for 14 days. (C and D) Expression of hepatic Cidea increased after 7 and 14 days of TRO administration. Administering 1049 mg/kg/day for 14 days caused the largest increase in hepatic Cidea expression. (E and F) Expression of Cidec in the livers of male mice increased with TRO treatment with the greatest increase in expression measured in livers of mice administered 1049 mg/kg/day TRO for 14 days. (G and H) Increased expression of S3-12 was detected in the livers of male mice administered TRO for 7 and 14 days. Mice administered 810 mg/kg/day TRO for 7 days and 1049 mg/kg/day TRO for 14 days had similar levels of hepatic S3-12 expression (data are mean ± SD (n=5), results are statistically significant at $*p<0.05$ for given group compared with controls by one-way ANOVA with post hoc Dunnett's test).
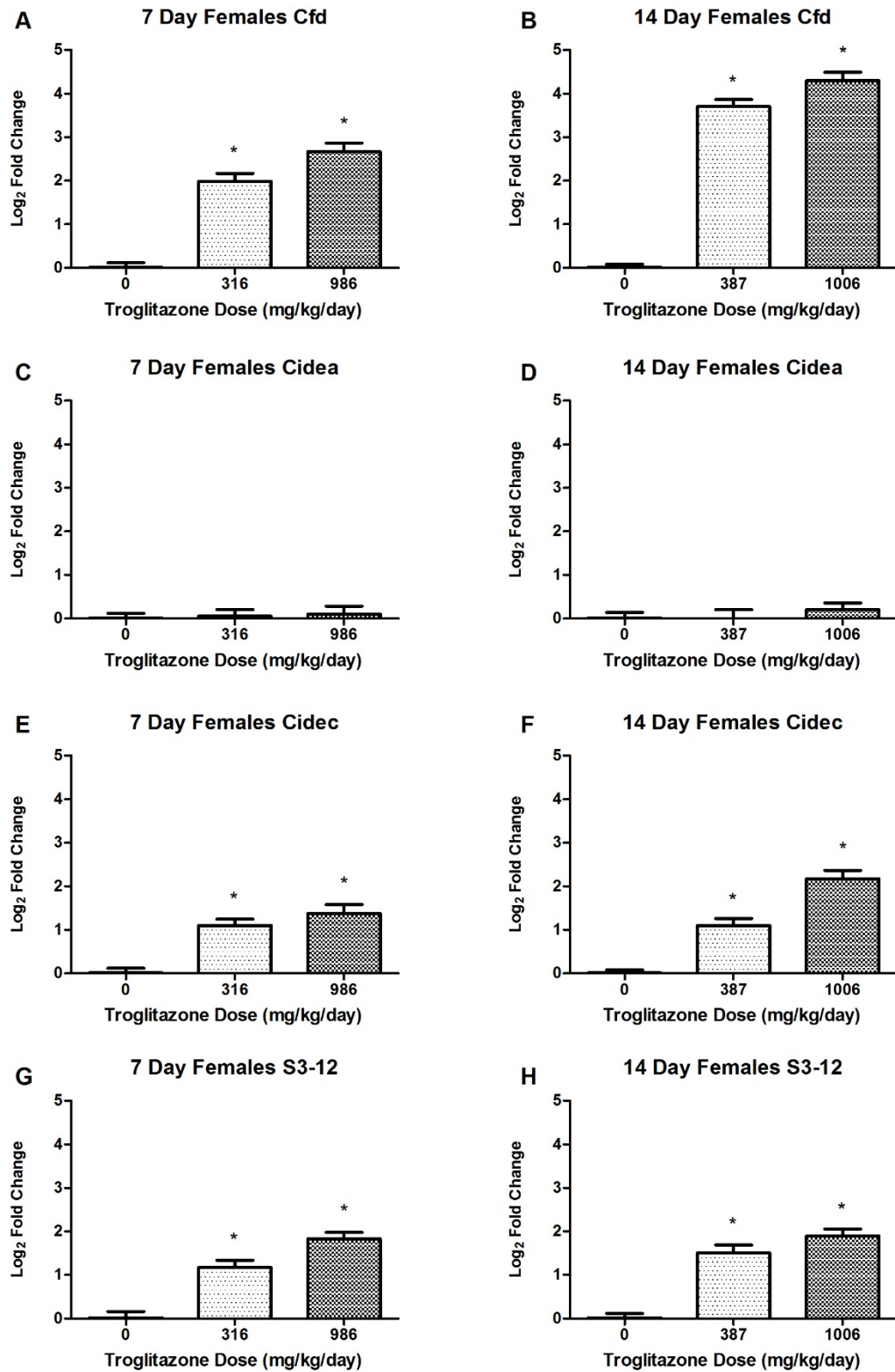
Figure 5.24 – Expression of genes involved in triglyceride accumulation in livers of HFD female mice administered TRO for 7 and 14 days. Please see next page for legend.

Figure 5.24 – Expression of genes involved in triglyceride accumulation in livers of HFD female mice administered TRO for 7 and 14 days. Expression of hepatic Cfd, Cidea, Cidec and S3-12 was assessed by RT-PCR in the livers of control mice and mice dosed with TRO for 7 and 14 days. (A and B) Expression of Cfd in the livers of female mice dosed with TRO increased in a time and dose dependent manner with the greatest induction of gene expression being observed in the livers of mice administered 1006 mg/kg/day TRO for 14 days. (C and D) Expression of Cidea in the livers of female mice was not altered by TRO treatment. (E and F) Expression of Cidec in the livers of female mice increased with TRO treatment with the greatest increase in expression measured in livers of mice administered 1006 mg/kg/day TRO for 14 days. (G and H) Increased expression of S3-12 was detected in the livers of female mice administered TRO for 7 and 14 days. Mice administered 986 mg/kg/day TRO for 7 days and 1006 mg/kg/day TRO for 14 days had similar levels of hepatic S3-12 expression (data are mean ± SD (n=5, n=4 for 7 day controls), results are statistically significant at *$p < 0.05$ for given group compared with controls by one-way ANOVA with post hoc Dunnett's test).
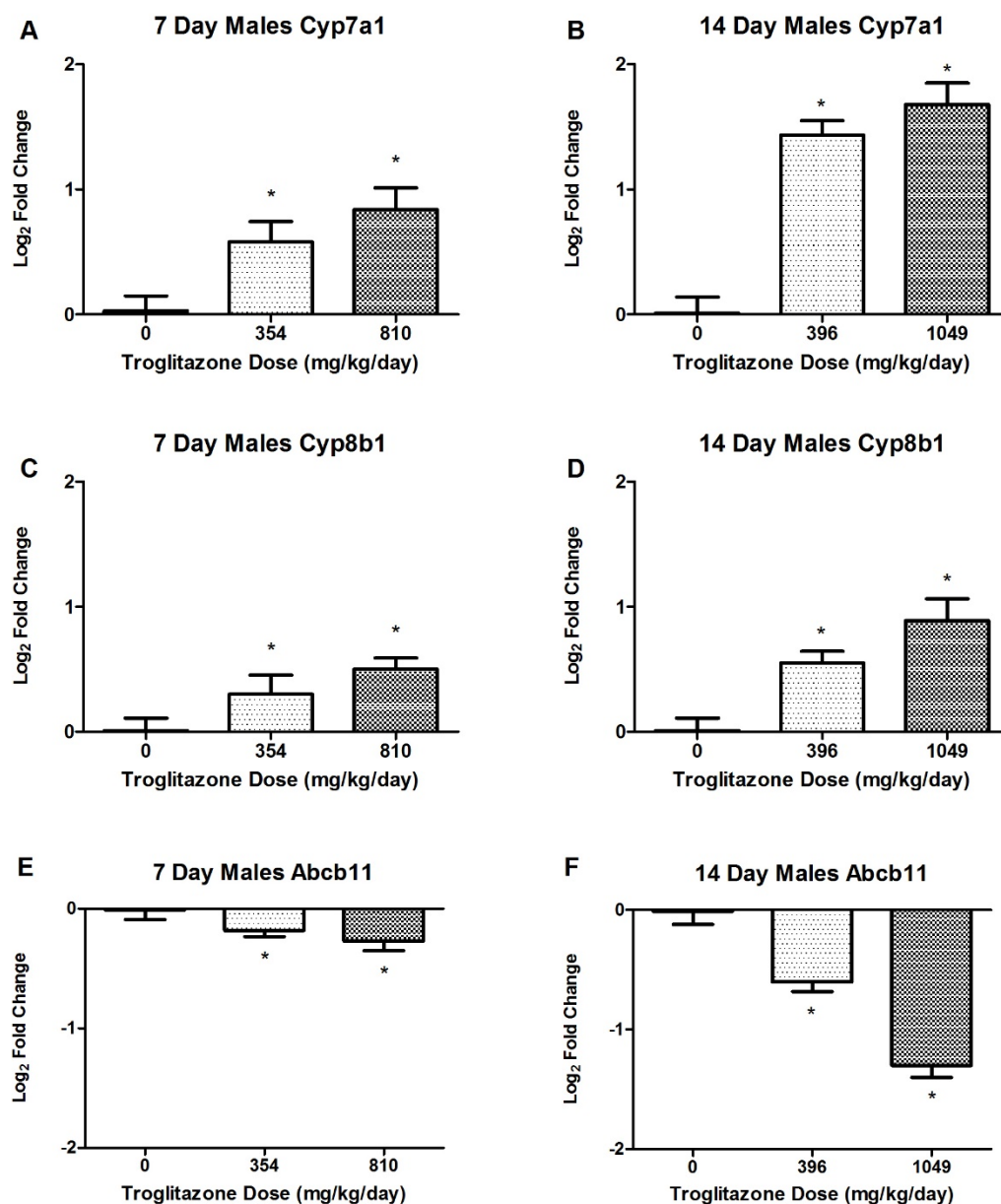
Figure 5.25 – Expression of genes involved in bile acid formation and secretion in livers of HFD male mice administered TRO for 7 and 14 days. (A-F) Expression of hepatic Cyp7a1, Cyp8b1 and Abcb11 was assessed by RT-PCR in the livers of control mice and mice dosed with TRO for 7 and 14 days. TRO treatment for 7 and 14 days resulted in increased expression of hepatic Cyp7a1, Cyp8b1 and Abcb11. The greatest increases in gene expression were observed in the livers of mice administered 1049 mg/kg/day TRO for 14 days (data are mean ± SD (n=5), *$p<0.05$ for given group compared with controls by one-way ANOVA with post hoc Dunnett's test).
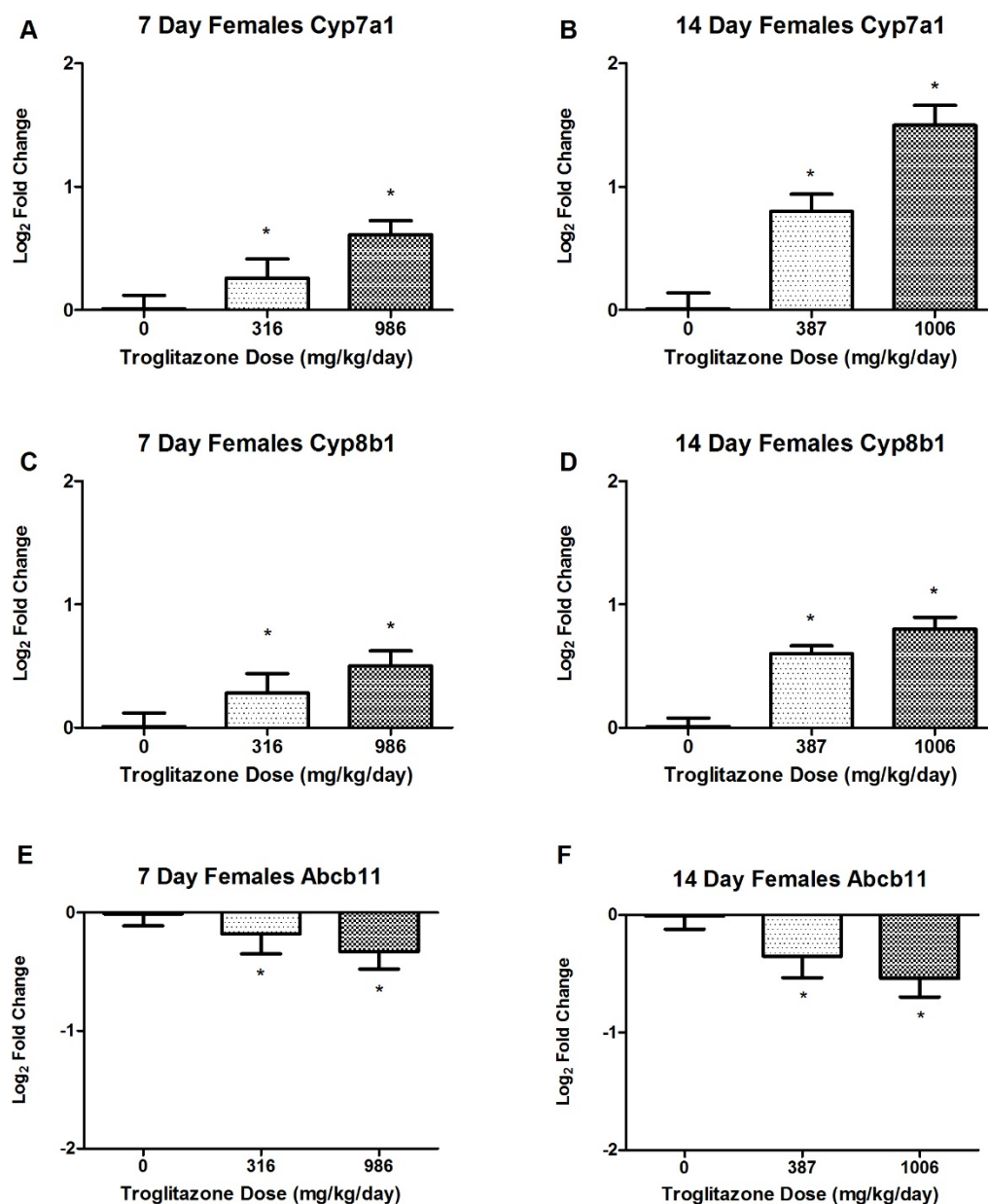
Figure 5.26 – Expression of genes involved in bile acid formation and secretion in livers of HFD female mice administered TRO for 7 and 14 days. (A-F) Expression of hepatic Cyp7a1, Cyp8b1 and Abcb11 was assessed by RT-PCR in the livers of control mice and mice dosed with TRO for 7 and 14 days. TRO treatment for 7 and 14 days resulted in increased expression of hepatic Cyp7a1, Cyp8b1 and Abcb11. The greatest increases in gene expression were observed in the livers of mice administered 1006 mg/kg/day TRO for 14 days (data are mean ± SD (n=5, n=4 for 7 day controls), *p<0.05 for given group compared with controls by one-way ANOVA with post hoc Dunnett's test).

5.4 Discussion

The aim of this chapter was to develop a HFD induced mouse model of T2D for use in deducing a profile of TRO induced transcriptional changes in a model that represented that pathophysiological changes associated with the disease in the patient population. The gene signatures of transcriptional changes in the heart and liver would be used to evaluate the utility of *in vitro* mES cell derived cardiomyocytes and hepatocytes as model systems for the evaluation of drug induced toxicity.

5.4.1 Inducing Diabetes in Mice using a HFD

TRO was used in the management of T2D until it was withdrawn from the market due to incidences of severe hepatotoxicity in a small subset of the patient population (Gale, 2001). The development of T2D has been associated with overnutrition, which is the excessive consumption of dietary components (Parillo and Riccardi, 2004). This effect can be mimicked in mice via administration of a HFD in which 60% of the calories are from fat. Feeding male and female adult mice a HFD for 18 weeks led to increased body weight and blood glucose levels, and impaired glucose tolerance. These traits are characteristic of insulin resistance as is observed in T2D patients (Reaven, 2005).Normally, PpARγ expression in the liver is relatively low however, in T2D patients it is elevated (Westerbacka et al., 2007). Feeding male and female mice a HFD resulted in increased Pparγ expression in the liver (Figure 5.16). The HFD diet mice developed pathophysiological characteristics that are associated with T2D.

5.4.2 Effects of TRO in HFD Induced Diabetic Mice

TRO was used in the treatment of T2D to sensitize tissues to the actions of insulin and subsequently reduce BG levels and improve glucose intolerance in patients.

TRO was administered via the diet and LC-MS analysis detected the parental compound in the plasma from all treated mice but not in the plasma from control mice (Figure 5.7). Decreased glucose intolerance was observed in both male and female mice at all doses (Figures 5.8-5.11). HFD mice administered TRO responded in the same manner as lean control mice in OGTTs, illustrating improved glucose tolerance in mice administered TRO. Presence of TRO in the plasma and reversal of glucose intolerance illustrated absorption of TRO from the diet and pharmacological activity of the drug.

5.4.2.1 Effects of TRO on the Hearts of Diabetic Mice

Investigation of TRO toxicity in a normal mouse model highlighted adaptive changes in cardiac structure in response to TRO treatment. However, such changes were not observed in the hearts of HFD mice. Decreased expression of Kcna5, which encodes for a cardiac potassium channel was observed in the hearts of male and female mice administered TRO for 7 and 14 days. Decreased Kcna5 activity has been associated with atrial fibrillation and total-loss of function results in heart failure (Olson et al., 2006). Decreased Kcna5 expression was not observed in the hearts of TRO dosed normal mice. It is possible that the cases of TRO induced heart failure that were reported to have occurred in the patient population occurred as a result of down-regulation of Kcna5. Increased expression of Aqp7 and Mgll, which are involved in the transport and metabolism of glycerol, were up-regulated in HFD mice administered TRO (Figures 5.14-5.15). A signature of TRO induced gene expression changes in the hearts of HFD mice was obtained that could be used to compare with the transcriptomic profiles produced *in vitro* using stem cell based models. The HFD *in vivo* gene signature of the effects of TRO on the heart did not identify toxicological mechanisms but

indicated at a potential role for TRO induced down-regulation of the potassium channel Kcna5 in TRO induced heart failure.

5.4.2.2 Effects of TRO on the Livers of Diabetic Mice

HFD consumption increased expression of hepatic Pparγ in both male and female mice. Expression of Pparγ in the livers of male and female mice was further increased by administration of TRO and this up-regulation was found to be both dose and time dependent (Figure 5.16). Transcriptomic profiling of liver tissue highlighted that the most significant gene changes were those related to lipid metabolism. A sub-set of these genes were highlighted as being involved in the synthesis and accumulation of triglycerides within the liver. Hepatic steatosis results from increased storage of triglycerides in the liver. Increased expression of the genes Slc27a1, Agpat6 and Mogat1, which encode for genes involved in triglyceride synthesis and increased expression of the genes Cfd, Cidea, Cidec and S3-12, which are involved in the storage of triglycerides in the liver were observed in male and female mice, with the exception of Cidea, which was only up-regulated in male mice (Figures 5.21 – 5.24). Over-expression of Pparγ has been reported to be involved in the development of hepatic steatosis (Inoue et al., 2005). Furthermore, genes involved in hepatic triglyceride accumulation such as Cidec, Cidea and S3-12 are known downstream targets of Pparγ (Ghazalpour et al., 2006, Gong et al., 2009). HFDs induce Pparγ expression in the liver, TRO treatment further induces expression of Pparγ and subsequently activates expression of downstream targets that are involved in storage of triglycerides in the liver. This indicates a potential mechanism for TRO induced hepatic steatosis through induction of Pparγ expression in the liver. Increased hepatic Pparγ in diabetic mice and development of hepatic steatosis in diabetic mice administered

Ppary agonists has been previously reported and supports the hypothesis that TRO induced hepatic steatosis occurs via a Ppary dependent pathway (Bedoucha et al., 2001).

At the point of necropsy it was noted that the livers of male mice administered 1049 mg/kg/day TRO were yellowish in colour and speckled in appearance, whereas the livers from the other male and female mice in the study were reddish-brown. This indicated that the livers from the top dose 14 day male mice were injured. In both the normal and HFD mouse models, increased expression of Cyp7a1 and Cyp8b1 were observed. These genes are involved in the production of bile acids from cholesterol and Cyp7a1 is the rate limiting enzyme in this pathway (Russell, 2003). Furthermore, in the HFD model, decreased expression of Abcb11, which encodes for the bile salt export pump (Bsep) was also observed, with the greatest suppression occurring in the livers of male mice administered 1049 mg/kg/day for 14 days. Bsep is the primary transporter of bile acids out of hepatocytes and into the bile canaliculus (Alrefai and Gill, 2007). Increased synthesis of bile acids coupled with inhibition of bile acid transport from hepatocytes into the bile canaliculus can lead to the development of cholestasis (Zollner et al., 2006). It is thus possible that change in colour of the livers from the male mice administered 1049 mg/kg/day was due to the intra-hepatic jaundice caused by damage to the liver by the onset of cholestasis. Development of cholestasis was observed in patients who suffered from TRO induced liver failure (Menon et al., 2001). This indicates that increased expression of genes involved in bole acid synthesis and decreased expression of genes involved in hepatic bile acid export are involved in the development of TRO induced hepatotoxicity.

5.4.3 Summary

Transcriptomic signatures of the effects of TRO on the hearts and livers of HFD induced diabetic mice were acquired. Greater gene changes were observed in the liver than in the heart and the majority of gene changes were associated with the pharmacological action of TRO. TRO was only toxic in a small sub set of a very large patient population and thus it is extremely difficult to characterize its toxicity. Administering TRO to HFD diet induced diabetic mice resulted in differential expression of genes involved in triglyceride synthesis and accumulation bile acid synthesis and transport. These gene expression changes are associated with development of hepatic steatosis and cholestasis, which were observed in the patient population (Chojkier, 2005). Genes involved in hepatic triglyceride accumulation are downstream targets of Pparγ and HFD administration was shown to increase Pparγ expression in the liver. This implies a Pparγ mediated mechanism of TRO induced toxicity. Adverse reactions to TRO were observed in a small sub-set of the patient population. Due to complex physiological states of patients suffering from metabolic diseases such as T2D, it is highly probable that the toxicity is patient specific and that the affected patients have an underlying vulnerability that makes them more susceptible to drug induced toxicity. Genetic differences between T2D patients have been reported and variability in PPARγ has been linked to susceptibility to development of T2D in normal patients (Freeman and Cox, 2006). Such underlying variability in gene expression may explain why TRO caused adverse reactions in a sub-set of the patient population.

Chapter 6: Modelling Troglitazone Toxicity in Differentiated Mouse Embryonic Stem Cells

6.1 Introduction

In vitro assays are a fundamental part of pre-clinical toxicity testing during drug development (Whitebread et al., 2005). These assays typically utilize primary cells and immortalised cancer derived cell lines, however these cells neither represent the normal physiological nor the diseased state of an organism. (McNeish, 2004). Primary cells are costly, genetically highly variable and begin to de-differentiate in culture losing expression of key genes such as the cytochrome P450 enzyme family. Immortalized cells are usually derived from cancerous tissues and are often phenotypically different from cells *in vivo* (Cezar, 2007). ES cells possess the ability to differentiate into any cell type and it is hoped that differentiated ES cells will be more representative of *in vivo* cell environments than primary cells and immortalised cell lines. The development of robust and reproducible differentiation protocols should allow for the generation of stable cell populations that are less variable than primary cell based assays that are currently being utilised. The combined use of stem cell derived *in vitro* assays and toxicogenomic analysis methods is anticipated to provide more accurate models for the prediction and detection of drug induced toxicity. Chapter 3 details the development of protocols for the differentiation of mES cells into cardiomyocytes and hepatocytes using chemicals. These differentiated cells expressed cardiac and hepatocyte specific gene markers and differentiated cardiomyocytes contracted spontaneously in culture. The compound of interest in this project was TRO and the *in vivo* transcriptional responses in heart and liver tissues of normal and diabetic mice in response to TRO is described in chapters 4 and 5, respectively.

6.2 Chapter Aims

Following on from the results of chapters 3, 4 and 5 the aims of this chapter were to assess the transcriptional responses of mES cell differentiated cardiomyocytes and hepatocytes to TRO, to evaluate if *in vitro* gene expression changes could provide information on the mechanisms of TRO induced toxicity and to compare these changes in gene expression with those observed in heart and liver tissues from *in vivo* normal and diabetic mouse studies.

6.3 Results

6.3.1 *In Vitro* Transcriptional Profile of TRO in mES Cell Derived Cardiomyocytes and Hepatocytes

6.3.1.1 Development of In Vitro Differentiated mES Cell Models for TRO Treatment

In vitro models of mES cell differentiated cardiomyocytes and hepatocytes were developed as described in chapter 3. These differentiated cells expressed key cardiac and hepatic marker genes but were not homogenous cultures of terminally differentiated cells. Differentiated cells aged between 20 and 24 days were utilised for *in vitro* experiments and 24 hours before TRO treatment, cell culture medium was changed to treatment medium. Treatment medium was free of LIF, FCS and differentiation inducing chemicals.

6.3.1.2 TRO Cytotoxicity in mES Cell Derived Cardiomyocytes and Hepatocytes

The cytotoxic effects of TRO on mES cell differentiated cardiomyocytes and hepatocytes were assessed using a cell viability assay as described in section 2.3.8.3. Cardiomyocytes and hepatocytes were exposed to a range of TRO concentrations (0-100 µM) for 24 hours following which cell viability was measured. Similar levels of cell viability were observed in both cardiomyocytes and hepatocytes when treated with 0-5 µM TRO for 24 hours (Figure 6.1). At TRO concentrations in excess of 5 µM hepatocytes had lower cell viability than cardiomyocytes. The 24 hour IC_{50} (concentration causing 50% inhibition of cell viability) value for mES cell derived cardiomyocytes was 27 µM and for hepatocytes was 18 µM. Total cell death (0% cell viability) was observed in

cardiomyocytes treated with TRO concentrations in excess of 45 μM and in hepatocytes treated with TRO concentrations in excess of 40 μM. For further experiments sub-toxic concentrations of 15 μM and 10 μM TRO were chosen for the treatment of mES cell derived cardiomyocytes and hepatocytes, respectively.
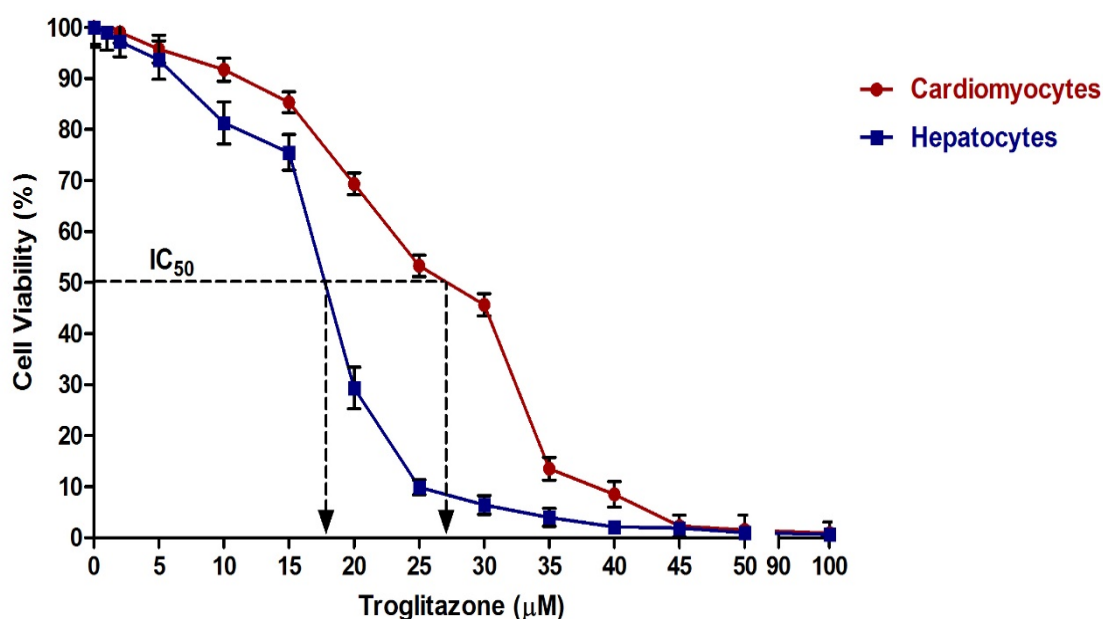
Figure 6.1 – Cytotoxicity of TRO in mES cell differentiated cardiomyocytes and hepatocytes. Differentiated hepatocytes and cardiomyocytes were treated with varying concentrations of TRO for 24 hours. TRO cytotoxicity was assessed using the CellTiter 96® Aqueous One Solution Cell Viability Assay. Differentiated hepatocytes were less viable than cardiomyocytes at TRO concentrations in excess of 5 μM. The IC_{50} for hepatocytes was 18 μM and for cardiomyocytes it was 27 μM (data are mean ± SD (n=3)).

6.3.1.3 Transcriptomic Profile of TRO Treated mES Cell Derived Cardiomyocytes

Differentiated cardiomyocytes were treated with 15 μM TRO or vehicle only (0.1% DMSO) for 24 hours following which RNA was extracted and microarray analysis was undertaken using in-house printed mouse whole genome microarrays. Microarrays were used to assess changes in gene expression of mES cell derived cardiomyocytes after TRO treatment. Microarray data was analysed and genes with $\log_2$ fold changes <-0.6 or >0.6 and significance $p<0.05$ were selected. The subsequent list of TRO induced changes in gene expression in mES cell derived cardiomyocytes consisted of 699 up-regulated and 1485 down-regulated genes (Figure 6.2).

TRO Induced Gene Expression Changes
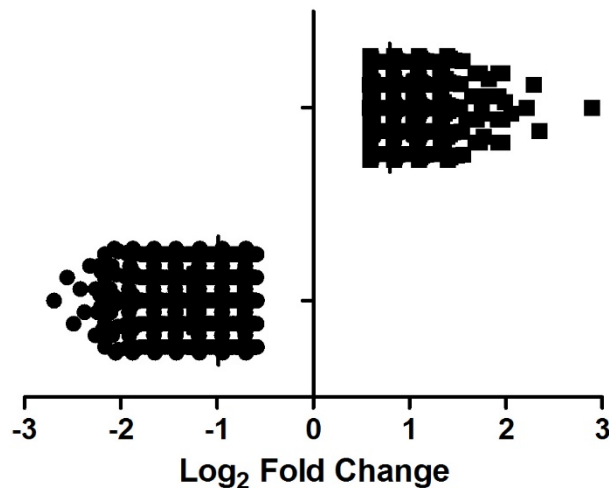
Figure 6.2 – Gene expression changes in mES cell differentiated cardiomyocytes treated with 15 μM TRO for 24 hours. Microarray analysis identified 699 up-regulated and 1485 down-regulated genes with $\log_2$ fold changes <-0.6 or >0.6 and with significance $p<0.05$ in differentiated cardiomyocytes treated with 15 μM TRO for 24 hours compared with controls (differentiated cardiomyocytes treated with vehicle only (0.1% DMSO)).

6.3.1.4 Transcriptomic Profile of TRO Treated mES Cell Derived Hepatocytes

Differentiated hepatocytes were treated with 10 µM TRO or vehicle only (0.1% DMSO) for 24 hours following which RNA was extracted and microarray analysis was undertaken using in-house printed mouse whole genome microarrays. Microarrays were used to assess changes in gene expression of mES cell derived hepatocytes after TRO treatment. Microarray data was analysed and genes with $\log_2$ fold changes <-0.6 or >0.6 and significance $p<0.05$ were selected. The subsequent list of TRO induced changes in gene expression in mES cell derived hepatocytes consisted of 826 up-regulated and 1047 down-regulated genes (Figure 6.3).

TRO Induced Gene Expression Changes
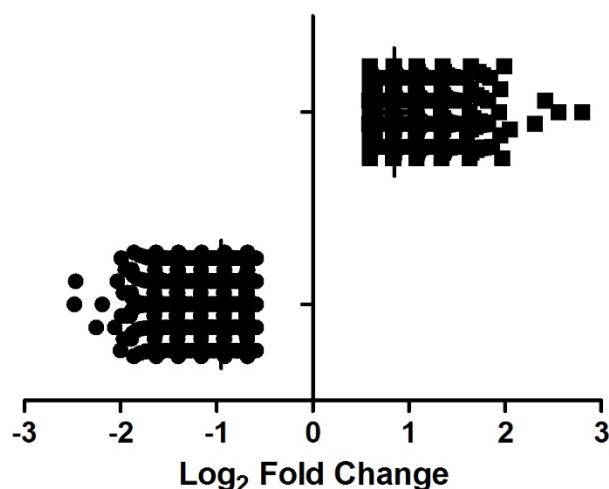
Figure 6.3 – Gene expression changes in mES cell differentiated hepatocytes treated with 10 µM TRO for 24 hours. Microarray analysis identified 826 up-regulated and 1047 down-regulated genes with $\log_2$ fold changes <-0.6 or >0.6 and with significance $p<0.05$ in differentiated hepatocytes treated with 10 µM TRO for 24 hours compared with controls (differentiated hepatocytes treated with vehicle only (0.1% DMSO)).

6.3.2 *In Vitro* Effects of TRO on mES Cell Derived Cardiomyocytes

6.3.2.1 TRO Increases Intracellular Calcium Levels

Spontaneously contracting cultures of mES cell derived cardiomyocytes were treated with 15 µM TRO for 24 hours. It was observed that cells treated with TRO ceased to spontaneously contract whilst control cells were unaffected. Contraction of cardiomyocytes is controlled by action potentials that are triggered by fluctuations in intracellular calcium levels (Bers, 2000). Intracellular calcium levels in mES cell derived cardiomyocytes were measured as described in section 2.3.8.4. Readings were taken for cells that were undisturbed (Blank), treated with vehicle only (Control), treated with TRO (5 and 15 µM) and treated with Ionomycin (Iono) (1 µM). Iono was used as a positive control as it is known to cause a maximum influx of calcium into the cytoplasm (Morgan and Jacob, 1994). Cells were treated at T0 and fluorescence readings were taken at intervals for 75 seconds (Figure 6.4). Treatment of cardiomyocytes with TRO caused an increase in intracellular calcium levels compared with controls. Calcium levels peaked 15 seconds after TRO was added following which levels plateaued and subsequently remained elevated for the remainder of the sampling period. Treatment with 5 and 15 µM TRO produced similar elevations in intracellular calcium levels. Exposure of cardiomyocytes to 1 µM Ionomycin induced a greater increase in intracellular calcium than treatment with 5 or 15 µM TRO. Iono caused calcium levels to increase for the initial 30 seconds of sampling and then decrease. After 75 seconds calcium levels in Iono and TRO treated cardiomyocytes were equivalent. These data indicate that TRO caused increases in intracellular calcium levels and this may be the mechanism via which TRO treatment caused inhibition of cardiomyocyte contraction.
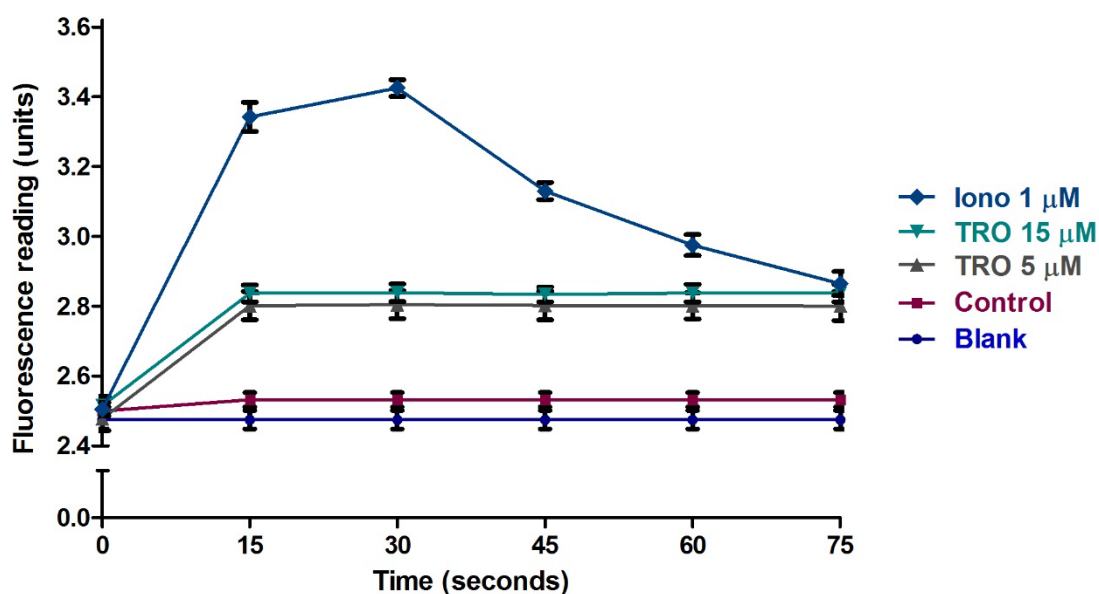
Figure 6.4 – TRO increases intracellular calcium levels in mES cell derived cardiomyocytes. Fluctuations in intracellular calcium levels in mES cell derived cardiomyocytes were measured using the fluorescent calcium indicator fluo-4 AM and the Cellomics ArrayScan VTI platform. Fluorescence readings were taken when for conditions where the cells were undisturbed (Blank), 0.1% DMSO (vehicle) was added (Control), troglitazone was added (TRO 5 and 15 µM) and ionomycin was added (Iono 1 µM); all compounds were added at T0. Blank and control readings were similar with $p > 0.05$ by student's t-test, illustrating no effect of the vehicle on intracellular calcium levels. Addition of the positive control ionomycin caused a rise and fall in intracellular calcium levels. Addition of TRO caused a rise intracellular calcium levels, which remained elevated for the duration of the sampling period. Similar effects were observed with 5 and 15 µM TRO (data are mean ± SD (n=3) with results statistically significant at $p < 0.05$ for cells treated with Iono and TRO compared with controls by one-way ANOVA with post hoc Dunnett's test).

6.3.2.2 TRO Induced Differential Expression of Genes Involved in Regulating Cardiomyocyte Contraction

In addition to fluctuations in calcium levels, generation of action potentials in contracting cardiomyocytes also involves changes in intracellular potassium levels (Luo and Rudy, 1991). Analysis of microarray data identified differential expression of genes involved in cardiac contraction in mES cell derived cardiomyocytes treated with 15 µM TRO for 24 hours (Figure 6.5). These genes encode for calcium and potassium channels, cardiac muscle genes and genes involved in regulating cardiomyocyte contraction. Several sarcomeric genes were down-regulated by TRO, these included genes encoding for tropomyosin (Tpm2, Tpm1, Tpm4), light and heavy chain myosin (Myl9, Myl6, Myl4, Myh8, Myh6), actinin (Actn2, Actn4, Actc1. Actg2), troponin (Tnni3) and dystrophin (Dmd). Increased expression of the calcium channels genes Cacna1c and Cacnb1 and the calcium dependant potassium channels genes Kcnh1 and Kcnn4 and decreased expression of the potassium channel genes Kcnk5, Kcna1, Kcnk6, Kcnmb1, Kcnq5, Kcnn2, Kcnk18 and Kcna5 and the calcium channel gene Cacnb3, were observed in TRO treated mES cell derived cardiomyocytes (Figure 6.6). These data illustrate that TRO caused differential expression of genes encoding for calcium and potassium channels and down-regulation of sarcomeric genes in mES cell derived cardiomyocytes. These data indicate that TRO inhibited mES cell derived cardiomyocyte contraction via mechanisms involving increases in intracellular calcium levels and differential expression of genes involved in regulating cardiomyocyte contraction.
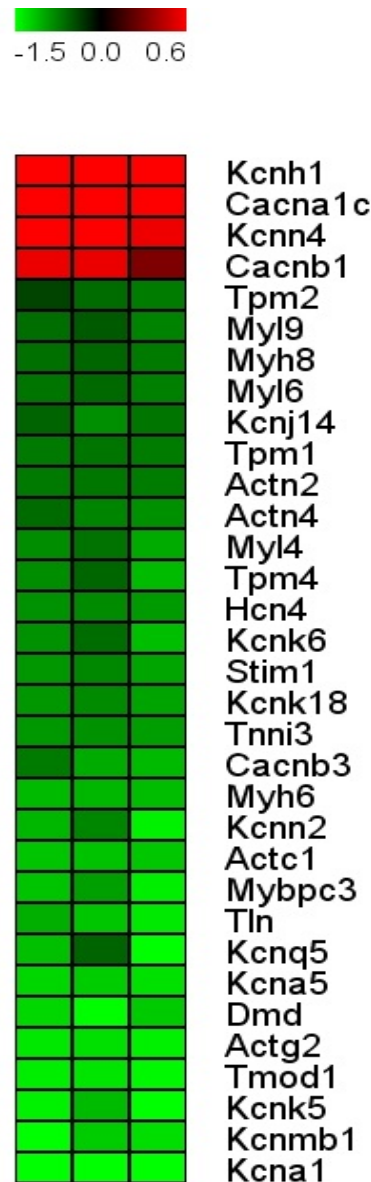
Figure 6.5 – TRO treatment of mES cell derived cardiomyocytes induced differential expression of genes involved in regulating cardiomyocyte contraction. Microarray analysis of mES cell derived cardiomyocytes treated with 15 μM TRO for 24 hours identified a number of gene expression changes. Pathway analysis and literature mining identified a sub-set of 33 genes that are involved in regulation of cardiomyocyte contraction (data are $\log_2$ fold changes of gene expression, each column represents an experimental replicate (n=3). Results are statistically significant at p<0.05 for comparison of TRO treated and control cardiomyocytes by Welch's t-test).
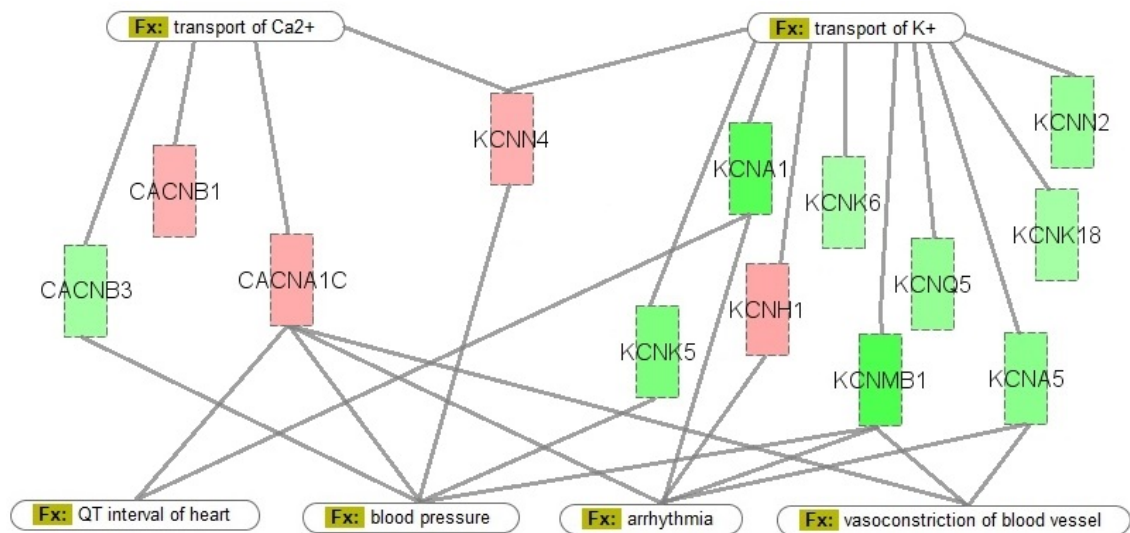
Figure 6.6 – TRO treatment of mES cell derived cardiomyocytes induced differential expression of genes encoding for calcium and potassium ion channels. Pathway analysis of microarray data from mES cell derived cardiomyocytes treated with 15 µM TRO for 24 hours identified changes in the expression of a number genes that encode for cardiac calcium (Ca2+) and potassium (K+) channels. Furthermore, changes to the expression of the genes Cacnb3, Cacna1c, Kcnn4, Kcnk5, Kcna1, Kcnh1, Kcnmb1 and Kcna5 have been linked to the alteration of QT intervals of cardiac action potentials, changes in blood pressure, development of arrhythmias and vasoconstriction of blood vessels. Up and down regulated genes are coloured red and green respectively, with the colour intensity correlating to the degree of gene expression change.

6.3.2.3 TRO Induced Differential Expression of Genes Involved in Regulating Cellular Responses to Stress

The endoplasmic reticulum (ER) plays a key role in regulating calcium homeostasis within cells and is involved in releasing calcium into and removing calcium from the cytoplasm. Disruption of calcium homeostasis can induce ER stress, which can result in apoptosis (Pizzo and Pozzan, 2007). Pathway analysis and literature mining identified significant changes in the expression of 61 genes that are involved in regulating cellular responses to stress (Figure 6.7). Within this sub-group several genes have been reported to be involved in pathways associated with onset of ER stress and apoptosis. Treatment of mES cell derived cardiomyocytes with 15 µM TRO caused up-regulation of the ER stress effector genes Atf4, Ddit4, Hspa5 and Trib3 and down-regulation of the anti-apoptotic genes Mcl1, Cflar, Bcl2l2 and Bcl2. TRO induced changes in the expression of these genes was detected by microarray analysis and confirmed using RT-PCR (Figure 6.8). These data indicate that TRO induced ER stress and apoptosis in mES cell derived cardiomyocytes.

-1.5 0.0 1.5

Trib3
Bbc3
Atf4
Mapkapk5
Tlr7
E2f1
Hspa9a
Ddit4
Dusp4
Arhgap10
Hspa4
Cad
Atf5
Anapc1
Vegfa
Mapk9
Arhgef1
Akt2
Slc7a11
Psmb2
Stk3
Hspa5
Psen
Gstp1
Plg
Ngfr
Ambra1
Cdk2
Mre11a
Apc
Mcl1
Psmb7
Aph1b
Eif2c4
Dnclc1
Rpn2
Dnm1l
Hist1h3f
Itgb3bp
Tnfrsf10b
Xbp1
Prg1
Bcl2
Vav2
Hist1h2bc
Hspa1l
Psma3
Gsn
Trf
Dlc1
Birc4
Asf1a
Atp7a
Hspa1a
Ppp3r1
Bcl2l2
Fkbp4
Cflar
Ccne2
Il1a
Tlr3
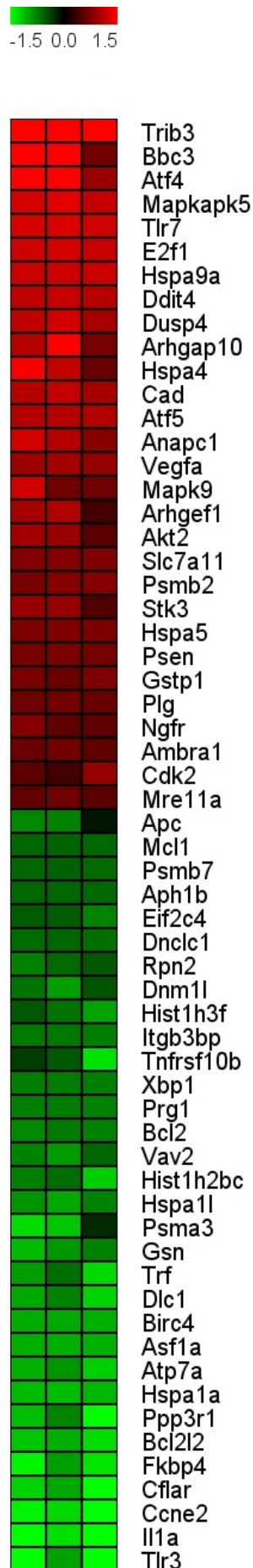
Figure 6.7 – TRO treatment of mES cell derived cardiomyocytes induced differential expression of genes involved in regulating cellular responses to stress. Microarray analysis of mES cell derived cardiomyocytes treated with 15 µM TRO for 24 hours identified a number of gene expression changes. Pathway analysis and literature mining identified a sub-set of 61 genes that are involved in regulation of cellular responses to stress (data are $\log_2$ fold changes of gene expression, each column represents an experimental replicate (n=3). Results are statistically significant at p<0.05 for comparison of TRO treated and control cardiomyocytes by Welch's t-test).
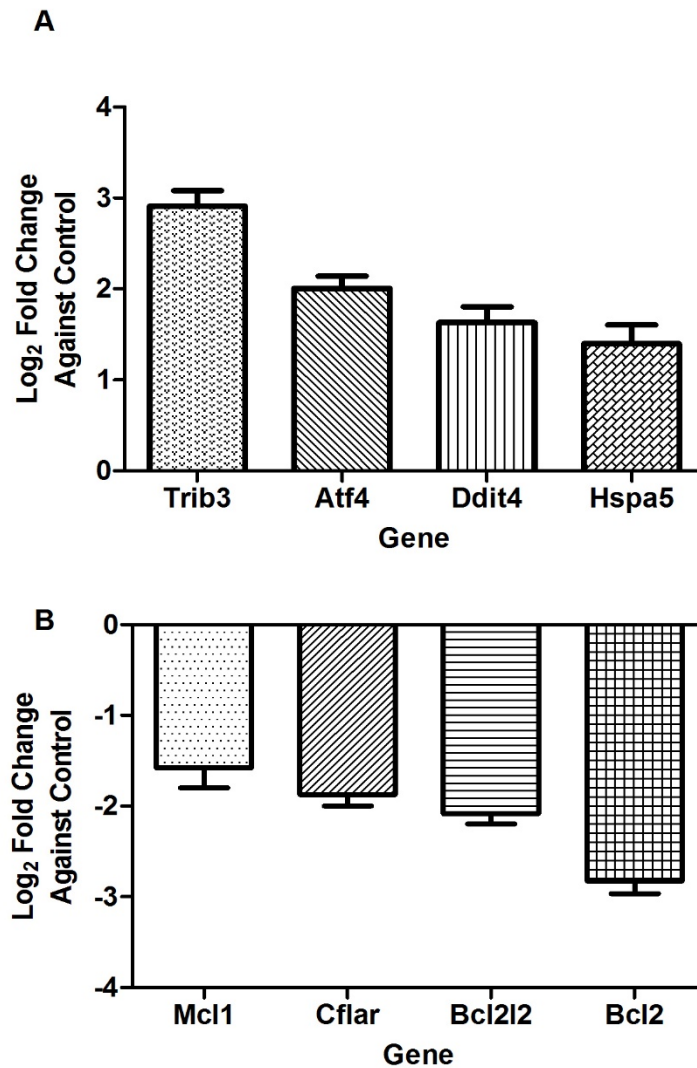
Figure 6.8 – TRO treatment of mES cell derived cardiomyocytes induced differential expression of ER stress and apoptosis genes. Expression of genes involved in cellular responses to ER stress and apoptosis in mES cell derived cardiomyocytes treated with 15 µM TRO for 24 hours was assessed by RT-PCR. (A) TRO treatment resulted in increased expression of Trib3, Atf4, Ddit3 and Hspa5. (B) Down-regulation of the genes Xbp1, Cflar, Bcl2l2 and Bcl2 was observed in TRO treated mES cell derived cardiomyocytes (data are mean ± SD (n=3), with results statistically significant at p<0.05 for comparison of TRO treated and control cardiomyocytes for all genes by student's t-test).

6.3.3 *In Vitro* Effects of TRO on mES Cell Derived Hepatocytes

6.3.3.1 Differential Expression of Genes Involved in Xenobiotic Metabolism in TRO Treated mES Cell Derived Hepatocytes

Microarray analysis of mES cell derived hepatocytes treated with 10 µM TRO for 24 hours identified 1873 differentially expressed genes. Pathway analysis and literature mining identified a sub-group of 65 genes that are involved in xenobiotic metabolism (Figure 6.9). Members of the cytochrome P450 (Cyp) family of proteins are involved in the Phase I metabolism of drugs and in the synthesis of endogenous compounds (Danielson, 2002). TRO treatment of mES cell derived hepatocytes affected the expression of Cyp1b1, Cyp26a1, Cyp2a4, Cyp3a13, Cyp3a16, Cyp4a12a and Cyp51. In addition, TRO treatment also affected the expression of genes involved in Phase II metabolism of xenobiotics. These genes encoded for enzymes involved in glutathione conjugation (Gclm, Gsta1, Gsta2, Gstp1, Gstt2 and Gstz1), glucuronidation (Ugdh, Ugt1a5, Ugt1a6, Ugt1a6a) and sulfation (Sult1b1) of drug compounds and their metabolites.
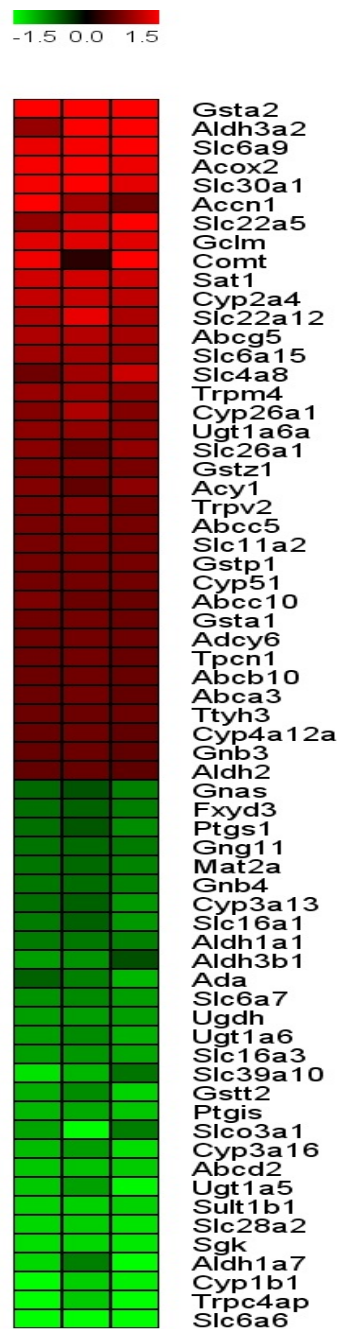
Figure 6.9 – TRO treatment of mES cell derived hepatocytes induced differential expression of genes involved in regulating xenobiotic metabolism. Microarray analysis of mES cell derived hepatocytes treated with 10 μM TRO for 24 hours identified a number of gene expression changes. Pathway analysis and literature mining identified a sub-set of 65 genes that are involved in regulation of xenobiotic metabolism (data are log_2 fold changes of gene expression, each column represents an experimental replicate (n=3). Results are statistically significant at $p<0.05$ for comparison of TRO treated and control hepatocytes by Welch's t-test)

6.3.3.2 Differential Expression of Genes Involved in Lipid and Carbohydrate Metabolism in TRO Treated mES Cell Derived Hepatocytes

In addition to altering expression of genes involved in xenobiotic metabolism, TRO treatment of mES cell derived hepatocytes also affected expression of genes involved in the metabolism of lipids and carbohydrates. Pathway analysis and literature mining of microarray data identified a sub-group of 114 genes that are involved in lipid and carbohydrate metabolism (Figure 6.10). The ligand activated nuclear receptor Pparα is a key regulator of lipid metabolism (Berger and Moller, 2002). TRO treatment increased expression of Pparα in mES cell derived hepatocytes, In addition, microarray analysis detected increased expression of the retinoid X receptor Rxra, which binds to Pparα to form a heterodimer complex that activates transcription of several genes. Microarray analysis detected TRO induced increased expression of the Pparα downstream target genes Acadl, Acox2, Acsl4, Carm1, Cyp4a12a, Fads1, Hmgcl, Pparbp, Rora and Trib3. These genes are involved in the transport and metabolism of fatty acids. TRO treatment of mES cell derived hepatocytes resulted in decreased expression of the genes Crk, Fgfr2, Insr and Ptpn11, which are involved in the insulin receptor signalling pathway. Furthermore, increased expression of the genes Gyg1 and Phkb, which are involved in glycogenolysis and decreased expression of Gys1, which is involved in glycogen synthesis, were also detected in TRO treated hepatocytes.
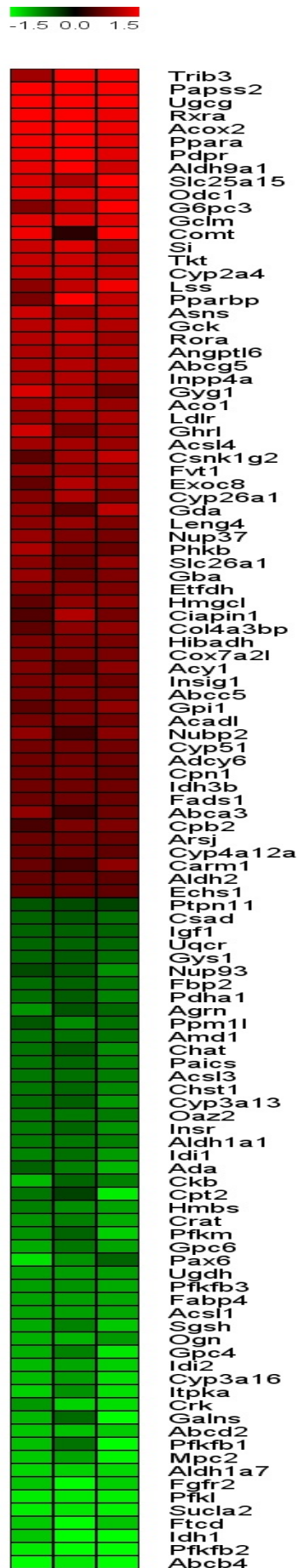
Figure 6.10 – TRO treatment of mES cell derived hepatocytes induced differential expression of genes involved in regulating lipid and carbohydrate metabolism. Microarray analysis of mES cell derived hepatocytes treated with 10 µM TRO for 24 hours identified a number of gene expression changes. Pathway analysis and literature mining identified a sub-set of 114 genes that are involved in regulation of lipid and carbohydrate metabolism (data are $\log_2$ fold changes of gene expression, each column represents an experimental replicate (n=3). Results are statistically significant at $p < 0.05$ for comparison of TRO treated and control hepatocytes by Welch's t-test).

6.3.3.3 Differential Expression of Genes Involved in Regulating Cellular Responses to Stress in TRO Treated mES Cell Derived Hepatocytes

Analysis of microarray data of mES cell derived hepatocytes treated with 10 μM TRO for 24 hours identified differential expression of 102 genes involved in regulating cellular responses to stress (Figure 6.11). Pathway analysis and literature mining highlighted that several genes within this sub-group are involved in the same cellular response pathways. TRO treatment of hepatocytes resulted in increased expression of genes Adam15, Cd44 and Mmp3 and decreased expression of the genes, Col11a1, Col1a1, Col2a1, Col3a1, Col5a2, Col6a3, Col8a1, Col8a2 and Ctsd, which are collectively involved in the degradation of the extracellular matrix. TRO treatment decreased expression of the genes mt-Co2 and mt-Co3, which encode for subunits of cytochrome C oxidase and the genes mt-Nd1 and mt-Nd4, which encode for subunits of NADH dehydrogenase 1. NADH dehydrogenase 1 is complex I and cytochrome C oxidase is complex IV of the electron transport chain (ETC) and disruption of the ETC can result in increased cellular stress through the production of reactive oxygen species (ROS). Increased expression of Sod2 gene, which encodes for the ROS detoxifying enzyme superoxide dismutase 2, was observed in TRO treated hepatocytes. Increased cellular levels of ROS can induce ER stress and TRO treatment of mES cell derived hepatocytes caused up-regulation of the genes Asns, Atf3, Atf4, Ddit3, Dnajb9, Hspa1b, Hspa5 and Trib3. TRO induced increased expression of the ER stress effector genes, Trib3, Atf4, Hspa5, Ddit3 and Dnajb9 and decreased expression of the anti-apoptotic genes Mcl1 and Bcl2 were confirmed by RT-PCR (Figure 6.12). These data indicate that TRO induced cellular stress in mES cell derived hepatocytes.
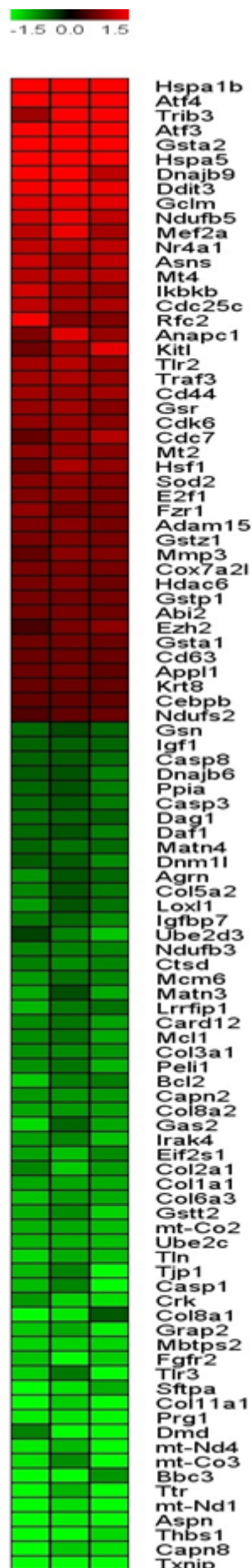
Figure 6.11 – TRO treatment of mES cell derived hepatocytes induced differential expression of genes involved regulation of cellular responses to stress. Microarray analysis of mES cell derive hepatocytes treated with 10 µM TRO for 24 hours identified a number of gene expression changes. Pathway analysis and literature mining identified a subset of 102 genes that are involved in regulation of cellular responses to stress (data are $\log_2$ fold changes of gene expression, each column represents an experimental replicate (n=3). Data are $p < 0.05$ for comparison of TRO treated and control hepatocytes by Welch's t-test).
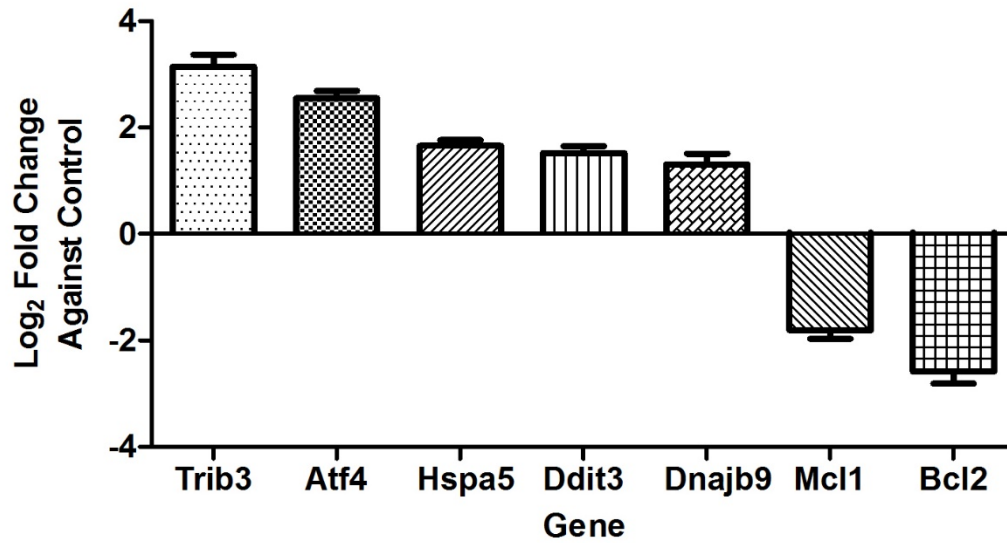
Figure 6.12 – TRO treatment of mES cell derived hepatocytes induced expression of ER stress marker genes. Expression of ER marker stress genes in mES cell derived hepatocytes treated with 10 µM TRO for 24 hours was assessed by RT-PCR. TRO treatment resulted in increased expression of the genes ER stress effector gens Trib3, Atf4, Hspa5, Ddit3 and Dnajb9 and decreased expression of the anti-apoptotic genes Mcl1 and Bcl2 in mES cell derived hepatocytes (data are mean ± SD (n=3), with results statistically significant at $p<0.05$ for comparison of each gene in TRO treated and control hepatocytes by student's t-test).

6.3.4 Comparison of *In Vivo* and *In Vitro* Cardiac TRO Gene Signatures

The first notable difference between *in vivo* (normal and diabetic) and *in vitro* cardiac gene signatures of TRO were the differences between the numbers of genes that had altered expression after TRO treatment (Figure 6.13). TRO treatment *in vivo* of normal and diabetic male mice with 1280 and 1049 mg/kg/day TRO respectively, for 14 days resulted in expression changes in similar numbers of genes. In the hearts of normal mice TRO treatment caused up-regulation of 42 genes and down-regulation of 23 genes and in the hearts of diabetic mice TRO treatment caused up-regulation of 34 genes and down-regulation of 18 genes. In contrast, TRO treatment *in vitro* of mES cell derived cardiomyocytes with 15 μM TRO for 24 hours resulted in the changed expression of many more genes with increased expression of 699 genes and decreased expression of 1485 genes.

Following comparison of the number of TRO induced gene expression changes *in vivo* and *in vitro*, Venn analysis was utilised to identify similarities between *in vivo* and *in vitro* cardiac gene signatures of TRO (Figure 6.14). Comparison of the gene signatures identified that the expression of the genes Ppp1r10, Aqp7, Ddit4 and Tfrc was altered after TRO treatment both *in vivo* and *in vitro.* However, only the change in expression of Ppp1r10 occurred in the same manner in normal and diabetic mouse *in vivo* models and the stem cell based *in vitro* cardiomyocyte model. TRO treatment decreased expression of the Ppp1r10 gene *in vivo* and *in vitro*. This gene encodes for a protein that interacts with protein phosphatase 1 and is involved in regulating numerous cellular processes. The expression of Aqp7, which encodes for a glycerol transporter, was up-regulated *in vivo* but down-regulated *in vitro* and the expression of the genes Ddit4 and Tfrc, which

291

encode for a protein involved in regulating responses to cellular stress and a transferrin receptor, respectively, were up-regulated *in vitro* but down-regulated *in vivo*.
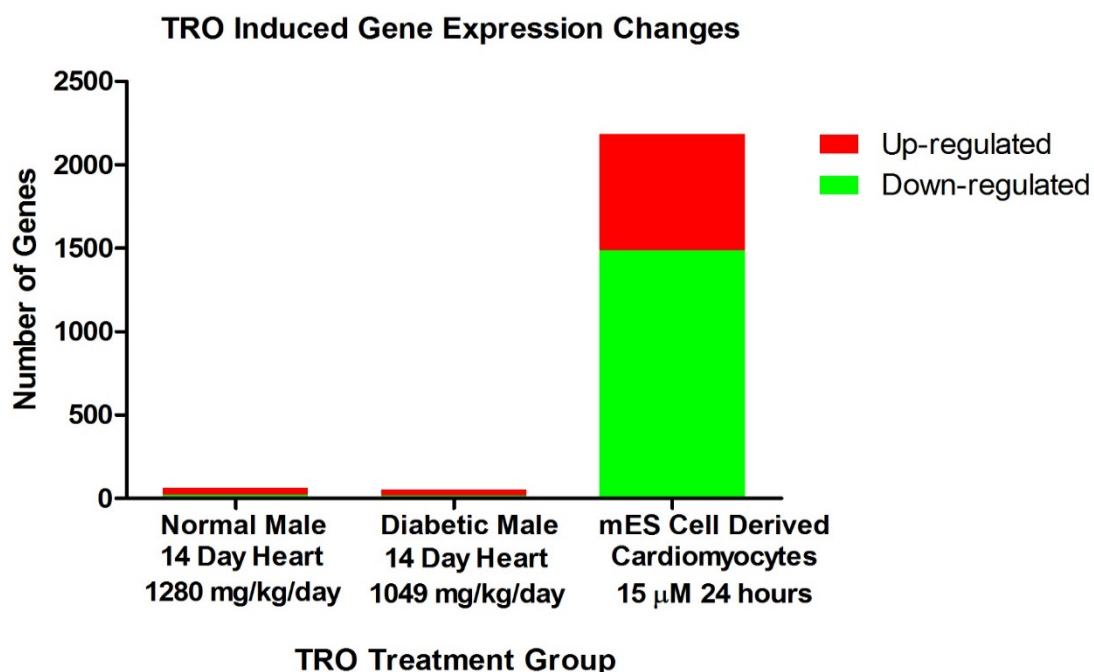
Figure 6.13 – Comparison of *in vivo* and *in vitro* TRO induced cardiac gene expression changes. Transcriptomic profiles of TRO induced gene expression changes in heart tissue from normal and diabetic male mice *in vivo* and in E14Tg2a.4 mES cell derived cardiomyocytes *in vitro* were obtained using microarray analysis. *In vivo* and *in vitro* gene signatures consisted of genes with $\log_2$ fold changes <-0.6 or >0.6 with significance $p<0.05$ after TRO treatment. In heart tissue from normal mice, TRO treatment induced up-regulation of 42 genes and down-regulation of 23 genes. In the hearts of diabetic mice, TRO treatment resulted in increased expression of 34 genes and decreased expression of 18 genes. In contrast, 699 genes were up-regulated and 1485 genes were down-regulated after TRO treatment of mES cell derived cardiomyocytes *in vitro*.

Comparison of *in vivo* and *in vitro* gene signatures identified 13 genes that were differentially expressed in heart tissue from normal mice and in mES cell derived cardiomyocytes. Expression of Dbp and Per1 was up-regulated and expression of Npas2 was down-regulated with TRO treatment *in vivo* and *in vitro*. These 3 genes are involved in the regulation of circadian rhythm. Decreased expression of the genes Akp2, Fbp2 and Tmem82, which encode for alkaline phosphatase 2, fructose-1,6-bisphosphatase 2 and a transmembrane protein respectively, was observed in both heart tissue from normal mice and mES cell derived cardiomyocytes treated with TRO. In addition, changes in the expression of the genes Actg2, Eef2, Fos, Gsn, Lrrn4, Slco2a1 and Vegfa were also detected both *in vivo* and *in vitro* however the changes in expression were in opposite directions. The genes Actg2, Eef2, Gsn Lrrn4 and Slco2a1 were up-regulated in the hearts of normal mice dosed with 1280 mg/kg/day TRO for 14 days and down-regulated in cardiomyocytes treated with 15 µM TRO for 24 hours. The genes Actg2 and Gsn are involved in formation of actin filaments, Eef2 is required for protein synthesis, Lrrn4 is a protein-coding gene with a peroxisome proliferator response element in its promoter region and Slco2a1 encodes for a prostaglandin transporter. Expression of the genes Fos and Vegfa was decreased *in vivo* and increased *in vitro;* Fos is involved in regulating cell transformation and apoptosis and Vegfa encodes for vascular endothelial growth factor A.

Comparison of *in vivo* and *in vitro* gene signatures identified 6 genes that were differentially expressed in heart tissue from diabetic mice dosed with 1049 mg/kg/day for 14 days and in mES cell derived cardiomyocytes treated with 15 µM TRO for 24 hours. Expression of Akap12, which encodes for a kinase anchor protein, was up-regulated and expression of Kcna5, which encodes for a

293

potassium channel and Timeless, a circadian clock component, was down-regulated *in vivo* and *in vitro*. Expression of the protein-coding gene Sh3gl2 was down-regulated *in vivo* and up-regulated *in vitro*. Expression of the genes Cxcl9, which encodes for a small cytokine and H2-Abl, which encodes for a major histocompatibility complex class II antigen, was increased in the hearts of diabetic mice but decreased in mES cell derived cardiomyocytes. These data illustrate that the mES cell derived cardiomyocytes detected some of the TRO induced gene expression changes that were observed *in vivo*.

Treatment of normal mice with 1280 mg/kg/day for 14 days resulted in increased expression of the genes Actg2, Bmp4, Myh11, Tcap, Timp3, Timp4 and Tpm2 (Chapter 4, Figure 4.8). These genes were associated with being involved in adverse cardiac events such as dilated cardiomyopathy, abnormal ventricle morphology and increased blood pressure. RT-PCR analysis of mES cell derived cardiomyocytes treated with 15 µM TRO for 24 hours revealed significant down-regulation of the genes Tcap, Tpm2, Myl2, Myh11, Timp4 and Actg2 and no significant change in the expression of Bmp4 (Figure 6.15). These data demonstrate that TRO induced opposing effects on the expression of cardiac structural genes *in vivo* and i*n vitro.*
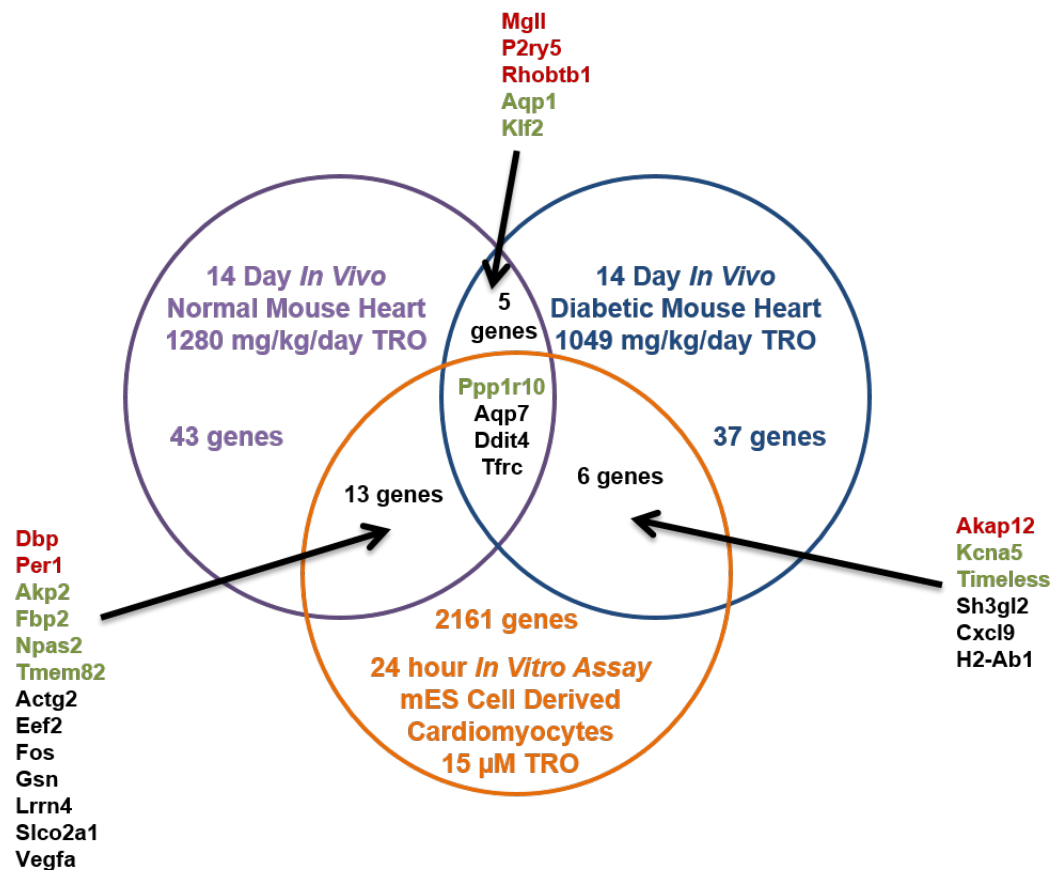
Figure 6.14 – Comparison of *in vivo* and *in vitro* TRO induced cardiac gene signatures. Transcriptomic profiles of TRO induced gene expression changes in heart tissue from male mice *in vivo* and in E14Tg2a.4 mES cell derived cardiomyocytes *in vitro* were obtained using microarray analysis. Gene signatures were produced consisting of genes with $\log_2$ fold changes <-0.6 or >0.6 with significance $p<0.05$ for *in vivo* and *in vitro* TRO treatment groups compared with their respective controls. *In vitro* TRO treatment induced more gene expression changes than *in vivo* dosing. Comparison of *in vitro* and *in vivo* TRO induced gene changes identified 13 genes that were differentially expressed in mES derived cardiomyocytes and in heart tissue from normal mice. In contrast, only 6 genes were differentially expressed in both cardiomyocytes and heart tissue from diabetic mice. Gene symbol colour represents direction of change in gene expression in each group; red denotes up-regulated genes, green denotes down-regulated genes and black represents genes that are up-regulated in one or two group(s) and down regulated in the other group(s).
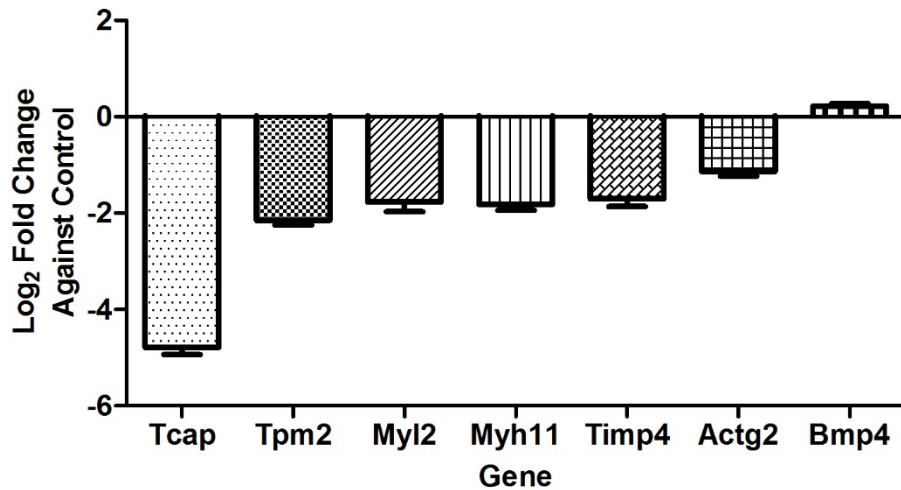
Figure 6.15 – TRO induced changes in the expression of cardiac structural genes in mES cell derived cardiomyocytes. Expression of Tcap, Tpm2, Myl2, Myh11, Timp4, Actg2 and Bmp4 in mES cell derived cardiomyocytes treated with 15 µM TRO for 24 hours was assessed by RT-PCR. TRO treatment resulted in significant down-regulation of the cardiac structural genes Tcap, Tpm2, Myl2, Myh11, Timp4 and Actg2. A significant difference in the expression of Bmp4 in TRO treated and control cardiomyocytes was not observed (data are mean ± SD (n=3), with results statistically significant at $p < 0.05$ for comparison of TRO treated and control cardiomyocytes for all genes except Bmp4 by student's t-test).

6.3.5 Comparison of *In Vivo* and *In Vitro* Hepatic TRO Gene Signatures

Gene signatures acquired from microarray analysis of liver tissue from normal male mice dosed with 1280 mg/kg/day TRO for 14 days, diabetic mice dosed with 1049 mg/kg/day TRO for 14 days and mES cell derived hepatocytes treated with 10 µM TRO for 24 hours were compared (Figure 6.16). The first visible difference between the three gene signatures was that the greatest number of TRO induced gene expression changes occurred *in vitro*. TRO treatment of mES cell derived hepatocytes resulted in up-regulation of 826 genes and down-regulation of 1047 genes. The smallest number of gene expression changes were observed in the livers of diabetic mice. Administering TRO to diabetic mice resulted in increased expression of 137 genes and decreased expression of 92. TRO treatment of normal mice resulted in a threefold increase, compared with diabetic mice, in the number of hepatic genes with altered expression. In the livers of normal mice TRO treatment caused increased expression of 297 genes and decreased expression of 473 genes.

Following comparison of the number of genes *in vivo* and *in vitro* with TRO induced expression changes, Venn analysis was utilised to identify similarities between *in vivo* and *in vitro* hepatic gene signatures of TRO (Figure 6.17). Venn analysis highlighted that 177 genes were differentially expressed in both the livers of normal mice dosed with 1280 mg/kg/day for 14 days and in mES cell derived hepatocytes treated with 10 µM TRO for 24 hours. For the majority of genes in this group their change in expression occurred in the same direction in both normal liver tissue and mES cell derived hepatocytes. There were 28 genes that had opposite changes in gene expression *in vivo* and *in vitro* after TRO treatment.
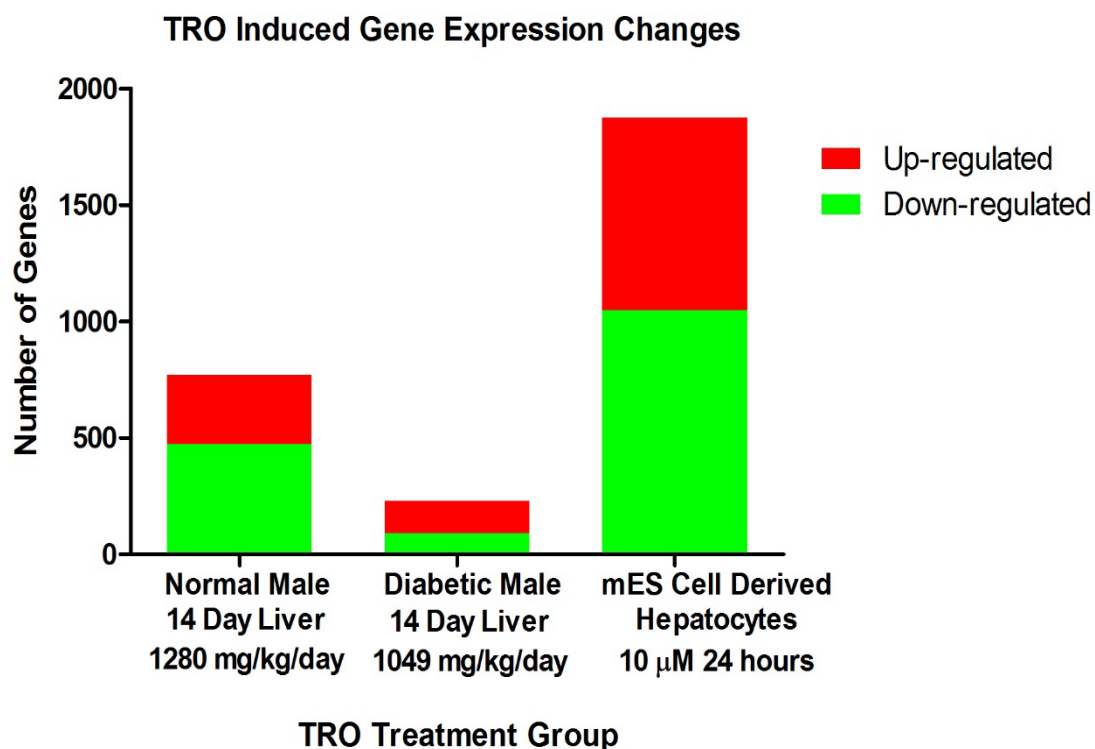
Figure 6.16 – Comparison of *in vivo* and *in vitro* TRO induced hepatic gene expression changes. Transcriptomic profiles of TRO induced gene expression changes in liver tissue from male mice *in vivo* and in E14Tg2a.4 mES cell derived hepatocytes *in vitro* were obtained using microarray analysis. Gene signatures were produced consisting of genes with $\log_2$ fold changes <-0.6 or >0.6 with significance p<0.05 for *in vivo* and *in vitro* TRO treatment groups compared with their respective controls. In livers of normal mice, TRO treatment induced up-regulation of 297 genes and down-regulation of 473 genes. In the livers of diabetic mice, TRO treatment resulted in the increased expression of 137 genes and decreased expression of 92 genes. In contrast, 826 genes were up-regulated and 1047 genes were down-regulated after TRO treatment of mES cell derived hepatocytes *in vitro.*

Abcb9 Dhodh Itgb3 Pacsin3
Acox2 Dnajb9 Lbr Prkra
Akap9 Dusp10 Lgals9 Prnpip1
Aldh3a2 Ell3 Lsm1 Rnf40
Apoc1 Eml4 Luc7l Sertad2
Aqp4 Ezh2 Mdm1 Sestd1
Atf4 Fdxr Mef2a Slc27a2
Bhlhb2 Gart Mt2 Ssfa1
Ccrn4l Gnl3 Narg1 Syt15
Cd44 Gosr2 Nol6 Tmco3
Ckap1 Gpr126 Nr1d1 Vldlr
Cyp2a4 Hoxd10 Nr1i3 Wrnip1
Ddit3 Il17e Osbpl1a

Ada Hba-a1 Mllt10 Sftpa
Ankrd27 Hccs Mon1b Sgk
Bzw1 Hmbs Ms4a4c Sin3a
Cdc2a Hprt Mup3 Slc4a3
Clecsf8 Iars Myo9a Spire1
Colec12 Igh-6 N4bp2l2 Stk23
Cspg6 Il10rb Nek9 Tax1bp3
Dchs1 Irak4 Nes Tbc1d8
Ddc Kazald1 Nphs2 Tdrkh
Dnase2a Kif21a Nucks1 Tfdp1
Dusp14 Klk24 Oas2 Tgfbr3
Elavl4 Klra12 Odd1 Thbs3
Epha1 Kpna2 Pcmt1 Tln
Fam166b Krt39 Pcsk2 Tmprss11f
Fbxw4 Lamb2 Pfkm Topbp1
Fpr-rs2 Lnp Phka2 Ube2g2
Fpr-rs7 Lrfn3 Polr2a Ube3a
Fst Lrp1 Postn Upf2
Galns Mapk11 Pphln1 Usp46
Galnt10 Mapkbp1 Ppp3r1 Vim
Gpc4 Matk Rcbtb1 Zfp2
Gpkow Mbd3l2 Rgs9bp Zfp318
Gsn Mettl4 Rnf125 Zfr
H2-Q2 Minpp1 Rpl13a Zmpste24

Agrn Epha10 Iqce Sfmbt1
Aldh3b1 Gabpa Kdelc2 Sorbs1
Cblb Gdi1 Mbnl1 Taf13
Chka Herc3 Megf11 Tef
Cpa6 Hhex Memo1 Tnfrsf5
Cspg3 Hspa5 Mtap6 Tomm7
Ctsd Igfbp4 Nags Zfp61

Acadm   Apoa4 Cobl
Acat1   Eef2
Cyp2a5
Cyp4a10
Cyp4a14
Ehhadh
Pex11a
Pparγ
S3-12

Atp9a Acat3 Abhd6
Ccl21b Cps1 Acsl1
Ccl9 Gpiap1 Afmid
Ctps Lypla1 Atf4
Odc1 Rnase4 Bach1
Pla2g12a Ccnd1
Slc22a5   Comt
Uap1l1   Cpb2
          Csad
          Cxcl1
          Cxcl9
          Ddit3
          Dsip1
          Efna5
          Gstp1
          Gstt2
          Hmox2
          Idb1
          Idb2
          Myadm
          Myom3
          Pvrl2
          Slc25a15

14 Day *In Vivo*
Normal Mouse Liver
1280 mg/kg/day TRO

578 genes

14 Day *In Vivo*
Diabetic Mouse Liver
1049 mg/kg/day TRO

178 genes

12 genes

Pparα
Trib3
Tmem24

177 genes

36 genes

1657 genes
24 hour *In Vitro* Assay
mES Cell Derived
Hepatocytes
10 µM TRO

Figure 6.17 – Comparison of *in vivo* and *in vitro* TRO induced hepatic gene expression changes. Transcriptomic profiles of TRO induced gene expression changes in liver tissue from male mice *in vivo* and in E14Tg2a.4 mES cell derived hepatocytes *in vitro* were obtained using microarray analysis. Gene signatures were produced consisting of genes with $\log_2$ fold changes <-0.6 or >0.6 with significance p<0.05 for *in vivo* and *in vitro* TRO treatment groups compared with their respective controls. *In vitro* TRO treatment induced more gene expression changes than *in vivo* dosing. Comparison of *in vitro* and *in vivo* TRO induced gene changes identified 177 genes that were differentially expressed in mES derived hepatocytes and in liver tissue from normal mice. In contrast, only 36 genes were differentially expressed in both hepatocytes and liver tissue from diabetic mice. Gene symbol colour represents direction of change in gene expression; red denotes up-regulated genes, green denotes down regulated genes and black represents genes that are up-regulated in one or two group(s) and down regulated in the other group(s).

TRO induced up-regulation of the genes Acox2, Aldh3a2, Cyp2a4, Dhodh, Gart, Slc27a2 and down-regulation of the genes Ada, Ddc, Galns, Galnt10, Hmbs, Minpp1, Pfkm, Phka2, Polr2a and Ppp3r1 occurred in both the livers of normal mice and in mES cell derived hepatocytes. Pathway analysis highlighted that this sub group of genes is involved in the regulation of various metabolic pathways including glycolysis/gluconeogenesis, insulin signalling, glucagon signalling and peroxisome proliferator activated receptor signalling. The genes, Pparα and Trib3 also feed into these pathways and their expression was affected by TRO in both *in vivo* models and in the *in vitro* model.

Comparison of the hepatic TRO gene signatures from diabetic mice administered 1049 mg/kg/day TRO for 14 days and mES cell derived hepatocytes treated with 10 µM TRO for 24 hours highlighted 36 genes, in addition to the genes Pparα, Trib3 and Tmem24, which had altered expression in both groups after TRO treatment. The TRO induced changes in the expression of half of these genes occurred in the same direction in both *in vivo* and *in vitro*. The expression of the other half of these genes was either up-regulated in the livers of diabetic mice and down-regulated in mES cell derived hepatocytes or vice versa. Pathway analysis grouped together genes that are involved in the same functional pathways. The genes Afmid, Comt, Cps1, Csad, Slc25a15 and Uap1l1 are involved in amino acid metabolism, Ccl21b, Ccl9, Cxcl1 and Cxcl9 are involved in chemokine signalling, Abhd6, Acat3, Acsl1, Pla2g12a and Slc22a5 are involved in fatty acid metabolism and transport, Gstp1, Gstt2 and Odc1 are involved in glutathione metabolism and Atf4 and Ddit3 are involved in the endoplasmic stress response pathway.

The hepatic expression of the genes Pparα, Trib3, and Tmem24 was altered after TRO treatment of normal mice, diabetic mice and mES cell derived hepatocytes. In all three TRO models, expressions of Pparα, Trib3 were increased after TRO treatment whereas expression of Tmem24 was increased in the livers of normal mice and mES cell derived hepatocytes after TRO treatment but decreased in the livers of diabetic mice. The genes Pparα, Trib3 and Tmem24 encode for the peroxisome proliferator activated alpha transcription factor, the tribbles pseudokinase protein and the C2 calcium-dependent domain containing 2-like transmembrane protein respectively.

TRO increased expression of the Pparγ was detected by microarray analysis in both *in vivo* mouse models but not in the *in vitro* mES cell derived hepatocyte model. TRO induced increased expression of Pparα was detected by microarray analysis in all three models. RT-PCR analysis was used to confirm the changes in expression of Pparγ and Pparα in the livers of normal and diabetic mice dosed with 1280 and 1049 mg/kg/day TRO, respectively, for 14 days and in mES cell derived hepatocytes treated with 10 µM TRO for 24 hours (Figure 6.18). TRO increased hepatic Pparγ expression in normal and diabetic mice with the greatest increase being observed in the livers of diabetic mice. However, *in vitro*, TRO treatment did not increase Pparγ expression in mES cell derived hepatocytes. In contrast, the greatest increase in expression of Pparα was found in TRO treated mES cell derived hepatocytes in comparison with control cells. Increased expression of Pparα was also observed in the livers of normal and diabetic mice. *In vivo*, greater up-regulation of Pparγ than Pparα occurred, whereas, *in vitro*, the opposite was observed where the expression of Pparα was increased but no

significant changes were measured between the expression of Ppary in control and TRO treated cells
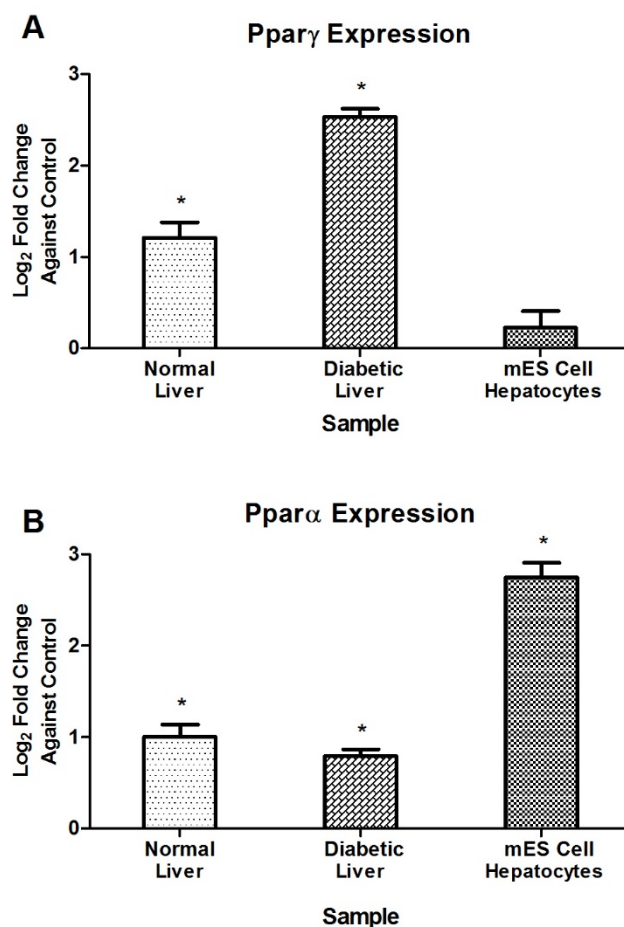
Figure 6.18 – Effect of TRO on Ppary and Pparα expression *in vivo* and *in vitro*. Expression of Ppary and Pparα in liver tissue of normal and diabetic male mice dosed with 1280 and 1049 mg/kg/day for 14 days respectively and in mES cell derived hepatocytes treated with 10 µM TRO for 24 hours, was assessed by RT-PCR. (A) TRO treatment resulted in increased expression of hepatic Ppary in normal and diabetic mice but did not significantly affect expression in mES cell derived hepatocytes. (B) Increased expression of Pparα was observed in all three models with the greatest up-regulation being observed in TRO treated mES cell derived hepatocytes (data are mean ± SD (n=6 for normal mice dose groups, n= 5 for diabetic mice dose groups and n=3 mES cell hepatocytes), *p<0.05 for comparison of TRO mice/cells compared with their respective controls by student's t-test).

TRO induced increased expression of Trib3 was identified by microarray analysis of liver tissue in both *in vivo* models and *in vitro* in mES cell derived hepatocytes. Expression of Trib3 in the livers of normal mice dosed with 326 and 925 mg/kg/day for 7 days and 279 and 1280 mg/kg/day for 14 days, diabetic mice dosed with 354 and 810 mg/kg/day for 7 days and 396 and 1049 mg/kg/day for 14 days and mES cell derived hepatocytes treated with 10 µM TRO for 24 hours was confirmed using RT-PCR (Figure 6.19). In normal and diabetic mice TRO induced an increase in hepatic Trib3 expression in a dose and time dependent manner. Administering 326 mg/kg/day TRO to normal male mice for 7 days did not induce a significant increase in Trib3 expression whereas in comparison, dosing of diabetic male mice with 354 mg/kg/day TRO for 7 days did cause a significant increase in Trib3 expression. In the normal mouse study, mice dosed with 279 mg/kg/day TRO for 14 days had lower levels of Trib3 expression than mice administered a higher dose of 925 mg/kg/day for 7 days. However, in the diabetic study, both 14 day TRO dose groups had higher levels of Trib3 expression than either of the 7 day TRO dose groups. In the diabetic mouse study, similar expression levels of Trib3 were detected in the livers of mice dosed with 396 and 1049 mg/kg/day for 14 days. At similar time and dose levels higher levels of hepatic Trib3 expression were observed in diabetic mice compared with normal mice. Treatment of mES cell derived hepatocytes with 10 µM TRO for 24 hours caused a greater increase in Trib3 expression than that observed in either *in vivo* study. Trib3 plays a role in cellular nutrient availability, insulin signalling and ER stress responses, thus up-regulation of Trib3 could be indicative of both TRO pharmacology and toxicity (Zhang et al., 2013).
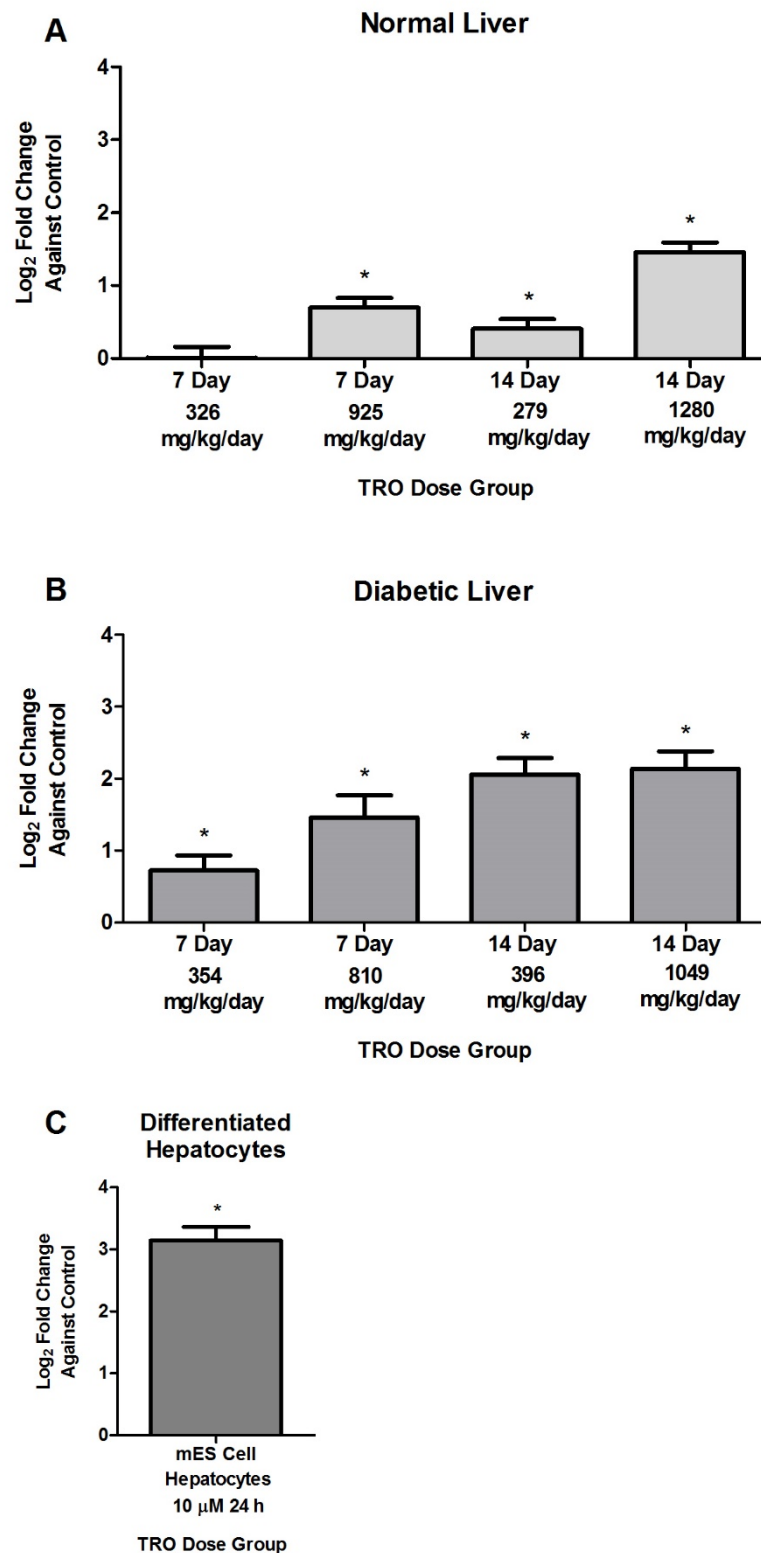
Figure 6.19 – Effect of TRO on Trib3 expression in vivo and in vitro.

Please see next page for figure legend.

Figure 6.16 – Effect of TRO on Trib3 expression *in vivo* and *in vitro*.
Expression of Trib3 in liver tissue of normal and diabetic male mice and in mES cell derived hepatocytes was assessed by RT-PCR. (A) Hepatic Trib3 expression was increased in the livers of normal mice dosed with 925 mg/kg/day for 7 days and 279 and 1280 mg/kg/day for 14 days. (B) Increased expression of Trib3 was observed at all TRO dose and time points in the diabetic mouse study. Similar degree of up-regulation of Trib3 was detected in diabetic mice dosed with 396 and 1049 mg/kg/day TRO. (C) Treatment of mES cell derived hepatocytes with 10 µM TRO for 24 hours resulted in up-regulation of Trib3 expression (data are mean ± SD (n=6, 5, 3 or normal mice, diabetic mice and hepatocytes respectively), $p < 0.05$ for comparison of TRO mice/cells compared with their respective controls by one way ANOVA with post hoc Dunnett's test for normal and diabetic mice and by student's t-test for mES cell derived hepatocytes).

6.4 Discussion

The aims of this chapter were to assess the *in vitro* transcriptional responses of mES cell differentiated cardiomyocytes and hepatocytes to TRO, to evaluate if *in vitro* gene expression changes could provide information on the mechanisms of TRO induced toxicity and to ascertain if TRO induced transcriptomic changes observed *in vivo* (chapters 4 and 5) could be mimicked *in vitro* using differentiated stem cell based assays.

6.4.1 Transcriptional Responses of mES Cell Derived Cardiomyocytes and Hepatocytes to TRO

To assess the transcriptional responses of mES cell derived cardiomyocytes and hepatocytes the differentiated cells were treated with 15 and 10 µM TRO respectively, for 24 hours. Microarray analysis was utilised to compare global gene expression profiles of control and TRO treated cells to deduce which genes had altered expression levels after TRO treatment. Treatment of mES cell derived cardiomyocytes with TRO induced down-regulation of 1485 and up-regulation of 699 genes and treatment of mES cell derived hepatocytes resulted in decreased expression of 1047 and increased expression of 826 genes (Figures 6.2 and 6.3). The unique combination of differentiated mES cells, TRO and microarray analysis in this project made it difficult to directly compare the findings of these experiments with results reported in literature. In the literature experiments often utilised primary cells or immortal cell lines in combination with RT-PCR analysis for the investigation of TRO toxicity and thus reported on the expression changes of a few genes as opposed to the global gene expression change across a tissue. To review the suitability of the mES cell derived hepatocytes as an *in vitro* model for the investigation of TRO induced hepatotoxicity, the transcriptomic gene

signature derived from these experiments was compared to hepatic gene expression changes reported in the literature. Analysis of literature revealed microarray data published by Rogue et al (2011), which showed that 24 hour treatment of primary rat hepatocytes with 40 µM TRO induced changes in the expression of 1600 genes (Rogue et al., 2011). In this project, 24 hour treatment of mES cell derived hepatocytes with 10 µM TRO induced changes in the expression of 1873 genes. Moreover, the data published by Rogue et al (2011) and the results from this study both identify lipid, xenobiotic and amino acid metabolism as common pathways that are affected by TRO treatment. Changes in the expression of genes involved in these pathways were observed in both studies. This supported the use of mES cell derived hepatocytes as a suitable model for acquiring an *in vitro* hepatic transcriptomic gene signature of TRO as the differentiated cells elicited similar TRO induced gene expression changes as those observed in primary rodent hepatocytes.

There is an absence of reports of transcriptomic data from TRO treated cardiomyocytes and thus a comparison could not be made between data reported in the literature and the data acquired in this project. The *in vitro* cardiac transcriptomic signature of TRO that was formulated during this project is a novel finding.

6.4.2 Evaluation of *In Vitro* Mechanisms of TRO Induced Toxicity

6.4.2.1 Inhibition of Cardiomyocyte Contractility

Data from TRO treated mES cell derived cardiomyocytes was analysed to ascertain if information could be acquired regarding possible mechanisms of TRO induced cardiotoxicity. During experiments it was observed that treatment of contracting mES cell derived cardiomyocytes with 15 µM TRO for 24 hours

caused the cells to stop contracting. Cardiomyocyte contractions are controlled by action potentials, which are generated by rhythmic fluctuations in intracellular calcium (Bers, 2000). Calcium imaging was utilised to observe the real time effect of TRO on intracellular calcium levels. It was observed that TRO caused a significant sustained rise in intracellular calcium levels (Figure 6.4). Literature mining and pathway analysis of microarray data identified that TRO treatment induced differential expression of genes involved in regulating cardiomyocyte contractions (Figure 6.5). These genes included several calcium and potassium ion transport channels, which are pathologically associated with alteration of the QT interval of cardiac action potentials, development of arrhythmias, changes in vasoconstriction of blood vessels and changes in blood pressure (Figure 6.6). These data indicate that TRO induced disruption of intracellular calcium levels and changes in the expression of genes involved in regulating cardiomyocyte contractions caused mES cell derived cardiomyocytes to stop contracting. TRO induced reduction and cessation of cardiomyocyte contractions has been previously reported by Ikeda and Watanabe (1998) who observed that 10 µM TRO affected the action potentials and excitability of rabbit ventricular myocytes. TRO was shown to inhibit intracellular calcium and potassium currents in ventricular myocytes, which lead to disruption of action potentials subsequently affecting cell contractility (Ikeda and Watanabe, 1998). TRO has also been shown to affect intracellular calcium and potassium levels in rat vascular myocytes leading to reduced contractility of the cells (Knock et al., 1999). These data collectively show that TRO induces changes to intracellular calcium and potassium levels that consequently affect cardiomyocyte contractility. TRO was notably withdrawn from the market due to its hepatotoxic effects, however, clinical

cardiotoxicity was also reported. (Gale, 2001, Smith, 2003). In 1999, 50 spontaneous adverse reaction cases of TRO induced heart failure, including six fatalities, were reported by the Endocrinologic and Metabolic Drugs Advisory Committee to the FDA (FDA, 1999a). Incidences of TRO induced deterioration of pre-existing heart failure resulted in physicians being prohibited from prescribing TRO to T2D patients with known cardiac abnormalities (Sarafidis, 2008).

The *in vitro* data in this project indicates that TRO induced cardiotoxicity may occur as a result of action potential disruption due to alterations in intracellular calcium levels.

6.4.2.2 Induction of ER Stress

TRO increased intracellular calcium levels in differentiated mES cells (Figure 6.4). The ER plays a key role in intracellular calcium homeostasis, both increasing and reducing calcium levels in the cytoplasm (Pizzo and Pozzan, 2007). Alterations in intracellular calcium levels can result in the onset of ER stress (Xu et al., 2005). Microarray analysis of TRO treated mES cell derived cardiomyocytes and hepatocytes detected differential expression of genes involved in regulating cellular responses to stress (Figures 6.7 and 6.11). Several genes that were up/down regulated by TRO treatment are cited in the literature to be deregulated by the onset of ER stress. In addition to regulating calcium homeostasis, the ER is also involved in protein synthesis, protein folding and lipid biosynthesis. Disruption to the ER through increases in protein synthesis, accumulation of unfolded proteins, cellular oxidative stress and disruption of calcium homeostasis results in activation of the unfolded protein response (UPR) pathway (Kim et al., 2008). Activation of the UPR is an adaptive mechanism that initially promotes cell survival and attempts to restore ER homeostasis; however

in instances of prolonged stress exposure the UPR contributes to the activation of apoptosis (Schröder, 2008).

Treatment of mES cell derived cardiomyocytes and hepatocytes with 15 µM and 10 µM TRO respectively, for 24 hours caused differential expression of a number of genes that were identified as being involved in the UPR pathway (Figures 6.8 and 6.12). Initiation of the UPR is mediated by activation of one or more of the ER transmembrane receptors, Perk, Atf6 and Ire1 (Szegezdi et al., 2006). In this project it was observed the TRO caused an increase in intracellular calcium levels in differentiated E14Tg2a.4 mES cells. Similar observations have previously been reported, which showed that TRO and its sister compound ciglitazone (CIG), increase cytoplasmic calcium levels by inducing release of calcium from intracellular stores in mES cells (Palakurthi et al., 2001). Furthermore, TRO and CIG induced increases in intracellular calcium levels have been reported to induce ER stress resulting in activation of Perk (Gardner et al., 2005). In the UPR pathway, activation of Perk leads to phosphorylation of the alpha subunit of translation initiation factor 2 (eIF2α), which subsequently induces increased expression and activation of the Atf4 transcription factor (Whitney et al., 2009). Microarray analysis detected that treatment of mES cell derived cardiomyocytes and hepatocytes with TRO caused increased expression of the Atf4 gene and this up-regulation was confirmed by RT-PCR (Figures 6.7, 6.8, 6.11 and 6.12). Atf4 is an ER stress induced apoptosis effector. Up-regulation of Atf4 consequently leads to transcriptional activation of target genes that contain amino acid response elements within their promotor regions (Ait Ghezala et al., 2012). Ddit3 and Ddit4 are downstream targets of ER stress mediated Perk activated Atf4 (Whitney et al., 2009, Dey et al., 2010). The expression of Ddit4 was

upregulated in TRO treated mES cell derived cardiomyocytes and the expression of Ddit3 was upregulated in TRO treated mES cell derived hepatocytes. Ddit3 has been shown to induce ER stress mediated apoptosis via inhibition of the anti-apoptotic genes Bcl2 and Mcl1 and up-regulation of Trib3 (Tabas and Ron, 2011). TRO induced decreased expression of Bcl2 and Mcl1 and increased expression of Trib3 was detected my microarray and confirmed by RT-PCR in both mES cell derived hepatocytes and cardiomyocytes (Figures 6.7, 6.8, 6.11 and 6.12). These data imply that *in vitro* TRO disrupts intracellular calcium homeostasis causing ER stress leading to initiation of the UPR pathway via Perk activation and subsequent Atf4 mediated apoptosis.

6.4.2.3 Trib3 as a Potential Biomarker of TRO Hepatotoxicity

TRO treatment resulted in increased Trib3 expression in the livers of normal and diabetic mice and in mES cell derived hepatocytes (Figure 6.16). The Trib3 gene is a member of the mammalian Tribbles gene family. There are three Tribbles isoforms, Trib1, Trib2 and Trib3 and all three can be found in the bone marrow and peripheral blood leukocytes. In addition, Trib1 is highly expressed in the pancreas and thyroid gland, Trib2 is expressed in the thymus, brain and skin and Trib3 is predominantly expressed in the liver but also found at lower levels in the kidney, heart, lung and small intestine (Dedhia et al., 2010). The Tribbles genes encode for pseudokinase proteins that contain serine/threonine kinase like domains but lack catalytic activity (Boudeau et al., 2006). It has been reported that Tribbles proteins function as scaffold proteins and protein kinase activators that support complex protein formation in signal transduction cascades (Kiss-Toth et al., 2004). Trib3 is regulated transcriptionally by its interaction with transcription factors such as Atf4 and Ddit3 and has been reported to be involved

311

in ER stress response pathways, apoptosis, lipid metabolism and nutrient availability (Carraro et al., 2009).

Increased expression of the ER stress effector genes Atf4, Ddit3 and Trib3 was observed in the livers of normal male mice administered 1280 mg/kg/day TRO for 14 days and in mES cell derived hepatocytes treated with 10 µM TRO for 24 hours (Figure 6.15). ER stress inducing agents such as thapsigargin and tunicamycin have been shown to increase Trib3 gene expression in a variety of cells including cardiac myocytes and hepatocytes (Ohoka et al., 2005, Avery et al., 2010). Furthermore, it has been shown that insulin has an additive effect on the expression of ER stress genes in insulin responsive cells. Du and Ding (2009) showed that treatment of HepG2 cells with thapsigargin increased the expression of the ER stress genes ATF4, Ddit3 and Trib3 and subsequent exposure of these cells to insulin resulted in further up-regulation of the ER stress genes (Du and Ding, 2009). TRO was used to treat T2D, a disease associated with increased ER stress (Ozcan et al., 2004). Pharmacologically, TRO increases insulin sensitivity in adipose tissue, the liver and skeletal muscle (Day, 1999). The degree of ER stress in T2D patients may vary greatly with some patients having much higher basal expression levels of stress response genes than others. Thus, it is possible that increased insulin sensitivity in the liver as a result of TRO treatment in patients with pre-existing high levels of ER stress gene expression leads to further increased expression of ER stress genes, which could result in a hepatotoxic reaction via an ER stress induced apoptosis mediated mechanism. ER stress induced apoptosis has been previously hypothesised as a mechanism in the onset of idiosyncratic TRO induced hepatotoxicity (Yokoi, 2010).

In addition to ER stress, increased hepatic Trib3 expression has also been associated with chemical induced glutathione (GSH) depletion. In cells, GSH helps to protect against oxidative stress and damage by binding to and detoxifying reactive oxygen species and electrophilic intermediates formed during metabolism (Wang and Ballatori, 1998). The toxicological effects of GSH depletion occur via two mechanisms; either by total conjugation of the cells GSH reserve by chemicals such as phorone and diethyl maleate or by disruption of GSH synthesis by chemicals such as buthionine sulfoximine, which inhibits γ-glutamylcysteine, the rate limiting enzyme in GSH production (Anderson, 1998). Drugs such as paracetamol can cause liver injury via GSH depletion. Paracetamol is metabolised in the liver by CYP3A4 and CYP2E1 into N-acetyl-*p*-benzoquinone (NAPQI), a highly reactive intermediate that binds to GSH. NAPQI is detoxified via conjugation with GSH and once cellular GSH reserves have been depleted, unbound NAPQI accumulates and binds to cellular proteins resulting in cell damage (Hinson et al., 2010). Using Crl:CD(SD) strain rats and microarray technology Gao et al (2010) showed that administering phorone or diethyl maleate to rats caused up-regulation of Trib3 in the liver. Whereas treatment with ∟-buthionine sulfoximine did not induce up-regulation of Trib3 (Gao et al., 2010). Similar results were also reported by Yamauchi et al (2011) who demonstrated that administering diethyl maleate to F344/DuCrlCrlj strain rats results in increased hepatic Trib3 mRNA expression (Yamauchi et al., 2011). These studies support the potential for Trib3 to be used as a mRNA biomarker of GSH depletion induced hepatotoxicity. TRO induced depletion of GSH has previously been hypothesised as a potential mechanism via which TRO caused hepatotoxicity. Metabolism of TRO by CYP3A4 and CYP2C8 produces a highly

electrophilic intermediate that is conjugated with GSH producing a non-toxic metabolite that is excreted. However, accumulation of the toxic intermediate in hepatocytes could cause depletion of GSH resulting in binding of the intermediate with cellular macromolecules resulting in toxicity (Narayanan et al., 2003).

TRO treatment of normal and diabetic mice and mES cell derived hepatocytes resulted in increased expression of hepatic Trib3 mRNA. Increased expression of hepatic Trib3 may have been caused by TRO induced ER stress or GSH depletion. The data in this project further supports the potential of Trib3 to be utilised as a mRNA biomarker of drug induced hepatotoxicity.

6.4.3 Mimicking *In Vivo* TRO Induced Gene Expression Changes *In Vitro* Using Differentiated Stem Cells

Gene signatures of TRO treatment *in vivo* and *in vitro* were compared to ascertain if TRO induced transcriptomic changes observed in *in vivo* mouse models could be mimicked *in vitro* using differentiated mES cells.

6.4.3.1 TRO Induced Changes in Cardiac Gene Expression

Six genes were differentially expressed after TRO treatment in both mES cell derived cardiomyocytes and in the hearts of diabetic mice. However, only the expression changes of three of the six genes occurred in the same direction in both groups. Thirteen genes were commonly affected by TRO in both cardiomyocytes and in the hearts of normal mice, however, only the expression of six of these genes occurred in the same direction. Twice as many gene expression change similarities were detected between cardiomyocytes and normal heart tissue than between cardiomyocytes and diabetic heart tissue. This was as expected considering cardiomyocytes were differentiated from the E14Tg2a.4 mES cell line, which is a physiologically normal stem cell line.

314

Differentiating cells from a normal stem cell line produces cells with a normal phenotype whereas a disease specific stem cell line produces differentiated cells with the same disease phenotype as the parental line (Verlinsky et al., 2005). Thus, it was expected and observed that more TRO induced gene change similarities would be detected between mES cell derived cardiomyocytes and heart tissue from normal mice than between mES cell derived cardiomyocytes and heart tissue from diabetic mice.

Transcriptional analysis using microarrays identified that TRO deregulated expression of more genes *in vitro* in mES cell derived cardiomyocytes than *in vivo* in the hearts of normal and diabetic mice (Figure 6.13). Changes in expression of the genes Ppp1r10, Aqp7, Ddit4 and Tfrc were common to all three models. However, only the expression of the gene Ppp1r10 was deregulated in the same manner in all three models. Ppp1r10 has been reported to be involved in apoptosis, DNA damage responses and cardiac remodelling (Bernardo et al., 2012, Boon et al., 2013). Changes in the expression of genes involved in cardiac remodelling were observed in the hearts of normal mice administered 1280 mg/kg/day TRO for 14 days. Increased expression of the cardiac structural genes Tcap, Tpm2, Myl2, Myh11, Timp4, Actg2 and Bmp4 were observed in the hearts of normal mice after TRO treatment. Changes in the expression of these genes was also observed *in vitro*, however treatment of mES cell derived cardiomyocytes with 15 µM TRO for 24 hours resulted in decreased expression of these cardiac structural genes (Figure 6.6). *In vivo* gene expression changes may have been the result of systemic responses to TRO mediated plasma volume increase. TRO is known to cause increased plasma volume in animals, healthy human volunteers and in patients (FDA, 1999b). Systemic responses

such as plasma volume increase cannot be modelled *in vitro* using 2-dimensional cell culture systems as the occurrence of such effects is dependent on whole organism physiological changes. This inability of in *vitro* cell models to mimic the physiological environments that the cells are found in *in vivo*, may be a primary reason why few genes were similarly affected by TRO in both *in vitro* and *in vivo* models.

6.4.3.2 TRO Induced Changes in Hepatic Gene Expression

Venn analysis of gene signatures from mES cell derived hepatocytes treated with 10 µM for 24 hours *in vitro* and liver tissue from normal and diabetic mice treated for 14 days with 1280 and 1049 mg/kg/day, respectively, *in vivo* highlighted 177 genes that were deregulated in both mES cell derived hepatocytes and normal livers, 36 genes that were deregulated in both mES cell derived hepatocytes and diabetic livers and 3 genes that were deregulated in all three models (Figure 6.17). Of the 177 genes deregulated after TRO treatment of normal mice and mES cell derived hepatocytes, 84% were up/down regulated in the same manner in both models. In comparison, only 36% of 36 genes deregulated after TRO treatment of diabetic mice and mES cell derived hepatocytes were up/down regulated in the same manner. As was noted earlier, the greater similarity between hepatic genes deregulated *in vitro* and *in vivo* in normal mice was expected because the differentiated hepatocytes were derived from a normal and not a disease specific stem cell line. Thus, the mES cell derived hepatocytes were more similar to the hepatocytes in the livers of normal mice than to the hepatocytes of diabetic mice.

The expression of the genes Pparα, Trib3 and Tmem24 was affected by TRO in both *in vivo* models and *in vitro*. TRO treatment caused increased expression of

Pparα and Trib3 in the livers of normal mice, diabetic mice and mES cell derived hepatocytes and the greatest increases in gene expression was observed in the mES cell derived hepatocytes (Figures 6.14 and 6.15).

6.4.4 Summary

The aims of this chapter were to assess the transcriptional responses of mES cell differentiated cardiomyocytes and hepatocytes to TRO, to evaluate if *in vitro* gene expression changes could provide information on the mechanisms of TRO induced toxicity and to compare these changes in gene expression with those observed in heart and liver tissues from *in vivo* normal and diabetic mouse studies.

The data in this chapter illustrates that it is possible to acquire an *in vitro* transcriptomic signature of drug treatment using differentiated mES cells. The observation that TRO elicited similar gene expression changes in primary rodent hepatocytes and in mES cell derived hepatocytes supports the potential for stem cell based assays to be integrated into the drug development process. The use of differentiated stem cells in place of primary rodent cells would support the UK National Center for the Replacement, Refinement and Reduction in Animal Research's initiative to reduce and replace the use of animals during pre-clinical drug development (Burden et al., 2015).

The *in vitro* data illustrated that TRO disrupted intracellular calcium homeostasis in mES cell derived cardiomyocytes and caused cessation of spontaneous cell contractions. TRO was also shown to induce expression of ER stress genes in both mES cell derived cardiomyocytes and hepatocytes.

TRO induced increased expression of hepatic Trib3 was observed in both normal and diabetic *in vivo* mouse studies and *in vitro* and indicates that TRO induced

hepatotoxicity may occur via GSH depletion or ER stress based mechanisms. Increased Trib3 mRNA has been observed in other studies of drug induced hepatotoxicity and thus there is potential for Trib3 to be tested further as a potential mRNA biomarker of drug induced hepatotoxicity.

Comparison of the *in vitro* and *in vivo* transcriptomic signatures of TRO treatment showed that the gene expression changes observed in differentiated mES cells were more similar to those observed in normal mice than in diabetic mice. There were some similarities between *in vitro* and *in vivo* transcriptomic signatures of TRO, in particular the up-regulation of Trib3. However it was not possible to mimic all *in vivo* gene expression changes *in vitro*.

In vitro assays utilised in pre-clinical toxicity testing typically utilize cells grown in a 2-dimensional (2D) format. Differentiated stem cells are proposed to be more similar to cells *in vivo* than cancer derived cell lines and primary cells. However when grown in 2D culture systems stem cells do not mimic tissue physiology. Advances in cell culture techniques and *in vitro* modelling have led to the development of Organ-On-Chip models (Huh et al., 2011). These microfluidic devices allow cells to be cultured in perfused chambers in a manner that allows cells to function as a specific tissue. This produces an *in vitro* model that better replicates the tissue physiology observed *in vivo* (Bhatia and Ingber, 2014). The differentiated mES cells utilised in this project were grown in a 2D format and mimicked some of the TRO induced gene changes that were observed *in vivo*. Utilising these differentiated cells in an Organ-On-Chip model may result in a better *in vitro* replication of *in vivo* TRO induced transcriptomic changes.

Chapter 7: General Discussion

7.1 Overview

The hypothesis for this thesis was that transcriptomic changes in mES cell derived cardiomyocytes and hepatocytes are signatures for cardiotoxic and hepatotoxic effects of troglitazone in the mouse. TRO was chosen as the test drug for this hypothesis because it was withdrawn from the market due to incidences of idiosyncratic toxicity and its ability to cause ADRs in some patients wasn't detected during drug development. To test the hypothesis a number of aims were devised and addressed in each of the results chapters.

The aim of Chapter 3 was to develop reproducible methods for the differentiation of pluripotent E14Tg2a.4 mES cells into cardiomyocytes and hepatocytes. Various EB formation techniques and media compositions were trialled in the development of protocols for the differentiation of mES cells into cardiomyocytes and hepatocytes. The devised methods were reproducible and generated differentiated cardiomyocytes and hepatocytes with no significant batch to batch variance. The cardiomyocytes spontaneously contracted in culture, both cardiomyocytes and hepatocytes expressed key cardiac and hepatic genes and the differentiated cells could be maintained in FCS free medium. Given that TRO is highly protein bound the use of FCS free medium allowed for the differentiated cells to be used in assays where the availability of free TRO would not be affected by the presence of BSA in cell culture medium.

The aims of Chapter 4 and 5 were to acquire *in vivo* transcriptomic signatures of TRO induced gene changes in the heart and liver using normal and diabetic mouse models, respectively. The normal mouse TRO study highlighted TRO induced increased expression of cardiac genes that play a role in plasma volume increase induced cardiac remodelling. The increased expression of the

sarcomeric Tcap gene was particularly interesting as this gene has previously been implicated as a novel biomarker of drug induced cardiac injury and has been shown to be up-regulated *in vitro* and *in vivo* by doxorubicin, a known cardiotoxic drug (Pointon et al., 2010). The hepatic gene signature from TRO treated normal mice contained several up-regulated genes that are known to be involved in fatty acid metabolism and bile acid synthesis. Increased expression of Ppary and a number of its downstream targets was also observed. These gene expression changes indicated at potential Ppary mediated mechanisms of TRO induced hepatotoxicity as the downstream Ppary targets are known to be involved in the onset of hepatic steatosis and ER stress. The use of a diabetic mouse model enabled a transcriptomic signature to be acquired using an *in vivo* disease model that was more representative of the patient population. The cardiac gene signature did not inform on the potential mechanisms of TRO toxicity but the TRO induced down-regulation of the potassium channel Kcna5 may play a role in TRO induced heart failure, which was observed in some patients. The hepatic TRO gene signature from diabetic mice contained genes involved in the onset of hepatic steatosis and cholestasis. Heart failure, hepatic steatosis and cholestasis were observed in patients admitted to hospital with TRO induced toxicity (FDA, 1999, Menon et al., 2001). The hepatic TRO gene signatures from both the normal and diabetic *in vivo* mouse studies identified differential expression of numerous Ppary downstream target genes that are known to be involved in drug induced hepatotoxicity. Undertaking the *in vivo* mouse studies followed by transcriptional analysis allowed gene signatures of the effects of TRO on the heart and liver to be acquired. The use of mES cells in this project meant that a

direct *in vivo-in vitro* comparison could be made of the TRO gene signatures because the same animal species was used for the *in vivo* and *in vitro* studies. The aims of Chapter 6 were to assess the transcriptional responses of mES cell differentiated cardiomyocytes and hepatocyte to TRO, to compare these changes in gene expression with those observed in heart and liver tissues from *in vivo* normal and diabetic mouse studies and to evaluate if *in vitro* gene expression changes could provide information on the mechanisms of TRO induced toxicity. Comparison of *in vitro* and *in vivo* cardiac and hepatic gene signatures of TRO treatment illustrated that the *in vitro* signatures were more similar to those acquired from the *in vivo* normal mouse study than those from the diabetic mouse study. This similarity was expected as the cardiomyocytes and hepatocytes were derived from a normal stem cell line and thus the differentiated stem cells had a normal phenotype. In order to produce cells with a type 2 diabetes phenotype the cardiomyocytes and hepatocytes would have to be derived from disease specific induced pluripotent stem (iPS) cells. Transcriptomic signatures of TRO from the *in vitro* studies indicated that TRO induced cardiotoxicity could occur via calcium homeostasis disruption, causing inhibition of cardiac contractions. Disruption of calcium homeostasis is associated with induction of ER stress and differential expression of genes involved in ER stress mediated apoptosis was observed in both TRO treated cardiomyocytes and hepatocytes. Data from the *in vivo* and *in vitro* studies highlighted TRO induced increased expression of Trib3 in the livers of normal and diabetic mice and in mES cell derived hepatocytes. Trib3 mRNA has previously been proposed as a biomarker of drug induced GSH depletion mediated hepatotoxicity and the data in this project implies that it may also be a biomarker of ER stress mediated hepatotoxicity.

7.2 TRO Toxicity

Idiosyncratic drug induced toxicity is a leading cause of post-marketing drug withdrawal. It often occurs in a small subset of the patient population, becoming apparent after hundreds of thousands of patients have been prescribed the drug and isn't detected during Phase III clinical trials that typically utilize a couple of thousand patients. TRO was removed from the market in 2000 due to incidences of severe hepatotoxicity in some patients. To date, the exact mechanism via which TRO causes hepatocellular damage has not been determined however, it has been hypothesised to occur as a consequence of the generation of reactive electrophilic metabolites, inhibition of BSEP, mitochondrial dysfunction, PPARγ activation and/or individual genetic susceptibility (Kostrubsky et al., 2000, Smith, 2003, Masubuchi, 2006). The *in vivo* and *in vitro* data from this project indicate that TRO toxicity occurs via a number of mechanisms that involve increased bile acid production and Bsep inhibition causing cholestasis, triglyceride accumulation as a result of Pparγ activation and ER stress induced apoptosis. Individual genetic variability may make some patients more susceptible to experiencing TRO induced ADRs. PPARγ expression in normal livers is low however its expression is increased in the livers of patients with T2D and the degree of PPARγ up-regulation may vary from patient to patient (Boelsterli and Bedoucha, 2002). There are known polymorphisms of BSEP in humans that affect the expression and activity of the transporter, thus making some patients more susceptible to developing TRO induced cholestasis (Meier et al., 2006). The basal expression levels of ER stress genes have been shown to vary between individuals and the prevalence of metabolic diseases can induce expression of ER stress genes (Ozcan and Tabas, 2012). Varying degrees of elevated basal

expression levels of ER stress genes in T2D patients may make some individuals more susceptible to hepatocellular damage via ER stress induced apoptosis as a result of TRO administration. The data from this project supports the hypothesis that TRO toxicity can occur via a number of mechanisms and its onset is influenced by individual genetic susceptibility. This also accounts for the idiosyncratic nature of TRO toxicity and the difficulty in replicating it using *in vivo* and *in vitro* models.

7.3 Stem Cells and Drug Development

The concept of individual genetic variability being a leading factor in the onset of idiosyncratic drug induced toxicity supports the development and use of disease specific ES and iPS cell based models in preclinical toxicity testing. This project utilized mES cells and involved developing methods for the differentiation of these cells into cardiomyocytes and hepatocytes for use in predictive toxicology studies. The exploration and development of stem cell technologies for use as novel *in vitro* models in preclinical drug development is centered on the use of human ES and iPS cells. Human ES cells are derived from embryos produced by *in vitro* fertilization. As with mES cells the ICM of blastocysts are extracted and the cells can be cultured indefinitely *in vitro* in a pluripotent state (Thomson et al., 1998). In comparison human iPS cells are generated via the process of reprogramming terminally differentiated somatic cells into pluripotent cells. Adult skin fibroblasts can be reprogrammed to produce human iPS cells that have similar morphology, gene expression and proliferation ability as hES cells (Takahashi et al., 2007). The advantage of using differentiated human stem cells in drug development assays is that they remove the need for inter-species extrapolation of data that would be required with the use of mES cells. The use

of human stem cells is anticipated to revolutionize the medical research and drug discovery fields as these cells will allow for the generation of disease specific in vitro models. Several disease specific hES cell lines have been generated for diseases such as cystic fibrosis and Huntington's disease. These cell lines were derived from embryos containing disease specific mutations which were identified using pre-implantation genetic diagnosis (Mateizel et al., 2006). There are many diseases for which disease specific hES cell lines do not exist and in these cases it is anticipated that iPS cells will provide a solution. Skin fibroblasts taken from patients with disease specific mutations could be used to generate iPS cells which could be expanded and differentiated in vitro to produce cell models for use in drug development (Tiscornia et al., 2011). The use of differentiated iPS cells will allow for the development of *in vitro* assays using cells that reflect the genotype and phenotype of the patient population. The potential of and demand for disease specific iPS cells lead to the launch of the European Bank for induced pluripotent Stem Cells (EBiSC) consortium in February 2014. EBiSC is supported by a €35 million grant to produce, store and distribute human iPS cells for use by academia and industry for the study of diseases and drug development (EBiSC, 2014).

Genetic variation is likely to be a contributing factor to the development of idiosyncratic drug induced toxicity in only a small percentage of patient populations. The most common variations are found in members of the cytochrome P450 enzyme family, which are involved in drug metabolism and bioactivation (Guengerich, 2007). Analysis of polymorphisms in CYP2C9 revealed that approximately 10% of the Caucasian population possess the CYP2C9*2. This same variant was observed in only 2% of the African population

and was absent in Asian populations. The CYP3A4*1B variants has been reported to occur in approximately 60% of the African population yet is found in only 5% of the Caucasian population. (Xie et al., 2001). Analysis of currently available hES cell lines by the Haplotype Mapping project identified that 80% of the cell lines were of Caucasian ancestry (Laurent et al., 2010, Mosher et al., 2010). Thus, differentiated cells from hES cell lines will predominantly represent the genetic variation in Caucasian populations. The use of iPS cells in drug development may allow for the development of differentiated cell models which more accurately represent targeted patient populations. This would increase the possibility of drug induced toxicity, where the mechanism is dependent on genetic variation within the population, to be detected in *in vitro* models during drug development.

7.4 Future Work

The requirement for more predictive *in vitro* toxicity assays in drug discovery and development is ever increasing. Currently utilised primary cell and cancer derived cell line base models do not always accurately predict drug induced toxicity especially idiosyncratic toxicities where the mechanism is patient specific. Stem cell based assays have been sought to meet the demand for more predictive toxicity assays. Genetic variance is hypothesised to be a leading factor that makes some patients more susceptible to experiencing ADRs. The use of disease specific ES cells and iPS cells, derived from individuals with varying drug sensitivities, is anticipated to provide more predictive assays for use in detecting drug induced toxicities during preclinical drug development. A leading obstacle in the full integration of differentiated stem cell based models into the drug development pipeline is the production of homogenous cultures of terminally

differentiated adult like cells. This challenge has not yet been overcome by the wider scientific community and future experiments would be directed towards developing reproducible and standardised differentiation protocols for the generation of cardiomyocytes and hepatocytes from disease specific human ES and iPS cells (Chen et al., 2013). Once this challenge and been overcome the cells would be used in HTS assays with transcriptomic analysis to profile the responses of the differentiated cells to known toxicants. This data would enable a reference database to be developed that could then be used to evaluate the toxicity of new drug entities.

7.5 Conclusions

The hypothesis for this thesis was that transcriptomic changes in mES cell derived cardiomyocytes and hepatocytes are signatures for cardiotoxic and hepatotoxic effects of troglitazone in the mouse. The data within this project illustrates the difficulties of using chemicals to induce differentiation of pluripotent mES cells into terminally differentiated adult cardiomyocytes and hepatocytes. As a result, the *in vitro* cardiotoxic and hepatotoxic transcriptomic signatures of TRO had limited similarity to the signatures acquired *in vivo* from the normal and diabetic mouse studies. The data highlights advantages of using transcriptomic analysis to characterise drug induced toxicity and supports the potential for Tcap and Trib3 to be further developed as mRNA biomarkers of drug induced cardio- and hepato- toxicity, respectively. Furthermore, the data supports the notion that idiosyncratic drug induced toxicities are patient specific and thus to enable better predication of ADRs during drug development the assays utilised should represent the genetic heterogeneity of the patient population. The limited similarities between the transcriptomic signatures of TRO toxicity acquired *in vivo*

and *in vitro* disprove the hypothesis that transcriptomic changes in mES cell derived cardiomyocytes and hepatocytes are signatures for cardiotoxic and hepatotoxic effects of troglitazone in the mouse.

In theory, stem cells are a potentially excellent tool for use in developing more predictive toxicity assays for use during drug development. Their ability to divide indefinitely in their pluripotent state and to differentiate in to any cell type present opportunities to build innovative *in vitro* cellular models. However, the lack of standardised differentiation protocols, poor reproducibility between different batches of differentiated stem cells, the heterogeneity of differentiated cultures, the high cost of and time intensive nature of stem cell culture and limited scale up ability of culture and differentiation methods is inhibiting the utilisation of stem cell based toxicity assays in preclinical drug development. In the future, stem cells may proceed to play an important role in toxicology studies undertaken during drug discovery and development however, there are numerous scientific and industrial challenges that need to be addressed before stem cell based assays become the gold standard for *in vitro* preclinical toxicity assays.

Appendicies

Appendix One: RT-PCR Primers

A1. RT-PCR primer sequence details for primers obtained from the Harvard Primer Bank (Wang and Seed, 2003, Spandidos et al., 2008, Spandidos et al., 2010)

Gene Symbol	NCBI Gene ID	Primer Bank ID	Amplicon Size	Primer Direction	Sequence (5' → 3')	Length	Tm	Location
Abcb11/Bsep	27413	120432046b3	79	Forward	CTGGCATCTACGCAGGAGTTG	21	62.8	425-445
				Reverse	GCCCCAGTGATTACCCACAA	20	61.8	503-484
Abcc2/Mrp2	12780	11184219a1	123	Forward	GTGTGGATTCCCTTGGGCTTT	21	62.6	94-114
				Reverse	CACAACGAACACCTGCTTGG	20	61.8	216-197
Actg2	11468	6752952a3	115	Forward	CCTTCCTTCATTGGCATGGAG	21	60.7	793-813
				Reverse	CCCCAGAGAGGACATTGTTAGC	22	62.1	907-886
Afp	11576	31982513a1	145	Forward	CTTCCCTCATCCTCCTGCTAC	21	61.1	20-40
				Reverse	ACAAACTGGGTAAAGGTGATGG	22	60.2	164-143
Agpat6	102247	227908857c2	91	Forward	TCAAAGAAATTCGTCGAAGTGGT	23	60.4	275-297
				Reverse	CCTTTCCGGCAAAAGTAGAAGAT	23	60.5	365-343
Alb	11657	33859506a1	167	Forward	TGCTTTTTCCAGGGGTGTGTT	21	62.4	45-65
				Reverse	TTACTTCCTGCACTAATTTGGCA	23	60.2	211-189
Aqp7	11832	6680712a1	126	Forward	AATATGGTGCGAGAGTTTCTGG	22	60.1	49-70
				Reverse	ACCCAAGTTGACACCGAGATA	21	60.5	174-154

Gene	Gene ID	Accession	Amplicon	Direction	Sequence	Length	Tm	Position
Atf4	11911	121949820c1	134	Forward	CCTGAACAGCGAAGTGTTGG	20	61.2	18-37
				Reverse	TGGAGAACCCATGAGGTTTCAA	22	61.2	151-130
Atp2a2	11938	6806903a1	120	Forward	GAGAACGCTCACACAAAGACC	21	61.2	4-24
				Reverse	CAATTCGTTGGAGCCCCAT	19	60.1	123-105
Bcl2	12043	4557355a1	94	Forward	GGGGAGGATTGTGGCCTTC	19	62.1	432-450
				Reverse	CAGGGCGATGTTGTCCACC	19	63.0	525-507
Bcl2l2	12050	6680774a1	136	Forward	GCGGAGTTCACAGCTCTATAC	21	60.0	433-453
				Reverse	AAAAGGCCCCTACAGTTACCA	21	60.7	568-548
Bmp4	12159	6680796a1	114	Forward	TTCCTGGTAACCGAATGCTGA	21	61.1	41-61
				Reverse	CCTGAATCTCGGCGACTTTTT	21	60.6	154-134
Cfd	11537	7304867a1	129	Forward	CATGCTCGGCCCTACATGG	19	62.6	103-121
				Reverse	CACAGAGTCGTCATCCGTCAC	21	62.4	231-211
Cflar/Flip	12633	2653420a1	115	Forward	GCTCCAGAATGGGCGAAGTAA	21	62.1	621-641
				Reverse	ACGGATGTGCGGAGGTAAAAA	21	62	735-715
Cidea	12683	162287226c1	84	Forward	TGACATTCATGGGATTGCAGAC	22	60.6	44-65
				Reverse	CATGGTTTGAAACTCGAAAAGGG	23	60.2	127-105
Cidec	14311	141802598c1	148	Forward	ATGGACTACGCCATGAAGTCT	21	60.7	1-21
				Reverse	CGGTGCTAACACGACAGGG	19	62.7	148-130
Cyp1b1	13078	6753568a1	144	Forward	CACCAGCCTTAGTGCAGACAG	21	62.7	6-26
				Reverse	GAGGACCACGGTTTCCGTTG	20	63.0	149-130
Cyp7a1	13122	31542445a1	100	Forward	GGGATTGCTGTGGTAGTGAGC	21	62.7	25-45
				Reverse	GGTATGGAATCAACCCGTTGTC	22	60.9	124-103
Cyp7b1	13123	160707926c2	110	Forward	AGCCGATTATCAGCGAAAGCC	21	62.9	340-360
				Reverse	GCATCCAAAGGTTTGCCTTGT	21	61.7	449-429
Cyp8b1	13124	31981808a1	112	Forward	CCTCTGGACAAGGGTTTGTG	21	60.8	97-117
				Reverse	GCACCGTGAAGACATCCCC	19	62.7	208-190

Gene				Direction	Sequence	Length	Tm	Position
Dbp	13170	8393240a3	133	Forward	CCTGATCCCGCTGATCTCG	19	61.6	619-637
				Reverse	CAGGCACCTGGACTTTCCTT	20	61.8	751-732
Ddit3	13198	31982415a1	121	Forward	CTGGAAGCCTGGTATGAGGAT	21	60.7	52-72
				Reverse	CAGGGTCAAGAGTAGTGAAGGT	22	60.8	172-151
Ddit4	74747	21312868a1	182	Forward	CAAGGCAAGAGCTGCCATAG	20	60.8	448-467
				Reverse	CCGGTACTTAGCGTCAGGG	19	61.5	629-611
Dnajb9	27362	31560495a1	128	Forward	CTCCACAGTCAGTTTTCGTCTT	22	60.2	8-29
				Reverse	GGCCTTTTTGATTTGTCGCTC	21	60.4	135-115
Foxa2	15376	6753898a1	222	Forward	CCCTACGCCAACATGAACTCG	21	63.0	376-396
				Reverse	GTTCTGCCGGTAGAAAGGGA	20	61.2	597-578
Gapdh	14433	6679937a1	123	Forward	AGGTCGGTGTGAACGGATTTG	21	62.6	8-28
				Reverse	TGTAGACCATGTAGTTGAGGTCA	23	60.2	130-108
Gata4	14463	6679953a1	139	Forward	CCCTACCCAGCCTACATGG	19	60.9	481-499
				Reverse	ACATATCGAGATTGGGGTGTCT	22	60.4	619-598
Hnf4a	15378	2895134a1	60	Forward	GTGGCGAGTCCTTATGACACG	21	62.8	34-54
				Reverse	GCTGTTGGATGAATTGAGGTTGG	23	61.9	93-71
Hspa5	14828	31981722a1	134	Forward	ACTTGGGGACCACCTATTCCT	21	62	104-124
				Reverse	ATCGCCAATCAGACGCTCC	19	62.2	237-219
Mcl1	17210	133892763c3	148	Forward	CAAAGATGGCGTAACAAACTGG	22	60.0	705-726
				Reverse	CCGTTTCGTCCTTACAAGAACA	22	60.5	852-831
Mef2c	17260	13384624a2	148	Forward	TGCTGGTCTCACCTGGTAAC	20	61.2	668-687
				Reverse	ATCCTTTGATTCACTGATGGCAT	23	60.0	815-793
Mgll	23945	261878513c1	75	Forward	AGGCGAACTCCACAGAATGTT	21	61.7	22-42
				Reverse	ACAAAAGAGGTACTGTCCGTCT	22	60.7	96-75
Mogat1	68393	229577407c3	78	Forward	TCCCGTTGTTCCGAGAATATCT	22	60.6	446-467
				Reverse	TGCTCAGCACATGAGACAAAC	21	60.8	523-503

331

Myh11	17880	7305295a2	131	Forward	GCTGCACGAGTATGAGACAGA	21	61.6	4791-4811
				Reverse	CCCTCCCTTTGATGGCTGAG	20	62	4921-4902
Myh6	17888	255918223c1	87	Forward	GCCCAGTACCTCCGAAAGTC	20	61.9	37-56
				Reverse	ATCAGGCACGAAGCACTCC	19	62.0	123-105
Myl2	17906	153791852c1	77	Forward	AGGACGAGTGAACGTGAAAAAT	22	60.2	168-189
				Reverse	ACACGGTGAAGTTAATTGGACC	22	60.5	244-223
Nanog	71950	153791181c1	87	Forward	CACAGTTTGCCTAGTTCTGAGG	22	60.6	25-46
				Reverse	GCAAGAATAGTTCTCGGGATGAA	23	60.1	111-89
Nkx 2.5	18091	6679068a2	153	Forward	GGTCTCAATGCCTATGGCTAC	21	60.0	718-738
				Reverse	GCCAAAGTTCACGAAGTTGCT	21	61.6	870-850
Plin4/S3-12	57435	157041251c1	121	Forward	CTGCTCCAACCTTCTGAACAG	21	60.6	229-249
				Reverse	GGACCATTCCTTTTGCAGCAT	21	61.2	349-329
Pou5f1	18999	7305399a1	211	Forward	GGCTTCAGACTTCGCCTCC	19	62.4	15-33
				Reverse	AACCTGAGGTCCACAGTATGC	21	61.5	225-205
PPARα	19013	31543500a1	153	Forward	AGAGCCCCATCTGTCCTCTC	20	62.3	14-33
				Reverse	ACTGGTAGTCTGCAAAACCAAA	22	60.0	166-145
PPARγ	19016	6755138a1	103	Forward	TCGCTGATGCACTGCCTATG	20	62.4	50-69
				Reverse	GAGAGGTCCACAGAGCTGATT	21	60.9	152-132
Ryr2	20191	13569850a1	153	Forward	ATGGCTTTAAGGCACAGCG	19	60.8	3413-3431
				Reverse	CAGAGCCCGAATCATCCAGC	20	62.7	3565-3546
Scp2	20280	293794a1	122	Forward	CCTTCTGTCGCTTTGAAATCTCC	23	61.4	4-26
				Reverse	GCTTCCTTTGCCATATCAGGAT	22	60.2	125-104
Slc27a1	26457	118129963c1	91	Forward	CTGGGACTTCCGTGGACCT	19	62.9	58-76
				Reverse	TCTTGCAGACGATACGCAGAA	21	61.5	148-128
Slc8a1	20541	163914366c3	114	Forward	ACCAAGACGACGGTGAGAATC	21	61.8	358-378
				Reverse	GTTATGGCCGCACACTTCAAT	21	61.3	471-451

Slco1b2/OATP2	28253	8347612a1	202	Forward	CCTGAGAAGTGTCCGCATAAC	21	60.4	495-515
				Reverse	GTCCGAGTGGCAGTAAGAAAG	21	60.4	696-676
Sox17	20671	6755604a1	136	Forward	GATGCGGGATACGCCAGTG	19	62.9	13-31
				Reverse	CCACCACCTCGCCTTTCAC	19	62.9	148-130
Tbx2	21385	6678231a1	123	Forward	CCGATGACTGCCGCTATAAGT	21	61.7	449-469
				Reverse	CCATCCACTGTTCCCCTGT	19	60.9	571-553
Tcap	21393	6755726a1	273	Forward	GATGCGCCTGGGTATCCTC	19	62.0	204-222
				Reverse	GATCGAGACAGGGTACGGC	19	61.6	476-458
Tef	21685	226958408c1	108	Forward	ATCTTTCAGCCCTCGGAAACC	21	62.8	388-408
				Reverse	GAAGTTCACATCGACCTCCAC	21	60.8	495-475
Thrsp	21835	31560631c1	63	Forward	ATGCAAGTGCTAACGAAACGC	21	62.1	1-21
				Reverse	GGAGTACCGATCCATGACTGTC	22	61.6	63-42
Timp3	21859	6755793a1	131	Forward	CTTCTGCAACTCCGACATCGT	21	62.4	102-122
				Reverse	GGGGCATCTTACTGAAGCCTC	21	62.2	232-212
Timp4	110595	31981528a1	130	Forward	TGTGGCTGCCAAATCACCA	19	62.2	466-484
				Reverse	TCATGCAGACATAGTGCTGGG	21	61.9	595-575
Tnni3	21954	6678393a1	135	Forward	TCTGCCAACTACCGAGCCTAT	21	62.5	70-90
				Reverse	CTCTTCTGCCTCTCGTTCCAT	21	61.3	204-184
Tpm2	22004	11875203a1	98	Forward	GTGGCTGAGAGTAAATGTGGG	21	60.4	553-573
				Reverse	TTGGTGGAATACTTGTCCGCT	21	61.4	650-630
Trib3	228775	21362365a1	64	Forward	TGCAGGAAGAAACCGTTGGAG	21	62.6	40-60
				Reverse	CTCGTTTTAGGACTGGACACTTG	23	60.8	103-81
Ttr	22139	7305599a1	125	Forward	TTGCCTCGCTGGACTGGTA	19	62.9	27-45
				Reverse	TTACAGCCACGTCTACAGCAG	21	61.8	151-131

(Tm – melting temperature)

B1. RT-PCR primer sequence details for Cyp3a11, designed using Primer Express software and checked using NCBI Primer Blast tool

Gene Symbol	NCBI Gene ID	Amplicon Size	Primer Direction	Sequence (5' → 3')	Length	Tm	Location
Cyp3a11	13112	73	Forward	GGATGAGATCGATGAGGCTCTG	22	60.1	1077-1098
			Reverse	CAGGTATTCCATCTCCATCACAGT	24	59.9	1149-1126

(Tm – melting temperature)

Appendix Two: RT-PCR Gapdh Standard Graphs

Normal Mouse Liver Control

$y = -3.1976x + 21.132$
$R^2 = 0.9911$

Normal Mouse Liver TRO

$y = -3.4643x + 21.457$
$R^2 = 0.9936$

Normal Mouse Heart Control

$y = -3.4349x + 21.821$
$R^2 = 0.9915$

Normal Mouse Heart TRO

$y = -3.2555x + 21.538$
$R^2 = 0.9975$

Diabetic Mouse Liver Control

$y = -3.1131x + 21.824$
$R^2 = 0.992$

Diabetic Mouse Liver TRO

$y = -3.4358x + 22.088$
$R^2 = 0.9972$

Diabetic Mouse Heart Control

$y = -3.5203x + 21.929$
$R^2 = 0.9843$

Diabetic Mouse Heart TRO

$y = -3.3124x + 21.51$
$R^2 = 0.9893$

Undifferentiated mES Cells

y = -3.284x + 20.84
R² = 0.9901

Differentiated Cardiomyocytes Control

y = -3.3504x + 21.28
R² = 0.9809

Differentiated Hepatocytes Control

y = -3.0846x + 20.622
R² = 0.9883

Differentiated Cardiomyocytes TRO

y = -3.3219x + 21.577
R² = 0.9902

Differentiated Hepatocytes TRO

y = -3.4168x + 21.019
R² = 0.9869

Appendix Three: Gene Symbols and Names

Aacs   Acetoacetyl-coa synthetase

Aadac   Arylacetamide deacetylase

Aadacl1   Neutral cholesterol ester hydrolase 1

Abca3   ATP-binding cassette, sub-family A, member 3

Abca6   ATP-binding cassette, sub-family A, member 6

Abcb10   ATP-binding cassette, sub-family B, member 10

Abcb11   ATP-binding cassette, sub-family B, member 11

Abcb4   ATP-binding cassette, sub-family B, member 4

Abcb9   ATP-binding cassette, sub-family B, member 9

Abcc10   ATP-binding cassette, sub-family C, member 10

Abcc2   ATP-binding cassette, sub-family C, member 2

Abcc3   ATP-binding cassette, sub-family C, member 3

Abcc4   ATP-binding cassette, sub-family C, member 4

Abcc5   ATP-binding cassette, sub-family C, member 5

Abcd1   ATP-binding cassette, sub-family D, member 1

Abcd2   ATP-binding cassette, sub-family D, member 2

Abcd3   ATP-binding cassette, sub-family D, member 3

Abcg5   ATP-binding cassette, sub-family G, member 5

Abcg8   ATP-binding cassette, sub-family G, member 8

Abhd6   Abhydrolase domain containing 6

Abi2   Abl-interactor 2

Acaa1   Acetyl-coa acyltransferase 1

Acaa1a   Acetyl-Coenzyme A acyltransferase 1A

Acaa1b   Acetyl-Coenzyme A acyltransferase 1B

Acaa2   Acetyl-coa acyltransferase 2

Acac   Acetyl-coa carboxylase alpha

Acacb   Acetyl-coa carboxylase beta

Acad10   Acyl-coa dehydrogenase family, member 10

Acadl   Acyl-coa dehydrogenase, long chain

Acadm   Acyl-coa dehydrogenase, C-4 to C-12 straight chain

Acads   Acyl-coa dehydrogenase, C-2 to C-3 short chain

Acat1   Acetyl-coa acetyltransferase 1

Acat2	Acetyl-coa acetyltransferase 2
Acat3	Acetyl-Coenzyme A acetyltransferase 3
Accn1	Acid sensing (proton gated) ion channel 2
Acly	ATP citrate lyase
Aco1	Aconitase 1, soluble
Aco2	Aconitase 2, mitochondrial
Acot2	Acyl-coa thioesterase 2
Acox1	Acyl-coa oxidase 1, palmitoyl
Acox2	Acyl-coa oxidase 2, branched chain
Acpp	Acid phosphatase, prostate
Acsl1	Acyl-coa synthetase long-chain family member 1
Acsl3	Acyl-coa synthetase long-chain family member 3
Acsl4	Acyl-coa synthetase long-chain family member 4
Acsl5	Acyl-coa synthetase long-chain family member 5
Acsm3	Acyl-coa synthetase medium-chain family member 3
Acta1	Actin, alpha 1
Acta2	Actin, alpha 2
Actb	Actin, beta
Actc1	Actin, alpha
Actg2	Actin, gamma 2
Actn1	Actinin, alpha 1
Actn2	Actinin, alpha 2
Actn4	Actinin, alpha 4
Acvr2b	Activin A receptor, type IIB
Acy1	Aminoacylase 1
Acy3	Aspartoacylase 3
Ada	Adenosine deaminase
Adam15	ADAM metallopeptidase domain 15
Adamts5	ADAM metallopeptidase with thrombospondin type 1 motif, 5
Adck4	Aarf domain containing kinase 4
Adck5	Aarf domain containing kinase 5
Adcy4	Adenylate cyclase 4
Adcy6	Adenylate cyclase 6

Adcy9	Adenylate cyclase 9
Adfp	Perilipin 2
Adh4	Alcohol dehydrogenase 4
Adh7	Alcohol dehydrogenase 7
Adk	Adenosine kinase
Admr	G protein-coupled receptor 182
Adora1	Adenosine A1 receptor
Adpn	Patatin-like phospholipase
Adrb2	Adrenoceptor beta 2, surface
Afg3l1	AFG3-like AAA atpase 1
Afmid	Arylformamidase
Afp	Alpha-fetoprotein
Agpat2	1-acylglycerol-3-phosphate O-acyltransferase 2
Agpat6	1-acylglycerol-3-phosphate O-acyltransferase 6
Agpat9	1-acylglycerol-3-phosphate O-acyltransferase 9
Agpt2	Angiopoietin 2
Agrn	Agrin
Agt	Angiotensinogen
Agtr1a	Angiotensin II receptor, type 1
Agtrl1	Apelin receptor
Agxt2l1	Ethanolamine-phosphate phospho-lyase
Aif1	Allograft inflammatory factor 1
Ak4	Adenylate kinase 4
Akap12	A kinase anchor protein 12
Akap9	A kinase anchor protein 9
Akp2	Alkaline phosphatase 2
Akr1b7	Aldo-keto reductase family 1, member B7
Akr1c19	Aldo-keto reductase family 1, member C19
Akt2	V-akt murine thymoma viral oncogene homolog 2
Alas1	5'-aminolevulinate synthase 1
Alas2	5'-aminolevulinate synthase 2
Alb	Albumin
Aldh1a1	Aldehyde dehydrogenase 1 family, member A1

Aldh1a7	Aldehyde dehydrogenase family 1, subfamily A7
Aldh1b1	Aldehyde dehydrogenase 1 family, member B1
Aldh1l2	Aldehyde dehydrogenase 1 family, member L2
Aldh2	Aldehyde dehydrogenase 2 family (mitochondrial)
Aldh3a2	Aldehyde dehydrogenase 3 family, member A2
Aldh3b1	Aldehyde dehydrogenase 3 family, member B1
Aldh5a1	Aldehyde dehydrogenase 5 family, member A1
Aldh9a1	Aldehyde dehydrogenase 9 family, member A1
Aldob	Aldolase B, fructose-bisphosphate
Ambra1	Autophagy/beclin-1 regulator 1
Amd1	Adenosylmethionine decarboxylase 1
Amn	Amnion associated transmembrane protein
Amy1	Amylase, alpha 1
Anapc1	Anaphase promoting complex subunit 1
Ang1	Angiopoietin 1
Ang2	Angiopoietin 2
Angptl4	Angiopoietin-like 4
Angptl6	Angiopoietin-like 6
Angptl7	Angiopoietin-like 7
Ankrd2	Ankyrin repeat domain 2
Ankrd27	Ankyrin repeat domain 27
Ankrd47	KN motif and ankyrin repeat domains 3
Ankrd56	Sosondowah ankyrin repeat domain family member B
Anxa2	Annexin A2
Ap3m1	Adaptor-related protein complex 3, mu 1 subunit
Apc	Adenomatous polyposis coli
Apcs	Amyloid P component, serum
Aph1b	APH1B gamma secretase subunit
Apoa2	Apolipoprotein A-II
Apoa4	Apolipoprotein A-IV
Apoa5	Apolipoprotein A-V
Apob	Apolipoprotein B
Apoc1	Apolipoprotein C-I

Apof	Apolipoprotein F
Appl1	Adaptor protein
Aprt	Adenine phosphoribosyltransferase
Aqp1	Aquaporin 1
Aqp4	Aquaporin 4
Aqp7	Aquaporin 7
Aqp8	Aquaporin 8
Ar	Androgen receptor
Arfl4	ADP-ribosylation factor-like 4D
Arhgap10	Rho gtpase activating protein 10
Arhgap18	Rho gtpase activating protein 18
Arhgef1	Rho guanine nucleotide exchange factor 1
Arhgef19	Rho guanine nucleotide exchange factor 19
Arl10c	ADP-ribosylation factor-like 8B
Arl6ip2	Atlastin gtpase 2
Arl6ip5	ADP-ribosylation factor-like 6 interacting protein 5
Arntl	Aryl hydrocarbon receptor nuclear translocator-like
Arpc3	Actin related protein 2/3 complex, subunit 3
Arsj	Arylsulfatase family, member J
As3mt	Arsenite methyltransferase
Asb13	Ankyrin repeat and SOCS box containing 13
Asb4	Ankyrin repeat and SOCS box containing 4
Asf1a	Anti-silencing function 1A histone chaperone
Asgr2	Asialoglycoprotein receptor 2
Asl	Argininosuccinate lyase
Asns	Asparagine synthetase
Aspn	Asporin
Ass1	Argininosuccinate synthase 1
Atad3a	Atpase family, AAA domain containing 3A
Atf3	Activating transcription factor 3
Atf4	Activating transcription factor 4
Atf5	Activating transcription factor 5
Atp10d	Atpase, class V, type 10D

Atp1a1	Atpase, Na+/K+ transporting, alpha 1 polypeptide
Atp2a2	Atpase, Ca++ transporting
Atp2a3	Atpase, Ca++ transporting
Atp5b	ATP synthase, H+ transporting, mitochondrial F1 complex, beta polypeptide
Atp7a	Atpase, Cu++ transporting, alpha polypeptide
Atp9a	Atpase, class II, type 9A
Avp	Arginine vasopressin
Axl	AXL receptor tyrosine kinase
B3bp	NEDD4 binding protein 2
Baat	Bile acid coa:amino acid N-acyltransferase
Bach1	BTB and CNC homology 1, basic leucine zipper transcription factor 1
Bag3	BCL2-associated athanogene 3
Bbc3	BCL2 binding component 3
Bcdo2	Beta-carotene oxygenase 2
Bche	Butyrylcholinesterase
Bckdhb	Branched chain keto acid dehydrogenase E1, beta polypeptide
Bcl2	B-cell CLL/lymphoma 2
Bcl2l2	BCL2-like 2
Bcl3	B-cell CLL/lymphoma 3
Bcl6	B-cell CLL/lymphoma 6
Bcmo1	Beta-carotene oxygenase 1
Bdh	3-hydroxybutyrate dehydrogenase, type 1
Bfar	Bifunctional apoptosis regulator
Bhlhb2	Basic helix-loop-helix family, member e40
Bhlhb4	Basic helix-loop-helix family, member e23
Bhlhb9	Basic helix-loop-helix domain containing, class B, 9
Bhmt	Betaine--homocysteine S-methyltransferase
Birc4	X-linked inhibitor of apoptosis, E3 ubiquitin protein ligase
Bmp4	Bone morphogenetic protein 4
Btbd14a	NACC family member 2
Btg1	B-cell translocation gene 1

Bzw1	Basic leucine zipper and W2 domains 1
C1qa	Complement component 1, q subcomponent, A chain
C1qb	Complement component 1, q subcomponent, B chain
C1qg	Complement component 1, q subcomponent, C chain
Cabc1	Aarf domain containing kinase 3
Cacna1c	Calcium channel, voltage-dependent, L type, alpha 1C subunit
Cacnb1	Calcium channel, voltage-dependent, beta 1 subunit
Cacnb3	Calcium channel, voltage-dependent, beta 3 subunit
Cad	Carbamoyl-phosphate synthetase 2
Camk2b	Calcium/calmodulin-dependent protein kinase II beta
Camk2n1	Calcium/calmodulin-dependent protein kinase II inhibitor 1
Capn10	Calpain 10
Capn2	Calpain 2, (m/II) large subunit
Capn8	Calpain 8
Car14	Carbonic anhydrase 14
Car4	Carbonic anhydrase IV
Car5a	Carbonic anhydrase 5a, mitochondrial
Card12	NLR family, CARD domain containing 4
Carhsp1	Calcium regulated heat stable protein 1, 24kda
Carm1	Coactivator-associated arginine methyltransferase 1
Casp1	Caspase 1
Casp3	Caspase 3
Casp6	Caspase 6
Casp8	Caspase 8
Catnbip1	Catenin beta interacting protein 1
Cav1	Caveolin 1
Cblb	Cbl proto-oncogene B, E3 ubiquitin protein ligase
Cbs	Cystathionine-beta-synthase
Cc1	RB1-inducible coiled-coil 1
Ccl19	Chemokine ligand 19
Ccl21b	Chemokine ligand 21B
Ccl21c	Chemokine ligand 21C
Ccl6	Chemokine ligand 6

Ccl7	Chemokine ligand 7
Ccl9	Chemokine ligand 9
Ccnd1	Cyclin D1
Ccne2	Cyclin E2
Ccrn4l	CCR4 carbon catabolite repression 4-like (S. Cerevisiae)
Cd163	CD163 molecule
Cd164	CD164 molecule
Cd200	CD200 molecule
Cd44	CD44 molecule
Cd63	CD63 molecule
Cd9	CD9 molecule
Cda	Cytidine deaminase
Cdc25c	Cell division cycle 25C
Cdc2a	Cyclin-dependent kinase 1
Cdc42ep5	CDC42 effector protein 5
Cdc7	Cell division cycle 7
Cdk2	Cyclin-dependent kinase 2
Cdk6	Cyclin-dependent kinase 6
Cdkn1a	Cyclin-dependent kinase inhibitor 1A
Cdkn1c	Cyclin-dependent kinase inhibitor 1C
Cdo1	Cysteine dioxygenase type 1
Cebpb	CCAAT/enhancer binding protein, beta
Cebpe	CCAAT/enhancer binding protein, epsilon
Celsr1	Cadherin, EGF LAG seven-pass G-type receptor 1
Ces3	Carboxylesterase 3
Cfd	Complement factor D (adipsin)
Cflar	CASP8 and FADD-like apoptosis regulator
Chat	Choline O-acetyltransferase
Chchd6	Coiled-coil-helix-coiled-coil-helix domain containing 6
Chd1	Chromodomain helicase DNA binding protein 1
Chi3l1	Chitinase 3-like 1
Chic1	Cysteine-rich hydrophobic domain 1
Chka	Choline kinase alpha

Chkb	Choline kinase beta
Chpt1	Choline phosphotransferase 1
Chrna2	Cholinergic receptor, nicotinic, alpha 2
Chst1	Carbohydrate sulfotransferase 1
Ciapin1	Cytokine induced apoptosis inhibitor 1
Cib3	Calcium and integrin binding family member 3
Cidea	Cell death-inducing DFFA-like effector a
Cidec	Cell death-inducing DFFA-like effector c
Cish	Cytokine inducible SH2-containing protein
Cited2	Cbp/p300-interacting transactivator
Ckap1	Tubulin folding cofactor B
Ckb	Creatine kinase, brain
Cldn1	Claudin 1
Cldn5	Claudin 5
Clecsf8	C-type lectin domain family 4, member D
Clock	Clock circadian regulator
Clpx	Caseinolytic mitochondrial matrix peptidase chaperone subunit
Clstn3	Calsyntenin 3
Cmas	Cytidine monophosphate N-acetylneuraminic acid synthetase
Cml1	Camello-like 1
Cml4	N-acetyltransferase 8
Coasy	Coa synthase
Cobl	Cordon-bleu WH2 repeat protein
Col11a1	Collagen, type XI, alpha 1
Col1a1	Collagen, type I, alpha 1
Col2a1	Collagen, type II, alpha 1
Col3a1	Collagen, type III, alpha 1
Col4a1	Collagen, type IV, alpha 1
Col4a3bp	Collagen, type IV, alpha 3, binding protein
Col5a2	Collagen, type V, alpha 2
Col6a3	Collagen, type VI, alpha 3
Col8a1	Collagen, type VIII, alpha 1
Col8a2	Collagen, type VIII, alpha 2

Colec11	Collectin sub-family member 11
Colec12	Collectin sub-family member 12
Comt	Catechol-O-methyltransferase
Cox7a2l	Cytochrome c oxidase subunit viia polypeptide 2 like
Coxvib2	Cytochrome c oxidase subunit vib polypeptide 2
Cpa6	Carboxypeptidase A6
Cpb2	Carboxypeptidase B2 (plasma)
Cpn1	Carboxypeptidase N, polypeptide 1
Cpn2	Carboxypeptidase N, polypeptide 2
Cpne8	Copine VIII
Cps1	Carbamoyl-phosphate synthase 1, mitochondrial
Cpt1a	Carnitine palmitoyltransferase 1A
Cpt1b	Carnitine palmitoyltransferase 1B
Cpt2	Carnitine palmitoyltransferase 2
Crat	Carnitine O-acetyltransferase
Creld2	Cysteine-rich with EGF-like domains 2
Crg-L1	Alkaline ceramidase 2
Crk	V-crk avian sarcoma virus CT10 oncogene homolog
Cry2	Cryptochrome circadian clock 2
Cryba4	Crystallin, beta A4
Cryl1	Crystallin, lambda 1
Csad	Cysteine sulfinic acid decarboxylase
Csnk1g2	Casein kinase 1, gamma 2
Cspg3	Neurocan
Cspg6	Structural maintenance of chromosomes 3
Csrp3	Cysteine and glycine-rich protein 3
Ctdsp2	CTD small phosphatase 2
Ctgf	Connective tissue growth factor
Ctps	CTP synthase 1
Ctsd	Cathepsin D
Ctsz	Cathepsin Z
Cxcl1	Chemokine ligand 1
Cxcl9	Chemokine ligand 9

Cyba	Cytochrome b-245, alpha polypeptide
Cyp11a1	Cytochrome P450, family 11, subfamily a, polypeptide 1
Cyp1b1	Cytochrome P450, family 1, subfamily b, polypeptide 1
Cyp26a1	Cytochrome P450, family 26, subfamily a, polypeptide 1
Cyp27a1	Cytochrome P450, family 27, subfamily a, polypeptide 1
Cyp2a4	Cytochrome P450, family 2, subfamily a, polypeptide 4
Cyp2a5	Cytochrome P450, family 2, subfamily a, polypeptide 5
Cyp2b20	Cytochrome P450, family 2, subfamily b, polypeptide 20
Cyp2b9	Cytochrome P450, family 2, subfamily b, polypeptide 9
Cyp2c37	Cytochrome P450, family 2, subfamily c, polypeptide 37
Cyp2c50	Cytochrome P450, family 2, subfamily c, polypeptide 50
Cyp2c54	Cytochrome P450, family 2, subfamily c, polypeptide 54
Cyp2c55	Cytochrome P450, family 2, subfamily c, polypeptide 55
Cyp2d13	Cytochrome P450, family 2, subfamily d, polypeptide 13
Cyp2e1	Cytochrome P450, family 2, subfamily e, polypeptide 1
Cyp2f2	Cytochrome P450, family 2, subfamily f, polypeptide 2
Cyp2j9	Cytochrome P450, family 2, subfamily j, polypeptide 9
Cyp39a1	Cytochrome P450, family 39, subfamily a, polypeptide 1
Cyp3a11	Cytochrome P450, family 3, subfamily a, polypeptide 11
Cyp3a13	Cytochrome P450, family 3, subfamily a, polypeptide 13
Cyp3a16	Cytochrome P450, family 3, subfamily a, polypeptide 16
Cyp3a25	Cytochrome P450, family 3, subfamily a, polypeptide 25
Cyp4a10	Cytochrome P450, family 4, subfamily a, polypeptide 10
Cyp4a12	Cytochrome P450, family 4, subfamily a, polypeptide 12
Cyp4a12a	Cytochrome P450, family 4, subfamily a, polypeptide 12a
Cyp4a14	Cytochrome P450, family 4, subfamily a, polypeptide 14
Cyp4b1	Cytochrome P450, family 4, subfamily b, polypeptide 1
Cyp4f14	Cytochrome P450, family 4, subfamily f, polypeptide 14
Cyp4f15	Cytochrome P450, family 4, subfamily f, polypeptide 15
Cyp4v3	Cytochrome P450, family 4, subfamily v, polypeptide 3
Cyp51	Cytochrome P450, family 51, subfamily a, polypeptide 1
Cyp7a1	Cytochrome P450, family 7, subfamily a, polypeptide 1
Cyp7b1	Cytochrome P450, family 7, subfamily b, polypeptide 1

Cyp8b1	Cytochrome P450, family 8, subfamily b, polypeptide 1
D3ucla1	Stress-associated endoplasmic reticulum protein 1
Daf1	CD55 antigen
Dag1	Dystroglycan 1
Dbp	D site of albumin promoter binding protein
Dchs1	Dachsous cadherin-related 1
Dci	Enoyl-coa delta isomerase 1
Dcn	Decorin
Dct	Dopachrome tautomerase
Ddah1	Dimethylarginine dimethylaminohydrolase 1
Ddc	Dopa decarboxylase
Ddit3	DNA-damage-inducible transcript 3
Ddit4	DNA-damage-inducible transcript 4
Ddit4l	DNA-damage-inducible transcript 4-like
Decr1	2,4-dienoyl coa reductase 1, mitochondrial
Decr2	2,4-dienoyl coa reductase 2, peroxisomal
Dhodh	Dihydroorotate dehydrogenase
Dhrs6	3-hydroxybutyrate dehydrogenase, type 2
Dhrs8	Hydroxysteroid (17-beta) dehydrogenase 11
Dlat	Dihydrolipoamide S-acetyltransferase
Dlc1	DLC1 Rho gtpase activating protein
Dlst	Dihydrolipoamide S-succinyltransferase
Dmd	Dystrophin
Dnaja3	Dnaj homolog, subfamily A, member 3
Dnajb1	Dnaj homolog, subfamily B, member 1
Dnajb11	Dnaj homolog, subfamily B, member 11
Dnajb6	Dnaj homolog, subfamily B, member 6
Dnajb9	Dnaj homolog, subfamily B, member 9
Dnajc19	Dnaj homolog, subfamily C, member 19
Dnase2a	Deoxyribonuclease II alpha
Dnclc1	Dynein light chain LC8-type 1
Dnm1l	Dynamin 1-like
Dock4	Dedicator of cytokinesis 4

Dpyd	Dihydropyrimidine dehydrogenase
Drctnnb1a	Family with sequence similarity 126, member A
Dscr1l1	Regulator of calcineurin 2
Dscr5	Phosphatidylinositol glycan anchor biosynthesis, class P
Dsip1	TSC22 domain family, member 3
Dusp1	Dual specificity phosphatase 1
Dusp10	Dual specificity phosphatase 10
Dusp14	Dual specificity phosphatase 14
Dusp4	Dual specificity phosphatase 4
Dusp8	Dual specificity phosphatase 8
Dynll1	Dynein, light chain, LC8-type 1
E2f1	E2F transcription factor 1
Ear1	Eosinophil-associated, ribonuclease A family, member 1
Ear11	Eosinophil-associated, ribonuclease A family, member 11
Ear2	Eosinophil-associated, ribonuclease A family, member 2
Ebpl	Emopamil binding protein-like
Ece1	Endothelin converting enzyme 1
Ech1	Enoyl coa hydratase 1, peroxisomal
Echs1	Enoyl coa hydratase, short chain, 1, mitochondrial
Eef1b2	Eukaryotic translation elongation factor 1 beta 2
Eef2	Eukaryotic translation elongation factor 2
Efcbp1	N-terminal EF-hand calcium binding protein 1
Efha1	Mitochondrial calcium uptake 2
Efna5	Ephrin-A5
Efnb1	Ephrin-B1
Egr1	Early growth response 1
Ehhadh	Enoyl-coa, hydratase/3-hydroxyacyl coa dehydrogenase
Eif2c4	Argonaute RISC catalytic component 4
Eif2s1	Eukaryotic translation initiation factor 2, subunit 1 alpha
Eif3s2	Eukaryotic translation initiation factor 3, subunit I
Eif4ebp3	Eukaryotic translation initiation factor 4E binding protein 3
Eif4g2	Eukaryotic translation initiation factor 4 gamma, 2
Ela1	Chymotrypsin-like elastase family, member 1

Elavl4	ELAV like neuron-specific RNA binding protein 4
Ell	Elongation factor RNA polymerase II
Ell3	Elongation factor RNA polymerase II-like 3
Eln	Elastin
Elovl2	ELOVL fatty acid elongase 2
Elovl3	ELOVL fatty acid elongase 3
Elovl5	ELOVL fatty acid elongase 5
Eltd1	EGF, latrophilin and seven transmembrane domain containing 1
Elys	AT hook containing transcription factor 1
Emcn	Endomucin
Eml4	Echinoderm microtubule associated protein like 4
Enc1	Ectodermal-neural cortex 1 (with BTB domain)
Enpp3	Ectonucleotide pyrophosphatase/phosphodiesterase 3
Entpd8	Ectonucleoside triphosphate diphosphohydrolase 8
Epha1	EPH receptor A1
Epha10	EPH receptor A10
Ercc1	Excision repair cross-complementation group 1
Ern1	Endoplasmic reticulum to nucleus signaling 1
Es22	Carboxylesterase 1E
Esm1	Endothelial cell-specific molecule 1
Esrra	Estrogen-related receptor alpha
Etfb	Electron-transfer-flavoprotein, beta polypeptide
Etfdh	Electron-transferring-flavoprotein dehydrogenase
Ethe1	Ethylmalonic encephalopathy 1
Exoc8	Exocyst complex component 8
Exosc5	Exosome component 5
Ezh2	Enhancer of zeste homolog 2
F11r	F11 receptor
F5	Coagulation factor V
Fabp4	Fatty acid binding protein 4
Fabp5	Fatty acid binding protein 5
Fads1	Fatty acid desaturase 1

Fads2	Fatty acid desaturase 2
Fah	Fumarylacetoacetate hydrolase
Falz	Bromodomain PHD finger transcription factor
Fam166b	Family with sequence similarity 166, member B
Fas	Fas cell surface death receptor
Fasn	Fatty acid synthase
Fbf1	Fas binding factor 1
Fbp1	Fructose-1,6-bisphosphatase 1
Fbp2	Fructose-1,6-bisphosphatase 2
Fbp3	Far upstream element binding protein 3
Fbxo21	F-box protein 21
Fbxo31	F-box protein 31
Fbxw4	F-box and WD repeat domain containing 4
Fcer1g	Fc fragment of ige
Fcna	Ficolin A
Fdps	Farnesyl diphosphate synthase
Fdxr	Ferredoxin reductase
Fez1	Fasciculation and elongation protein zeta 1
Fgd6	FYVE, rhogef and PH domain containing 6
Fgf16	Fibroblast growth factor 16
Fgfr2	Fibroblast growth factor receptor 2
Fgfrl1	Fibroblast growth factor receptor-like 1
Fgl1	Fibrinogen-like 1
Fibp	Fibroblast growth factor intracellular binding protein
Fkbp11	FK506 binding protein 11
Fkbp4	FK506 binding protein 4
Flt1	Fms-related tyrosine kinase 1
Fn1	Fibronectin 1
Fn3k	Fructosamine 3 kinase
Folr2	Folate receptor 2
Fos	FBJ murine osteosarcoma viral oncogene homolog
Fosl2	FOS-like antigen 2
Foxa2	Forkhead box A2

Fpr-rs2	Formyl peptide receptor 2
Fpr-rs7	Formyl peptide receptor 7
Fscn1	Fascin actin-bundling protein 1
Fst	Follistatin
Ftcd	Formimidoyltransferase cyclodeaminase
Fus	FUS RNA binding protein
Fvt1	3-ketodihydrosphingosine reductase
Fxyd1	FXYD domain containing ion transport regulator 1
Fxyd3	FXYD domain containing ion transport regulator 3
Fzd6	Frizzled class receptor 6
Fzr1	Fizzy/cell division cycle 20 related 1 (Drosophila)
G0s2	G0/G1 switch 2
G1p2	ISG15 ubiquitin-like modifier
G6pc	Glucose-6-phosphatase, catalytic subunit
G6pc2	Glucose-6-phosphatase, catalytic, 2
G6pc3	Glucose 6 phosphatase, catalytic, 3
Gabpa	GA binding protein transcription factor, alpha subunit
Gadd45a	Growth arrest and DNA-damage-inducible, alpha
Gal3st1	Galactose-3-O-sulfotransferase 1
Gale	UDP-galactose-4-epimerase
Galk1	Galactokinase 1
Galm	Galactose mutarotase
Galns	Galactosamine (N-acetyl)-6-sulfatase
Galnt10	Polypeptide N-acetylgalactosaminyltransferase 10
Galt	Galactose-1-phosphate uridylyltransferase
Gart	Phosphoribosylglycinamide formyltransferase
Gas2	Growth arrest-specific 2
Gas6	Growth arrest-specific 6
Gata4	GATA binding protein 4
Gba	Glucosidase, beta, acid
Gck	Glucokinase
Gckr	Glucokinase regulator
Gclm	Glutamate-cysteine ligase, modifier subunit

Gcs1	Mannosyl-oligosaccharide glucosidase
Gda	Guanine deaminase
Gdf15	Growth differentiation factor 15
Gdi1	GDP dissociation inhibitor 1
Ggta1	Glycoprotein, alpha-galactosyltransferase 1 pseudogene
Ggtla1	Gamma-glutamyltransferase 5
Ghr	Growth hormone receptor
Ghrl	Ghrelin/obestatin prepropeptide
Gig2	Tribbles pseudokinase 1
Glb1	Galactosidase, beta 1
Gldc	Glycine dehydrogenase
Gls2	Glutaminase 2
Gm2a	GM2 ganglioside activator
Gna14	Guanine nucleotide binding protein, alpha 14
Gnas	GNAS complex locus
Gnat1	Guanine nucleotide binding protein, alpha transducing activity polypeptide 1
Gnb3	Guanine nucleotide binding protein, beta polypeptide 3
Gnb4	Guanine nucleotide binding protein, beta polypeptide 4
Gne	Glucosamine (UDP-N-acetyl)-2-epimerase/N-acetylmannosamine kinase
Gng11	Guanine nucleotide binding protein (G protein), gamma 11
Gnl3	Guanine nucleotide binding protein-like 3 (nucleolar)
Gnmt	Glycine N-methyltransferase
Gosr2	Golgi SNAP receptor complex member 2
Gpc1	Glypican 1
Gpc4	Glypican 4
Gpc6	Glypican 6
Gpd	Atypical chemokine receptor 1
Gpd1	Glycerol-3-phosphate dehydrogenase 1
Gpd2	Glycerol-3-phosphate dehydrogenase 2
Gpi1	Phosphatidylinositol glycan anchor biosynthesis, class Q
Gpiap1	Cell cycle associated protein 1

Gpihbp1	Glycosylphosphatidylinositol anchored high density lipoprotein binding protein 1
Gpkow	G patch domain and KOW motifs
Gpr116	G protein-coupled receptor 116
Gpr125	G protein-coupled receptor 125
Gpr126	G protein-coupled receptor 126
Gpr146	G protein-coupled receptor 146
Gpr160	G protein-coupled receptor 160
Gpr22	G protein-coupled receptor 22
Gpr23	Lysophosphatidic acid receptor 4
Gprc5b	G protein-coupled receptor, class C, group 5, member B
Gpt1	Glutamic-pyruvate transaminase
Gpx7	Glutathione peroxidase 7
Grap2	GRB2-related adaptor protein 2
Gsdmdc1	Gasdermin D
Gsn	Gelsolin
Gsr	Glutathione reductase
Gss	Glutathione synthetase
Gsta1	Glutathione S-transferase alpha 1
Gsta2	Glutathione S-transferase alpha 2
Gsta3	Glutathione S-transferase alpha 3
Gstm1	Glutathione S-transferase mu 1
Gstm2	Glutathione S-transferase mu 2
Gstm4	Glutathione S-transferase mu 4
Gstm6	Glutathione S-transferase, mu 6
Gstp1	Glutathione S-transferase pi 1
Gstp2	Glutathione S-transferase, pi 2
Gstt1	Glutathione S-transferase theta 1
Gstt2	Glutathione S-transferase theta 2
Gstt3	Glutathione S-transferase, theta 3
Gstz1	Glutathione S-transferase zeta 1
Gulo	Gulonolactone (L-) oxidase
Gyg1	Glycogenin 1

Gyk	Glycerol kinase
Gys1	Glycogen synthase 1
H2-Aa	Histocompatibility 2, class II antigen A, alpha
H2-Ab1	Histocompatibility 2, class II antigen A, beta 1
H2afv	H2A histone family, member V
H2-Eb1	Histocompatibility 2, class II antigen E, beta
H2-Q2	Histocompatibility 2, Q region locus 2
H3f3b	H3 histone, family 3B
Hadh2	Hydroxysteroid (17-beta) dehydrogenase 10
Hadha	Hydroxyacyl-coa dehydrogenase/3-ketoacyl-coa thiolase/enoyl-coa hydratase (trifunctional protein), alpha subunit
Hadhsc	Hydroxyacyl-coa dehydrogenase
Hal	Histidine ammonia-lyase
Hamp2	Hepcidin antimicrobial peptide 2
Hapln4	Hyaluronan and proteoglycan link protein 4
Hax1	HCLS1 associated protein X-1
Hba-A1	Hemoglobin alpha, adult chain 1
Hbb-B1	Hemoglobin, beta adult major chain
Hccs	Holocytochrome c synthase
Hcn4	Hyperpolarization activated cyclic nucleotide gated potassium channel 4
Hdac11	Histone deacetylase 11
Hdac6	Histone deacetylase 6
Hdc	Histidine decarboxylase
Hdhd3	Haloacid dehalogenase-like hydrolase domain containing 3
Herc3	HECT and RLD domain containing E3 ubiquitin protein ligase 3
Herpud1	Homocysteine-inducible, endoplasmic reticulum stress-inducible, ubiquitin-like domain member 1
Hes6	Hes family bhlh transcription factor 6
Hgfac	HGF activator
Hhex	Hematopoietically expressed homeobox

Hibadh	3-hydroxyisobutyrate dehydrogenase
Hip1r	Huntingtin interacting protein 1 related
Hist1h2ad	Histone cluster 1, h2ad
Hist1h2af	Histone cluster 1, h2af
Hist1h2ag	Histone cluster 1, h2ag
Hist1h2ah	Histone cluster 1, h2ah
Hist1h2ai	Histone cluster 1, h2ai
Hist1h2ak	Histone cluster 1, h2ak
Hist1h2an	Histone cluster 1, h2an
Hist1h2ao	Histone cluster 1, h2ao
Hist1h2bc	Histone cluster 1, h2bc
Hist1h3f	Histone cluster 1, h3f
Hist1h4h	Histone cluster 1, h4h
Hist1h4i	Histone cluster 1, h4i
Hist1h4j	Histone cluster 1, h4j
Hist2h2ab	Histone cluster 2, h2ab
Hk2	Hexokinase 2
Hlcs	Holocarboxylase synthetase
Hmbs	Hydroxymethylbilane synthase
Hmgcl	3-hydroxymethyl-3-methylglutaryl-coa lyase
Hmgcs1	3-hydroxy-3-methylglutaryl-coa synthase 1
Hmgcs2	3-hydroxy-3-methylglutaryl-coa synthase 2
Hmgn1	High mobility group nucleosome binding domain 1
Hmox2	Heme oxygenase 2
Hnf4a	Hepatocyte nuclear factor 4, alpha
Hoxd10	Homeobox D10
Hprt	Hypoxanthine phosphoribosyltransferase 1
Hr	Hair growth associated
Hsd11b1	Hydroxysteroid (11-beta) dehydrogenase 1
Hsd17b11	Hydroxysteroid (17-beta) dehydrogenase 11
Hsd17b2	Hydroxysteroid (17-beta) dehydrogenase 2
Hsf1	Heat shock transcription factor 1
Hsp105	Heat shock 105kda/110kda protein 1

Hspa1a	Heat shock 70kda protein 1A
Hspa1b	Heat shock 70kda protein 1B
Hspa1l	Heat shock 70kda protein 1-like
Hspa4	Heat shock 70kda protein 4
Hspa5	Heat shock 70kda protein 5
Hspa8	Heat shock 70kda protein 8
Hspa9a	Heat shock protein 9
Htatip2	HIV-1 Tat interactive protein 2, 30kda
Hyal1	Hyaluronoglucosaminidase 1
Hyou1	Hypoxia up-regulated 1
Iars	Isoleucyl-trna synthetase
Icam1	Intercellular adhesion molecule 1
Idb1	Inhibitor of DNA binding 1
Idb2	Inhibitor of DNA binding 2
Idb3	Inhibitor of DNA binding 3
Idh1	Isocitrate dehydrogenase 1 (NADP+)
Idh3b	Isocitrate dehydrogenase 3 (NAD+) beta
Idi1	Isopentenyl-diphosphate delta isomerase 1
Idi2	Isopentenyl-diphosphate delta isomerase 2
Ifi205	Interferon activated gene 205
Ifitm2	Interferon induced transmembrane protein 2
Ifitm3	Interferon induced transmembrane protein 3
Ift81	Intraflagellar transport 81
Igf1	Insulin-like growth factor 1
Igf2bp2	Insulin-like growth factor 2 mrna binding protein 2
Igfals	Insulin-like growth factor binding protein
Igfbp2	Insulin-like growth factor binding protein 2
Igfbp4	Insulin-like growth factor binding protein 4
Igfbp5	Insulin-like growth factor binding protein 5
Igfbp7	Insulin-like growth factor binding protein 7
Igh-6	Immunoglobulin heavy constant mu
Igsf1	Immunoglobulin superfamily, member 1
Ihpk1	Inositol hexakisphosphate kinase 1

Ikbkb	Inhibitor of kappa light polypeptide gene enhancer in B-cells, kinase beta
Ikbke	Inhibitor of kappa light polypeptide gene enhancer in B-cells, kinase epsilon
Il10rb	Interleukin 10 receptor, beta
Il13ra2	Interleukin 13 receptor, alpha 2
Il17e	Interleukin 25
Il17rb	Interleukin 17 receptor B
Il18	Interleukin 18
Il1a	Interleukin 1, alpha
Il1b	Interleukin 1, beta
Il1rap	Interleukin 1 receptor accessory protein
Il1rn	Interleukin 1 receptor antagonist
Il6ra	Interleukin 6 receptor, alpha
Impa2	Inositol(myo)-1(or 4)-monophosphatase 2
Impact	Impact RWD domain protein
Inhba	Inhibin, beta A
Inhbc	Inhibin, beta C
Inhbe	Inhibin, beta E
Inmt	Indolethylamine N-methyltransferase
Inpp4a	Inositol polyphosphate-4-phosphatase, type I, 107kda
Inpp5f	Inositol polyphosphate-5-phosphatase F
Insig1	Insulin induced gene 1
Insig2	Insulin induced gene 2
Insr	Insulin receptor
Iqce	IQ motif containing E
Irak4	Interleukin-1 receptor-associated kinase 4
Irf1	Interferon regulatory factor 1
Irf2	Interferon regulatory factor 2
Irf2bp2	Interferon regulatory factor 2 binding protein 2
Irs2	Insulin receptor substrate 2
Irx3	Iroquois homeobox 3
Itgb3	Integrin, beta 3

Itgb3bp	Integrin beta 3 binding protein
Itgb6	Integrin, beta 6
Itih4	Inter-alpha-trypsin inhibitor heavy chain family, member 4
Itpka	Inositol-trisphosphate 3-kinase A
Ivd	Isovaleryl-coa dehydrogenase
Iyd	Iodotyrosine deiodinase
Kazald1	Kazal-type serine peptidase inhibitor domain 1
Kcna1	Potassium channel, voltage gated shaker related subfamily A, member 1
Kcna5	Potassium channel, voltage gated shaker related subfamily A, member 5
Kcnh1	Potassium channel, voltage gated eag related subfamily H, member 1
Kcnj14	Potassium channel, inwardly rectifying subfamily J, member 14
Kcnk1	Potassium channel, two pore domain subfamily K, member 1
Kcnk18	Potassium channel, two pore domain subfamily K, member 18
Kcnk5	Potassium channel, two pore domain subfamily K, member 5
Kcnk6	Potassium channel, two pore domain subfamily K, member 6
Kcnmb1	Potassium channel subfamily M regulatory beta subunit 1
Kcnn2	Potassium channel, calcium activated intermediate, member 2
Kcnn4	Potassium channel, calcium activated intermediate, member 4
Kcnq5	Potassium channel, voltage gated KQT-like subfamily Q, member 5
Kcns2	Potassium voltage-gated channel, modifier subfamily S, member 2
Kctd12	Potassium channel tetramerization domain containing 12
Kdelc2	KDEL containing 2
Khk	Ketohexokinase
Kif21a	Kinesin family member 21A
Kitl	KIT ligand
Klf12	Kruppel-like factor 12
Klf2	Kruppel-like factor 2
Klk24	Kallikrein 1-related peptidase b24

Klra10	Killer cell lectin-like receptor subfamily A, member 10
Klra12	Killer cell lectin-like receptor subfamily A, member 12
Klra3	Killer cell lectin-like receptor, subfamily A, member 3
Knsl5	Kinesin family member 23
Kpna2	Karyopherin alpha 2
Krt1-18	Keratin 18
Krt1-23	Keratin 23
Krt39	Keratin 39, type I
Krt8	Keratin 8, type II
Kynu	Kynureninase
Lama3	Laminin, alpha 3
Lamb2	Laminin, beta 2
Laptm5	Lysosomal protein transmembrane 5
Lbh	Limb bud and heart development
Lbr	Lamin B receptor
Lcn2	Lipocalin 2
Ldlr	Low density lipoprotein receptor
Leng4	Membrane bound O-acyltransferase domain containing 7
Leng9	Leukocyte receptor cluster member 9
Lep	Leptin
Lgals1	Lectin, galactoside-binding, soluble, 1
Lgals3bp	Lectin, galactoside-binding, soluble, 3 binding protein
Lgals4	Lectin, galactoside-binding, soluble, 4
Lgals8	Lectin, galactoside-binding, soluble, 8
Lgals9	Lectin, galactoside-binding, soluble, 9
Limk1	LIM domain kinase 1
Lipf	Lipase, gastric
Lman1	Lectin, mannose-binding, 1
Lnp	Nucleolar and spindle associated protein 1
Loxl1	Lysyl oxidase-like 1
Loxl4	Lysyl oxidase-like 4
Lpin1	Lipin 1
Lpl	Lipoprotein lipase

Lpp	LIM domain containing preferred translocation partner in lipoma
Lrfn3	Leucine rich repeat and fibronectin type III domain containing 3
Lrg1	Leucine-rich alpha-2-glycoprotein 1
Lrig1	Leucine-rich repeats and immunoglobulin-like domains 1
Lrp1	Low density lipoprotein receptor-related protein 1
Lrp12	Low density lipoprotein receptor-related protein 12
Lrp4	Low density lipoprotein receptor-related protein 4
Lrrc21	Leucine-rich repeat, immunoglobulin-like and transmembrane domains 1
Lrrc22	Leucine-rich repeat, immunoglobulin-like and transmembrane domains 2
Lrrfip1	Leucine rich repeat interacting protein 1
Lrrn4	Leucine rich repeat neuronal 4
Lsm1	LSM1, U6 small nuclear RNA associated
Lss	Lanosterol synthase (
Luc7l	LUC7-like (S. Cerevisiae)
Luc7l2	LUC7-like 2 (S. Cerevisiae)
Ly6e	Lymphocyte antigen 6 complex, locus E
Lypla1	Lysophospholipase I
Lyrm5	LYR motif containing 5
Lzf	Rogdi homolog (Drosophila)
Magee1	Melanoma antigen family E, 1
Man1a	Mannosidase 1, alpha
Manba	Mannosidase, beta A, lysosomal
Map3k6	Mitogen-activated protein kinase kinase kinase 6
Map3k7ip2	TGF-beta activated kinase 1/MAP3K7 binding protein 2
Mapk11	Mitogen-activated protein kinase 11
Mapk9	Mitogen-activated protein kinase 9
Mapkapk5	Mitogen-activated protein kinase-activated protein kinase 5
Mapkbp1	Mitogen-activated protein kinase binding protein 1
Marcks	Myristoylated alanine-rich protein kinase C substrate

Masp1	Mannan-binding lectin serine peptidase 1
Mast3	Microtubule associated serine/threonine kinase 3
Mat2a	Methionine adenosyltransferase II, alpha
Matk	Megakaryocyte-associated tyrosine kinase
Matn3	Matrilin 3
Matn4	Matrilin 4
Mbd1	Methyl-cpg binding domain protein 1
Mbd3l2	Methyl-cpg binding domain protein 3-like 2
Mbl2	Mannose-binding lectin (protein C) 2
Mbnl1	Muscleblind-like splicing regulator 1
Mbtps2	Membrane-bound transcription factor peptidase, site 2
Mcc	Mutated in colorectal cancers
Mcl1	Myeloid cell leukemia 1
Mcm6	Minichromosome maintenance complex component 6
Mdm1	Mdm1 nuclear protein homolog
Mef2a	Myocyte enhancer factor 2A
Mef2c	Myocyte enhancer factor 2C
Megf11	Multiple EGF-like-domains 11
Memo1	Mediator of cell motility 1
Mettl4	Methyltransferase like 4
Mgll	Monoglyceride lipase
Mgst3	Microsomal glutathione S-transferase 3
Mid1	Midline 1
Midn	Midnolin
Mif	Macrophage migration inhibitory factor
Mif4gd	MIF4G domain containing
Minpp1	Multiple inositol-polyphosphate phosphatase 1
Mir16	Glycerophosphodiester phosphodiesterase 1
Mknk2	MAP kinase interacting serine/threonine kinase 2
Mllt10	Myeloid/lymphoid or mixed-lineage leukemia, translocated to, 10
Mlxipl	MLX interacting protein-like
Mlycd	Malonyl-coa decarboxylase

Mmd	Monocyte to macrophage differentiation-associated
Mmd2	Monocyte to macrophage differentiation-associated 2
Mmp3	Matrix metallopeptidase 3
Mocs1	Molybdenum cofactor synthesis 1
Mod1	Chromobox homolog 1
Mogat1	Monoacylglycerol O-acyltransferase 1
Mon1b	MON1 secretory trafficking family member B
Moxd1	Monooxygenase, DBH-like 1
Mpc2	Mitochondrial pyruvate carrier 2
Mpra	Progestin and adipoq receptor family member VII
Mrc1	Mannose receptor, C type 1
Mre11a	MRE11 meiotic recombination 11 homolog A (S. Cerevisiae)
Mreg	Melanoregulin
Mrpl17	Mitochondrial ribosomal protein L17
Mrpl46	Mitochondrial ribosomal protein L46
Ms4a4c	Membrane-spanning 4-domains, subfamily A, member 4C
Msc	Musculin
Mscp	Solute carrier family 25, member 37
Mt1	Metallothionein 1
Mt2	Metallothionein 2
Mt4	Metallothionein 4
Mtap6	Microtubule-associated protein 6
mt-Co2	Mitochondrially encoded cytochrome c oxidase II
mt-Co3	Mitochondrially encoded cytochrome c oxidase III
Mtl5	Metallothionein-like 5
mt-Nd1	Mitochondrially encoded NADH dehydrogenase 1
mt-Nd4	Mitochondrially encoded NADH dehydrogenase 4
Mug2	Murinoglobulin 2
Mup3	Major urinary protein 3
Mvd	Mevalonate decarboxylase
Mvp	Major vault protein
Myadm	Myeloid-associated differentiation marker
Mybpc3	Myosin binding protein C

Myd88	Myeloid differentiation primary response 88
Myh11	Myosin, heavy chain 11
Myh6	Myosin, heavy chain 6
Myh8	Myosin, heavy chain 8
Myl2	Myosin, light chain 2
Myl4	Myosin, light chain 4
Myl6	Myosin, light chain 6
Myl7	Myosin, light chain 7
Myl9	Myosin, light chain 9
Mylk	Myosin light chain kinase
Myo1b	Myosin IB
Myo9a	Myosin IXA
Myom3	Myomesin 3
N4bp2l2	NEDD4 binding protein 2-like 2
Nags	N-acetylglutamate synthase
Nanog	Nanog homeobox
Narg1	N(alpha)-acetyltransferase 15, nata auxiliary subunit
Ncor1	Nuclear receptor corepressor 1
Ndfip2	Nedd4 family interacting protein 2
Ndrg1	N-myc downstream regulated 1
Ndst1	N-deacetylase/N-sulfotransferase 1
Ndufb3	NADH dehydrogenase 1 beta subcomplex, 3
Ndufb5	NADH dehydrogenase 1 beta subcomplex, 5
Ndufs2	NADH dehydrogenase Fe-S protein 2
Nedd4l	Neural precursor cell expressed, developmentally down-regulated 4-like, E3 ubiquitin protein ligase
Nedd9	Neural precursor cell expressed, developmentally down-regulated 9
Nek9	NIMA-related kinase 9
Nenf	Neudesin neurotrophic factor
Nes	Nestin
Net1	Neuroepithelial cell transforming 1
Neu1	Sialidase 1

Neu2	Sialidase 2
Nfe2	Nuclear factor, erythroid 2
Nfil3	Nuclear factor, interleukin 3 regulated
Nfix	Nuclear factor I/X (CCAAT-binding transcription factor)
Nfkbiz	Nuclear factor of kappa light polypeptide gene enhancer in B-cells inhibitor, zeta
Ngfa	Kallikrein 1-related pepidase b4
Ngfr	Nerve growth factor receptor
Nln	Neurolysin
Nnmt	Nicotinamide N-methyltransferase
Nol5	NOP58 ribonucleoprotein
Nol6	Nucleolar protein 6
Nola1	GAR1 ribonucleoprotein
Nostrin	Nitric oxide synthase trafficking
Nox4	NADPH oxidase 4
Npas2	Neuronal PAS domain protein 2
Nphs2	Nephrosis 2
Npr3	Natriuretic peptide receptor 3
Nr1d1	Nuclear receptor subfamily 1, group D, member 1
Nr1d2	Nuclear receptor subfamily 1, group D, member 2
Nr1i3	Nuclear receptor subfamily 1, group I, member 3
Nr4a1	Nuclear receptor subfamily 4, group A, member 1
Nrarp	NOTCH-regulated ankyrin repeat protein
Nrn1	Neuritin 1
Nsbp1	High mobility group nucleosome binding domain 5
Nsdhl	NAD(P) dependent steroid dehydrogenase-like
Nt5e	5'-nucleotidase, ecto
Ntrk2	Neurotrophic tyrosine kinase, receptor, type 2
Nubp2	Nucleotide binding protein 2
Nucks1	Nuclear casein kinase and cyclin-dependent kinase substrate 1
Nudt12	Nudix-type motif 12
Nudt4	Nudix-type motif 4

Nup133	Nucleoporin 133kda
Nup37	Nucleoporin 37kda
Nup93	Nucleoporin 93kda
Nxt2	Nuclear transport factor 2-like export factor 2
Oas2	2'-5'-oligoadenylate synthetase 2
Oaz2	Ornithine decarboxylase antizyme 2
Odc1	Ornithine decarboxylase 1
Odd1	Odd-skipped related 1 (Drosophila)
Ogn	Osteoglycin
Olfm3	Olfactomedin 3
Olfml1	Olfactomedin-like 1
Olfml2b	Olfactomedin-like 2B
Olig1	Oligodendrocyte transcription factor 1
Oplah	5-oxoprolinase
Orm1	Orosomucoid 1
Orm2	Orosomucoid 2
Osbpl1a	Oxysterol binding protein-like 1A
Osbpl3	Oxysterol binding protein-like 3
Osr1	Odd-skipped related transciption factor 1
Ostb	Solute carrier family 51, beta subunit
P2ry1	Purinergic receptor P2Y, G-protein coupled, 1
P2ry13	Purinergic receptor P2Y, G-protein coupled, 13
P2ry5	Lysophosphatidic acid receptor 6
P4ha1	Prolyl 4-hydroxylase, alpha polypeptide I
Pacsin3	Protein kinase C and casein kinase substrate in neurons 3
Pah	Phenylalanine hydroxylase
Paics	Phosphoribosylaminoimidazole carboxylase
Paox	Polyamine oxidase
Papss2	3'-phosphoadenosine 5'-phosphosulfate synthase 2
Paqr9	Progestin and adipoq receptor family member IX
Parp3	Poly (ADP-ribose) polymerase family, member 3
Pax6	Paired box 6
Pcdh12	Protocadherin 12

Pcmt1	Protein-L-isoaspartate O-methyltransferase
Pcp4l1	Purkinje cell protein 4 like 1
Pcsk2	Proprotein convertase subtilisin/kexin type 2
Pcsk4	Proprotein convertase subtilisin/kexin type 4
Pcx	Pyruvate carboxylase
Pdcd1lg1	CD274 molecule
Pde4b	Phosphodiesterase 4B
Pde8a	Phosphodiesterase 8A
Pdha1	Pyruvate dehydrogenase alpha 1
Pdhb	Pyruvate dehydrogenase beta
Pdia5	Protein disulfide isomerase family A, member 5
Pdk1	Pyruvate dehydrogenase kinase, isozyme 1
Pdk4	Pyruvate dehydrogenase kinase, isozyme 4
Pdpr	Pyruvate dehydrogenase phosphatase regulatory subunit
Peci	Enoyl-coa delta isomerase 2
Peg3	Paternally expressed 3
Peli1	Pellino E3 ubiquitin protein ligase 1
Per1	Period circadian clock 1
Per2	Period circadian clock 2
Per3	Period circadian clock 3
Pes1	Pescadillo ribosomal biogenesis factor 1
Pet112l	Glutamyl-trna amidotransferase, subunit B
Pex11a	Peroxisomal biogenesis factor 11 alpha
Pex16	Peroxisomal biogenesis factor 16
Pfc	Complement factor properdin
Pfkfb1	6-phosphofructo-2-kinase/fructose-2,6-biphosphatase 1
Pfkfb2	6-phosphofructo-2-kinase/fructose-2,6-biphosphatase 2
Pfkfb3	6-phosphofructo-2-kinase/fructose-2,6-biphosphatase 3
Pfkl	Phosphofructokinase, liver
Pfkm	Phosphofructokinase, muscle
Pfkp	Phosphofructokinase, platelet
Pgm3	Phosphoglucomutase 3
Phka2	Phosphorylase kinase, alpha 2

Phkb	Phosphorylase kinase, beta
Phkg1	Phosphorylase kinase, gamma 1
Phlda1	Pleckstrin homology-like domain, family A, member 1
Pi16	Peptidase inhibitor 16
Pi4k2b	Phosphatidylinositol 4-kinase type 2 beta
Pigr	Polymeric immunoglobulin receptor
Pim3	Pim-3 proto-oncogene, serine/threonine kinase
Pipox	Pipecolic acid oxidase
Pja2	Praja ring finger 2, E3 ubiquitin protein ligase
Pkd2	Polycystic kidney disease 2
Pkig	Protein kinase inhibitor gamma
Pkp4	Plakophilin 4
Pla2g12a	Phospholipase A2, group XIIA
Pla2g6	Phospholipase A2, group VI
Plekhg3	Pleckstrin homology domain containing, family G, member 3
Plg	Plasminogen
Plscr1	Phospholipid scramblase 1
Plscr2	Phospholipid scramblase 2
Pltp	Phospholipid transfer protein
Plxna1	Plexin A1
Pnpla2	Patatin-like phospholipase domain containing 2
Pnpo	Pyridoxamine 5'-phosphate oxidase
Polg2	Polymerase, gamma 2, accessory subunit
Polr2a	Polymerase (RNA) II, polypeptide A
Polr2e	Polymerase (RNA) II, polypeptide E
Por	P450 (cytochrome) oxidoreductase
Postn	Periostin, osteoblast specific factor
Pou5f1	POU class 5 homeobox 1
Ppa2	Pyrophosphatase 2
Ppara/α	Peroxisome proliferator-activated receptor alpha
Pparbp	Mediator complex subunit 1
Pparg/γ	Peroxisome proliferator-activated receptor gamma

Ppargc1b	Peroxisome proliferator-activated receptor gamma, coactivator 1 beta
Ppfia1	Protein tyrosine phosphatase, receptor type, f polypeptide, interacting protein, alpha 1
Ppfibp1	PTPRF interacting protein, binding protein 1
Pphln1	Periphilin 1
Ppia	Peptidylprolyl isomerase A
Ppib	Peptidylprolyl isomerase B
Ppm1k	Protein phosphatase, Mg2+/Mn2+ dependent, 1K
Ppm1l	Protein phosphatase, Mg2+/Mn2+ dependent, 1L
Ppnr	Per-pentamer repeat gene
Ppp1r10	Protein phosphatase 1, regulatory subunit 10
Ppp1r3b	Protein phosphatase 1, regulatory subunit 3B
Ppp1r3c	Protein phosphatase 1, regulatory subunit 3C
Ppp2r2d	Protein phosphatase 2, regulatory subunit B, delta
Ppp3ca	Protein phosphatase 3, catalytic subunit, alpha isozyme
Ppp3r1	Protein phosphatase 3, regulatory subunit B, alpha
Prc1	Protein regulator of cytokinesis 1
Prdx3	Peroxiredoxin 3
Prdx6	Peroxiredoxin 6
Prg1	Immediate early response 3
Prg4	Proteoglycan 4
Prkra	Protein kinase, interferon-inducible double stranded RNA dependent activator
Prkrir	Protein-kinase, interferon-inducible double stranded RNA dependent inhibitor
Prnpip1	Exoribonuclease 3
Prss8	Protease, serine, 8
Prtn3	Proteinase 3
Prune	Prune exopolyphosphatase
Psen	Presenilin 1
Psma3	Proteasome subunit, alpha type, 3
Psma7	Proteasome subunit, alpha type, 7

Psmb2	Proteasome subunit, beta type, 2
Psmb7	Proteasome subunit, beta type, 7
Psmb8	Proteasome subunit, beta type, 8
Psmb9	Proteasome subunit, beta type, 9
Psmd4	Proteasome subunit, non-atpase, 4
Pte2a	Acyl-coa thioesterase 3
Pte2b	Acyl-coa thioesterase 4
Pter	Phosphotriesterase related
Ptgds	Prostaglandin D2 synthase
Ptgis	Prostaglandin I2 synthase
Ptgs1	Prostaglandin-endoperoxide synthase 1
Ptms	Parathymosin
Ptp4a2	Protein tyrosine phosphatase type IVA, member 2
Ptpla	3-hydroxyacyl-coa dehydratase 1
Ptpn11	Protein tyrosine phosphatase, non-receptor type 11
Pvrl2	Poliovirus receptor-related 2
Pygl	Phosphorylase, glycogen, liver
Qpct	Glutaminyl-peptide cyclotransferase
Qprt	Quinolinate phosphoribosyltransferase
Qscn6	Quiescin Q6 sulfhydryl oxidase 1
Rad52b	RAD52 motif containing 1
Raet1b	Retinoic acid early transcript beta
Raet1c	Retinoic acid early transcript gamma
Ranbp10	RAN binding protein 10
Rapgef4	Rap guanine nucleotide exchange factor 4
Rapgef5	Rap guanine nucleotide exchange factor 5
Rassf4	Ras association domain family member 4
Rassf5	Ras association domain family member 5
Rbp1	Retinol binding protein 1
Rbpms	RNA binding protein with multiple splicing
Rcbtb1	RCC and BTB domain containing protein 1
Rdh11	Retinol dehydrogenase 11
Rdh6	Retinol dehydrogenase 16

Rdh9	Retinol dehydrogenase 9
Rdx	Radixin
Refbp2	Aly/REF export factor 2
Rfc2	Replication factor C 2
Rgpr	SEC16 homolog B (S. Cerevisiae)
Rgs5	Regulator of G-protein signaling 5
Rgs9bp	Regulator of G protein signaling 9 binding protein
Rhbdd2	Rhomboid domain containing 2
Rhbdf1	Rhomboid 5 homolog 1 (Drosophila)
Rhob	Ras homolog family member B
Rhobtb1	Rho-related BTB domain containing 1
Rin3	Ras and Rab interactor 3
Rnase4	Ribonuclease, rnase A family, 4
Rnf125	Ring finger protein 125
Rnf40	Ring finger protein 40
Rora	RAR-related orphan receptor A
Rorc	RAR-related orphan receptor C
Rpain	RPA interacting protein
Rpl13a	Ribosomal protein l13a
Rpl23a	Ribosomal protein l23a
Rpn2	Ribophorin II
Rps17	Ribosomal protein S17
Rps2	Ribosomal protein S2
Rps7	Ribosomal protein S7
Rps8	Ribosomal protein S8
Rsad1	Radical S-adenosyl methionine domain containing 1
Rshl2	Radial spoke 3 homolog (Chlamydomonas)
Rtn4	Reticulon 4
Rtp3	Receptor transporter protein 3
Rxra	Retinoid X receptor, alpha
Ryd5	Secretoglobin, family 1C, member 1
Ryr2	Ryanodine receptor 2 (cardiac)
S100a8	S100 calcium binding protein A8

S100a9	S100 calcium binding protein A9
S3-12	Perilipin 4
Saa1	Serum amyloid A1
Saa2	Serum amyloid A2
Saa3	Serum amyloid A3
Saa4	Serum amyloid A4
Sag	S-antigen
Sah	Acyl-coa synthetase medium-chain family member 3
Sar1b	Secretion associated, Ras related gtpase 1B
Sardh	Sarcosine dehydrogenase
Sat1	Solute carrier family 38, member 1
Sc5d	Sterol-C5-desaturase
Scara5	Scavenger receptor class A, member 5
Scd1	Stearoyl-Coenzyme A desaturase 1
Scfd1	Sec1 family domain containing 1
Scn4b	Sodium channel, voltage gated, type IV beta subunit
Scnn1a	Sodium channel, non voltage gated 1 alpha subunit
Scnn1g	Sodium channel, non voltage gated 1 gamma subunit
Scp2	Sterol carrier protein 2
Sdc2	Syndecan 2
Sdc4	Syndecan 4
Sdha	Succinate dehydrogenase complex, subunit A, flavoprotein
Sdpr	Serum deprivation response
Sdro	Short chain dehydrogenase/reductase family 9C, member 7
Sds	Serine dehydratase
Sec14l4	SEC14-like 4 (S. Cerevisiae)
Sel1l	Sel-1 suppressor of lin-12-like (C. Elegans)
Sephs2	Selenophosphate synthetase 2
Sepp1	Selenoprotein P, plasma, 1
Sepx1	Methionine sulfoxide reductase B1
Serinc2	Serine incorporator 2
Serpina12	Serpin peptidase inhibitor, clade A, member 12
Serpina3g	Serine (or cysteine) peptidase inhibitor, clade A, member 3G

Serpina3m	Serine (or cysteine) peptidase inhibitor, clade A, member 3M
Serpina3n	Serine (or cysteine) peptidase inhibitor, clade A, member 3N
Serpina7	Serpin peptidase inhibitor, clade A, member 7
Serpinb1a	Serine (or cysteine) peptidase inhibitor, clade B, member 1a
Serpinb6b	Serine (or cysteine) peptidase inhibitor, clade B, member 6b
Serpinh1	Serpin peptidase inhibitor, clade H, member 1
Sertad2	SERTA domain containing 2
Sestd1	SEC14 and spectrin domains 1
Sfmbt1	Scm-like with four mbt domains 1
Sfrs5	Serine/arginine-rich splicing factor 5
Sfxn1	Sideroflexin 1
Sfxn2	Sideroflexin 2
Sgk	Serum/glucocorticoid regulated kinase 1
Sgk2	Serum/glucocorticoid regulated kinase 2
Sgpl1	Sphingosine-1-phosphate lyase 1
Sgsh	N-sulfoglucosamine sulfohydrolase
Sh3bgrl2	SH3 domain binding glutamate-rich protein like 2
Sh3gl2	SH3-domain GRB2-like 2
Shb	Src homology 2 domain containing adaptor protein B
Shmt1	Serine hydroxymethyltransferase 1
Si	Sucrase-isomaltase
Siat9	ST3 beta-galactoside alpha-2,3-sialyltransferase 5
Sin3a	SIN3 transcription regulator family member A
Siva	SIVA1, apoptosis-inducing factor
Slamf9	SLAM family member 9
Slc11a2	Solute carrier family 11 (proton-coupled divalent metal ion transporter), member 2
Slc13a4	Solute carrier family 13 (sodium/sulfate symporter), member 4
Slc16a1	Solute carrier family 16 (monocarboxylate transporter), member 1
Slc16a10	Solute carrier family 16 (aromatic amino acid transporter), member 10
Slc16a13	Solute carrier family 16, member 13

Slc16a2	Solute carrier family 16, member 2 (thyroid hormone transporter)
Slc16a3	Solute carrier family 16 (monocarboxylate transporter), member 3
Slc16a5	Solute carrier family 16 (monocarboxylate transporter), member 5
Slc16a6	Solute carrier family 16, member 6
Slc17a8	Solute carrier family 17 (vesicular glutamate transporter), member 8
Slc1a2	Solute carrier family 1 (glial high affinity glutamate transporter), member 2
Slc1a4	Solute carrier family 1 (glutamate/neutral amino acid transporter), member 4
Slc22a12	Solute carrier family 22 (organic anion/urate transporter), member 12
Slc22a5	Solute carrier family 22 (organic cation/carnitine transporter), member 5
Slc22a7	Solute carrier family 22 (organic anion transporter), member 7
Slc23a2	Solute carrier family 23 (ascorbic acid transporter), member 2
Slc25a10	Solute carrier family 25 (mitochondrial carrier; dicarboxylate transporter), member 10
Slc25a15	Solute carrier family 25 (mitochondrial carrier; ornithine transporter) member 15
Slc25a16	Solute carrier family 25 (mitochondrial carrier), member 16
Slc25a25	Solute carrier family 25 (mitochondrial carrier; phosphate carrier), member 25
Slc26a1	Solute carrier family 26 (anion exchanger), member 1
Slc27a1	Solute carrier family 27 (fatty acid transporter), member 1
Slc27a2	Solute carrier family 27 (fatty acid transporter), member 2
Slc28a2	Solute carrier family 28 (concentrative nucleoside transporter), member 2
Slc2a1	Solute carrier family 2 (facilitated glucose transporter), member 1

Slc2a2	Solute carrier family 2 (facilitated glucose transporter), member 2
Slc30a1	Solute carrier family 30 (zinc transporter), member 1
Slc30a10	Solute carrier family 30, member 10
Slc35b1	Solute carrier family 35, member B1
Slc37a4	Solute carrier family 37 (glucose-6-phosphate transporter), member 4
Slc39a10	Solute carrier family 39 (zinc transporter), member 10
Slc3a1	Solute carrier family 3 (amino acid transporter heavy chain), member 1
Slc41a2	Solute carrier family 41 (magnesium transporter), member 2
Slc44a1	Solute carrier family 44 (choline transporter), member 1
Slc4a1	Solute carrier family 4 (anion exchanger), member 1 (Diego blood group)
Slc4a3	Solute carrier family 4 (anion exchanger), member 3
Slc4a8	Solute carrier family 4, sodium bicarbonate cotransporter, member 8
Slc5a6	Solute carrier family 5 (sodium/multivitamin and iodide cotransporter), member 6
Slc6a12	Solute carrier family 6 (neurotransmitter transporter), member 12
Slc6a15	Solute carrier family 6 (neutral amino acid transporter), member 15
Slc6a6	Solute carrier family 6 (neurotransmitter transporter), member 6
Slc6a7	Solute carrier family 6 (neurotransmitter transporter), member 7
Slc6a9	Solute carrier family 6 (neurotransmitter transporter, glycine), member 9
Slc7a11	Solute carrier family 7 (anionic amino acid transporter light chain, xc- system), member 11
Slc8a1	Solute carrier family 8 (sodium/calcium exchanger), member 1
Slco1b2	Solute carrier organic anion transporter family, member 1b2

Slco2a1	Solute carrier organic anion transporter family, member 2a1
Slco2b1	Solute carrier organic anion transporter family, member 2B1
Slco3a1	Solute carrier organic anion transporter family, member 3A1
Slitl2	Vasorin
Slpi	Secretory leukocyte peptidase inhibitor
Smek1	SMEK homolog 1, suppressor of mek1 (Dictyostelium)
Smek2	SMEK homolog 2, suppressor of mek1 (Dictyostelium)
Sn	Sialic acid binding Ig-like lectin 1, sialoadhesin
Snai2	Snail family zinc finger 2
Snai3	Snail family zinc finger 3
Snca	Synuclein, alpha
Snn	Stannin
Snx10	Sorting nexin 10
Socs2	Suppressor of cytokine signaling 2
Sod2	Superoxide dismutase 2, mitochondrial
Sorbs1	Sorbin and SH3 domain containing 1
Sort1	Sortilin 1
Sox17	SRY-box 17
Sox18	SRY-box 18
Sparc	Secreted protein, acidic, cysteine-rich
Sparcl1	SPARC-like 1
Spata13	Spermatogenesis associated 13
Spire1	Spire-type actin nucleation factor 1
Spnb3	Spectrin beta, non-erythrocytic 2
Spon2	Spondin 2, extracellular matrix protein
Spp1	Secreted phosphoprotein 1
Srd5a2l	Steroid 5 alpha-reductase 3
Srgap2	SLIT-ROBO Rho gtpase activating protein 2
Ssfa1	NHP2 non-histone chromosome protein 2-like 1 (S. Cerevisiae)
St3gal4	ST3 beta-galactoside alpha-2,3-sialyltransferase 4
St5	Suppression of tumorigenicity 5
St7l	Suppression of tumorigenicity 7 like

St8sia4	ST8 alpha-N-acetyl-neuraminide alpha-2,8-sialyltransferase 4
Stard10	Star-related lipid transfer domain containing 10
Stat1	Signal transducer and activator of transcription 1
Stim1	Stromal interaction molecule 1
Stip1	Stress-induced phosphoprotein 1
Stk23	SRSF protein kinase 3
Stk3	Serine/threonine kinase 3
Sucla2	Succinate-coa ligase, ADP-forming, beta subunit
Suclg2	Succinate-coa ligase, GDP-forming, beta subunit
Sucnr1	Succinate receptor 1
Sulf2	Sulfatase 2
Sult1a1	Sulfotransferase family, cytosolic, 1A, phenol-preferring, member 1
Sult1b1	Sulfotransferase family, cytosolic, 1B, member 1
Supt3h	Suppressor of Ty 3 homolog (S. Cerevisiae)
Supt4h2	Suppressor of Ty 4 homolog 2 (S. Cerevisiae)
Synj2bp	Synaptojanin 2 binding protein
Syt15	Synaptotagmin XV
Sytl1	Synaptotagmin-like 1
Sytl4	Synaptotagmin-like 4
Taf13	TAF13 RNA polymerase II
Taf15	TAF15 RNA polymerase II
Taldo1	Transaldolase 1
Tax1bp3	Tax1 binding protein 3
Tbc1d8	TBC1 domain family, member 8
Tbx3	T-box 3
Tbxas1	Thromboxane A synthase 1
Tcap	Titin-cap
Tcea3	Transcription elongation factor A (SII), 3
Tcf15	Transcription factor 15
Tcfcp2l2	Grainyhead-like 1 (Drosophila)
Tdrkh	Tudor and KH domain containing
Tef	Thyrotrophic embryonic factor

Temt	Indolethylamine N-methyltransferase
Tes3	DCN1, defective in cullin neddylation 1, domain containing 1
Tesc	Tescalcin
Tfdp1	Transcription factor Dp-1
Tfrc	Transferrin receptor
Tgfb1i4	TSC22 domain family, member 1
Tgfbr3	Transforming growth factor, beta receptor III
Tgoln1	Trans-golgi network protein
Tgoln2	Trans-golgi network protein 2
Thbd	Thrombomodulin
Thbs1	Thrombospondin 1
Thbs3	Thrombospondin 3
Them2	Acyl-coa thioesterase 13
Thrsp	Thyroid hormone responsive
Tiam2	T-cell lymphoma invasion and metastasis 2
Timeless	Timeless circadian clock
Timp3	TIMP metallopeptidase inhibitor 3
Timp4	TIMP metallopeptidase inhibitor 4
Tjp1	Tight junction protein 1
Tkt	Transketolase
Tlcd1	TLC domain containing 1
Tln	Talin 1
Tlr2	Toll-like receptor 2
Tlr3	Toll-like receptor 3
Tlr5	Toll-like receptor 5
Tlr7	Toll-like receptor 7
Tm4sf3	Tetraspanin 8
Tmco3	Transmembrane and coiled-coil domains 3
Tmem134	Transmembrane protein 134
Tmem24	C2 calcium-dependent domain containing 2-like
Tmem25	Transmembrane protein 25
Tmem43	Transmembrane protein 43
Tmem7	Receptor (chemosensory) transporter protein 3

Tmem82	Transmembrane protein 82
Tmem86b	Transmembrane protein 86B
Tmem98	Transmembrane protein 98
Tmie	Transmembrane inner ear
Tmod1	Tropomodulin 1
Tmpit	Transmembrane protein 120A
Tmprss11f	Transmembrane protease, serine 11F
Tmprss2	Transmembrane protease, serine 2
Tmprss7	Transmembrane protease, serine 7
Tnfrsf10b	Tumor necrosis factor receptor superfamily, member 10b
Tnfrsf5	CD40 molecule, TNF receptor superfamily member 5
Tnni3	Troponin I type 3
Tomm7	Translocase of outer mitochondrial membrane 7 homolog (yeast)
Top1	Topoisomerase (DNA) I
Topbp1	Topoisomerase (DNA) II binding protein 1
Tox	Thymocyte selection-associated high mobility group box
Tpcn1	Two pore segment channel 1
Tpm1	Tropomyosin 1
Tpm2	Tropomyosin 2
Tpm4	Tropomyosin 4
Tpst1	Tyrosylprotein sulfotransferase 1
Tra1	Heat shock protein, member 1
Traf3	TNF receptor-associated factor 3
Tram1	Translocation associated membrane protein 1
Trappc4	Trafficking protein particle complex 4
Treh	Trehalase
Trf	Interleukin 5
Trib3	Tribbles pseudokinase 3
Trim25	Tripartite motif containing 25
Trp53inp1	Transformation related protein 53 inducible nuclear protein 1
Trp53inp2	Transformation related protein 53 inducible nuclear protein 2

Trpc3	Transient receptor potential cation channel, subfamily C, member 3
Trpc4ap	Transient receptor potential cation channel, subfamily C, member 4 associated protein
Trpm4	Transient receptor potential cation channel, subfamily M, member 4
Trpv2	Transient receptor potential cation channel, subfamily V, member 2
Trub2	Trub pseudouridine synthase family member 2
Tsc22d3	TSC22 domain family, member 3
Tspo	Translocator protein
Ttc3	Tetratricopeptide repeat domain 3
Ttr	Transthyretin
Ttyh3	Tweety family member 3
Tuba4	Tubulin, alpha 4b
Tuba6	Tubulin, alpha 1c
Tuft1	Tuftelin 1
Txndc7	Protein disulfide isomerase family A, member 6
Txnip	Thioredoxin interacting protein
Txnl4b	Thioredoxin-like 4B
Uap1l1	UDP-N-acetylglucosamine pyrophosphorylase 1 like 1
Ubd	Ubiquitin D
Ube1l	Ubiquitin-like modifier activating enzyme 7
Ube2c	Ubiquitin-conjugating enzyme E2C
Ube2d3	Ubiquitin-conjugating enzyme E2D 3
Ube2g2	Ubiquitin-conjugating enzyme E2G 2
Ube3a	Ubiquitin protein ligase E3A
Ucp3	Uncoupling protein 3
Ugcg	UDP-glucose ceramide glucosyltransferase
Ugdh	UDP-glucose 6-dehydrogenase
Ugp2	UDP-glucose pyrophosphorylase 2
Ugt1a1	UDP glucuronosyltransferase 1 family, polypeptide A1
Ugt1a10	UDP glucuronosyltransferase 1 family, polypeptide A10

Ugt1a2	UDP glucuronosyltransferase 1 family, polypeptide A2
Ugt1a5	UDP glucuronosyltransferase 1 family, polypeptide A5
Ugt1a6	UDP glucuronosyltransferase 1 family, polypeptide A6
Ugt1a6a	UDP glucuronosyltransferase 1 family, polypeptide A6A
Ugt1a9	UDP glucuronosyltransferase 1 family, polypeptide A9
Unc84b	Sad1 and UNC84 domain containing 2
Uox	Urate oxidase, pseudogene
Upf2	UPF2 regulator of nonsense transcripts homolog (yeast)
Upp1	Uridine phosphorylase 1
Upp2	Uridine phosphorylase 2
Uqcr	Ubiquinol-cytochrome c reductase, complex III subunit XI
Urml	Up-regulated in Myc liver
Ush2a	Usher syndrome 2A
Usp46	Ubiquitin specific peptidase 46
Usp6nl	USP6 N-terminal like
V1rd6	Vomeronasal 1 receptor 65
Vav2	Vav 2 guanine nucleotide exchange factor
Vegfa	Vascular endothelial growth factor A
Vegfb	Vascular endothelial growth factor B
Vim	Vimentin
Vldlr	Very low density lipoprotein receptor
Vnn3	Vanin 3
Vsig4	V-set and immunoglobulin domain containing 4
Wbscr21	Abhydrolase domain containing 11
Wdr51b	POC1 centriolar protein B
Wdr6	WD repeat domain 6
Wfdc12	WAP four-disulfide core domain 12
Wfdc15	WAP four-disulfide core domain 15B
Wrnip1	Werner helicase interacting protein 1
Wsb1	WD repeat and SOCS box containing 1
Xbp1	X-box binding protein 1
Xlkd1	Lymphatic vessel endothelial hyaluronan receptor 1

Xrcc3	X-ray repair complementing defective repair in Chinese hamster cells 3
Ybx3	Y box binding protein 3
Yod1	YOD1 deubiquitinase
Zap70	Zeta-chain associated protein kinase 70kda
Zbtb16	Zinc finger and BTB domain containing 16
Zdhhc13	Zinc finger, DHHC-type containing 13
Zfp2	ZFP2 zinc finger protein
Zfp288	Zinc finger and BTB domain containing 20
Zfp318	Zinc finger protein 318
Zfp467	Zinc finger protein 467
Zfp61	Zinc finger protein 61
Zfpm1	Zinc finger protein, FOG family member 1
Zfr	Zinc finger RNA binding protein
Zmpste24	Zinc metallopeptidase STE24

Appendix Four: Microarray Data

Microarray data can be found on the CD-ROM attached to the inside of the back cover of this thesis.

Appendix Five: Immunostaining Isotype Controls of E14Tg2a.4 mES Cell Derived Cardiomyocytes
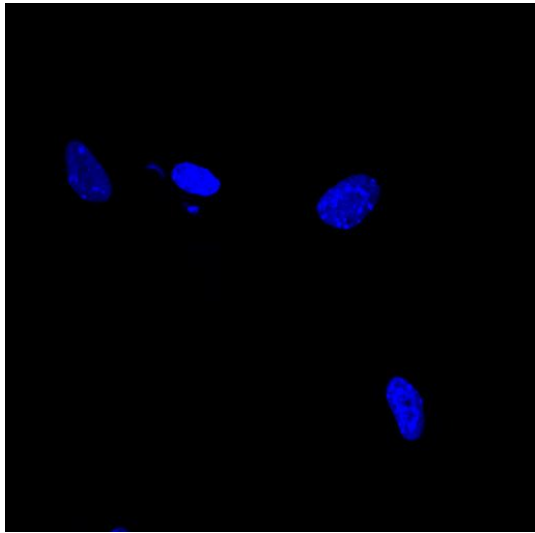
Mouse IgG Control
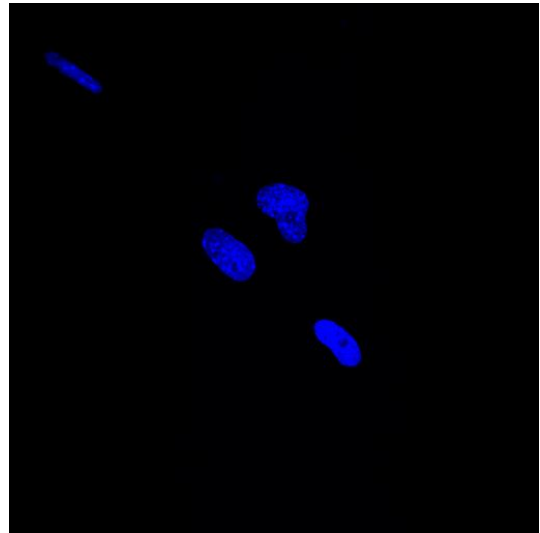
Rabbit IgG Control
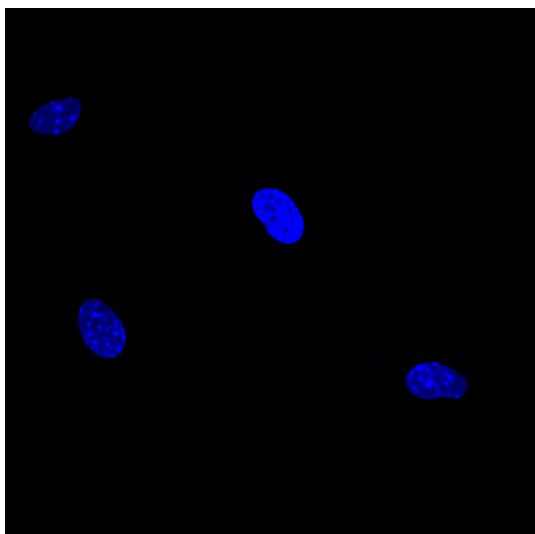
Sheep IgG Control

Bibliography

ABPI. 2012. *Guidelines for phase 1 clinical trials* [Online]. Available: http://www.abpi.org.uk/our-work/library/guidelines/Documents/guidelines_phase1_clinical_trials.pdf.

ABPI. 2014. *Clinical trial simulations - an essential tool in drug development* [Online]. Available: http://www.abpi.org.uk/our-work/library/industry/Documents/trial_design.pdf.

Adler, S., Basketter, D., Creton, S., Pelkonen, O., Van Benthem, J., Zuang, V., Andersen, K. E., Angers-Loustau, A., Aptula, A. & Bal-Price, A. 2011. Alternative (non-animal) methods for cosmetics testing: current status and future prospects. *Archives of Toxicology,* 85**,** 367-485.

Agarwal, S., Holton, K. L. & Lanza, R. 2008. Efficient differentiation of functional hepatocytes from human embryonic stem cells. *Stem Cells,* 26**,** 1117-1127.

Ait Ghezala, H., Jolles, B., Salhi, S., Castrillo, K., Carpentier, W., Cagnard, N., Bruhat, A., Fafournoux, P. & Jean-Jean, O. 2012. Translation termination efficiency modulates ATF4 response by regulating ATF4 mRNA translation at 5' short ORFs. *Nucleic Acids Research,* 40**,** 9557-70.

Aleo, M. D., Lundeen, G. R., Blackwell, D. K., Smith, W. M., Coleman, G. L., Stadnicki, S. W. & Kluwe, W. M. 2003. Mechanism and implications of brown adipose tissue proliferation in rats and monkeys treated with the thiazolidinedione darglitazone, a potent peroxisome proliferator-activated receptor-γ agonist. *Journal of Pharmacology and Experimental Therapeutics,* 305**,** 1173-1182.

Allegrucci, C. & Young, L. E. 2007. Differences between human embryonic stem cell lines. *Human Reproduction Update,* 13**,** 103-120.

Alrefai, W. A. & Gill, R. K. 2007. Bile acid transporters: structure, function, regulation and pathophysiological implications. *Pharmaceutical Research,* 24**,** 1803-1823.

American Diabetes Association 2004. Screening for type 2 diabetes. *Diabetes Care,* 27**,** s11-s14.

Anderson, C. C. & Matzinger, P. 2000. Danger: the view from the bottom of the cliff. *Seminars in Immunology Elsevier*, 231-238.

Anderson, M. E. 1998. Glutathione: an overview of biosynthesis and modulation. *Chemico-Biological Interactions,* 111**,** 1-14.

Ault, A. 1997. Troglitazone may cause irreversible liver damage. *The Lancet,* 350**,** 1451.

Avery, J., Etzion, S., DeBosch, B. J., Jin, X., Lupu, T. S., Beitinjaneh, B., Grand, J., Kovacs, A., Sambandam, N. & Muslin, A. J. 2010. TRB3 function in cardiac endoplasmic reticulum stress. *Circulation Research,* 106**,** 1516-1523.

Bailey, C. J. 2000. The rise and fall of troglitazone. *Diabetic Medicine,* 17**,** 414-415.

Barrow, P. C. 2009. Reproductive toxicity testing for pharmaceuticals under ICH. *Reproductive Toxicology,* 28**,** 172-179.

Baselga, J., Campone, M., Piccart, M., Burris III, H. A., Rugo, H. S., Sahmoud, T., Noguchi, S., Gnant, M., Pritchard, K. I. & Lebrun, F. 2012. Everolimus in postmenopausal hormone-receptor–positive advanced breast cancer. *New England Journal of Medicine,* 366**,** 520-529.

Bechtold, D. A., Gibbs, J. E. & Loudon, A. S. I. 2010. Circadian dysfunction in disease. *Trends In Pharmacological Sciences,* 31**,** 191-198.

Bedoucha, M., Atzpodien, E. & Boelsterli, U. A. 2001. Diabetic KKAy mice exhibit increased hepatic PPARγ1 gene expression and develop hepatic steatosis upon chronic treatment with antidiabetic thiazolidinediones. *Journal of Hepatology,* 35**,** 17-23.

Berg, J. M., Tymoczko, J. L. & Stryer, L. 2002. Biochemistry, Fifth Edition*. W.H. Freeman, 608.*

Berger, J. & Moller, D. E. 2002. The mechanisms of action of PPARs. *Annual Review of Medicine,* 53**,** 409-435.

Bernardo, B. C., Gao, X.-M., Winbanks, C. E., Boey, E. J., Tham, Y. K., Kiriazis, H., Gregorevic, P., Obad, S., Kauppinen, S. & Du, X.-J. 2012. Therapeutic inhibition of the miR-34 family attenuates pathological cardiac remodeling and improves heart function. *Proceedings of the National Academy of Sciences,* 109**,** 17615-17620.

Bers, D. M. 2000. Calcium fluxes involved in control of cardiac myocyte contraction. *Circulation Research,* 87**,** 275-281.

Betteridge, D. 2004. Treating dyslipidaemia in the patient with type 2   diabetes. *European Heart Journal Supplements,* 6**,** C28-C33.

Bhatia, S. N. & Ingber, D. E. 2014. Microfluidic organs-on-chips. *Nature Biotechnology,* 32**,** 760-772.

Bleicher, K. H., Böhm, H.-J., Müller, K. & Alanine, A. I. 2003. Hit and lead generation: beyond high-throughput screening. *Nature Reviews Drug Discovery,* 2**,** 369-378.

Blomme, E. A. G. & Warder, S. E. 2008. Gene Expression-Based Biomarkers of Drug Safety*. Humana Press*, 27-49.

Boelsterli, U. A. & Bedoucha, M. 2002. Toxicological consequences of altered peroxisome proliferator-activated receptor γ expression in the liver: insights from models of obesity and type 2 diabetes. *Biochemical Pharmacology,* 63**,** 1-10.

Boheler, K. R., Czyz, J., Tweedie, D., Yang, H. T., Anisimov, S. V. & Wobus, A. M. 2002. Differentiation of pluripotent embryonic stem cells into cardiomyocytes. *Circulation Research,* 91**,** 189-201.

Boiani, M. & Schöler, H. R. 2005. Regulatory networks in embryo-derived pluripotent stem cells. *Nature Reviews Molecular Cell Biology,* 6**,** 872-881.

Bolstad, B. M., Irizarry, R. A., Åstrand, M. & Speed, T. P. 2003. A comparison of normalization methods for high density oligonucleotide array data based on variance and bias. *Bioinformatics,* 19**,** 185-193.

Boon, R. A., Iekushi, K., Lechner, S., Seeger, T., Fischer, A., Heydt, S., Kaluza, D., Treguer, K., Carmona, G., Bonauer, A., Horrevoets, A. J., Didier, N., Girmatsion, Z., Biliczki, P., Ehrlich, J. R., Katus, H. A., Muller, O. J., Potente, M., Zeiher, A. M., Hermeking, H. & Dimmeler, S. 2013. MicroRNA-34a regulates cardiac ageing and function. *Nature,* 495**,** 107-10.

Boudeau, J., Miranda-Saavedra, D., Barton, G. J. & Alessi, D. R. 2006. Emerging roles of pseudokinases. *Trends in Cell Biology,* 16**,** 443-452.

Bradford, M. M. 1976. A rapid and sensitive method for the quantitation of microgram quantities of protein utilizing the principle of protein-dye binding. *Analytical Biochemistry,* 72**,** 248-254.

Brandon, E. F., Raap, C. D., Meijerman, I., Beijnen, J. H. & Schellens, J. H. 2003. An update on in vitro test methods in human hepatic drug biotransformation research: pros and cons. *Toxicology and Applied Pharmacology,* 189**,** 233-46.

Breider, M., Gough, A., Haskins, J., Sobocinski, G. & De La Iglesia, F. 1999. Troglitazone-induced heart and adipose tissue cell proliferation in mice. *Toxicologic Pathology,* 27**,** 545-552.

Breuker, C., Moreau, A., Lakhal, L., Tamasi, V., Parmentier, Y., Meyer, U., Maurel, P., Lumbroso, S., Vilarem, M. J. & Pascussi, J. M. 2010. Hepatic expression of thyroid hormone-responsive spot 14 protein is regulated by constitutive androstane receptor. *Endocrinology,* 151**,** 1653.

Buck, W. R., Waring, J. F. & Blomme, E. A. 2008. Use of Traditional End Points and Gene Dysregulation to Understand Mechanisms of Toxicity: Toxicogenomics in Mechanistic Toxicology. *Humana Press*, 23-44.

Burden, N., Chapman, K., Sewell, F. & Robinson, V. 2015. Pioneering better science through the 3Rs: an introduction to the National Centre for the Replacement, Refinement, and Reduction of Animals in Research (NC3Rs). *Journal of the American Association for Laboratory Animal Science,* 54**,** 198-208.

Bushel, P., Heinloth, A., Li, J., Huang, L., Chou, J., Boorman, G., Malarkey, D., Houle, C., Ward, S. & Wilson, R. 2007. Blood gene expression signatures predict

exposure levels. *Proceedings of the National Academy of Sciences,* 104**,** 18211-18216.

Camp, H. S., Li, O., Wise, S. C., Hong, Y. H., Frankowski, C. L., Shen, X., Vanbogelen, R. & Leff, T. 2000. Differential activation of peroxisome proliferator-activated receptor-gamma by troglitazone and rosiglitazone. *Diabetes,* 49**,** 539-547.

Campion, S., Aubrecht, J., Boekelheide, K., Brewster, D. W., Vaidya, V. S., Anderson, L., Burt, D., Dere, E., Hwang, K. & Pacheco, S. 2013. The current status of biomarkers for predicting toxicity. *Expert Opinion on Drug Metabolism and Toxicology,* 9**,** 1391-1408.

Carraro, V., Maurin, A., Lambert-Langlais, S., Averous, J., Chaveroux, C., Parry, L., Jousse, C., Ord, D., Ord, T. & Fafournoux, P. 2009. Amino acid availability controls TRB3 transcription in liver through the GCN2/eIF2α/ATF4 pathway. *PloS One,* 5**,** e15716-e15716.

Caspi, O., Itzhaki, I., Kehat, I., Gepstein, A., Arbel, G., Huber, I., Satin, J. & Gepstein, L. 2009. In vitro electrophysiological drug testing using human embryonic stem cell derived cardiomyocytes. *Stem Cells and Development,* 18**,** 161-172.

Cezar, G. G. 2007. Can human embryonic stem cells contribute to the discovery of safer and more effective drugs? *Current Opinion in Chemical Biology,* 11**,** 405-409.

Chaggar, P. S., Shaw, S. M. & Williams, S. G. 2009. Review article: thiazolidinediones and heart failure. *Diabetes and Vascular Disease Research,* 6**,** 146-152.

Chambers, I. 2004. The molecular basis of pluripotency in mouse embryonic stem cells. *Cloning and Stem Cells,* 6**,** 386-391.

Cheatham, B. & Kahn, C. R. 1995. Insulin action and the insulin signaling network. *Endocrine Reviews,* 16**,** 117-142.

Chen, Kevin G., Mallon, Barbara S., McKay, Ronald D. G. & Robey, Pamela G. 2013. Human pluripotent stem cell culture: considerations for maintenance, expansion, and therapeutics. *Cell Stem Cell,* 14**,** 13-26.

Chen, S., Hilcove, S. & Ding, S. 2006. Exploring stem cell biology with small molecules. *Molecular BioSystems,* 2**,** 18-24.

Cheon, C. W., Kim, D. H., Cho, Y. H. & Kim, J. H. 2009. Effects of ciglitazone and troglitazone on the proliferation of human stomach cancer cells. *World Journal of Gastroenterology,* 15**,** 310.

Chojkier, M. 2005. Troglitazone and liver injury: In search of   answers. *Hepatology,* 41**,** 237-246.

Cumming, J. G., Davis, A. M., Muresan, S., Haeberlein, M. & Chen, H. 2013. Chemical predictive modelling to improve compound quality. *Nature Reviews Drug Discovery,* 12**,** 948-962.

D'Amour, K. A., Agulnick, A. D., Eliazer, S., Kelly, O. G., Kroon, E. & Baetge, E. E. 2005. Efficient differentiation of human embryonic stem cells to definitive endoderm. *Nature Biotechnology,* 23**,** 1534-1541.

Daheron, L., Opitz, S. L., Zaehres, H., Lensch, W. M., Andrews, P. W., Itskovitz-Eldor, J. & Daley, G. Q. 2004. LIF/STAT3 signaling fails to maintain self-renewal of human embryonic stem cells. *Stem Cells,* 22**,** 770-778.

Daly, A. K. 2013. Pharmacogenomics of adverse drug reactions. *Genome Medicine*, 5, 1-12.

Danielson, P. 2002. The cytochrome P450 superfamily: biochemistry, evolution and drug metabolism in humans. *Current Drug Metabolism,* 3**,** 561-597.

Davies, G. F., Khandelwal, R. L. & Roesler, W. J. 1999. Troglitazone induces expression of PPARγ in liver. *Molecular Cell Biology Research Communications,* 2**,** 202-208.

Day, C. 1999. Thiazolidinediones: a new class of antidiabetic drugs. *Diabetic Medicine,* 16**,** 179-192.

Dearfield, K. L., Cimino, M. C., McCarroll, N. E., Mauer, I. & Valcovic, L. R. 2002. Genotoxicity risk assessment: a proposed classification strategy. *Mutation Research/Genetic Toxicology and Environmental Mutagenesis,* 521**,**121-135.

DeCristofaro, M. F. & Daniels, K. K. 2008. Toxicogenomics in Biomarker Discovery. *Humana Press*, 185-194.

Dedhia, P. H., Keeshan, K., Uljon, S., Xu, L., Vega, M. E., Shestova, O., Zaks-Zilberman, M., Romany, C., Blacklow, S. C. & Pear, W. S. 2010. Differential ability of tribbles family members to promote degradation of C/EBPα and induce acute myelogenous leukemia. *Blood,* 116**,**1321-1328.

Deferme, S., Annaert, P. & Augustijns, P. 2008. In vitro screening models to assess intestinal drug absorption and metabolism. *Drug Absorption Studies Springer*, 182-215.

DeRisi, J., Penland, L., Brown, P. O., Bittner, M. L., Meltzer, P. S., Ray, M., Chen, Y., Su, Y. A. & Trent, J. M. 1996. Use of a cDNA microarray to analyse gene expression patterns in human cancer. *Nature Genetics,* 14**,**457-460.

Desbaillets, I., Ziegler, U., Groscurth, P. & Gassmann, M. 2000. Embryoid bodies: an in vitro model of mouse embryogenesis. *Experimental Physiology,* 85**,** 645-651.

Dey, S., Baird, T. D., Zhou, D., Palam, L. R., Spandau, D. F. & Wek, R. C. 2010. Both transcriptional regulation and translational control of ATF4 are central to the integrated stress response. *The Journal of Biological Chemistry,* 285**,** 33165-33174.

Doetschman, T. C., Eistetter, H., Katz, M., Schmidt, W. & Kemler, R. 1985. The in vitro development of blastocyst-derived embryonic stem cell lines: formation of visceral yolk sac, blood islands and myocardium. *Journal of Embryology and Experimental Morphology,* 87**,**27-45.

Du, K. & Ding, J. 2009. Insulin regulates TRB3 and other stress-responsive gene expression through induction of C/EBPβ. *Molecular Endocrinology,* 23**,**475-485.

Durgan, D. J. & Young, M. E. 2010. The cardiomyocyte circadian clock. *Circulation Research,* 106**,** 647-658.

Dykens, J. A. & Will, Y. 2007. The significance of mitochondrial toxicity testing in drug development. *Drug Discovery Today,* 12**,** 777-785.

EBiSC. 2014. *EBiSC - the first European bank for induced pluripotent stem cells* [Online]. Available: www.ebisc.eu.

Edwards, I. R. & Aronson, J. K. 2000. Adverse drug reactions: definitions, diagnosis, and management. *The Lancet,* 356**,** 1255-1259.

Evans, M. J. & Kaufman, M. H. 1981. Establishment in culture of pluripotential cells from mouse embryos. *Nature,* 292**,** 154-156.

FDA. 1999a. *Endocrinologic and metabolic drugs advisory committee meeting no. 72* [Online].
Available: http://www.fda.gov/AdvisoryCommittees/CommitteesMeetingMaterial s/Drugs/EndocrinologicandMetabolicDrugsAdvisoryCommittee/default.htm.

FDA. 1999b. *Rezulin drug label* [Online].
Available: http://www.accessdata.fda.gov/drugsatfda_docs/label/1999/20720s12 lbl.pdf.

FDA. 2006. *The future of drug safety — promoting and protecting the health of the public* [Online].
Available: http://www.fda.gov/downloads/Drugs/DrugSafety/PostmarketDrugSaf etyInformationforPatientsandProviders/UCM171627.pdf.

FDA. 2009. *Inside clinical trials: testing medical products in people* [Online].
Available: http://www.fda.gov/Drugs/ResourcesForYou/Consumers/ucm143531. htm.

FDA. 2014. *Pharmacogenomic biomarkers in drug labeling* [Online].
Available: http://www.fda.gov/drugs/scienceresearch/researchareas/pharmacog enetics/ucm083378.htm.

Fleckenstein, A. 1977. Specific pharmacology of calcium in myocardium, cardiac pacemakers, and vascular smooth muscle. *Annual Review of Pharmacology and Toxicology,* 17**,** 149-166.

Frayn, K., Arner, P. & Yki-Jarvinen, H. 2006. Fatty acid metabolism in adipose tissue, muscle and liver in health and disease. *Essays in Biochemistry,* 42**,** 89-103.

Frayn, K. N. 2001. Adipose tissue and the insulin resistance syndrome. *Proceedings of the Nutrition Society of London*, *Cambridge University Press,* 375-380.

Freeman, H. & Cox, R. D. 2006. Type-2 diabetes: a cocktail of genetic discovery. *Human Molecular Genetics,* 15**,** R202-R209.

Funk, C., Pantze, M., Jehle, L., Ponelle, C., Scheuermann, G., Lazendic, M. & Gasser, R. 2001. Troglitazone-induced intrahepatic cholestasis by an interference with the hepatobiliary export of bile acids in male and female rats. Correlation with the gender difference in troglitazone sulfate formation and the inhibition of the canalicular bile salt export pump (Bsep) by troglitazone and troglitazone sulfate. *Toxicology,* 167**,** 83-98.

Gachon, F., Olela, F. F., Schaad, O., Descombes, P. & Schibler, U. 2006. The circadian PAR-domain basic leucine zipper transcription factors DBP, TEF, and HLF modulate basal and inducible xenobiotic detoxification. *Cell Metabolism,* 4**,** 25-36.

Gale, E. A. M. 2001. Lessons from the glitazones: a story of drug development. *The Lancet,* 357**,** 1870-1875.

Gao, W., Mizukawa, Y., Nakatsu, N., Minowa, Y., Yamada, H., Ohno, Y. & Urushidani, T. 2010. Mechanism-based biomarker gene sets for glutathione depletion-related hepatotoxicity in rats. *Toxicology and Applied Pharmacology,* 247**,** 211-221.

Gardner, O. S., Shiau, C.-W., Chen, C.-S. & Graves, L. M. 2005. Peroxisome proliferator-activated receptor gamma-independent activation of p38 MAPK   by

thiazolidinediones involves calcium/calmodulin-dependent protein kinase II and protein kinase R: correlation with endoplasmic reticulum stress. *Journal of Biological Chemistry,* 280**,** 10109-10118.

Genschow, E., Spielmann, H., Scholz, G., Pohl, I., Seiler, A., Clemann, N., Bremer, S. & Becker, K. 2004. Validation of the embryonic stem cell test in the international ECVAM validation study on three in vitro embryotoxicity tests. *Alternatives to Laboratory Animals,* 32**,** 209-244.

Genschow, E., Spielmann, H., Scholz, G., Seiler, A., Brown, N., Piersma, A., Brady, M., Clemann, N., Huuskonen, H. & Paillard, F. 2002. The ECVAM international validation study on in vitro embryotoxicity tests: results of the definitive phase and evaluation of prediction models. *Alternatives to Laboratory Animals,* 30**,** 151-176.

Ghazalpour, A., Doss, S., Zhang, B., Wang, S., Plaisier, C., Castellanos, R., Brozell, A., Schadt, E. E., Drake, T. A. & Lusis, A. J. 2006. Integrating genetic and network analysis to characterize genes related to mouse weight. *PLoS Genetics,* 2**,** e130.

Ginis, I., Luo, Y., Miura, T., Thies, S., Brandenberger, R., Gerecht-Nir, S., Amit, M., Hoke, A., Carpenter, M. K. & Itskovitz-Eldor, J. 2004. Differences between human and mouse embryonic stem cells. *Developmental Biology,* 269**,** 360-380.

Gong, J., Sun, Z. & Li, P. 2009. CIDE proteins and metabolic disorders. *Current Opinion in Lipidology,* 20**,** 121-126.

Gonzalez, F. J. 2005. Role of cytochromes P450 in chemical toxicity and oxidative stress: studies with CYP2E1. *Mutation Research/Fundamental and Molecular Mechanisms of Mutagenesis,* 569**,** 101-110.

Gotto Jr, A. M. 2006. Statins, cardiovascular disease and drug safety. *The American Journal of Cardiology,* 97**,** S3-S5.

Gough, N. M., Gearing, D. P., King, J. A., Willson, T. A., Hilton, D. J., Nicola, N. A. & Metcalf, D. 1988. Molecular cloning and expression of the human homologue of the murine gene encoding myeloid leukemia-inhibitory factor. *Proceedings of the National Academy of Sciences,* 85**,** 2623-2627.

Graham, D., J. , Drinkard, C., R. & Shatin, D. 2003. Incidence of idiopathic acute liver failure and hospitalized liver injury in patients treated with troglitazone. *American Journal of Gastroenterology,* 98**,** 175-179.

Gregorio, C. C., Trombitás, K., Centner, T., Kolmerer, B., Stier, G., Kunke, K., Suzuki, K., Obermayr, F., Herrmann, B. & Granzier, H. 1998. The NH2 terminus of titin spans the Z-disc: its interaction with a novel 19-kD ligand (T-cap) is required for sarcomeric integrity. *The Journal of Cell Biology,* 143**,** 1013.

Guengerich, F. P. 2007. Cytochrome P450 and chemical toxicology. *Chemical Research in Toxicology,* 21**,** 70-83.

Gupta, P., Gupta, V. & Gupta, Y. K. 2012. Phase I clinical trials of anticancer drugs in healthy volunteers: need for critical consideration. *Indian Journal of Pharmacology,* 44**,** 540-542.

Han, J., Back, S. H., Hur, J., Lin, Y.-H., Gildersleeve, R., Shan, J., Yuan, C. L., Krokowski, D., Wang, S. & Hatzoglou, M. 2013. ER-stress-induced transcriptional regulation increases protein synthesis leading to cell death. *Nature Cell Biology,* 15**,** 481-490.

Hancox, J. C., McPate, M. J., El Harchi, A. & Zhang, Y. h. 2008. The hERG potassium channel and hERG screening for drug-induced torsades de pointes. *Pharmacology and Therapeutics,* 119**,** 118-132.

Hartung, T. 2013. Food for thought look back in anger–What clinical studies tell us about preclinical work. *Altex,* 30**,** 275.

He, S., Nakada, D. & Morrison, S. 2009. Mechanisms of stem cell self-renewal. *Annual Review of Cell and Developmental Biology,* 25**,** 377.

Health, U. N. I. O. 2010. *Clinical trial: mechanism of fatty acid-induced impairment of glucose-simulated insulin secretion - effect of buphenyl* [Online]. Available: http://clinicaltrials.gov/ct2/show/study/NCT00533559.

Herman, J. R., Dethloff, L. A., McGuire, E. J., Parker, R. F., Walsh, K. M., Gough, A. W., Masuda, H. & de la Iglesia, F. A. 2002. Rodent carcinogenicity with the thiazolidinedione antidiabetic agent troglitazone. *Toxicological Sciences,* 68**,** 226-236.

Hewitt, R. G. 2002. Abacavir hypersensitivity reaction. *Clinical Infectious Diseases,* 34**,** 1137-1142.

Hibuse, T., Maeda, N., Nakatsuji, H., Tochino, Y., Fujita, K., Kihara, S., Funahashi, T. & Shimomura, I. 2009. The heart requires glycerol as an energy substrate through aquaporin 7, a glycerol facilitator. *Cardiovascular Research,* 83**,** 34-41.

Hildebrandt, M., Salavaggione, O., Martin, Y., Flynn, H., Jalal, S., Wieben, E. & Weinshilboum, R. 2004. Human SULT1A3 pharmacogenetics: gene duplication and functional genomic studies. *Biochemical and Biophysical Research Communications,* 321**,** 870-878.

Hinson, J. A., Roberts, D. W. & James, L. P. 2010. Adverse Drug Reactions*. Springer,* 369-405.

Hoffman, J. A. & Merrill, B. J. 2007. New and renewed perspectives on embryonic stem cell pluripotency. *Frontiers Bioscience,* 12**,** 3321-32.

Hu, F. B., Manson, J. A. E., Stampfer, M. J., Colditz, G., Liu, S., Solomon, C. G. & Willett, W. C. 2001. Diet, lifestyle, and the risk of type 2 diabetes mellitus in women. *New England Journal of Medicine,* 345**,** 790-797.

Hu, P., Han, Z., Couvillon, A. D. & Exton, J. H. 2004. Critical role of endogenous Akt/IAPs and MEK1/ERK pathways in counteracting endoplasmic reticulum stress-induced cell death. *Journal of Biological Chemistry,* 279**,** 49420-49429.

Hughes, J., Rees, S., Kalindjian, S. & Philpott, K. 2011. Principles of early drug discovery. *British Journal of Pharmacology,* 162**,** 1239-1249.

Huh, D., Hamilton, G. A. & Ingber, D. E. 2011. From three-dimensional cell culture to organs-on-chips. *Trends in Cell Biology,* 21**,** 745-754.

Hulin, B., McCarthy, P. A. & Gibbs, E. M. 1996. The glitazone family of antidiabetic agents. *Current Pharmaceutical Design, 2,* 85-102.

ICH 2008. *E15 definitions for genomic biomarkers, pharmacogenomics, pharmacogenetics, genomic data and sample coding categories*. [Online]. Available:http://www.ich.org/products/guidelines/efficacy/efficacy-single/article/definitions-for-genomic-biomarkers-pharmacogenomics-pharmacogenetics-genomic-data-and-sample-cod.html.

Ikeda, S. & Watanabe, T. 1998. Effects of troglitazone and pioglitazone on the action potentials and membrane currents of rabbit ventricular myocytes. *European Journal of Pharmacology,* 357, 243-250.

Inoue, M., Ohtake, T., Motomura, W., Takahashi, N., Hosoki, Y., Miyoshi, S., Suzuki, Y., Saito, H., Kohgo, Y. & Okumura, T. 2005. Increased expression of PPARγ in high fat diet-induced liver steatosis in mice. *Biochemical and Biophysical Research Communications,* 336, 215-222.

Jacobs, A. C. & Hatfield, K. P. 2012. History of chronic toxicity and animal carcinogenicity studies for pharmaceuticals. *Veterinary Pathology Online*, 50, 324-333

Jin, M., Takahashi, M., Moto, M., Muguruma, M., Ito, K., Watanabe, K., Kenmochi, Y., Kono, T., Hasumi, K. & Mitsumori, K. 2007. Carcinogenic susceptibility of rasH2 mice to troglitazone. *Archives of Toxicology,* 81, 883-894.

Jogl, G., Hsiao, Y.-S. & Tong, L. 2004. Structure and function of carnitine acyltransferases. *Annals of the New York Academy of Sciences,* 1033, 17-29.

Jousse, C., Deval, C., Maurin, A.-C., Parry, L., Chérasse, Y., Chaveroux, C., Lefloch, R., Lenormand, P., Bruhat, A. & Fafournoux, P. 2007. TRB3 inhibits the transcriptional activation of stress-regulated genes by a negative feedback on the ATF4 pathway. *Journal of Biological Chemistry,* 282, 15851-15861.

Kahn, S. E., Hull, R. L. & Utzschneider, K. M. 2006. Mechanisms linking obesity to insulin resistance and type 2 diabetes. *Nature,* 444, 840-846.

Kehat, I. & Molkentin, J. D. 2010. Molecular pathways underlying cardiac remodeling during pathophysiological stimulation. *Circulation,* 122**,**2727-2735.

Keller, G. 2005. Embryonic stem cell differentiation: emergence of a new era in biology and medicine. *Genes and Development,* 19**,**1129-1155.

Kim, I., Xu, W. & Reed, J. C. 2008. Cell death and endoplasmic reticulum stress: disease relevance and therapeutic opportunities. *Nature Reviews Drug Discovery,* 7**,** 1013-1030.

Kim, S., Sohn, I., Ahn, J. I., Lee, K. H. & Lee, Y. S. 2004. Hepatic gene expression profiles in a long-term high-fat diet-induced obesity mouse model. *Gene,* 340**,** 99-109.

Kiss-Toth, E., Bagstaff, S. M., Sung, H. Y., Jozsa, V., Dempsey, C., Caunt, J. C., Oxley, K. M., Wyllie, D. H., Polgar, T. & Harte, M. 2004. Human tribbles, a protein family controlling mitogen-activated protein kinase cascades. *Journal of Biological Chemistry,* 279**,**42703-42708.

Knock, G. A., Mishra, S. K. & Aaronson, P. I. 1999. Differential effects of insulin-sensitizers troglitazone and rosiglitazone on ion currents in rat vascular myocytes. *European Journal of Pharmacology,* 368**,**103-109.

Koressaar, T. & Remm, M. 2007. Enhancements and modifications of primer design program primer3. *Bioinformatics,* 23**,**1289-1291.

Kostrubsky, V. E., Sinclair, J. F., Ramachandran, V., Venkataramanan, R., Wen, Y. H., Kindt, E., Galchev, V., Rose, K., Sinz, M. & Strom, S. C. 2000. The role of conjugation in hepatotoxicity of troglitazone in human and porcine hepatocyte cultures. *Drug Metabolism and Disposition,* 28**,**1192-1197.

Kumar, D. & Sun, B. 2005. Transforming growth factor-β2 enhances differentiation of cardiac myocytes from embryonic stem cells. *Biochemical and Biophysical Research Communications,* 332**,**135-141.

Lago, R. M., Singh, P. P. & Nesto, R. W. 2007. Congestive heart failure and cardiovascular death in patients with prediabetes and type 2 diabetes given

thiazolidinediones: a meta-analysis of randomised clinical trials. *The Lancet,* 370**,** 1129-1136.

Lauer, B., Tuschl, G., Kling, M. & Mueller, S. O. 2009. Species-specific toxicity of diclofenac and troglitazone in primary human and rat hepatocytes. *Chemico-Biological Interactions,* 179**,** 17-24.

Laurent, L. C., Nievergelt, C. M., Lynch, C., Fakunle, E., Harness, J. V., Schmidt, U., Galat, V., Laslett, A. L., Otonkoski, T. & Keirstead, H. S. 2010. Restricted ethnic diversity in human embryonic stem cell lines. *Nature Methods,* 7**,** 6-7.

Leahy, A., Xiong, J.-W., Kuhnert, F. & Stuhlmann, H. 1999. Use of developmental marker genes to define temporal and spatial patterns of differentiation during embryoid body formation. *Journal of Experimental Zoology,* 284**,** 67-81.

Lehrke, M. & Lazar, M. A. 2005. The many faces of PPARγ. *Cell,* 123**,** 993-999.

Levi, F. & Schibler, U. 2007. Circadian rhythms: mechanisms and therapeutic implications. *Pharmacology and Toxicology,* 47**,** 593.

Liu, X. & Jia, L. 2007. The conduct of drug metabolism studies considered good practice: analytical systems and in vivo studies. *Current Drug Metabolism,* 8**,** 815-821.

Lizcano, J. M. & Alessi, D. R. 2002. The insulin signalling pathway. *Current Biology,* 12**,** 236.

Lloyd, M. & Wolfensohn, S. 2003. Handbook of Laboratory Animal Management and Welfare*. Blackwell Science*, 235

Loh, Y.-H., Wu, Q., Chew, J.-L., Vega, V. B., Zhang, W., Chen, X., Bourque, G., George, J., Leong, B., Liu, J., Wong, K.-Y., Sung, K. W., Lee, C. W. H., Zhao, X.-D., Chiu, K.-P., Lipovich, L., Kuznetsov, V. A., Robson, P., Stanton, L. W., Wei, C.-L., Ruan, Y., Lim, B. & Ng, H.-H. 2006. The Oct4 and Nanog transcription network regulates pluripotency in mouse embryonic stem cells. *Nature Genetics*, 38, 431-440.

Lord, P. G. 2004. Progress in applying genomics in drug development. *Toxicology Letters,* 149**,** 371-375.

Luo, C.-h. & Rudy, Y. 1991. A model of the ventricular cardiac action potential: depolarization, repolarization, and their interaction. *Circulation Research,* 68**,** 1501-1526.

Mabilleau, G., Chappard, D. & Baslé, M. F. 2011. Cellular and molecular effects of thiazolidinediones on bone cells: a review. *International Journal of Biochemistry and Molecular Biology,* 2**,** 240-246.

Magkos, F., Yannakoulia, M., Chan, J. L. & Mantzoros, C. S. 2009. Management of the metabolic syndrome and type 2 diabetes through lifestyle modification. *Annual Review of Nutrition,* 29**,** 223-256.

Mah, N., Thelin, A., Lu, T., Nikolaus, S., Kühbacher, T., Gurbuz, Y., Eickhoff, H., Klöppel, G., Lehrach, H., Mellgård, B., Costello, C. M. & Schreiber, S. 2004. A comparison of oligonucleotide and cDNA-based microarray systems. *Physiological Genomics,* 16**,** 361-370.

Mallal, S., Nolan, D., Witt, C., Masel, G., Martin, A., Moore, C., Sayer, D., Castley, A., Mamotte, C. & Maxwell, D. 2002. Association between presence of HLA-B* 5701, HLA-DR7, and HLA-DQ3 and hypersensitivity to HIV-1 reverse-transcriptase inhibitor abacavir. *The Lancet,* 359**,** 727-732.

Manuilova, E. S., Gordeeva, O. F., Grivennikov, I. A. & Ozernyuk, N. D. 2001. Embryonic stem cells: spontaneous and directed differentiation. *Biology Bulletin of the Russian Academy of Sciences,* 28**,** 595-600.

Martin, G. R. 1981. Isolation of a pluripotent cell line from early mouse embryos cultured in medium conditioned by teratocarcinoma stem cells. *Proceedings of the National Academy of Sciences,* 78**,** 7634-7638.

Masubuchi, Y. 2006. Metabolic and non-metabolic factors determining troglitazone hepatotoxicity: a review. *Drug Metabolism and Pharmacokinetics,* 21**,** 347-356.

Mateizel, I., De Temmerman, N., Ullmann, U., Cauffman, G., Sermon, K., Van de Velde, H., De Rycke, M., Degreef, E., Devroey, P., Liebaers, I. & Van Steirteghem, A. 2006. Derivation of human embryonic stem cell lines from embryos obtained after IVF and after PGD for monogenic disorders. *Human Reproduction,* 21**,** 503-511.

Mathivanan, S., Ji, H. & Simpson, R. J. 2010. Exosomes: extracellular organelles important in intercellular communication. *Journal of Proteomics,* 73**,** 1907-1920.

McGivern, J. V. & Ebert, A. D. 2014. Exploiting pluripotent stem cell technology for drug discovery, screening, safety, and toxicology assessments. *Advanced Drug Delivery Reviews,* 69**,** 170-178.

McNeish, J. 2004. Embryonic stem cells in drug discovery. *Nature Reviews Drug Discovery,* 3**,** 70-80.

Meier, Y., Pauli-Magnus, C., Zanger, U. M., Klein, K., Schaeffeler, E., Nussler, A. K., Nussler, N., Eichelbaum, M., Meier, P. J. & Stieger, B. 2006. Interindividual variability of canalicular ATP-binding-cassette (ABC)–transporter expression in human liver. *Hepatology,* 44**,** 62-74.

Menon, K. V. N., Angulo, P. & Lindor, K. D. 2001. Severe cholestatic hepatitis from troglitazone in a patient with nonalcoholic steatohepatitis and diabetes mellitus. *The American Journal of Gastroenterology,* 96**,** 1631-1634.

Metcalf, D. 2003. The unsolved enigmas of leukemia inhibitory factor. *Stem Cells,* 21**,** 5-14.

MHRA. 2010. *Rosiglitazone (avandia, avandamet): withdrawal from clinical use* [Online].
Available: http://www.mhra.gov.uk/Safetyinformation/Safetywarningsalertsandrecalls/Safetywarningsandmessagesformedicines/CON094121.

Mitchell, P. 1997. Shock as troglitazone withdrawn in UK. *The Lancet,* 350**,** 1685.

Morgan, A. J. & Jacob, R. 1994. Ionomycin enhances Ca2+ influx by stimulating store-regulated cation entry and not by a direct action at the plasma membrane. *Biochemical Journal,* 300**,** 665.

Morgan, S., Grootendorst, P., Lexchin, J., Cunningham, C. & Greyson, D. 2011. The cost of drug development: a systematic review. *Health Policy,* 100**,** 4-17.

Mosher, J. T., Pemberton, T. J., Harter, K., Wang, C., Buzbas, E. O., Dvorak, P., Simón, C., Morrison, S. J. & Rosenberg, N. A. 2010. Lack of population diversity in commonly used human embryonic stem-cell lines. *New England Journal of Medicine,* 362**,** 183-185.

Mudaliar, S. & Henry, R. R. 2001. New oral therapies for type 2 diabetes mellitus: the glitazones or insulin sensitizers 1. *Annual Review of Medicine,* 52**,** 239-257.

Müller, L., Kikuchi, Y., Probst, G., Schechtman, L., Shimada, H., Sofuni, T. & Tweats, D. 1999. ICH-harmonised guidances on genotoxicity testing of pharmaceuticals: evolution, reasoning and impact. *Mutation Research/Reviews in Mutation Research,* 436**,** 195-225.

Mummery, C. 2010. Sorting cardiomyocytes: a simple solution after all? *Nature Methods,* 7**,** 40-42.

Murry, C. E. & Keller, G. 2008. Differentiation of embryonic stem cells to clinically relevant populations: lessons from embryonic development. *Cell,* 132**,** 661-680.

Narayanan, P. K., Hart, T., Elcock, F., Zhang, C., Hahn, L., McFarland, D., Schwartz, L., Morgan, D. G. & Bugelski, P. 2003. Troglitazone-induced intracellular oxidative stress in rat hepatoma cells: A flow cytometric assessment. *Cytometry Part A,* 52A**,** 28-35.

Nathwani, R. A., Pais, S., Reynolds, T. B. & Kaplowitz, N. 2005. Serum alanine aminotransferase in skeletal muscle diseases. *Hepatology,* 41**,** 380-382.

Newell, D. R., Burtles, S. S., Fox, B. W., Jodrell, D. I. & Connors, T. A. 1999. Evaluation of rodent-only toxicology for early clinical trials with novel cancer therapeutics. *British Journal of Cancer,* 81**,** 760-768.

Nichols, J. & Smith, A. 2011. The origin and identity of embryonic stem cells. *Development,* 138**,** 3-8.

Niggli, E. 1999. Localized intracellular calcium signaling in muscle: calcium sparks and calcium quarks. *Annual Review of Physiology,* 61**,** 311-335.

Ohoka, N., Yoshii, S., Hattori, T., Onozaki, K. & Hayashi, H. 2005. TRB3, a novel ER stress-inducible gene, is induced via ATF4–CHOP pathway and is involved in cell death. *The EMBO Journal,* 24**,** 1243-1255.

Okita, K. & Yamanaka, S. 2006. Intracellular signaling pathways regulating pluripotency of embryonic stem cells. *Current Stem Cell Research and Therapy,* 1**,** 103-111.

Olson, T. M., Alekseev, A. E., Liu, X. K., Park, S., Zingman, L. V., Bienengraeber, M., Sattiraju, S., Ballew, J. D., Jahangir, A. & Terzic, A. 2006. Kv1. 5 channelopathy due to KCNA5 loss-of-function mutation causes human atrial fibrillation. *Human Molecular Genetics,* 15**,** 2185-2191.

Ozcan, L. & Tabas, I. 2012. Role of endoplasmic reticulum stress in metabolic disease and other disorders. *Annual Review of Medicine,* 63**,** 317-328.

Ozcan, U., Cao, Q., Yilmaz, E., Lee, A.-H., Iwakoshi, N. N., Ozdelen, E., Tuncman, G., Gorgun, C., Glimcher, L. H. & Hotamisligil, G. S. 2004. Endoplasmic reticulum stress links obesity, insulin action, and type 2 diabetes. *Science Signaling,* 306**,** 457.

Ozcan, U., Yilmaz, E., Ozcan, L., Furuhashi, M., Vaillancourt, E., Smith, R. O., Gorgun, C. Z. & Hotamisligil, G. S. 2006. Chemical chaperones reduce ER stress and restore glucose homeostasis in a mouse model of type 2 diabetes. *Science Signaling,* 313**,** 1137.

Ozer, J., Ratner, M., Shaw, M., Bailey, W. & Schomaker, S. 2008. The current state of serum biomarkers of hepatotoxicity. *Toxicology,* 245**,** 194-205.

Pacheco, S. E., Anderson, L. M., Sandrof, M. A., Vantangoli, M. M., Hall, S. J. & Boekelheide, K. 2012. Sperm mRNA transcripts are indicators of sub-chronic low dose testicular injury in the Fischer 344 rat. *PloS One,* 7**,** e44280.

Palakurthi, S. S., Aktas, H., Grubissich, L. M., Mortensen, R. M. & Halperin, J. A. 2001. Anticancer effects of thiazolidinediones are independent of peroxisome proliferator-activated receptor γ and mediated by inhibition of translation initiation. *Cancer Research,* 61**,** 6213-6218.

Pan, G. J., Chang, Z. Y., Scholer, H. R. & Pei, D. 2002. Stem cell pluripotency and transcription factor Oct4. *Cell Research,* 12**,** 321-329.

Pang, K. S. 2003. Modeling of intestinal drug absorption: roles of transporters and metabolic enzymes *Drug Metabolism and Disposition,* 31**,** 1507-1519.

Parasuraman, S. 2011. Toxicological screening. *Journal of Pharmacology and Pharmacotherapeutics,* 2**,** 74-79.

Parillo, M. & Riccardi, G. 2004. Diet composition and the risk of type 2 diabetes: epidemiological and clinical evidence. *British Journal of Nutrition,* 92**,** 7-19.

Park, B., Pirmohamed, M. & Kitteringham, N. 1992. Idiosyncratic drug reactions: a mechanistic evaluation of risk factors. *British Journal of Clinical Pharmacology,* 34**,** 377.

Park, B. K., Boobis, A., Clarke, S., Goldring, C. E. P., Jones, D., Kenna, J. G., Lambert, C., Laverty, H. G., Naisbitt, D. J., Nelson, S., Nicoll-Griffith, D. A., Obach, R. S., Routledge, P., Smith, D. A., Tweedie, D. J., Vermeulen, N., Williams, D. P., Wilson, I. D. & Baillie, T. A. 2011. Managing the challenge of chemically reactive metabolites in drug development. *Nature Reviews Drug Discovery,* 10**,** 292-306.

Park, B. K., Laverty, H., Srivastava, A., Antoine, D. J., Naisbitt, D. & Williams, D. P. 2010. Drug bioactivation and protein adduct formation in the pathogenesis of drug-induced toxicity. *Chemico-Biological Interactions,* 192, 30-36.

Park, B. K., Pirmohamed, M. & Kitteringham, N. R. 1998. Role of drug disposition in drug hypersensitivity: a chemical, molecular, and clinical perspective. *Chemical Research in Toxicology,* 11**,** 969-988.

Paschos, G. K., Baggs, J. E., Hogenesch, J. B. & FitzGerald, G. A. 2010. The role of clock genes in pharmacology. *Annual Review of Pharmacology and toxicology,* 50**,** 187-214.

Petersen, K. F., Krssak, M., Inzucchi, S., Cline, G. W., Dufour, S. & Shulman, G. I. 2000. Mechanism of troglitazone action in type 2 diabetes. *Diabetes,* 49**,** 827.

Pettinelli, P. & Videla, L. A. 2011. Up-regulation of PPAR-γ mRNA expression in

the liver of obese patients: an additional reinforcing lipogenic mechanism to SREBP-1c induction. *Journal of Clinical Endocrinology and Metabolism,* 96**,** 1424-1430.

Pi-Sunyer, X. 2009. The medical risks of obesity. *Postgraduate Medicine,* 121**,** 21.

Picard, F. & Auwerx, J. 2002. PPARγ and glucose homeostasis. *Annual Review of Nutrition,* 22**,** 167-197.

Pirmohamed, M., James, S., Meakin, S., Green, C., Scott, A. K., Walley, T. J., Farrar, K., Park, B. K. & Breckenridge, A. M. 2004. Adverse drug reactions as cause of admission to hospital: prospective analysis of 18 820 patients. *The BMJ,* 329**,** 15-19.

Pizzo, P. & Pozzan, T. 2007. Mitochondria-endoplasmic reticulum choreography: structure and signaling dynamics. *Trends in Cell Biology,* 17**,** 511-517.

Pointon, A. V., Walker, T. M., Phillips, K. M., Luo, J., Riley, J., Zhang, S. D., Parry, J. D., Lyon, J. J., Marczylo, E. L. & Gant, T. W. 2010. Doxorubicin in vivo rapidly alters expression and translation of myocardial electron transport chain genes, leads to ATP loss and caspase 3 activation. *PloS One,* 5**,** e12733.

Pouton, C. W. & Haynes, J. M. 2007. Embryonic stem cells as a source of models for drug discovery. *Nature Reviews Drug Discovery,* 6**,** 605-616.

Pritchard, J. F., Jurima-Romet, M., Reimer, M. L. J., Mortimer, E., Rolfe, B. & Cayen, M. N. 2003. Making better drugs: decision gates in non-clinical drug development. *Nature Reviews Drug Discovery,* 2**,** 542-553.

Quednau, B. D., Nicoll, D. A. & Philipson, K. D. 2004. The sodium/calcium exchanger family—SLC8. *Pflügers Archiv - European Journal of Physiology,* 447**,** 543-548.

Rakhshandehroo, M., Knoch, B., Müller, M. & Kersten, S. 2010. Peroxisome proliferator-activated receptor alpha target genes. *PPAR Research,* 612089. http://doi.org/10.1155/2010/612089.

Reaven, G. M. 2005. The insulin resistance syndrome: definition and dietary

approaches to treatment. *Annual Review of Nutrition,* 25**,** 391-406.

Reddy, J. K. & Sambasiva Rao, M. 2006. Lipid metabolism and liver inflammation II: fatty liver disease and fatty acid oxidation. *American Journal of Physiology - Gastrointestinal and Liver Physiology,* 290**,** G852-G858.

Reppert, S. M. & Weaver, D. R. 2001. Molecular analysis of mammalian circadian rhythms. *Physiology,* 63**,** 647.

Reya, T., Morrison, S. J., Clarke, M. F. & Weissman, I. L. 2001. Stem cells, cancer, and cancer stem cells. *Nature,* 414**,** 105-111.

Rogue, A., Renaud, M. P., Claude, N., Guillouzo, A. & Spire, C. 2011. Comparative gene expression profiles induced by PPARγ and PPARα/γ agonists in rat hepatocytes. *Toxicology and Applied Pharmacology,* 254**,** 18-31.

Rogue, A., Spire, C., Brun, M., Claude, N. & Guillouzo, A. 2010. Gene expression changes induced by PPAR gamma agonists in animal and human liver. *PPAR Research,* 325183. http://doi.org/10.1155/2010/325183.

Rosen, E. D., Walkey, C. J., Puigserver, P. & Spiegelman, B. M. 2000. Transcriptional regulation of adipogenesis. *Genes and Development,* 14**,** 1293-1307.

Russell, D. W. 2003. The enzymes, regulation, and genetics of bile acid synthesis. *Annual Review of Biochemistry,* 72**,** 137-174.

Saltiel, A. R. & Kahn, C. R. 2001. Insulin signalling and the regulation of glucose and lipid metabolism. *Nature,* 414**,** 799-806.

Sanderson, J. P., Naisbitt, D. J. & Park, B. K. 2006. Role of bioactivation in drug-induced hypersensitivity reactions. *The AAPS journal,* 8**,** 55-64.

Sanguinetti, M. C. & Tristani-Firouzi, M. 2006. hERG potassium channels and cardiac arrhythmia. *Nature,* 440**,** 463-469.

Sarafidis, P., A. 2008. Thiazolidinedione derivatives in diabetes and cardiovascular disease: an update. *Fundamental & Clinical Pharmacology,* 22**,** 247-264.

SC4SM. 2008. *Stem Cells 4 Safer Medicine* [Online]. Available: http://www.sc4sm.org/.

Schernthaner, G., Currie, C. J. & Schernthaner, G.-H. 2013. Do we still need pioglitazone for the treatment of type 2 diabetes? *Diabetes Care,* 36**,** S155-S161.

Schmidt, C. W. 2009. TOX 21: new dimensions of toxicity testing. *Environmental Health Perspectives,* 117**,** A348.

Scholz, G., Genschow, E., Pohl, I., Bremer, S., Paparella, M., Raabe, H., Southee, J. & Spielmann, H. 1999. Prevalidation of the embryonic stem cell test — a new in vitro embryotoxicity test. *Toxicology In Vitro,* 13**,** 675-681.

Schröder, M. 2008. Endoplasmic reticulum stress responses. *Cellular and Molecular Life Sciences,* 65**,** 862-894.

Shen, Y., Meunier, L. & Hendershot, L. M. 2002. Identification and characterization of a novel endoplasmic reticulum (ER) DnaJ homologue, which stimulates ATPase activity of BiP in vitro and is induced by ER stress. *The Journal of Biological Chemistry,* 277**,** 15947-56.

Shiroi, A., Yoshikawa, M., Yokota, H., Fukui, H., Ishizaka, S., Tatsumi, K. & Takahashi, Y. 2002. Identification of insulin-producing cells derived from embryonic stem cells by zinc-chelating dithizone. *Stem Cells,* 20**,** 284-292.

Smith, A. G. 2001. Embryo-derived stem cells: of mice and men. *Annual Review of Cell and Developmental Biology,* 17**,** 435-462.

Smith, A. G., Heath, J. K., Donaldson, D. D., Wong, G. G., Moreau, J., Stahl, M. & Rogers, D. 1988. Inhibition of pluripotential embryonic stem cell differentiation by purified polypeptides. *Nature,* 336**,** 688-690.

Smith, M. T. 2003. Mechanisms of troglitazone hepatotoxicity. *Chemical Research in Toxicology,* 16**,** 679-687.

Smyth, G. K. & Speed, T. 2003. Normalization of cDNA microarray data. *Methods,* 31**,** 265-273.

Spandidos, A., Wang, X., Wang, H., Dragnev, S., Thurber, T. & Seed, B. 2008. A

comprehensive collection of experimentally validated primers for polymerase chain reaction quantitation of murine transcript abundance. *BMC Genomics,* 9**,** 633.

Spandidos, A., Wang, X., Wang, H. & Seed, B. 2010. PrimerBank: a resource of human and mouse PCR primer pairs for gene expression detection and quantification. *Nucleic Acids Research,* 38**,** D792-D799.

Straub, S. G. & Sharp, G. W. G. 2002. Glucose-stimulated signaling pathways in biphasic insulin secretion. *Diabetes/Metabolism Research and Reviews,* 18**,** 451-463.

Stumvoll, M., Goldstein, B. J. & van Haeften, T. W. 2005. Type 2 diabetes: principles of pathogenesis and therapy. *The Lancet,* 365**,** 1333-1346.

Suzuki, A., Raya, Á., Kawakami, Y., Morita, M., Matsui, T., Nakashima, K., Gage, F. H., Rodríguez-Esteban, C. & Belmonte, J. C. I. 2006. Nanog binds to Smad1 and blocks bone morphogenetic protein-induced differentiation of embryonic stem cells. *Proceedings of the National Academy of Sciences,* 103**,** 10294-10299.

Szegezdi, E., Logue, S. E., Gorman, A. M. & Samali, A. 2006. Mediators of endoplasmic reticulum stress-induced apoptosis. *EMBO Reports,* 7**,** 880-885.

Tabas, I. & Ron, D. 2011. Integrating the mechanisms of apoptosis induced by endoplasmic reticulum stress. *Nature Cell Biology,* 13**,** 184-190.

Takahashi, K., Tanabe, K., Ohnuki, M., Narita, M., Ichisaka, T., Tomoda, K. & Yamanaka, S. 2007. Induction of pluripotent stem cells from adult human fibroblasts by defined factors. *Cell,* 131**,** 861-872.

Takahashi, T., Lord, B., Schulze, P. C., Fryer, R. M., Sarang, S. S., Gullans, S. R. & Lee, R. T. 2003. Ascorbic acid enhances differentiation of embryonic stem cells into cardiac myocytes. *Circulation***,** 14, 1912-1916.

Takaki, M., Nakayama, S., Misawa, H., Nakagawa, T. & Kuniyasu, H. 2006. In vitro formation of enteric neural network structure in a gut-like organ differentiated from mouse embryonic stem cells. *Stem Cells,* 24**,** 1414-1422.

Thomson, H. 2007. Bioprocessing of embryonic stem cells for drug discovery. *Trends in Biotechnology,* 25**,** 224-230.

Thomson, J. A., Itskovitz-Eldor, J., Shapiro, S. S., Waknitz, M. A., Swiergiel, J. J., Marshall, V. S. & Jones, J. M. 1998. Embryonic stem cell lines derived from human blastocysts. *Science,* 282**,** 1145-1147.

Tiscornia, G., Vivas, E. L. & Belmonte, J. 2011. Diseases in a dish: modeling human genetic disorders using induced pluripotent cells. *Nature Medicine,* 17**,** 1570-1576.

Tong, W., Cao, X., Harris, S., Sun, H., Fang, H., Fuscoe, J., Harris, A., Hong, H., Xie, Q. & Perkins, R. 2003. ArrayTrack--supporting toxicogenomic research at the US Food and Drug Administration National Center for Toxicological Research. *Environmental Health Perspectives,* 111**,** 1819.

Tontonoz, P. & Spiegelman, B. M. 2008. Fat and beyond: the diverse biology of PPARγ. *Annual Review of Biochemistry,* 77**,** 289-312.

Tyers, M. & Mann, M. 2003. From genomics to proteomics. *Nature,* 422**,** 193-197.

Verdugo, R. A. & Medrano, J. F. 2006. Comparison of gene coverage of mouse oligonucleotide microarray platforms. *BMC Genomics,* 7**,** 58-58.

Verlinsky, Y., Strelchenko, N., Kukharenko, V., Rechitsky, S., Verlinsky, O., Galat, V. & Kuliev, A. 2005. Human embryonic stem cell lines with genetic disorders. *Reproductive BioMedicine Online,* 10**,** 105-110.

Vidal-Puig, A., Jimenez-Liñan, M., Lowell, B. B., Hamann, A., Hu, E., Spiegelman, B., Flier, J. S. & Moller, D. E. 1996. Regulation of PPAR gamma gene expression by nutrition and obesity in rodents. *Journal of Clinical Investigation,* 97**,** 2553.

Videla, L. A. 2009. Oxidative stress signaling underlying liver disease and hepatoprotective mechanisms. *World Journal of Hepatology,* 1**,** 72.

Wang, S., Sim, T. B., Kim, Y.-S. & Chang, Y.-T. 2004. Tools for target identification and validation. *Current Opinion in Chemical Biology,* 8**,** 371-377.

Wang, W. & Ballatori, N. 1998. Endogenous glutathione conjugates: occurrence

and biological functions. *Pharmacological Reviews,* 50**,** 335-356.

Wang, X. & Seed, B. 2003. A PCR primer bank for quantitative gene expression analysis. *Nucleic Acids Research,* 31**,** e154.

Wang, X. & Yang, P. 2008. In vitro differentiation of mouse embryonic stem (mES) cells using the hanging drop method. *Journal of Visualized Experiments*, 17, 825.

Waters, M. D. & Fostel, J. M. 2004. Toxicogenomics and systems toxicology: aims and prospects. *Nature Reviews Genetics,* 5**,** 936-948.

Weir, M. R. 2010. Hypervolemia and blood pressure: powerful indicators of increased mortality among hemodialysis patients. *Hypertension,* 56**,** 341-343.

Westerbacka, J., Kolak, M., Kiviluoto, T., Arkkila, P., Sirén, J., Hamsten, A., Fisher, R. M. & Yki-Järvinen, H. 2007. Genes involved in fatty acid partitioning and binding, lipolysis, monocyte/macrophage recruitment, and inflammation are overexpressed in the human fatty liver of insulin-resistant subjects. *Diabetes,* 56**,** 2759-2765.

Whitebread, S., Hamon, J., Bojanic, D. & Urban, L. 2005. Keynote review: In vitro safety pharmacology profiling: an essential tool for successful drug development. *Drug Discovery Today,* 10**,** 1421-1433.

Whitney, M. L., Jefferson, L. S. & Kimball, S. R. 2009. ATF4 is necessary and sufficient for ER stress-induced upregulation of REDD1 expression. *Biochemical and Biophysical Research Communications,* 379**,** 451-455.

WHO. 2006. *Definition and diagnosis of diabetes mellitus and intermediate hyperglycemia: report of a WHO/IDF consultation* [Online].
Available: http://www.who.int/diabetes/publications/diagnosis_diabetes2006/en/.

WHO. 2012. *List of globally identified websites of medicines regulatory authorities* [Online].
Available: http://www.who.int/medicines/areas/quality_safety/regulation_legislation/en/.

Wilkening, S. & Bader, A. 2003. Influence of culture time on the expression of

drug-metabolizing enzymes in primary human hepatocytes and hepatoma cell line HepG2. *Journal of Biochemical and Molecular Toxicology,* 17**,** 207-213.

Williams, R. L., Hilton, D. J., Pease, S., Willson, T. A., Stewart, C. L., Gearing, D. P., Wagner, E. F., Metcalf, D., Nicola, N. A. & Gough, N. M. 1988. Myeloid leukaemia inhibitory factor maintains the developmental potential of embryonic stem cells. *Nature,* 336**,** 684-687.

Willson, T. M., Lambert, M. H. & Kliewer, S. A. 2001. Peroxisome proliferator-activated receptor γ and metabolic disease. *Annual Review of Biochemistry,* 70**,** 341-367.

Winzell, M. S. & Ahrén, B. 2004. The high-fat diet–fed mouse. *Diabetes,* 53**,** S215.

Wobus, A. M. 2001. Potential of embryonic stem cells. *Molecular Aspects of Medicine,* 22**,** 149-164.

Wobus, A. M. & Boheler, K. R. 2005. Embryonic stem cells: prospects for developmental biology and cell therapy. *Physiological Reviews,* 85**,** 635-678.

Wobus, A. M. & Guan, K. 1998. Embryonic stem cell-derived cardiac differentiation: modulation of differentiation and "loss-of-function" analysis in vitro. *Trends in Cardiovascular Medicine,* 8**,** 64-74.

Wobus, A. M., Kaomei, G., Shan, J., Wellner, M.-C., Rohwedel, J., Guanju, J., Fleischmann, B., Katus, H. A., Hescheler, J. & Franz, W.-M. 1997. Retinoic acid accelerates embryonic stem cell-derived cardiac differentiation and enhances development of ventricular cardiomyocytes. *Journal of Molecular and Cellular Cardiology,* 29**,** 1525-1539.

Wuttke, H., Rau, T., Heide, R., Bergmann, K., Böhm, M., Weil, J., Werner, D. & Eschenhagen, T. 2002. Increased frequency of cytochrome P450 2D6 poor metabolizers among patients with metoprolol-associated adverse effects. *Clinical Pharmacology and Therapeutics,* 72**,** 429-437.

Xie, H.-G., Kim, R. B., Wood, A. J. & Stein, C. M. 2001. Molecular basis of ethnic differences in drug disposition and response. *Annual Review of Pharmacology*

and Toxicology, 41**,** 815-850.

Xu, C., Bailly-Maitre, B. & Reed, J. C. 2005. Endoplasmic reticulum stress: cell life and death decisions. *The Journal of Clinical Investigation,* 115**,** 2656-2664.

Yamauchi, S., Kiyosawa, N., Ando, Y., Watanabe, K., Niino, N., Ito, K., Yamoto, T., Manabe, S. & Sanbuissho, A. 2011. Hepatic transcriptome and proteome responses against diethyl maleate-induced glutathione depletion in the rat. *Archives of Toxicology,* 85**,** 1045-1056.

Yang, Y. H., Dudoit, S., Luu, P., Lin, D. M., Peng, V., Ngai, J. & Speed, T. P. 2002. Normalization for cDNA microarray data: a robust composite method addressing single and multiple slide systematic variation. *Nucleic Acids Research,* 30**,** e15-e15.

Yap, Y. G. & Camm, A. J. 2003. Drug induced QT prolongation and torsades de pointes. *Heart,* 89**,** 1363-1372.

Ying, Q. L., Nichols, J., Chambers, I. & Smith, A. 2003. BMP induction of Id proteins suppresses differentiation and sustains embryonic stem cell self-renewal in collaboration with STAT3. *Cell,* 115**,** 281-292.

Yokoi, T. 2010. Adverse Drug Reactions. *Springer Berlin Heidelberg,* 419-435.

Zaret, K. S. 2009. Using small molecules to great effect in stem cell differentiation. *Cell Stem Cell,* 4**,** 373-374.

Zhang, S.-D. & Gant, T. W. 2008. A simple and robust method for connecting small-molecule drugs using gene-expression signatures. *BMC Bioinformatics,* 9**,** 258.

Zhang, W., Liu, J., Tian, L., Liu, Q., Fu, Y. & Garvey, W. T. 2013. TRIB3 mediates glucose-induced insulin resistance via a mechanism that requires the hexosamine biosynthetic pathway. *Diabetes,* 62**,** 4192-4200.

Zhou, M., Li, P., Tan, L., Qu, S., Ying, Q. L. & Song, H. 2010. Differentiation of mouse embryonic stem cells into hepatocytes induced by a combination of cytokines and sodium butyrate. *Journal of Cellular Biochemistry,* 109**,** 606-614.

Zimmermann, R., Lass, A., Haemmerle, G. & Zechner, R. 2009. Fate of fat: The

role of adipose triglyceride lipase in lipolysis. *BBA Molecular and Cell Biology of Lipids,* 1791**,** 494-500.

Zollner, G., Marschall, H.-U., Wagner, M. & Trauner, M. 2006. Role of nuclear receptors in the adaptive response to bile acids and cholestasis: pathogenetic and therapeutic considerations. *Molecular Pharmaceutics,* 3**,** 231-251.Zorn, A. M. & Wells, J. M. 2009. Vertebrate endoderm development and organ formation. *Annual Review of Cell and Developmental Biology,* 25**,**221.

Zucco, F., De Angelis, I., Testai, E. & Stammati, A. 2004. Toxicology investigations with cell culture systems: 20 years after. *Toxicology In Vitro,* 18**,** 153-163.